ATP-dependent nucleosome remodeling by ISWI: Insights into mechanism and regulation

Dissertation zur Erlangung des Doktorgrades
der Naturwissenschaften (Dr. rer. nat.)

vorgelegt der Fakultät für Biologie der
Ludwig-Maximilians-Universität München

Johanna Ludwigsen
2017

Tag der Abgabe:	06.06.2017
Tag der mündlichen Prüfung:	14.11.2017

Erstgutachter:	Prof. Dr. Peter B. Becker
Zweitgutachter:	Prof. Dr. Dirk Eick

Eidesstattliche Erklärung

Ich versichere hiermit an Eides statt, dass die vorgelegte Dissertation von mir selbständig und ohne unerlaubte Hilfe angefertigt ist.

München, den 02.02.2018 …….
(Johanna Ludwigsen)

Erklärung

Hiermit erkläre ich, dass die Dissertation **nicht** ganz oder in wesentlichen Teilen einer anderen Prüfungskommission vorgelegt worden ist. Ich habe mich **nicht** anderweitig einer Doktorprüfung ohne Erfolg unterzogen.

München, den 02.02.2018 …….
(Johanna Ludwigsen)

CONTENTS

I. PREFACE

The research I conducted in the laboratory of Dr. Felix Müller-Planitz resulted in three original research papers on the mechanism and regulation of the nucleosome remodeling enzyme ISWI. The research papers are presented in the results section (page 17) of this cumulative thesis along with an additional manuscript describing the establishment of two *in vitro* assays to study nucleosome remodeling. Since the publications build on one another, they are presented in a chronological order. My contributions are stated at the beginning of each research paper and in the comprehensive 'declaration of contributions' (page IV). Each chapter of the results section contains the corresponding reference list and supplementary material. References from the introduction and the discussion are included subsequent to the discussion (page 144).

II. ABBREVIATIONS

Å	Ångström
Aa	Amino acids
ACF	ATP-utilizing chromatin assembly and remodeling factor
AcidicN	Acidic region in the N-terminus of ISWI
ADP	Adenosine diphosphate
AFM	Atomic force microscope
ATP	Adenosine triphosphate
ATRX	α-thalassaemia/mental retardation X-linked
AutoN	N-terminal autoinhibitory region in ISWI
Bp	Base pairs
CARD	Caspase activation and recruitment domain
CERF	CECR2-containing remodeling factor
Chd1/2	Chromodomain helicase DNA binding protein 1/2
CHRAC	Chromatin accessibility complex
Chromodomain	Chromatin organization modifier domain
CtBP	C-terminal binding protein
DAXX	Death domain-associated protein
DDX3	DEAD-box protein 3
DBD	DNA-binding domain
Dbp5	DEAD-box protein 5
DNA	Desoxyribonucleic acid
EM	Electron microscopy
FRET	Fluorescence resonance energy transfer
g-H4	Globular histone H4 (histone H4 lacking the N-terminal tail)
HSS	HAND SANT SLIDE domain
ISW1/2	Imitation switch 1/2 (complexes in yeast)
(Dm)ISWI	Imitation switch (enzyme in *D. melanogaster*)
Mfd	mutation frequency decline protein
mRNA	Messenger RNA
MtISWI	ISWI ortholog of *M. thermophila*
NAP1	Nucleosome assembly protein 1
NegC	C-terminal autoinhibitory motif in ISWI
NoRC	Nucleolar remodeling complex
NTR	N-terminal region
Nup159	Nuclear pore protein 159
NURF	Nucleosome remodeling factor
Prp5	Pre-mRNA processing 5
PTM	Post-translational modification
RIG-I	Retinoic acid inducible gene I
RNA	Ribonucleic acid
RSC	Remodels the structure of chromatin (enzyme in yeast)
ScSnf2	*S. cerevisiae* Snf2
SHL	Super-helical location
Snf2	Sucrose non-fermentable 2
ToRC	Toutatis-containing chromatin remodeling complex

III. LIST OF PUBLICATIONS AND MANUSCRIPTS

List of the publications included in this thesis

Mueller-Planitz F, Klinker H**, Ludwigsen J**, Becker PB (2013)
The ATPase domain of ISWI is an autonomous nucleosome remodeling machine.
Nature Structural & Molecular Biology 20, 82-89.

Ludwigsen J, Klinker H, Mueller-Planitz F (2013)
No need for a power stroke in ISWI-mediated nucleosome sliding.
EMBO reports 14, 1092-1097.

Ludwigsen J, Pfennig S, Singh AK, Schindler C, Harrer N, Forné I, Zacharias M, Mueller-Planitz F (2017)
Concerted regulation of ISWI by an autoinhibitory domain and the H4 N-terminal tail.
Elife, 6:e21477.

Unpublished manuscript included in this thesis

Ludwigsen J, Hepp N, Klinker H, Pfennig S, Mueller-Planitz F
Remodeling and repositioning of nucleosomes in nucleosomal arrays.
invited book chapter in the Methods in Molecular Biology series (Springer), Molecular Motors volume
in revision

Publications not included in this thesis

Lieleg C, Ketterer P, Nuebler J, **Ludwigsen J**, Gerland U, Dietz H, Mueller-Planitz F, Korber P (2015)
Nucleosome spacing generated by ISWI and CHD1 remodelers is constant regardless of nucleosome density.
Molecular and Cellular Biology, 35(9):1588-605.

IV. DECLARATION OF CONTRIBUTIONS AS CO-AUTHOR

Declaration of contributions to: Mueller-Planitz et al. (2013) The ATPase domain of ISWI is an autonomous remodeling machine. Nature Structural & Molecular Biology.

This study was conceived by F. Müller-Planitz and P.B. Becker. I performed most of the restriction enzyme accessibility experiments employing g-H4 arrays that are summarized in Figure 6 and Supplementary Figure 7. Together with H. Klinker, I prepared Figure 6 including the Figure legend and the respective materials and methods sections. I assisted in developing and revising the manuscript that was mainly written by F. Mueller-Planitz and P.B. Becker and edited it at all stages of the publication process.

Declaration of contributions to: Ludwigsen et al. (2013) No need for a power stroke in ISWI-mediated nucleosome sliding. EMBO reports.

This study was conceived by F. Müller-Planitz and me. I performed all experiments except for the nucleosome sliding experiment shown in Figure 4, which was done by H. Klinker. She also wrote the corresponding materials and methods section and revised the figure legend. The manuscript was written by Felix-Mueller-Planitz and me. Furthermore, I prepared all figures and figure legends.

Declaration of contributions to: Ludwigsen et al. (2017) Concerted regulation of ISWI by an autoinhibitory domain and the H4 N-terminal tail. Elife.

This study was conceived by F. Müller-Planitz and me. I performed experiments, analyzed data and prepared the figures with the exceptions listed below. All yeast experiments were performed by A. Singh (Figure 2 and Figure 2 – Figure supplement 1). S. Pfennig crosslinked nucleosomes containing benzophenone-labeled H4 to ISWI and performed the corresponding control experiments (Figure 5A–D, Figure 5 – Figure supplement 1G–J, Figure 5 – Figure supplement 2B,C). C. Schindler performed all *in silico* docking studies (Figure 4F, Figure 4 – Figure supplement 3A–C, Figure 5E). I. Forné performed mass spectrometry measurements and helped with data analysis. N. Harrer helped preparing Figure 7 and all figures involving spectra obtained from mass spectrometry. N. Harrer also helped to analyze mass spectrometry data. The manuscript was written and revised by F. Mueller-Planitz and me. The materials and methods sections were written by the author, who performed the corresponding experiment.

Declaration of contributions to: Ludwigsen et al., Remodeling and repositioning of nucleosomes in nucleosomal arrays. Invited book chapter, in revision.

N. Hepp and I contributed equally to this work. N. Hepp designed and prepared all materials and developed the original protocol for the quantitative polynucleosome remodeling assay (sections 2.2, 3.1). H. Klinker developed the polynucleosome repositioning assay (sections 2.3, 3.2). I applied and optimized the protocols. Moreover, I wrote the first draft of the manuscript and developed the enclosed version together with F. Mueller-Planitz, N. Hepp and H. Klinker. S. Pfennig helped writing the introduction and prepared Figure 1. I prepared all remaining figures.

V. SUMMARY

Eukaryotic cells store their genome in a protein-DNA complex called chromatin. The fundamental building unit of chromatin is the nucleosome, which consists of DNA that is wrapped around a protein core. Nucleosomes pose an obstacle to nuclear DNA-binding factors by inherently restricting access to the DNA that is wrapped around them. To allow for the progression of essential nuclear processes, cells have evolved sophisticated mechanisms that regulate the dynamic access of specific DNA target sequences. Key players ensuring the rapid and reliable rearrangement of chromatin are conserved ATP-dependent nucleosome remodeling enzymes. These molecular motors assemble, evict, restructure or reposition nucleosomes. Remodelers of the ISWI family translocate DNA across the histone core to reposition nucleosomes along DNA in a process termed nucleosome sliding. Efficient nucleosome mobilization relies on the presence of the nucleosomal H4 N-terminal tail. The ATPase domain of ISWI is flanked by the DNA-binding HAND-SANT-SLIDE (HSS) module on the C-terminus and a largely uncharacterized N-terminal region (NTR). Gaps in the understanding of a basic sliding reaction and its regulation exist and prevent us from obtaining a detailed mechanistic view of nucleosome remodeling.

This thesis presents a combination of quantitative biochemical and structural studies that provide insights into the function of the HSS domain during nucleosome sliding and the regulatory potential of the ISWI NTR. To facilitate the quantitative analysis of nucleosome remodeling, we developed an *in vitro* remodeling assay employing nucleosomal arrays.

Prominent mechanistic models suggested that the HSS domain is essential for nucleosome sliding by ISWI. Furthermore, a conformational change between the ATPase and the HSS domain was proposed to mechanically pull DNA into the nucleosome. In contrast, we now revealed that the HSS domain is dispensable for nucleosome sliding. In fact, we demonstrated that an ISWI mutant lacking the HSS domain displayed all attributes of a basic remodeling machine. Its ATPase activity was stimulated by DNA and nucleosomes, it repositioned nucleosomes and was sensitive towards the H4 N-terminal tail. Notably, flexible linkers inserted at strategic positions between the ATPase and HSS domain did not compromise the catalytic activity of ISWI. This indicates that the HSS domain does not simply serve as a mechanical element that pushes DNA into the nucleosome. We thus hypothesize that the ATPase domain combines all aspects of a rudimentary remodeling machine and that flanking domains including the HSS domain regulate and optimize the sliding reaction.

The ISWI NTR contains several conserved sequence motifs. The AutoN motif has previously been suggested to negatively regulate the ISWI ATPase domain, whereas the function of the remaining motifs has not been studied to date. We systematically analyzed the function of the acidic region, which we termed AcidicN, the post-post-helicase-SANT-associated (ppHSA) motif and the AT-hook. We found the ppHSA motif to be important for the structural stability of ISWI. Furthermore, we demonstrated that AcidicN cooperates with AutoN to regulate the ISWI ATPase domain. AcidicN furnished ISWI with the ability to discriminate between DNA and nucleosomes and conferred sensitivity towards the H4 N-terminal tail. To understand the molecular basis of H4 tail recognition we mapped its binding site and resolved the overall structural architecture of the NTR-ATPase module. Contrary to prevalent expectations, we found the binding sites of AutoN-AcidicN and the H4 tail to be adjacent, but not overlapping. We interpret our results with a comprehensive model for the combined inhibition of ISWI by the NTR and recognition of the histone H4 tail.

VI. ZUSAMMENFASSUNG

Eukaryotische Zellen verpacken ihr Genom in einem Protein-DNA Komplex, der Chromatin genannt wird. Die grundlegende Verpackungseinheit des Chromatins ist das Nukleosom, welches aus DNA besteht, die sich um einen Proteinkern windet. Nukleosomen stellen ein Hindernis für DNA-bindende Faktoren dar, da sie die aufgewickelte DNA verdecken. Zellen haben daher komplexe Mechanismen entwickelt, die die dynamische Zugänglichkeit spezifischer DNA-Sequenzen gewährleisten. So gewährleisten konservierte, ATP-abhängige Nukleosomen-*Remodeling*-Enzyme den schnellen und zuverlässigen Übergang zwischen verschiedenen Chromatinzuständen. Diese Enzyme sind molekulare Motoren, die sowohl die Assemblierung von Nukleosomen als auch deren Ab- und Umbau katalysieren. *Remodeling*-Enzyme der ISWI-Familie sind beispielsweise in der Lage Nukleosomen entlang der DNA an eine neue Position zu verschieben. Dieser Prozess wird als Nukleosomen Repositionierung bezeichnet. Für eine effiziente Nukleosomen Repositionierungs-Aktivität benötigt ISWI den flexiblen N-terminus von Histon H4. Die ATPase-Domäne von ISWI wird durch ein C-terminales DNA-Bindungsmodul, die HAND-SANT-SLIDE (HSS) Domäne, und die weitestgehend unerforschte N-terminale Region (NTR) flankiert. Ebenso ist sowohl der grundlegende molekulare Mechanismus als auch die Regulation der Nukleosomen Repositionierungs-Reaktion bis heute nicht im Detail aufgeklärt.

In der vorliegenden Dissertation wurde eine Kombination aus quantitativen biochemischen Methoden und strukturellen Studien genutzt, um Einblicke in die Funktion der HSS-Domäne während der Repositionierung von Nukleosomen zu erhalten. Außerdem wurde das regulatorische Potential der NTR von ISWI näher untersucht. Dafür wurde ein Protokoll entwickelt, dass die quantitative Analyse der Nukleosomen Repositionierung innerhalb von *in vitro* assemblierten Chromatinfasern ermöglicht.

Vorherrschende Modelle postulieren, dass die HSS-Domäne von ISWI essentiell für dessen Repositionierungs-Aktivität ist. Des Weiteren wurde angenommen, dass eine Konformationsänderung zwischen der ATPase und der HSS-Domäne nötig ist, um DNA mechanisch in das Nukleosom hinein zu ziehen. Im Gegensatz dazu haben wir nun gezeigt, dass die HSS-Domäne nicht essentiell für die Repositionierung von Nukleosomen ist. In der Tat besaß eine ISWI-Mutante, der die HSS-Domäne fehlte, alle Attribute einer grundlegenden Nukleosomen-*Remodeling* Maschine. Ihre ATPase-Aktivität wurde durch DNA und Nukleosomen stimuliert, sie besaß Repositionierungs-Aktivität und reagierte zudem auf den N-terminus von H4. Bemerkenswert war, dass flexible Linker, die an strategischen Positionen zwischen der ATPase- und der HSS-Domäne eingefügt wurden, die katalytische Aktivität von ISWI nicht beeinträchtigten. Unsere Ergebnisse deuten darauf hin, dass die HSS-Domäne nicht als ein simples mechanisches Element fungiert, das DNA in das Nukleosom hineinzieht. Wir vermuten vielmehr, dass die ATPase-Domäne alle Aspekte einer rudimentären *Remodeling*-Maschine vereint und dass die HSS-Domäne die Aktivität von ISWI reguliert und optimiert.

Die NTR von ISWI enthält eine Vielzahl konservierter Sequenzmotive. Während das AutoN Motiv bereits in die negative Regulation der ISWI ATPase Domäne impliziert wurde, ist die Funktion der verbleibenden Motive bis heute völlig unbekannt. Wir untersuchten systematische die Funktion der sauren Region, die wir als AcidicN definieren, des post-post-helicase-SANT-associated (ppHSA) Motivs und des AT-*hook*. Wir konnten zeigen, dass ppHSA wichtig für die strukturelle Stabilität von ISWI ist. Weiterhin, legten wir dar, dass AcidicN zusammen mit AutoN die ATPase Domäne

von ISWI reguliert. AcidicN stattete ISWI mit der Fähigkeit aus zwischen DNA und Nukleosomen zu unterscheiden und gewährleistete die Sensitivität von ISWI gegenüber dem N-terminus von H4. Um den molekularen Mechanismus der H4 N-terminus Erkennung zu verstehen, identifizierten wir dessen Bindungsstelle in ISWI und klärten die generelle strukturelle Architektur des NTR-ATPase Moduls auf. Im Gegensatz zu vorherrschenden Erwartungen überlappten die Bindungsstellen von AutoN-AcidicN und dem H4 N-terminus nicht, sondern lagen nebeneinander. Wir interpretieren unsere Ergebnisse mit einem übergreifenden Modell, dass sowohl die Inhibierung von ISWI durch die NTR als auch die Erkennung des H4 N-terminus erklärt.

1. INTRODUCTION

1.1 Chromatin structure

The genetic material of eukaryotic cells is stored in a dynamic nucleoprotein complex called chromatin. This organization ensures that DNA can be accommodated in the restricted confines of the cell's nucleus. However, chromatin is not just a scaffold for DNA, but a highly dynamic structure that is intricately linked to the regulation of many essential cellular processes. The following section discusses structural details of the nucleosome, the basic building unit of chromatin, and higher-order compaction levels of chromatin.

1.1.1 Nucleosomes: beads on a string

The repeating unit of chromatin is the nucleosome, which consists of DNA that is wrapped around a core of histone proteins. Early evidence for the existence of nucleosomes came from negative stain micrographs of chromatin fibers that resembled 'beads on a string' (Figure 1A) (1, 2). Years later, Luger et al. reported the 2.8 Å crystal structure of the nucleosome and set a scientific milestone (Figure 1B,C) (3).

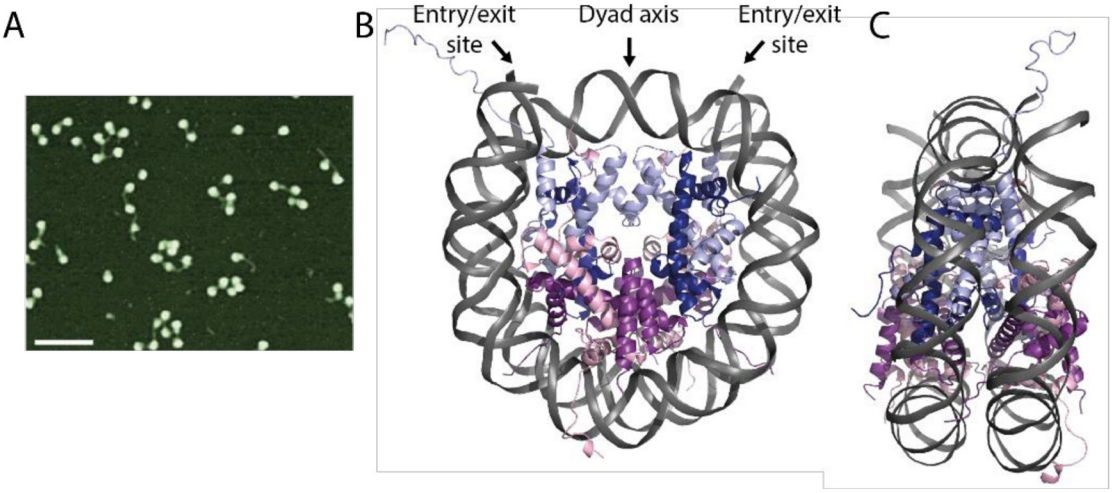

Figure 1: The nucleosome. (A) Cryo-AFM image of purified chromatin fragments from chicken erythrocytes. Chromatin fibers resemble 'beads on a string', with linker DNA and nucleosomes well resolved. Scale bar: 100 nm. (Reprinted from (Sheng et al., 2006) with permission from Elsevier) **(B)** Crystal structure of the nucleosome core particle at 2.8 Å resolution (PDB: 1AOI, Luger et al., 1997). 146 bp of DNA are wrapped around the core of histone proteins in a left-handed superhelix. The pseudo-twofold dyad axis and the entry/exit site of DNA are indicated by arrows. H2A: pink, H2B: purple, H3: light blue, H4: dark blue, DNA: grey. **(C)** 90° rotation of the nucleosome particle as shown in **(B)**. All molecular graphics included in this thesis were prepared using PyMOL (www.pymol.org).

To form a nucleosome, 145–147 bp of DNA are wrapped around a histone octamer core in a left-handed superhelix. The histone octamer comprises two copies of each of the four core histones H2A, H2B, H3 and H4 (Figure 1B,C). Canonical histones are small (11–15 kDa), highly conserved and very basic proteins that feature two characteristic parts. Each core histone contains a largely unstructured N-terminal 'tail' region, which is required for nucleosome stability and formation of higher-order structures (section 1.1.2). Moreover, histones are characterized by the presence of a central 'histone fold' domain (4). This domain is comprised of three α-helices connected by two loops and serves as a dimerization interface that drives heterodimerization of histones H2A with H2B and H3 with H4 via a 'handshake motif'. Two H3/H4 dimers associate via a H3:H3 interface to form a stable $(H3/H4)_2$ tetramer. Single H2A/H2B dimers then assemble on either side of the

tetramer to form a histone octamer. Nucleosomes are subject to numerous post-translational modifications (PTMs), which are dynamically added and removed (see section 1.2.2).

The nucleosome core particle exhibits a pseudo-twofold dyad symmetry. The symmetry axis passes through the $(H3\text{-}H4)_2$ tetramer and coincides with the central base-pair (Figure 1B,C). This central position is commonly referred to as super-helical location 0 (SHL0) with other DNA locations described by the number of helical turns away from the dyad (SHL±1-SHL±7). The DNA major groove faces inward at integer SHL values whereas the minor groove faces inward at half-integer SHL values. DNA is highly contorted by wrapping around the histone core and the tight association requires several electrostatic and van der Waals interactions as well as direct and water-mediated hydrogen bonds (5). The majority of contacts are observed between the histone folds and the DNA backbone. The flexible histone tails extend away from DNA and are mainly involved in interactions with neighboring nucleosomes or with regulatory factors. Specific histone-DNA contacts occur at 14 distinct sites where the minor groove approaches the protein surface and are mediated by highly conserved arginine residues. Notably, these interactions are energetically not equivalent. The strongest interactions occur around the nucleosomal dyad whereas particularly weak interactions exist at the entry/exit site of the nucleosome (6). Moreover, none of the interactions are base-pair specific, suggesting that histone–DNA contacts are sequence independent (5). However, global determination of nucleosome positioning *in vivo* indicates certain DNA sequence preferences that likely result from inherent differences in the ability of DNA sequences to bend and adapt to the contour of the octamer surface (7, 8).

Nucleosomes have been suggested to be assembled in a stepwise manner (9, 10). First, the $(H3\text{-}H4)_2$ tetramer is deposited onto DNA to form a tetrasome. The assembly then proceeds by the addition of two H2A-H2B dimers flanking the $(H3\text{-}H4)_2$ tetramer on both sides and the wrapping of DNA around the histone octamer. Nucleosome disassembly is thought to be the reversal of this process such that eviction of H2A-H2B occurs before $(H3\text{-}H4)_2$ is removed. *In vivo*, histones are escorted by chaperones that prevent the highly basic histones from engaging in non-specific interactions and facilitate the assembly process (11). Recent studies identified sub-nucleosomal structures, such as half-nucleosomes consisting of one copy of each histone as well as hexasomes (nucleosomes lacking one H2A-H2B dimer) (12-17). These findings suggest the existence of alternative nucleosome assembly/disassembly pathways.

Each nucleosome core is connected to its neighbor via a stretch of 'linker DNA' to form nucleosomal arrays. The length of the linker DNA varies from ~10–90 bp in a species- and tissue-specific manner. *In vivo*, linker DNA is typically associated with a fifth class of histones, the 'linker histones' (H1s) (18). H1-bound nucleosome core particles are commonly referred to as 'chromatosomes' (19). Compared to core histones, the H1 family of histones is less conserved and exhibits a considerable sequence variability between species. Linker histones appear to be involved in stabilizing nucleosomes and in the assembly of higher-order chromatin structures, which are discussed below (20-22).

1.1.2 Higher-order chromatin structures

The organization into nucleosome allows for a sixfold compaction of the eukaryotic genome, therefore accounting for only a small fraction of the approximately 1000-fold compaction observed. To form structures as condensed as a mitotic chromosome, it was postulated that chromatin hierarchically folds into higher-order structures. According to this concept, the primary 'beads on

a string' structure (also referred to as the 10 nm fiber) folds into a regular secondary structure, the '30 nm fiber'. These fibers have been suggested to form interstrand contacts and sequentially fold into a well-defined tertiary structure.

The structure of the 30 nm fiber has been at the heart of debate for decades. Two competing models have emerged as possible candidates. The solenoid model was derived from electron microscopy (EM) studies and proposes consecutive nucleosomes to interact with each other and follow a helical trajectory. Linker DNA connecting adjacent nucleosomes is bent (23). This model has recently been supported by single-molecule force spectroscopy (24) and EM (25) of nucleosomal arrays. In contrast, the zig-zag model favors the formation of a two-start helix such that alternate nucleosomes become interacting partners. Linker DNA is expected to be straight and criss-cross the interstitial space (26, 27). Disulfide crosslinking studies (28), the crystal structure of a tetranucleosome (29) as well as cryo-EM studies (30) provide evidence for the zig-zag structure.

Whereas 30 nm fibers certainly form *in vitro*, their existence in living cells has recently been called into question (31-34). Concerns were raised that conditions used for chromatin extraction such as fixation and staining procedures may favor the assembly of 30 nm fibers and introduce *in vitro* artifacts. Moreover, evidence for a different chromatin organization accumulated. Data obtained from cryo-EM (35), SAXS (36) and energy spectroscopic imaging (ESI) experiments (37, 38) suggested that even heterochromatin is exclusively composed of 10 nm fibers (39). Moreover, it was proposed that 30 nm fibers primarily form in transcriptionally inactive or terminally differentiated cells such as starfish sperm (26) or chicken erythrocytes (40, 41). Although local or transient formation of 30 nm fiber structures cannot be excluded *in vivo*, most chromatin fibers appear to adopt alternative structures. Lately, the development of chromosome conformation capture (3C) techniques offer the possibility to obtain high-resolution information on the three-dimensional structure of the genome (42, 43). A recent micro-C study found no evidence for a repeating 30 nm fiber in *Saccharomyces cerevisiae* cells. Instead, the data supported a tri- or tetranucleosome folding motif with domains of one to five genes forming compact folds (44).

1.2 Chromatin Dynamics

The organization of DNA into chromatin generally leads to the occlusion of DNA sequences. Nucleosomal DNA is bent and distorted in a manner that prevents regulatory factors from recognizing and binding their cognate sequences. Moreover, nucleosomes may organize into higher-order structures that are even less accessible. However, chromatin is far from being an inert DNA packaging material. Instead, it functions as a signaling hub and aids in the regulation of virtually all DNA-based processes. Eukaryotic cells have evolved several mechanisms to guarantee the dynamic accessibility of the genome, which will be discussed in the following section.

1.2.1 Inherent nucleosome dynamics

The basic building unit of chromatin, the nucleosome, is not a static entity. In contrast, the intrinsic features of the canonical nucleosome structure itself render it a remarkably dynamic structure undergoing spontaneous fluctuations. Polach and Widom were the first to demonstrate that DNA near the entry/exit site of the nucleosome transiently and reversibly unwrapped from the protein surface in a process called 'breathing' (45). Their pioneering study probed DNA accessibility using restriction enzymes. Supporting evidence for spontaneous un- and rewrapping of nucleosomal DNA came from fluorescence resonance energy transfer (FRET) studies (46-49). The transient exposure of nucleosomal DNA was shown to be sufficient for the binding of transcription factors (TFs) to

their target sequence within nucleosomal DNA (46, 47). Moreover, the extent of breathing was shown to be strongly governed by the nucleosomal DNA sequence (45, 46, 50-52). The breathing characteristics of nucleosomes may thus be an important pathway for DNA-binding proteins to access their cognate sequence. Furthermore, nucleosomes exhibit internal conformational dynamics that are characterized by the transient disruption of the H2A-H2B dimer as well as the $(H3\text{-}H4)_2$ tetramer interfaces (53). In a slow (1-10 min) process called 'gaping', nucleosomes spontaneously open in the direction normal to the DNA plane (54-56). Taken together, the nucleosome itself is an inherently dynamic particle and undergoes various conformational transitions that may offer pathways for the binding of regulatory factors.

1.2.2 Post-translational modifications (PTMs) of histones

Post-translational modifications (PTMs) of histones can fundamentally change the organization and function of chromatin (57). According to the 'histone code' hypothesis, the combination of different histone modifications considerably extends the information potential of the genetic code (58). Numerous different modifications are dynamically set and erased from histones by chromatin-modifying enzymes in a highly regulated manner. Chemical alterations of histones predominantly occur at the flexible and accessible histone tails. Although less frequent, also the globular histone cores can be targeted by modifications (59, 60). A multitude of different modifications on different histone residues have been identified and continue to be discovered. Among the best studied modifications are histone methylation, acetylation, phosphorylation, ubiquitylation and ADP-ribosylation. More recently, a variety of other modifications including succinylation, malonylation and crotonylation have been reported (61).

Histone modifications on the one hand serve as highly selective recruitment platforms and are recognized by chromatin 'readers', which harbor conserved domains capable of binding specific marks (62, 63). ATP-dependent chromatin remodeling complexes (section 1.2.4) frequently display such domains. For example, nearly all Snf2 family members contain bromodomains that often bind acetylated lysine residues (64-66). On the other hand, histone modifications can stimulate structural changes of nucleosomes and impact chromatin compaction. A prominent example for a histone modification affecting chromatin structure is the acetylation of the H4 N-terminal tail at lysine 16 (H4K16). The H4 N-terminal tail was shown to interact with the acidic patch formed by H2A and H2B on an adjacent nucleosome, thereby promoting the formation of higher-order structures (28). This interaction was suggested to be disturbed by H4K16ac resulting in reduced chromatin compaction (67). Interestingly, H4K16ac was also implicated in modulating nucleosome remodeling by Imitation switch (ISWI) remodelers (discussed in section 1.3.5) (67-71). Modifications within the histone fold domain near the DNA entry/exit site have the potential to affect histone-DNA or histone-histone contacts. H3K56 for example is situated on the lateral surface of the nucleosome that contacts DNA. Conceivably, acetylation of H3K56 was shown to increase the rate of spontaneous unwrapping of DNA at the entry/exit site (72, 73).

1.2.3 Histone variants

In addition to canonical histones, eukaryotic genomes encode several 'histone variants', which are incorporated at specific genomic locations and confer specific structural and functional properties on the nucleosome. The bulk of DNA is packaged by nucleosomes containing so-called canonical histones (H2A, H2B, H3, H4). By definition, canonical histones exhibit an expression peak in S-phase and provide the main histone supply during replication. They are encoded by multiple gene copies that are organized in tandem and are devoid of introns enabling a coordinated transcription.

Transcripts of canonical histones are not polyadenylated. Instead, they contain a 3' stem-loop structure that is crucial for their regulation (74). In contrast, histone variant genes often contain introns and are expressed mostly during the cell cycle in a replication-independent manner (75, 76). Their corresponding mRNAs are polyadenylated. Incorporation of histone variants into nucleosomes is mediated by histone chaperones and specialized nucleosome remodeling enzymes (discussed in section 1.2.4).

Most histone variants exist for H3 and H2A (77, 78). There are also variants of H2B and H1, but no variant for H4 has yet been described. Variants may differ from canonical histones in only few amino acids (for example H3.3 (79)) or may contain additional large non-histone domains (for example macroH2A (80)). Incorporation of histone variants can change multiple histone-DNA and histone-histone contacts simultaneously and can thus induce structural changes of nucleosomes and affect their stability. MacroH2A, for example, wraps DNA more tightly in comparison to the canonical H2A (81) and localizes to repressive chromatin such as the inactive X chromosome (82). In contrast, nucleosomes substituted with the variant H2A.Bbd (Barr body deficient) wrap DNA much more poorly and prevent formation of compact chromatin fibers (83, 84). Histone variants can acquire specific PTMs and recruit specific interactors thereby further modulating the chromatin landscape (85).

1.2.4 ATP-dependent nucleosome remodeling

Nucleosome remodeling enzymes use the energy derived from ATP-hydrolysis to alter or disrupt histone-DNA contacts inside the nucleosome (86, 87). Thereby, they endow chromatin with structural flexibility and ensure the dynamic accessibility of the eukaryotic genome. Virtually all DNA-based processes in the nucleus require the action of nucleosome remodelers, which facilitate the establishment of specific chromatin states. Nucleosome remodelers are highly abundant enzymes and have been identified in all eukaryotes from yeast to man (88-90). Mutations of nucleosome remodelers are frequently associated with human cancers and developmental disorders underscoring their importance for biological processes (91, 92). *In vivo*, nucleosome remodelers typically reside in multi-subunit complexes (termed 'remodeling factors' hereafter) that contain one or several accessory subunits in addition to the nucleosome remodeling ATPase. The clear majority of associated subunits are non-catalytic albeit critically involved in targeting and regulating the complex.

Nucleosome remodeling ATPases belong to the diverse SF2 superfamily of helicases characterized by the presence of two RecA-like domains that form a bi-lobed motor (93, 94). Within the SF2 superfamily, nucleosome remodelers constitute the specialized Snf2 family (Figure 2). Based on sequence conservation of the ATPase domain, the Snf2 family can further be subdivided into 24 distinct subfamilies (95). In addition to the motor, the catalytic subunits display a wide variety of N- and C-terminal accessory domains, which regulate the motor and allow for interaction with binding partners.

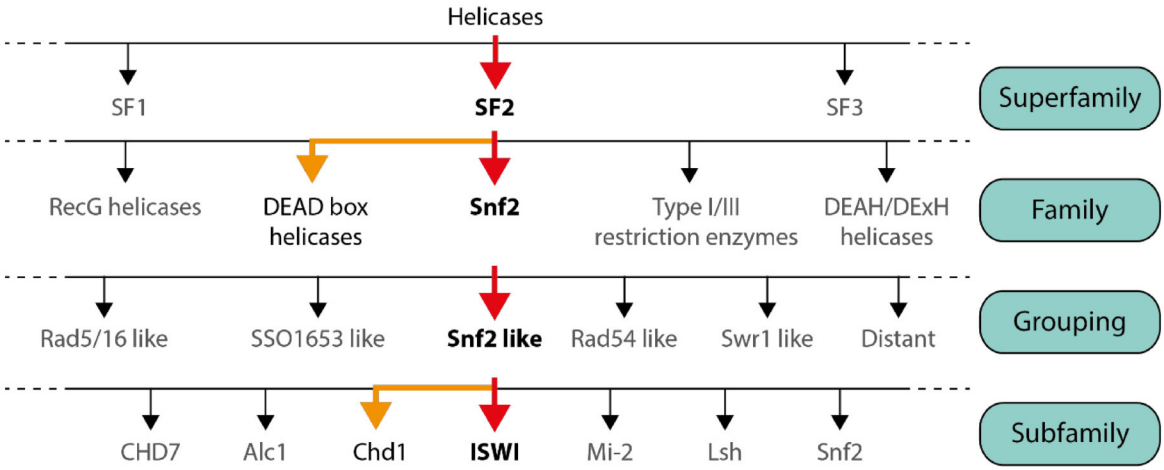

Figure 2: Family tree depicting the sequence relationship of Snf2 family remodelers to distant helicases. Nucleosome remodeling enzymes belong to the SF2 superfamily of helicases (96). Within the SF2 superfamily, they constitute the Snf2 family, which can further be classified into six groupings of subfamilies based on alignment of the ATPase domain of 1306 family members (95). The nucleosome remodeler ISWI studied in this work belongs to the Snf2-like grouping (hierarchical path indicated in red). The related Chd1 remodeler and DEAD box helicases (hierarchical path indicated in orange) are discussed in section 3 of this thesis. Figure is adapted from reference (97).

Remodeling enzymes catalyze a remarkably diverse set of nucleosome transformations (Figure 3). They modify the octamer composition, evict the entire octamer or reposition nucleosomes along DNA. For example, remodelers of the Swr1 and Ino80 families alter nucleosomes by either incorporating or removing the histone variant H2A.Z (98, 99). The variant H3.3 is deposited at telomeres and pericentric heterochromatin by combined action of the α-thalassaemia/mental retardation X-linked (ATRX) remodeler and the histone chaperone death domain-associated protein (DAXX). Members of the Snf2 family have been implicated in generating accessible chromatin and partially or completely disassemble nucleosomes (100-103). SWI/SNF, for instance, has been proposed to initially displace a H2A/H2B dimer and subsequently eject the complete octamer off a dinucleosomal substrate (104). In contrast, the ISWI and Chromodomain helicase DNA binding protein 1 (Chd1) remodelers slide nucleosomes along DNA and guide nucleosome assembly and spacing (105-108). Among all remodelers, ISWI is probably the best characterized enzyme and has served as a model to study the basic nucleosome remodeling mechanism. Composition, function and regulation of ISWI-containing nucleosome remodeling complexes are discussed in the following chapter.

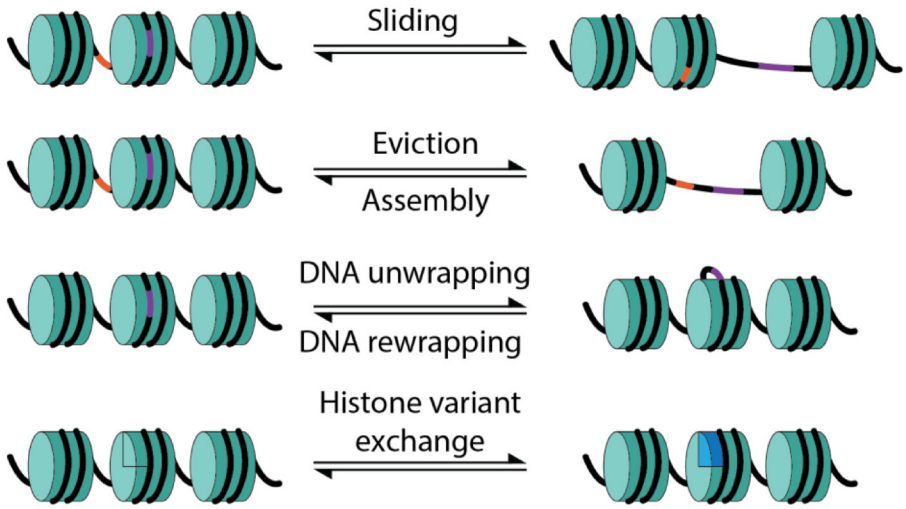

Figure 3: Physiological consequences of ATP-dependent nucleosome remodeling. Remodeling factors catalyze diverse reactions. Repositioning the histone octamer (turquoise) along DNA ('sliding'), eviction of the complete octamer or its assembly can either result in occlusion or clearance of specific DNA loci. Similarly, local distortions of DNA may expose stretches of nucleosomal DNA ('DNA unwrapping'). Specialized remodelers modify the histone octamer by replacing canonical histones with histone variants (blue). DNA stretches colored orange or violet represent sequences, which are either masked or rendered accessible upon nucleosome remodeling.

1.3 ATP-dependent nucleosome remodeling by ISWI-type remodelers

1.3.1 Composition of ISWI remodeling complexes

The nucleosome remodeler ISWI was originally identified due to its sequence similarity to the Swi2/Snf2 proteins of yeast and *Drosophila melanogaster* (109). Subsequently, the enzyme was described to be the catalytic subunit of the nucleosome remodeling factor (NURF) present in *Drosophila* embryos (110). In addition to ISWI, NURF contains the accessory subunits Nurf301, Nurf38 and Nurf55 (111). To date, five additional remodeling factors containing ISWI as the catalytic subunit have been discovered in *Drosophila*. Among them are ACF (ATP-dependent nucleosome assembly and remodeling factor) (112) as well as CHRAC (chromatin accessibility complex) (113). ACF and CHRAC share the common non-catalytic subunit Acf1, but CHRAC features the unique subunits CHRAC14 and CHRAC16 in addition. NoRC (nucleolar remodeling complex) (114) contains the accessory subunit Toutatis and interacts with the transcriptional co-repressor CtBP to form ToRC (Toutatis-containing chromatin remodeling complex) (115). RSF is characterized by the non-catalytic subunit Rsf1 (116) (Figure 4). *Saccharomyces cerevisiae* contains two ISWI homologs, Isw1 and Isw2 that form distinct complexes (Figure 4). Similarly, humans carry two ISWI homologs called SNF2H (sucrose non-fermenting 2 homolog) and SNF2L (sucrose non-fermenting 2 like). SNF2L incorporates into the NURF (117) and CERF (118) complex whereas SNF2L appears to be the catalytic subunit of the remaining complexes (Figure 4). Besides this combinatorial complexity, the different subunits may have restricted expression patterns depending on cell type and developmental stage (119, 120). For SNF2L, there even exist cell type-specific splice variants with distinct activities and localizations (121-123).

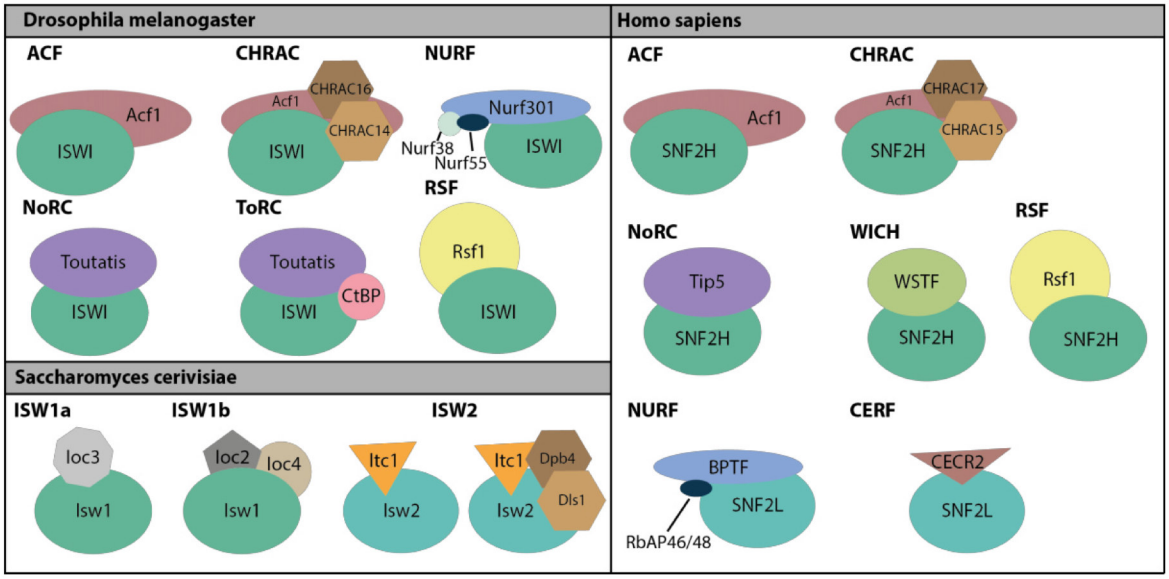

Figure 4: ISWI factors in different organisms. Schematic representation of ISWI factors discovered in *D. melanogaster*, *S. cerevisiae* and *H. sapiens* to date. Orthologous subunits in different organisms are colored identically. Subunit sizes are not drawn to scale. This study mainly focuses on the *D. melanogaster* ISWI ATPase subunit. Selected experiments were carried out with the human ortholog SNF2H (see section 2.3). The Isw1 ATPase subunit of the *S. cerevisiae* complexes ISW1a and ISW1b was analyzed *in vivo* (see section 2.3).

1.3.2 Function of ISWI complexes

The *in vivo* functions of ISWI factors are diverse and manifold. They play critical roles in a variety of nuclear processes including *de novo* nucleosome assembly, transcriptional regulation and DNA damage repair (87, 124). Consistently, loss of SNF2H in mice is embryonic lethal (125). Depletion

of ISWI in *D. melanogaster* is accompanied by larval lethality, induces a massive decondensation of the male X-chromosome on polytene chromosomes (126) and decompacts metaphase chromosomes (127). Whole-genome microarrays analyzing 15.000 genes in *Drosophila* larvae revealed that the expression of 500 genes changed by at least twofold upon loss of ISWI. Nearly 75% of these genes showed increased expression hinting at a predominant role for ISWI in transcriptional repression (127). Notably however, accumulating evidence suggests a role for NURF in transcriptional activation (128-130). ISWI factors appear to be involved also in replication. Acf1, WSTF and SNF2H have been found to be enriched at pericentric heterochromatin suggesting a role in replication of condensed chromatin (131). In yeast, ISW2 localizes to sites of active replication aiding in progression of the replication fork (132). Moreover, Acf1 and SNF2H rapidly accumulate at DNA-damage sites in human cells and have been suggested to be required for efficient repair of DNA double-strand breaks (133, 134).

In vitro, all ISWI factors studied to date mobilize nucleosomes along DNA in an ATP-dependent manner without disrupting the histone octamer in a process referred to as 'nucleosome sliding' (116, 135-137). The sliding activity is intrinsic to the isolated ISWI ATPase (138), but is fine-tuned by accessory subunits. For instance, association of ISWI with Acf1 markedly increases the efficiency of nucleosome sliding (139). Remarkably, ISWI not only slides nucleosomes, but catalyzes the conversion of randomly distributed nucleosomes with irregular linker lengths into evenly spaced nucleosomal arrays with characteristic linker lengths (138). ACF and CHRAC both possess such 'nucleosome spacing' activity. ACF was suggested to sense the length of linker DNA between adjacent nucleosomes. According to a recent model, the remodeler samples linker lengths on both sides of the nucleosome and preferentially slides the nucleosome towards the longer linker. Nucleosome sliding would thus result in arrays with equalized linkers (107, 140). Accordingly, linker length would not primarily be set by the remodeler itself, but rather be dictated by nucleosome density. Recent evidence however points to the fact that ISWI factors set a certain constant linker length independent of nucleosome density (141, 142).

ISWI factors not only slide nucleosomes, but also facilitate the *de novo* formation of nucleosomes. ISWI, ACF, CHRAC and ToRC have been shown to conduct nucleosome assembly *in vitro* in reactions containing the respective remodeler in conjunction with the histone chaperone NAP1, native core histones and DNA (105, 113, 115, 138, 143). In contrast, RSF does not require the help of an extrinsic factor and was suggested to have a built-in histone chaperone function (144, 145).

As outlined above, *in vivo* studies have revealed ISWI factors to be involved in numerous chromatin-based activities. However, the complexity of a living organism oftentimes makes it difficult to discriminate direct from secondary effects. In the past, much has been learned from *in vitro* studies, which aimed at the specific characterization of the enzymatic activities of remodelers. *In vitro*, ISWI factors display two distinct activities, nucleosome spacing and nucleosome assembly. According to current models, remodelers initially deposit nucleosomes onto the DNA template in a random fashion. Regularly spaced mature nucleosomal arrays are then generated by the regulated sliding of nucleosomes along DNA. In fact, for Chd1 it was shown that nucleosome assembly and nucleosome sliding are functionally distinct activities as a remodeling-defective Chd1 mutant retained its assembly function (146).

1.3.3 The structure of ISWI-type remodelers

ISWI consists of a catalytic bi-lobed ATPase domain, which is flanked by regulatory domains. C-terminal of the ATPase follows the regulatory NegC region and the DNA-binding HAND-SANT-SLIDE (HSS) module. The domain required for interaction with Acf1 was mapped to the very C-terminus of ISWI (139). The AutoN motif located in the ISWI N-terminus has been proposed to negatively regulate ISWI (see section 1.3.5) (147). AutoN is embedded in the so-called N-terminal region (NTR) of ISWI, which contains additional conserved motifs. Among them are an acidic region (AcidicN), the 'post-post-helicase-SANT-associated' (ppHSA) motif and a poorly conserved AT-hook (148) (Figure 5) (see sections 2.1 and 2.3). Their functions have not been studied to date. The related Chd1 remodeler harbors two chromodomains in the N-terminus and contains a C-terminal SANT-SLIDE domain (Figure 5).

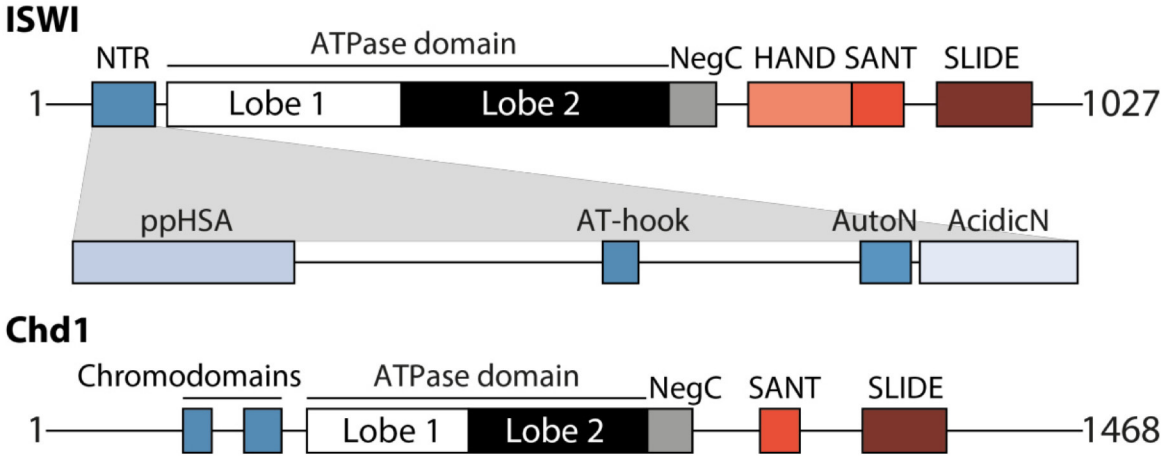

Figure 5: Schematic representation of the ISWI and Chd1 domain compositions. The grey inset shows the conserved motifs of the ISWI NTR. The N-termini of ISWI and Chd1 are not conserved. Amino acids in ISWI required for interaction with Acf1 are found C-terminal to the SLIDE domain(139) and are not indicated.

Crystal structures of few Snf2-type helicase domains have been solved. Among the existing structures are Rad54 from zebrafish (149), Sso1653 from *Sulfolobus solfataricus* (150) and RapA from *E.coli* (151). Crystal structures of the catalytic cores of Swi2/Snf2 (152) of the thermophilic yeast *Myceliophtora thermophila* and *S. cerevisiae* Chd1 (153) were solved in the Apo state. Recently, also the structure of the *M. thermophila* ISWI (MtISWI) catalytic core was reported (154). The structures revealed the common architecture of Snf2 ATPases, which consist of two RecA-like lobes connected by a structured linker. The ATPase domain contains at least 12 conserved sequence motifs required for ATP-binding and hydrolysis as well as nucleic acid binding (96). The Walker A motif (also called P-loop) contains the lysine residue, which is critically involved in binding the β-phosphate group of ATP (149, 151). The conserved aspartate residue within the DEAH box of the Walker B motif coordinates the Mg^{2+} ion, whereas the glutamate residue appears to be important for ATP hydrolysis. Walker A and Walker B are both located inside lobe 1. The second ATPase lobe harbors two arginine fingers on motif VI, which interact with the ATP γ-phosphate and are thought to stabilize a transition state during ATP hydrolysis (155). In the active conformation, both ATPase lobes are oriented such that catalytically important residues face towards the central cleft between the lobes.

Notably, in the *M. thermophila* Swi2/Snf2 and ISWI structures as well as in the *S. cerevisiae* Chd1 structure, the conformation of the ATPase lobes considerably deviates from the catalytically competent state. The two ATPase lobes of Swi2/Snf2 are trapped through direct interaction with

each other. The arginine fingers and the P-loop are twisted towards opposite directions rendering the domain incompatible with ATP-hydrolysis. Notably, DNA-binding elements are exposed to solvent. DNA-binding was therefore suggested to activate the ATPase by inducing a ~90° rotation of lobe 2 relative to lobe 1 (152). In contrast, in the Chd1 crystal structure the ATPase lobes assume an open conformation, which does not allow for efficient ATP hydrolysis. The arginine fingers are too far apart to make direct contact with the nucleotide phosphates. Furthermore, several DNA-binding sites are masked by the N-terminal double chromodomains of Chd1, which directly contact ATPase lobe 2. Transformation into an active state was suggested to require ATPase lobe 2 to rotate by 52°, which would close the cleft between the two ATPase lobes and allow for ATP-hydrolysis (153). Notably, distance information obtained from site-directed crosslinking of the ISWI ATPase domain in solution is indeed consistent with a rotation of both ATPase lobes against each other (156).

The C-terminal portion of ISWI contains three well conserved domains, the so-called HAND, SANT and SLIDE (HSS) domains (157). A SANT-SLIDE module was also identified in the C-terminal part of the remodeler Chd1 by crystallization, even though it could not be inferred from the amino acid sequence alone (149) (Figure 5). SANT and SLIDE domains each consist of three α-helices and are structurally related to the DNA-binding domain of the transcription factor c-Myb (157-160). In fact, the isolated SANT-SLIDE and HSS modules of *S. cerevisiae* Chd1 and Isw1 could be crystallized in complex with DNA. DNA-binding was shown to be mediated by negatively charged amino acids in the N-terminal helix of the SANT domain and C-terminal helix of the SLIDE domain (161, 162). In the nucleosome-bound state, DNA-crosslinking studies confirmed that the SANT and SLIDE domains of ISW2 bind to linker DNA.

At present, structural information on ISWI-type remodelers is limited. Although high-resolution structures of single domains in complex with DNA have been solved, detailed structural information on the nucleosome-bound state is missing. At present, the only nucleosome-bound structure of an ISWI-family member available is the low-resolution negative stain EM structure of SNF2H on a mononucleosome (107). Recently, a high-resolution cryo-EM structure of *S. cerevisiae* Snf2 (ScSnf2) bound to a nucleosome was reported (163). Importantly, the structure of a multi-subunit ISWI factor is still lacking.

1.3.4 Mechanism of nucleosome sliding

Despite years of intense research, the molecular mechanism of nucleosome sliding remains elusive. Nucleosome sliding requires the numerous histone-DNA contacts within the nucleosome to be broken and reformed without dissociation of the histone octamer. Remodelers therefore constitute sophisticated molecular machines, which pass through a complex succession of catalytic steps to fulfill their tasks. This chapter discusses models for nucleosome sliding that were controversially discussed at the outset of this thesis. Brief summaries of mechanistic aspects can furthermore be found in the introductions of the research articles presented in sections 2.1 and 2.2.

Prerequisite for understanding the remodeling mechanism is knowledge about how a remodeler interacts with nucleosomal DNA and histones. Several elegant experiments identified the binding sites of ISWI on the nucleosome. The ISWI ATPase domain was shown to engage the nucleosome at an internal site two helical turns off the dyad axis at SHL-2. Reassuringly, site-directed DNA-protein crosslinking also placed the Isw2 ATPase domain close to SHL-2 (164, 165). Consistent with this physical interaction, introduction of DNA gaps or nicks near SHL-2 inhibited nucleosome

sliding by ISWI. In contrast, no major effect on sliding was observed when gaps and nicks were inserted at locations distant from SHL-2 (166, 167). Similar to ISWI, also RSC (168), SWI/SNF (163, 167, 169) and Chd1 (170) were shown to contact the nucleosome at SHL-2 suggesting a common nucleosome-binding site shared between different remodeler families.

Binding of remodelers to SHL-2 may be advantageous for several reasons. First, this site is in close proximity to the strongest histone-DNA contacts in the nucleosome, which are found at the dyad (6). Second, the H4 tail N-terminal tail, which is required for ISWI activity, emerges from the nucleosome in close proximity to SHL-2 (3). Moreover, crystal structures confirmed that the region around SHL-2 can accommodate structural variability, which may facilitate remodeling (171).

Another strategic binding site of ISWI on the nucleosome is located at the nucleosomal entry site and in the adjacent linker. The C-terminal HSS domain of ISWI, which constitutes a DNA-binding module, was shown to contact approximately 30 bp of linker DNA (162, 165). For Isw2, the C-terminal SLIDE domain was identified to interact with linker DNA 19 bp away from the entry site. Similarly, also the SANT-SLIDE module of Chd1 binds to linker DNA at the edge of the nucleosome (158, 161, 170). Notably, the HSS domain of ISWI remodelers has recently been proposed to play an essential role in nucleosome sliding.

According to the ‘loop propagation’ model, remodelers initiate sliding by pulling additional DNA into the nucleosome from the entry side. Detachment of DNA would then lead to the formation of a DNA loop travelling around the histone octamer surface. Eventually, the loop would emerge at the exit site resulting in the translational repositioning of DNA relative to the histone octamer (172-174). Binding of the HSS domain to linker DNA and engagement of SHL-2 by the ATPase domain was suggested to define a topological domain of nucleosomal DNA. A conformational change between the HSS domain and the ATPase was predicted to destabilize histone-DNA contacts and initiate loop formation (174, 175). The described reaction step, which converts chemical energy derived from ATP-hydrolysis into mechanical work, will be referred to as a ‘power stroke’ in the following. The power stroke hypothesis predicts nucleosome sliding to be abolished in absence of the HSS domain. Indeed, deletion of the *Drosophila* ISWI (157) HSS domain was shown to markedly reduce the nucleosome sliding efficiency. Similarly, deletion of the SANT-SLIDE module of yeast Chd1 impaired sliding (158). Contradictory results came from a different study, where deletion of the SANT-SLIDE domain of Chd1 did not abolish sliding, but instead impaired its mononucleosome centering activity (176). The mechanism proposed by the loop propagation model has the advantage that DNA can maintain its rotational phasing on the histone octamer (177). However, loss of several histone–DNA contacts at a time make a DNA loop energetically unfavorable. As the strongest histone–DNA contacts cluster around the dyad, a DNA loop forming at the entry site would need to travel energetically uphill to traverse the dyad (6). Moreover, a recent single-molecule study shows that ISWI moves DNA out of the nucleosome before feeding DNA into the nucleosome, a result that is difficult to reconcile with formation of a DNA loop (178).

The ‘twist diffusion’ model predicts that remodelers introduce a twist defect into a segment of nucleosomal DNA, which propagates around the histone octamer such that the position of the nucleosome is shifted in 1-bp steps (179-181). In crystal structures, it was indeed observed that nucleosomes can accommodate additional base pairs (3, 182, 183). Furthermore, this model is energetically favorable since it requires only minimal disruption of histone-DNA contacts. However, several observations indicate that ‘twist diffusion’ may not be the exclusive remodeling mechanism. First, introduction of single-strand DNA nicks at several positions around the

nucleosome, which would be expected to dissipate torsional stress, did not prevent remodeling by ISWI (175) and RSC (173). Second, branches inside nucleosomal DNA that would sterically hinder rotation of DNA on the octamer surface did not abrogate remodeling (184). Moreover, remodeling of nucleosomes coupled to magnetic beads via a biotin-streptavidin linkage did not disrupt nucleosomes as predicted by the model (174).

As outlined above, the fundamental mechanism of nucleosome sliding by ISWI is still not fully understood. Resolving the mechanochemical cycle of ISWI and deciphering the role of the HSS domain during nucleosome sliding remain major goals.

1.3.5 Regulation of ISWI-type remodelers

Nucleosome sliding by ISWI plays critical roles in chromatin organization and gene regulation such that its activities must be tightly regulated to meet the cellular demands. The complex and intertwined network of mechanisms recruiting and regulating the remodeler are only starting to be unraveled. As ISWI usually resides in multi-subunit complexes, its activity supposedly is customized by non-catalytic subunits. For example, Acf1 has been shown to both influence the directionality of nucleosome sliding and to increase the efficiency of the sliding reaction (137, 140, 185). Moreover, post-translational modifications may be involved in ISWI regulation. Indeed, poly-ADP-ribosylation of ISWI has been proposed to interfere with nucleosome binding (186). The HAND domain of ISWI was shown to be a target of the acetyltransferase Gcn5 (187). However, the functional relevance of acetylation remains unknown.

This chapter focuses on the regulation of ISWI by nucleosomal features and their interplay with regulatory modules in ISWI itself. Short overviews of ISWI regulation are furthermore presented in the introductions of the research articles in section 2.1 and section 2.3.

Regulation by nucleosomal features

Two nucleosomal features are crucial for the regulation of ISWI: The length of linker DNA flanking the nucleosome (106, 140, 164) and the N-terminal tail of H4 (68, 141, 188, 189). In contrast to other histone tails, the H4 tail is critically required to stimulate the enzymatic activity of ISWI. Upon deletion of the H4 tail both ATPase activity as well as nucleosome sliding activity are severely compromised. How ISWI senses the H4 tail is largely unknown. However, as swapping the locations of the H4 and H3 tails on the nucleosome led to a marked decrease of ISWI activity, the specific location of the tail appears to be critical (68, 189). The H4 tail emerges from the nucleosome close to SHL-2. Since the ISWI ATPase domain was shown to contact the nucleosome at SHL-2, it seems likely that the ATPase domain is involved in H4 tail recognition. A recent study suggests that H4 tail-binding induces a conformational change in the ATPase domain and promotes closure of the ATP-binding pocket (190). This may indicate the H4 tail-binding pocket to reside in the ATPase domain. However, also the HSS domain has been implicated in H4 tail binding (157, 191). The activating epitope within the H4 tail was mapped to the amino acids $R_{17}H_{18}R_{19}$, which are part of a region in the tail called basic patch (68, 189, 192). Interestingly, this exact peptide motif is also found in the N-terminal tail of ISWI, here called AutoN (see below).

Notably, the H4 tail plays an important role in chromatin compaction. Formation of higher-order chromatin structures is promoted by binding of the H4 N-terminal tail to the acidic patch of an adjacent nucleosome (3, 193, 194) (see also chapter 1.1.2). This interaction is expected to sequester the H4 tail rendering it incapable of activating ISWI. The remodeler would thus display decreased

activity on condensed chromatin. The H4 tail dependence of ISWI could therefore be a means to ensure the unidirectionality of the sliding reaction.

Interestingly, acetylation of lysine 16 within the H4 tail (H4K16ac) was shown to reduce compaction of chromatin arrays *in vitro* (67, 195, 196) and correlates with open and accessible chromatin regions *in vivo* (197, 198). Given the importance of the H4 tail for ISWI activity, it is conceivable that posttranslational modifications of the tail contribute to ISWI regulation. Indeed, several studies suggest an inhibitory effect of H4K16ac on ISWI activity. Both, ACF and ISW2 were shown to display reduced sliding activity on H4 tail-acetylated mononucleosomes (67, 70). Moreover, site-specific acetylation of lysines 12 or 16 markedly reduced the ATPase activity of ISWI (68, 147). Also *in vivo*, H4K16 acetylation was shown to directly counteract chromatin compaction mediated by ISWI (69). Contradictory to this, another study reported that hyperacetylation of the chromatin fiber permitted faster remodeling by *Drosophila* ACF-type complexes and ISWI (199). This finding is supported by a recent quantitative biochemical study involving defined nucleosomal arrays, which showed that H4K16ac did neither inhibit ISWI nor ACF remodeling activity (71). The effect of H4K16ac on ISWI activity thus remains highly controversial.

Besides PTMs of histones, also histone variants may be implicated in ISWI regulation. For example, the ACF complex was found to be incapable of sliding mononucleosomes containing the H2A.Bbd variant (200). H2A.Z incorporation in contrast was reported to stimulate ISWI activity presumably due to the presence of an extended acidic patch on H2A.Z (201).

Another nucleosomal feature which is critically involved in ISWI regulation is the length of linker DNA flanking the nucleosome. Deletion of linker DNA reduces the affinity of ISWI to the nucleosome and decreases ATP turnover and sliding capacity (106, 140, 202, 203). With the help of its HSS domain, ISWI can sample linker lengths on both sides of the nucleosome and preferentially slides nucleosomes towards the longer linker. As a result, mononucleosomes are centered on stretches of DNA and nucleosomal arrays are evenly spaced (140, 164). By sampling the length of linker DNA, ISWI may not only recognize the presence of neighboring nucleosomes, but may also detect transcription factors bound to DNA. In fact, the Gal4 DNA-binding domain was recently demonstrated to act as an effective barrier for nucleosome sliding by the ISW1a complex. ISW1a may thus use bound transcription factors as reference points for nucleosome spacing (204). Similarly, Chd1 was shown to respond to a DNA-bound Lac repressor by preferentially shifting nucleosomes away from the barrier (205).

Regulation by motifs flanking the ATPase domain

Nucleosome remodelers contain conserved sequences N- and C-terminal to their ATPase domains, which are critical for remodeler regulation. While Chd1 contains regulatory chromodomains (153), ISWI harbors the peptide motif AutoN in the N-terminus (147). C-terminal adjacent to the ATPase domains of ISWI and Chd1 is the NegC region, which is also referred to as the ‘bridge’. Clapier and Cairns identified the autoinhibitory NegC region by serially truncating ISWI from the C-terminus. NegC was suggested to prevent the efficient coupling of ATP hydrolysis to nucleosome sliding, although the mechanism of this effect remains unclear (147). The crystal structure of Chd1 revealed the NegC region to contact both ATPase lobes and form a bridge between them (153). These contacts were suggested to prevent the ATPase lobes to adopt a conformation competent for ATP hydrolysis. Notably, NegC crystallized in a different conformation in the recent MtISWI structure. Here, NegC protrudes from the ATPase domain and binds to ATPase lobe 2 of an adjacent

molecule in the crystal (154). Autoinhibition by NegC was proposed to be counteracted by association of the HSS domain with nucleosomal linker DNA. DNA binding was further suggested to relieve NegC from the ATPase lobes allowing them to reorient. Consistent with an inhibitory function, deletion of NegC restored the nucleosome sliding defect imposed by deletion of the HSS domain (147).

The second auto-inhibitory motif, AutoN, resides in the N-terminal region (NTR) of ISWI and consists of only four amino acids (RHRK) (147). Interestingly, AutoN displays sequence similarity to the basic patch of the H4 N-terminal tail (see above). Mutation of AutoN's two arginine residues to alanines ($ISWI_{2RA}$) was shown to severely deregulate ISWI. Specifically, $ISWI_{2RA}$ displayed increased DNA-stimulated ATPase activity. The mutant also mobilized nucleosomes more efficiently compared to the wild-type enzyme. In fact, mutation of AutoN also partially relieved the dependence of ISWI on the H4 tail. In contrast to wild-type ISWI ($ISWI_{WT}$), $ISWI_{2RA}$ efficiently mobilized nucleosomes lacking the H4 tail. These data suggested a model, where AutoN competes with the H4 tail for a binding site on the ISWI ATPase domain (147). However, at the onset of this thesis neither the H4 tail-binding site within ISWI nor the conformation of the NTR were known.

In contrast to ISWI, Chd1 contains two regulatory chromodomains in the N-terminus. Both chromodomains are connected by two helices. In the crystal structure, the double chromodomain unit binds within the central cleft of the ATPase domain such that it contacts both ATPase lobes (also see section 1.3.3) (153). The second one of the chromodomain-connecting helices is highly acidic and packs against a basic surface on ATPase lobe 2. As this basic surface constitutes a nucleic acid-binding site, binding of the acidic helix is expected to interfere with DNA binding (153). Consistently, truncation of the chromodomains allowed naked DNA to fully activate the Chd1 ATPase activity. In contrast, wild-type Chd1 requires nucleosomes for full activation. The Chd1 N-terminus may thus act as a 'gatekeeper' for DNA binding and may furthermore ensure the substrate specificity of the remodeler (153). Interestingly, ISWI contains an acidic region adjacent to AutoN, the function of which is unknown.

Taken together, the ATPase domains of ISWI and Chd1 are regulated by modules flanking the ATPase domains. These modules guarantee substrate specificity for the nucleosome and they prevent wasteful ATP hydrolysis in the absence of an appropriate substrate. Upon substrate binding and during the remodeling cycle, the regulatory modules are predicted to undergo conformational changes. Much remains to be unraveled about the exact mechanisms of autoregulation. Especially in the case of the ISWI remodeler, detailed information on how the various modules are structurally organized with respect to each other is missing. *In vivo*, the situation is potentially even more complex as the ISWI ATPase associates with accessory subunits that may contribute additional regulatory modules.

1.4 Aims of this study

The conserved nucleosome remodeler ISWI is an important structural modulator of chromatin. Mechanistic details on how the different ISWI domains cooperate to translate the energy derived from ATP-hydrolysis into nucleosome sliding is scarce. Furthermore, little is known on how the ATPase motor is regulated. The goal of this study was to elucidate the molecular mechanism of nucleosome sliding by ISWI and to gain a deeper insight into how catalysis is regulated.

To investigate the requirement of the HSS domain during nucleosome sliding, we employed several quantitative biochemical assays to determine critical catalytic parameters of recombinant wild-type

ISWI and various ISWI mutants. The results are presented in section 2.1. Moreover, we sought to understand whether direct communication between the HSS and the ATPase domain resulting in transmission of force is essential for nucleosome sliding (see section 2.2). To facilitate our biochemical studies, we developed a restriction enzyme-based remodeling assay that allowed us to quantitatively assess nucleosome repositioning in nucleosomal arrays (see section 2.4).

A major focus of this study was further to explore the regulatory role of the H4 tail for ISWI remodeling. Specifically, we systematically analyzed the functions of the motifs found in the ISWI NTR and probed for potential crosstalk with the H4 tail. Using protein crosslinking followed by high-resolution mass spectrometry, we mapped the H4 tail-binding site within ISWI and obtained information about the overall structural architecture of the NTR-ATPase module (section 2.3).

2. RESULTS

2.1 The ATPase domain of ISWI is an autonomous remodeling machine

Felix Mueller-Planitz, Henrike Klinker, Johanna Ludwigsen and Peter B. Becker

Adolf Butenandt Institute and Center for Integrated Protein Science Munich,

Ludwig-Maximilians-Universität München, Munich, Germany

Published in *Nature Structural and Molecular Biology*, 20, 82-89 (2013);

doi: 10.1038/nsmb.2457

Declaration of contributions

This study was conceived by F. Müller-Planitz and P.B. Becker. I performed most of the restriction enzyme accessibility experiments employing g-H4 arrays that are summarized in Figure 6 and Supplementary Figure 7. Together with H. Klinker, I prepared Figure 6 including the Figure legend and the respective materials and methods sections. I assisted in developing and revising the manuscript that was mainly written by F. Mueller-Planitz and P.B. Becker and edited it at all stages of the publication process.

nature structural & molecular biology

The ATPase domain of ISWI is an autonomous nucleosome remodeling machine

Felix Mueller-Planitz[1,2], Henrike Klinker[1,2], Johanna Ludwigsen[1,2] & Peter B Becker[1,2]

ISWI slides nucleosomes along DNA, enabling the structural changes of chromatin required for the regulated use of eukaryotic genomes. Prominent mechanistic models imply cooperation of the ISWI ATPase domain with a C-terminal DNA-binding function residing in the HAND-SANT-SLIDE (HSS) domain. Contrary to these models, we show by quantitative biochemical means that all fundamental aspects of nucleosome remodeling are contained within the compact ATPase module of *Drosophila* ISWI. This domain can independently associate with DNA and nucleosomes, which in turn activate ATP turnover by inducing a conformational change in the enzyme, and it can autonomously reposition nucleosomes. The role of the HSS domain is to increase the affinity and specificity for nucleosomes. Nucleosome-remodeling enzymes may thus have evolved directly from ancestral helicase-type motors, and peripheral domains have furnished regulatory capabilities that bias the remodeling reaction toward different structural outcomes.

Chromatin organization endows eukaryotic genomes with stability and regulates gene expression. DNA within chromatin is spooled around histone proteins, forming nucleosomes. Arrays of nucleosomes are further folded to accommodate the genome in the nuclear volume. Tight packaging inevitably leads to the occlusion of DNA sequences that can no longer be accessed by regulatory proteins. However, chromatin has to be dynamic to permit cells to respond to environmental or developmental challenges. Crucial to a dynamic and regulated use of the genome are the actions of ATP-consuming nucleosome-remodeling enzymes[1,2].

Nucleosome-remodeling enzymes use energy from ATP hydrolysis to weaken or disrupt histone-DNA contacts in the otherwise extremely stable nucleosome particle. They thereby catalyze histone exchange, partial or complete nucleosome disassembly and formation of new nucleosomes or repositioning of existing ones. The precise outcome of a remodeling reaction is frequently determined by regulatory subunits that associate with the ATPase[2–5].

The ATPase domains of all nucleosome-remodeling complexes are conserved and distantly related to superfamily 2 (SF2) DNA helicases. On the basis of similarity of their ATPase domain sequences, all known or presumed nucleosome-remodeling enzymes constitute 24 subfamilies[4,6]. Despite this complexity, it is becoming clear that the remodeling enzymes studied to date are related in structure and mechanism. Deciphering the fundamental mechanism of a basic remodeling reaction remains an important goal[2–5].

Most insight into the mechanism of nucleosome remodeling has been obtained by studying representatives of three subfamilies of remodelers: ISWI, Snf2 and Chd1. They all slide nucleosomes along DNA, and although differences have been noted[7,8], they share a strategic interaction site on the nucleosome. Their ATPase 'motor' domain engages the nucleosomal DNA about two helical turns off the nucleosomal dyad at superhelix location 2 (SHL2)[9–11]. This site is characterized by structural variability of the histone-DNA interactions. It can accommodate a gain or loss of one base pair (bp), a feature that could be exploited during the remodeling reaction[12–14]. Furthermore, the histone H4 N terminus, which is mechanistically involved in remodeling reactions catalyzed by ISWI and Chd1, emanates from the nucleosome core around SHL2 (refs. 15–19). At SHL2, the ATPase domain is thought to translocate on DNA in accord with its helicase ancestry[9,20,21]. The ATPase domain may thereby force additional DNA into the nucleosome, change the twist in the DNA or otherwise perturb histone-DNA contacts[2,4,22].

In several cases it was observed that successful remodeling required accessory domains in addition to the ATPase. These domains are thought to provide the appropriate mechanical or topological context for remodeling. For ISWI-type enzymes, the C terminus harbors a DNA-binding module in the form of the HSS domain (**Fig. 1a**). Deletion of the HSS domain markedly reduced the ability of *Drosophila* ISWI to associate with and remodel nucleosomes[23]. Subsequent cross-linking and cryo-EM studies with the ISWI orthologs in yeast revealed interactions of the HSS domain with DNA flanking the nucleosome, so-called linker or extranucleosomal DNA[24,25]. Deletion of this DNA diminished not only the binding affinity but also the ATP turnover and the remodeling capacity of ISWI[26,27].

These results collectively support models in which the nucleosomal contacts made by the ISWI ATPase and HSS modules delimit a topological domain of nucleosomal DNA. Conceivably, a conformational change between the ATPase and the HSS modules, mediated by a

[1]Adolf Butenandt Institut, Ludwig-Maximilians-Universität, Munich, Germany. [2]Center for Integrated Protein Science Munich, Ludwig-Maximilians-Universität, Munich, Germany. Correspondence should be addressed to F.M.-P. (Felix.Mueller-Planitz@med.uni-muenchen.de) or P.B.B. (pbecker@med.uni-muenchen.de).

Received 3 May; accepted 1 November; published online 2 December 2012; doi:10.1038/nsmb.2457

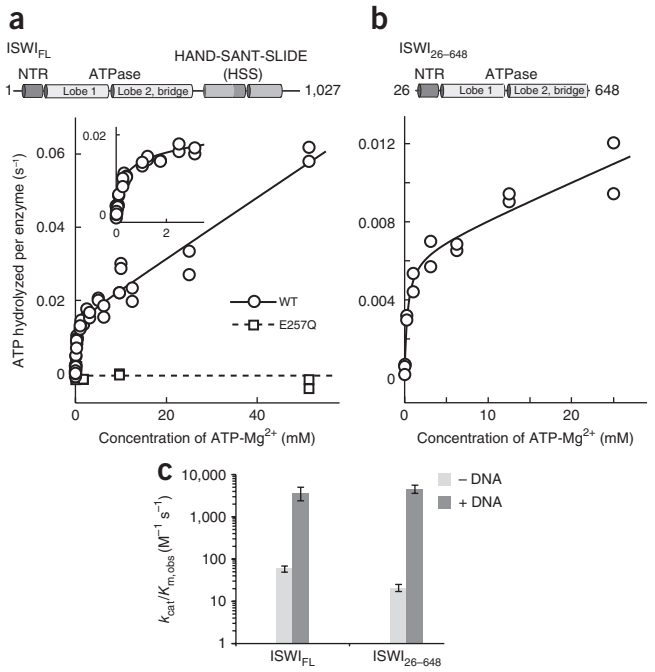

Figure 1 Steady-state ATP hydrolysis. (**a**,**b**) ATP concentration dependence of ATP turnover by DNA-free ISWI$_{FL}$ (**a**) and ISWI$_{26–648}$ (**b**), both 4 μM. The response was biphasic, with the first phase completed with submillimolar concentrations of ATP (**a**, inset). Steady-state ATPase parameters extracted from fits (lines) are listed in **Table 1**. Domain schematics for ISWI$_{FL}$ and ISWI$_{26–648}$ are shown on top. In addition to wild-type (WT), an ATPase-deficient mutant (E257Q) was used as a negative control in **a**. (**c**) Strong stimulation of ATP hydrolysis of ISWI$_{FL}$ and ISWI$_{26–648}$ by saturating concentrations of a 39-bp-long DNA duplex (80 to 400 nM). The assays were performed with 100 mM Mg^{2+}; similar results were obtained in a buffer containing lower Mg^{2+} concentrations or varying enzyme concentrations (**Supplementary Table 1** and **Supplementary Fig. 2a,b** and data not shown).

'hinge' that connects the two, may destabilize the DNA-histone contacts in this domain and pull linker DNA into the nucleosome[16,18]. The excess DNA would initially bulge out from the histone surface. Eventually it may escape from the other side of the nucleosome and re-form the canonical nucleosome structure at a different position on DNA.

This model predicts that the HSS domain plays an integral part during the remodeling reaction. Underscoring its importance, deletion of a related domain in Chd1 strongly reduced the overall remodeling efficiency[28]. Unexpectedly, a different study concluded that deletion of the DNA-binding module in the C terminus of Chd1 does not completely abolish the nucleosome sliding activity. Rather, the C terminus was suggested to affect the directionality of the process[11]. Thus, the DNA-binding domain may not be essential for the remodeling process as such. It might instead determine the overall outcome of the remodeling reaction, either the direction of nucleosome sliding[11] or the positioning of the substrate nucleosome in the context of nucleosome spacing[28]. This conclusion is not readily compatible with the hinge model, which was mainly derived from studies on ISWI-type enzymes. Do these studies reveal a fundamental difference between ISWI- and Chd1-type remodelers with respect to their use of binding domains for linker DNA? How can ATP hydrolysis–driven conformational changes be productive in the absence of the main linker DNA–binding domain?

We set out to address these issues in the context of *Drosophila* ISWI. Our quantitative analysis reveals two ATPase domain conformations, which drastically differ in their catalytic competency. Nucleic acids induce a change of conformation, thereby activating the enzyme. Furthermore, we show that the ATPase domain has an intrinsic ability to bind nucleosomes, to functionally interact with the H4 N terminus and to remodel nucleosomes. Accessory domains in chromatin remodelers may thus have evolved to regulate an autonomous basic remodeling module. Our data place firm limits on the mechanistic models of nucleosome remodeling and favor models in which the ATPase domain performs the fundamental steps involved in remodeling, such as breaking histone-DNA contacts and moving nucleosomes, whereas the HSS domain fulfills auxiliary duties, such as increasing the affinity and specificity for nucleosomes.

RESULTS

The ATPase domain adopts different conformations in solution

The ATPase activity of ISWI is activated by free and nucleosomal DNA[23,29]. To dissect this effect in a quantitative manner, we obtained highly purified enzyme preparations by using an optimized purification protocol that included affinity, ion-exchange and size-exclusion chromatography. Further purification did not affect the results.

We first measured ATP turnover by unliganded ISWI and determined the reaction velocities for varying ATP concentrations. Whereas enzymes typically show a simple saturation behavior with increasing substrate concentrations, ISWI featured a more complex biphasic response. After an initial rise of the reaction velocity with increasing ATP concentrations, the curve entered a second phase and continued to rise until at least 50 mM of ATP (**Fig. 1a**).

The two phases of the curve indicated that different enzyme populations existed with strongly differing observed Michaelis ($K_{m,obs}$) values. We hypothesized that these populations may correspond to ISWI molecules in different conformations. Kinetic and thermodynamic modeling confirmed that this scenario could indeed account for the data (**Supplementary Fig. 1**).

However, the biphasic ATPase response could also be due to a number of trivial reasons. Most importantly, we ruled out a contaminating ATPase being responsible for one of the two phases by analyzing a point mutant with an amino acid change in the Walker B motif of the ISWI ATPase domain (E257Q), that prevents ATP hydrolysis. Although this mutant was expressed at similar levels and prepared in the same way as the wild type, we could not detect any ATP hydrolysis for this mutant (**Fig. 1a**). We have ruled out additional scenarios, such as enzyme dimerization and contamination with DNA, that could, in principle, explain the unusual shape of the curve (discussed in **Supplementary Note**; **Supplementary Fig. 2a**,**b**).

According to prominent models of ISWI function, the HSS and ATPase domains intimately cooperate during nucleosome remodeling[2–4,24,30]. In this scenario the HSS domain might be expected to directly influence ATP hydrolysis. We tested this hypothesis by truncating ISWI in a poorly conserved region that separates the ATPase domain from the HSS domain (**Fig. 1b**). Our construct spanned a conserved N-terminal region (NTR; **Supplementary Fig. 3**), both ATPase lobes and the 'bridge' at the C-terminal end, which is conserved between ISWI and Chd1 remodelers and docks against both ATPase lobes[31,32]. In most experiments, we used a construct that lacked nonconserved amino acids at the N terminus, spanning amino acids 26–648 (ISWI$_{26–648}$). We repeated a number of experiments with ISWI$_{1–697}$, which also included less-conserved regions on both termini.

Table 1 Steady-state ATPase parameters[a]

		$ISWI_{FL}$			$ISWI_{26–648}$		
		$k_{cat}/K_{m,obs}$ (M^{-1} s^{-1})	$k_{cat,obs}$ (s^{-1})	$K_{m,obs}$ (mM)	$k_{cat}/K_{m,obs}$ (M^{-1} s^{-1})	$k_{cat,obs}$ (s^{-1})	$K_{m,obs}$ (mM)
– DNA	Phase 1	60 ± 10	0.014 ± 0.004	0.24 ± 0.03	21 ± 3*	0.007 ± 0.002	0.36 ± 0.02*
	Phase 2	NA	>0.046	>50	NA	>0.02	>25
+ DNA		3,700 ± 900*	0.51 ± 0.09	0.15 ± 0.05	4,100 ± 900*	1.0 ± 0.1	0.25 ± 0.01

[a]Values were measured in reaction buffer containing 100 mM Mg^{2+}. Where indicated (asterisks), errors are minimum and maximum values of two independent measurements. Otherwise, errors are s.d. of at least three independent measurements. DNA reactions contained saturating concentrations of a 39-bp DNA duplex. NA, Not applicable.

As in the case with full-length ISWI ($ISWI_{FL}$), the ATP concentration dependencies of unliganded $ISWI_{26–648}$ and $ISWI_{1–697}$ were biphasic, which suggested that the two conformations involve the ATPase domain (**Fig. 1b** and data not shown). Unexpectedly, steady-state ATPase parameters ($k_{cat}/K_{m,obs}$, $k_{cat,obs}$ and $K_{m,obs}$) differed by less than three-fold between the three enzymes (**Fig. 1** and **Table 1** and data not shown). This similarity attested to the integrity of the two truncated proteins and showed that the C terminus did not substantially influence ATP hydrolysis, at least when no DNA ligand was bound.

DNA ligands strongly influence the ATP hydrolysis mechanism

To test how DNA binding affected the catalytic parameters, we repeated the analyses in the presence of a 39-bp-long DNA duplex. Varying the length of the DNA from 19 to ~3,000 bp did not considerably affect the $k_{cat,obs}$ (below and data not shown). In contrast to the ligand-free enzyme, DNA-bound $ISWI_{FL}$ exhibited standard Michaelis-Menten–type kinetics (data not shown). Furthermore, DNA strongly stimulated $k_{cat}/K_{m,obs}$ (61-fold; **Fig. 1c** and **Table 1**).

Like stimulation by DNA, stimulation by chromatin abolished the biphasic response to the ATP concentration (data not shown). Relative to DNA, chromatin binding increased the affinity for nucleotides by six-fold (**Supplementary Fig. 4**). In addition, $k_{cat,obs}$ increased by 4- to 14-fold, depending on the enzyme concentration (**Supplementary Fig. 2c** and **Supplementary Table 1**; here we employed lower Mg^{2+} concentrations to prevent aggregation of chromatin). This dependence of $k_{cat,obs}$ on the enzyme concentration is consistent with binding of two functionally interacting ISWI molecules per nucleosome, as previously suggested (**Supplementary Fig. 2d,e**)[33].

DNA binding to the ATPase domain activates ATP hydrolysis

Nucleic acids typically directly bind the ATPase domain of SF2 helicases[34,35]. Using the $ISWI_{26–648}$ construct, we confirmed in a double-filter binding assay that the ATPase domain of ISWI indeed harbors a DNA-binding site (**Supplementary Fig. 5**). Consistent with its DNA-binding function[23–25,36], the HSS domain increased the DNA affinity by 20-fold.

DNA could, in principle, activate ATP hydrolysis by binding to either of the two binding sites or to both. Whereas nucleic acids often directly bind and stimulate the ATPase activity of SF2 helicases[34,35], we previously suggested that it was DNA binding to the HSS domain that conferred most DNA stimulation[23]. However, at that time we did not account for the reduced DNA affinity when the HSS domain is missing. To differentiate between the two sites and to probe their involvement in the regulation of ATP turnover, we titrated DNA to the ISWI constructs that lacked the HSS domain and measured ATP turnover. DNA was a potent activator of ATP hydrolysis of $ISWI_{26–648}$ and $ISWI_{1–697}$ (**Fig. 1c** and data not shown). Overall, their ATPase parameters were strikingly similar to those of $ISWI_{FL}$, indicating that DNA binding at the ATPase domain, not the HSS domain, drives the stimulation (**Table 1**).

DNA binding affects the conformation of the ATPase domain

To test whether DNA binding activated ATP turnover by triggering a conformational change in the ATPase domain, as seen for evolutionarily related proteins[37], we turned to limited proteolysis experiments. Consistent with a structural change, limited digestion with trypsin led to a different cleavage pattern and a substantially faster cleavage of $ISWI_{26–648}$ in the presence of DNA (**Fig. 2a**). A different protease (GluC) and partial trypsin digests of $ISWI_{FL}$ yielded analogous results (data not shown).

Additional proteolysis experiments firmly ruled out that the different cleavage pattern was simply due to occlusion of the predominant cleavage sites by DNA. From a comparison of the electrophoretic mobility of proteolytic fragments obtained with trypsin, which cleaves at lysines and arginines, and LysC, which is specific for lysine, we concluded that the major tryptic digestion product of the DNA-free enzyme arose from a cut next to a lysine (**Supplementary Fig. 6**).

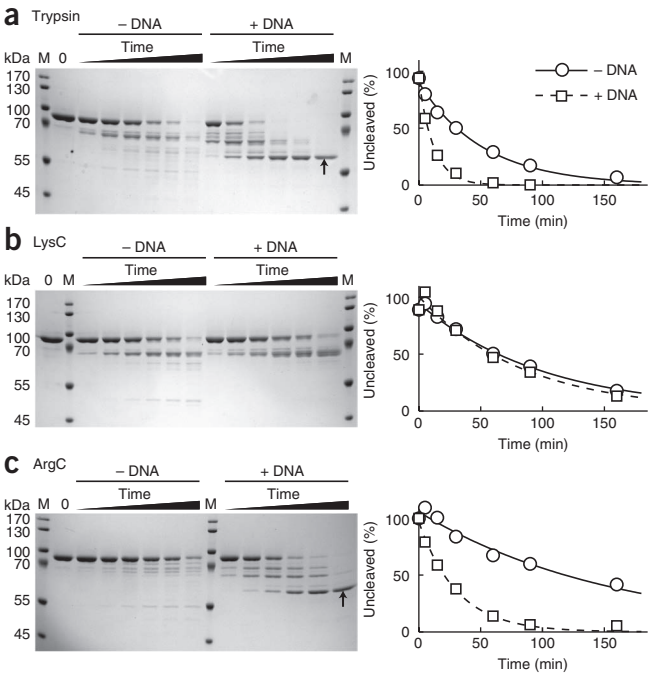

Figure 2 Limited proteolysis revealed a DNA-induced conformational change within the ATPase domain of ISWI. (**a–c**) Protease digestion of DNA-free and DNA-bound $ISWI_{26–648}$ by trypsin (**a**), LysC (**b**) and ArgC (**c**) for 5, 15, 30, 60, 90 and 160 min. Left, SDS-PAGE gels. Undigested protein served as the zero time point (0). M, molecular-weight marker. Right, quantification of the gel bands. The data were fit by a single exponential function (lines). Addition of 39-bp-long DNA duplexes (10 μM) led to a different banding pattern and 4.4-fold and 5.1-fold faster digestion rates by trypsin and ArgC, respectively, without affecting LysC digests. Arrows indicate a protease-stable fragment only seen in the presence of DNA.

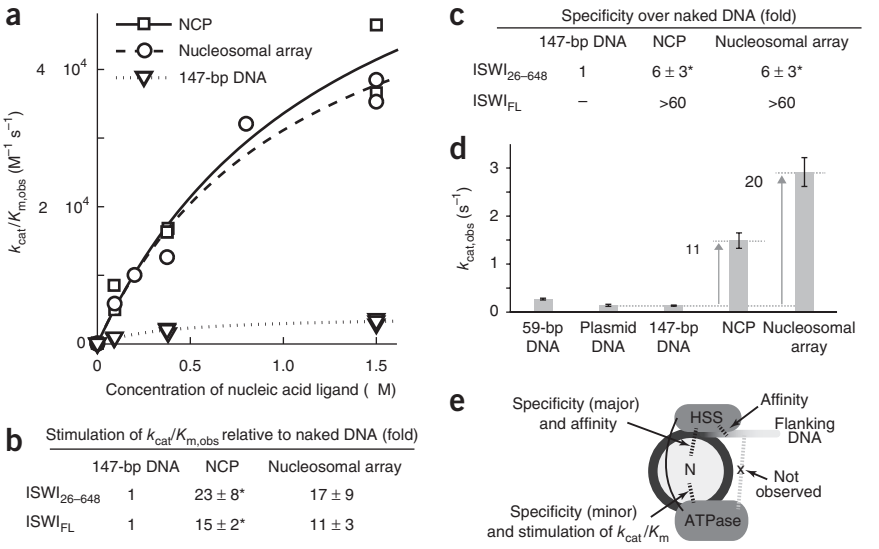

Figure 3 Interactions between domains of ISWI and the nucleosome and their importance for catalysis and substrate specificity. (**a**) Marked stimulation of $k_{cat}/K_{m,obs}$ for ATP hydrolysis of $ISWI_{26–648}$ (80 nM) by NCPs and nucleosomal arrays. Data were fit to a simple binding isotherm (lines). Results of two or more independent experiments are superimposed. (**b**) Stimulation of $k_{cat}/K_{m,obs}$ by NCPs and arrays relative to DNA. $k_{cat}/K_{m,obs}$ values for saturating concentrations of NCPs and arrays were normalized by corresponding values for 147-bp-long DNA (**Supplementary Table 1**). Where indicated (asterisks), errors are minimum and maximum values of two independent measurements. Otherwise, errors are s.d. ($n = 3$). (**c**) Discrimination between nucleosomal and naked DNA. $k_{cat}/K_{m,obs}$ values at subsaturating NCP and array concentrations were normalized by corresponding values for DNA-stimulated $ISWI_{26–648}$. Errors as in **b**. (**d**) Strong stimulation of $k_{cat,obs}$ of $ISWI_{FL}$ by saturating NCPs and arrays (200 nM enzyme; 0.5 mM ATP). Errors represent 95% confidence intervals of fits to a binding isotherm. (**e**) Summary of functional interactions (dashed lines) between ISWI and the nucleosome.

Notably, DNA binding did not affect the digestion kinetics of LysC, which provided strong evidence against occlusion (**Fig. 2b**). If accessibility of the lysine remained the same, then arginine residues must become more exposed with DNA to explain the trypsin results. We confirmed this prediction with the arginine-specific protease ArgC. ArgC produced a similar cleavage pattern as trypsin in the presence of DNA and experienced a similar rate enhancement by DNA (**Fig. 2a**,**c**). In summary, the proteolysis experiments showed that the enzyme conformation changed upon DNA binding. We suggest that these conformations are related to the conformations detected independently by the ATP-hydrolysis results above.

We noted that an ~60 kDa fragment accumulated in trypsin and ArgC digests when DNA was present (**Fig. 2a**,**c**), which suggested that DNA binding led to a well-folded, protease-resistant structure. N-terminal Edman sequencing and LC-MS/MS analysis of this fragment mapped the cleavage sites to accessory sequences outside of the ATPase core (Arg91 and Arg93 in the NTR and Arg589 at the C terminus; **Supplementary Fig. 3**). These accessory regions therefore took part in regulatory conformational changes induced by DNA binding (Discussion).

Nucleosome recognition involves the ATPase and HSS domains

Our data showed that the ISWI ATPase domain independently reacted to DNA association. We asked next whether the ATPase domain alone could specifically recognize an entire nucleosome, whether the HSS domain increased this specificity and to what extent stimulation of ATP hydrolysis by nucleosomes required the HSS domain.

We started by titrating nucleosomal arrays to $ISWI_{26–648}$ and $ISWI_{FL}$ under subsaturating ATP conditions, measuring the $k_{cat}/K_{m,obs}$ (**Fig. 3a**,**b**). Effects of nucleosomes on the affinity of ATP (discussed above) should be detectable under these conditions, whereas they are masked with saturating ATP. Much to our surprise, saturating concentrations of nucleosomal arrays stimulated $ISWI_{26–648}$ much more strongly than DNA (17-fold). The level of stimulation and even the absolute hydrolysis rates were comparable between $ISWI_{26–648}$ and $ISWI_{FL}$ (**Fig. 3b** and **Supplementary Table 1**). These results indicated that $ISWI_{FL}$ and $ISWI_{26–648}$ could form the same important contacts to the nucleosome that mediated the stimulation.

We next probed whether these contacts were to linker DNA by deleting the linker altogether, using nucleosome core particles (NCPs). NCPs stimulated hydrolysis of $ISWI_{26–648}$ just as well as arrays. Also the apparent affinity of arrays and NCPs remained unaffected (**Fig. 3a**). Notably, even $ISWI_{FL}$ did not react to deletion of the linker (**Fig. 3b**). These results ruled out that the contact responsible for ATPase stimulation was between the HSS domain and linker DNA.

When ATP and DNA ligand are subsaturating, the specificity with which ISWI discriminates between different DNA ligands can be determined (ref. 38 and mathematical derivation not shown). $ISWI_{26–648}$ possessed a moderate ability to distinguish between naked and nucleosomal DNA (six-fold for both NCPs and arrays). In contrast, $ISWI_{FL}$ strongly discriminated between naked and nucleosomal DNA (>60-fold for both NCPs and arrays; **Fig. 3c**). This result indicated that the HSS domain formed important contacts to the NCP, which increased the specificity for nucleosomes. Because of tight binding, we could only extract lower limits for the specificity of $ISWI_{FL}$. For the same reason, we could not test whether HSS-linker interactions provided additional specificity. In addition to specificity, the HSS domain markedly improved the apparent affinity for nucleosomes, as $ISWI_{FL}$ saturated with much lower concentrations of nucleosomes than $ISWI_{26–648}$ (≤25 nM versus >0.5 μM, respectively; **Fig. 3a** and data not shown).

We confirmed that the HSS–linker DNA interaction is also negligible for ATPase activation under saturating ATP conditions (**Fig. 3d**). NCPs stimulated the $k_{cat,obs}$ by 11-fold relative to naked DNA, whereas nucleosomal arrays stimulated $k_{cat,obs}$ at most by ~two-fold more than NCPs. Notably, $ISWI_{26–648}$ apparently lost its ability to discriminate free DNA from NCPs or arrays with saturating ATP, as all these ligands gave indistinguishable stimulation at similar concentrations (data not shown). This result suggested that the relatively poor discriminatory power that $ISWI_{26–648}$ possessed at subsaturating ATP concentrations was further reduced when the enzyme was saturated with nucleotides, which resulted in enzyme that did not profit from the nucleosomal activation at SHL2 (discussed below) but instead sampled DNA elsewhere on the surface of the nucleosome (**Supplementary Note**). **Figure 3e** summarizes ISWI-nucleosome interactions and their functions uncovered in this section.

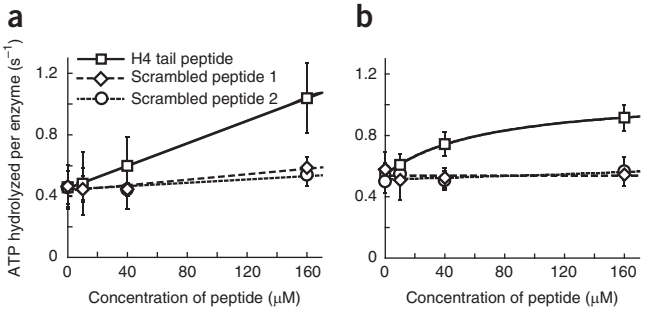

Figure 4 An N-terminal peptide of histone H4 activated ISWI ATP turnover. (**a**,**b**) ATP hydrolysis rates of $ISWI_{FL}$ (**a**) and $ISWI_{26–648}$ (**b**), both 0.5 μM, in the presence of DNA (1.2 mg ml^{-1} salmon sperm DNA) and saturating ATP concentrations (1 mM). Two peptides with a scrambled amino acid sequence served as specificity controls. Error bars, s.d. ($n = 4$).

The ATPase domain senses the histone H4 N-terminal tail

Stimulation of ATP turnover by nucleosomes has been shown to require the histone H4 N-terminal tail[17,19]. The location of the H4 tail near the interaction site of the ATPase domain at SHL2 would be consistent with a direct effect of the H4 tail on the ATPase domain. Structural similarity of the SANT domain with histone tail–binding proteins, however, would point to the HSS domain as the sensor of the H4 tail[23,39]. Using $ISWI_{26–648}$, we directly tested whether the HSS domain is required to detect the H4 tail.

In a previous publication, we showed that ATP turnover was faster when $ISWI_{FL}$ was presented with a synthetic H4 tail peptide in addition to DNA[40]. Surprisingly, $ISWI_{26–648}$ was similarly sensitive to the presence of the peptide (**Fig. 4**). On the basis of these results, we suggest that the HSS domain is not necessary for the recognition of the H4 tail, a conclusion that is further corroborated below.

The ATPase domain is sufficient to remodel nucleosomes

Our results so far argued that many important functionalities of ISWI are built into its ATPase module. We were curious as to whether these functionalities also sufficed to remodel nucleosomes, which would be consistent with recent evidence obtained for Chd1 (refs. 11,31), or whether additional conformational changes between the HSS and ATPase were required for remodeling, as previously suggested[2,3,24,30].

We analyzed nucleosome remodeling in three different ways. First, we probed whether $ISWI_{26–648}$ could reposition the histone octamer in mononucleosomes, an activity that is well documented for $ISWI_{FL}$[41]. Differently positioned nucleosomes can be visualized through their different mobility in native gels. Unexpectedly, the reaction products generated by $ISWI_{26–648}$ in this assay resembled those of $ISWI_{FL}$ (**Fig. 5a**).

Second, we tested nucleosome repositioning in the context of 25-mer nucleosomal arrays, a more physiological substrate (**Fig. 5b**). Each linker DNA contained an exposed AvaI restriction site. As expected, AvaI fully digested unremodeled arrays to mononucleosomes. After remodeling by $ISWI_{26–648}$, in contrast, AvaI could not fully digest the arrays, which indicated occlusion of a fraction of AvaI sites by nucleosomes (**Fig. 5c**). Protection of these sites by binding of ISWI was ruled out by experiments that lacked ATP and by exhaustive AvaI digests.

The third assay probed accessibility of restriction sites that were protected by nucleosomes in the array before remodeling[42]. Accessibility of four restriction enzyme sites, distributed over an entire gyre of nucleosomal DNA, dramatically changed upon incubation with $ISWI_{26–648}$ in an ATP hydrolysis–dependent manner (**Fig. 5d**).

To quantify the effect of the deletion of the HSS domain on remodeling, we adapted a previously described assay[43]. We generated nucleosomal arrays in which the central nucleosome protected a unique restriction site before remodeling (KpnI; **Fig. 6a**). By following the accessibility of the KpnI site, we collected time courses for increasing ISWI concentrations at saturating ATP and plotted the observed remodeling rate constants over the enzyme concentration to obtain the maximal reaction velocity (**Fig. 6b–d** and **Supplementary Fig. 7**). Comparison of the maximal velocities showed that $ISWI_{FL}$ remodeled arrays approximately an order of magnitude faster than $ISWI_{26–648}$ (**Fig. 6e**). As shown above, $ISWI_{FL}$ also hydrolyzed ATP at an order of magnitude faster than $ISWI_{26–648}$ under similar conditions, owing to improved binding specificity. Thus, per ATP hydrolyzed, the efficiency of remodeling was similar for both enzymes.

Deletion of the histone H4 tail was shown to impair remodeling by $ISWI_{FL}$[15–19]. Remodeling by $ISWI_{26–648}$ should be similarly affected if, as we suggested above, the ATPase domain directly recognized the H4 tail. By monitoring remodeling of nucleosomal arrays that lacked the H4 N-terminal tail, we found that $ISWI_{26–648}$ was at least

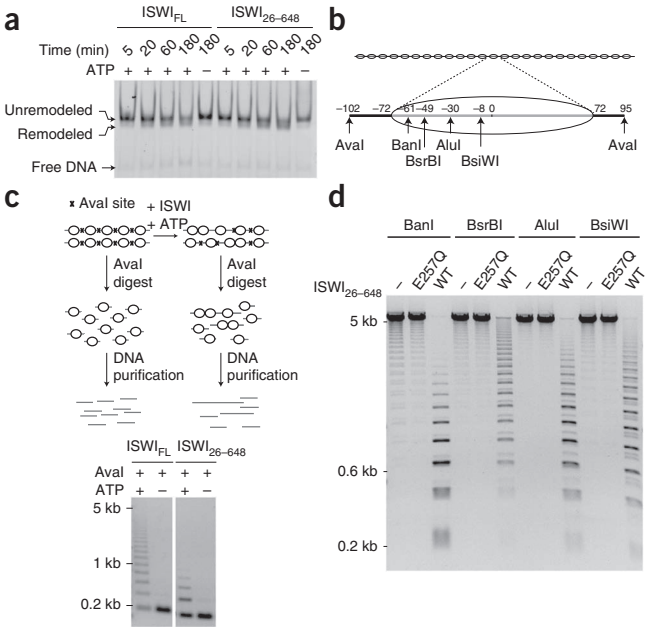

Figure 5 The HSS domain is not required for repositioning mononucleosomes or nucleosomes within arrays. (**a**) Mononucleosome-sliding assay. Mononucleosomes, centrally positioned on a 197-bp Widom-601 DNA, were incubated for the indicated time with ATP and ISWI and analyzed by native PAGE. Quench DNA migrated more slowly and was cut off for clarity. Control reactions (–) were depleted of ATP with apyrase before addition of ISWI. (**b**) Schematic depiction of the 25-mer nucleosomal arrays used in **c** and **d**. Each nucleosome protected the indicated restriction enzyme sites, whereas the linker DNA contained an exposed AvaI site (magnification). Numbers specify base pairs relative to the pseudodyad axis (0). (**c**) Polynucleosome-sliding assay. Top, schematic depiction of the assay. Bottom, nucleosomal arrays incubated with ISWI and ATP as indicated. Control reactions were depleted of ATP as above (–). kb, kilobases. (**d**) Restriction enzyme accessibility assays. Nucleosomal arrays were incubated with ATP, the indicated restriction enzymes and wild-type (WT) or mutant $ISWI_{26–648}$ (E257Q). DNA was then deproteinized and resolved by gel electrophoresis. Samples incubated without enzyme (–) served as controls.

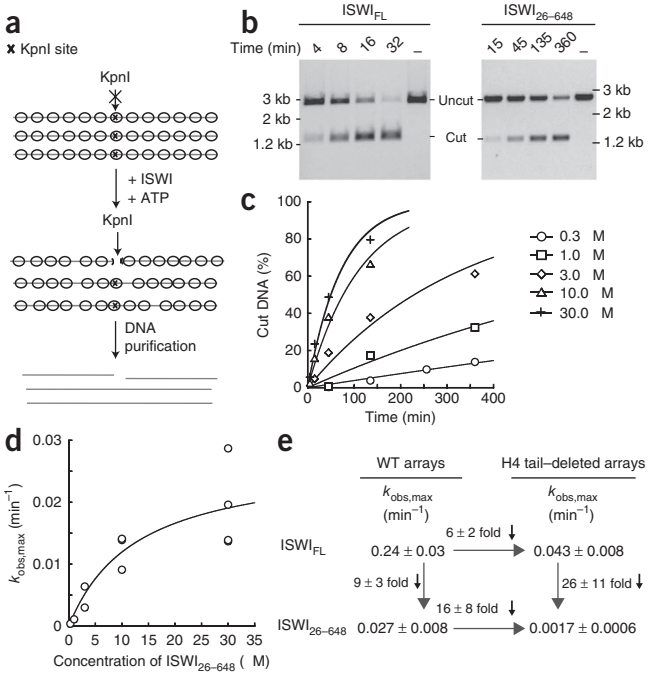

Figure 6 Remodeling by ISWI$_{26–648}$ is only moderately slower than remodeling by ISWI$_{FL}$, and it is sensitive to H4 tail deletion. (**a**) Schematic depiction of the remodeling assay. The central nucleosome in a 13-mer nucleosomal array occluded a unique KpnI site. (**b**) Exemplary time courses for remodeling by ISWI$_{FL}$ and ISWI$_{26–648}$ (both 3 μM). In control reactions (–), the quench solution was added together with ATP. (**c**) Time-course data collected for varying ISWI$_{26–648}$ concentrations and fit to a single exponential function to extract the rate constant k_{obs} (line). (**d**) Maximal velocity with which ISWI$_{26–648}$ remodeled nucleosomes ($k_{obs,max}$), obtained by extrapolating to saturating enzyme concentrations (lines). Data points were from several independent experiments. (**e**) Effects of HSS and H4 tail deletion on the maximal remodeling velocities $k_{obs,max}$. Values for $k_{obs,max}$ for ISWI$_{FL}$ and ISWI$_{26–648}$ were obtained as above at saturating ATP concentrations (**Supplementary Fig. 7**). Errors are standard errors of the fit.

as sensitive toward deletion of the H4 tail as ISWI$_{FL}$, confirming our previous conclusion (16-fold; **Fig. 6e**).

DISCUSSION

Our major conclusion is that—contrary to widespread belief—all fundamental aspects of nucleosome-remodeling catalysis are contained within the compact ATPase domain of ISWI. The ATPase module alone was able to recognize the DNA and histone moiety of substrate nucleosomes. Substrate binding triggered a conformational change within the ATPase domain along with an increased affinity for ATP. The ATPase module alone was able to remodel nucleosomes. In conjunction with recent related observations for the Chd1 remodeler[11], these findings suggest that nucleosome remodeling could have evolved from helicase-type motors without further requirements for accessory domains[44].

Mechanistic implications for nucleosome remodeling

Several current models ascribe critical functions to the HSS domain during remodeling. The HSS domain was suggested to bind and release DNA and drag it into the nucleosome upon cues from the ATPase domain, to form channels for nucleosomal DNA or to stabilize high-energy structures such as DNA bulges off the histone surface[2–4,16,24,30]. Notably, we found that ISWI lacking its HSS domain still remodeled nucleosomes, although the reaction proceeded an order of magnitude more slowly. This defect, however, was accounted for by a proportionally decreased ATP turnover. We therefore conclude that the HSS domain is not an integral component of the motor core of ISWI.

Whereas passive secondary roles of the HSS during remodeling are fully consistent with our results (discussed below), our ATPase data do not favor models that postulate active coordination, that is, transduction of energy, between the ATPase and the HSS domains. Steady-state ATP hydrolysis parameters ($k_{cat}/K_{m,obs}$) of ligand-free, DNA-bound and nucleosome-bound ISWI largely remained unaffected when the HSS was deleted. Notably, the characteristic biphasic ATP concentration dependence of hydrolysis was preserved when the HSS domain was missing. It remains possible, though, that energy is transduced only after the rate-limiting step of ATP hydrolysis, because steady-state measurements are blind to that regime.

The autonomy of the ATPase domain does not appear to be a specialty of ISWI, because Chd1 derivatives that lack their C-terminal DNA-binding domain can still slide nucleosomes[11,31]. This commonality adds to the growing list of shared functional properties of ISWI and Chd1 remodelers (ref. 28 and references therein). In fact, substantial parts of both enzymes are also structurally related. Chd1 harbors a SANT-SLIDE domain in place of the HSS domain of ISWI[28], and both enzymes contain the bridge motif adjacent to the conserved ATPase domain[31,32]. Although the N-terminal parts of both enzymes lack any apparent homology, they nevertheless may perform similar functions (discussed below).

How does ISWI remodel nucleosomes without the involvement of the HSS domain? Previous studies placed the ATPase region of several remodelers close to SHL2 of the nucleosome, whereas the HSS domain of ISWI was found to bind the linker DNA[9–11,18,24,25,45]. As ISWI$_{26–648}$ discriminates between nucleosomes and DNA and is sensitive to the H4 tail, at least a fraction of ISWI$_{26–648}$ can productively bind at SHL2 (**Fig. 7a**, step 1).

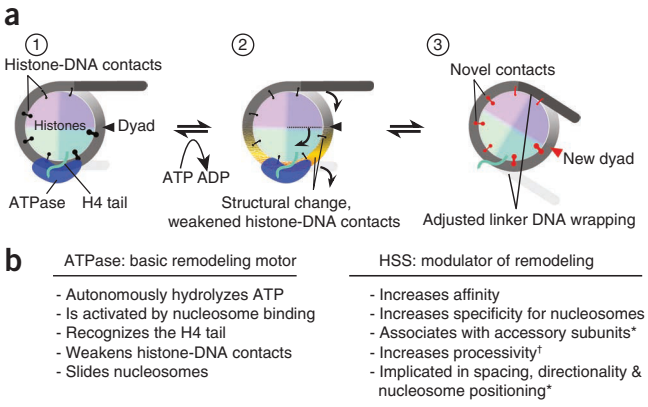

Figure 7 Model for the mechanism of nucleosome remodeling. (**a**) Suggested remodeling mechanism. The HSS domain was omitted from the model, as it is not required for the basic mechanism. Histones and DNA form multiple contacts of varying strength (black clamps; shown only for the top gyre of DNA). The ATPase domain attaches to histones, for example the H4 N terminus (1). Upon ATP hydrolysis, the ATPase domain translocates DNA relative to the histones, thereby distorting the nucleosome structure and disrupting DNA-histone interactions in the vicinity of SHL2 (2). With the strongest histone-DNA contacts destabilized, the histones rearrange relative to DNA to optimize interactions, forming a new set of contacts and thus a repositioned nucleosome (red clamps; 3). (**b**) Division of labor between the ATPase and HSS domains. Asterisks indicate prior work; dagger, anticipated function.

Strong histone-DNA contacts are present around SHL2 (refs. 46,47). Weakening the strongest contacts is expected to be rate limiting for remodeling. This could occur when the binding energy of the remodeler toward the nucleosome is exploited[48] or when the ATPase domain tries to translocate on DNA while interacting with histones, for example, at the H4 tail. Translocation puts a strain on the nucleosome, caused either by the presence of excess DNA or by a change in the twist of the DNA, which locally destabilizes histone-DNA interactions (**Fig. 7a**, step 2)[12,13,22]. The ATPase domain may even be strong enough to pump more DNA toward the dyad than the nucleosomal surface can accommodate, causing it to detach and bulge out[2,16,18,30,49]. The latter model is difficult to envision for remodeling by the truncated ISWI enzyme, owing to a lack of domains that help form and stabilize the bulge.

Once key contacts between histones and DNA are weakened, alternative sets of histone-DNA contacts might become energetically more preferable, leading to a repositioning of the histones relative to DNA (**Fig. 7a**, step 3). DNA-histone contacts may adjust concertedly or—perhaps more probably—only locally, such that the strain propagates in multiple steps around the nucleosome[4,22].

Accessory domains may have evolved to optimize catalysis and modulate the outcome of the reaction, which explains their diversity among remodeling machines (**Fig. 7b**)[2,4]. We showed that, consistent with previous findings[23], the HSS domain increased the affinity of ISWI toward DNA, a feature that is expected to enhance processivity[16,50,51]. In agreement with cross-linking results[24], we obtained evidence for direct contacts between the HSS domain and the NCP. This interaction was a major source for specificity toward the nucleosome. As such, the HSS domain improves the productive association of the ATPase domain at SHL2, which in turn enhances remodeling. The HSS domain could also optimize catalysis by weakening the DNA-histone interactions at the edge of the nucleosome[11,16]. Through interactions with additional subunits and the linker DNA[23–25,36,52], the HSS may assist sensing the length of the linker or a preferred DNA sequence and therefore bias the remodeling reaction toward specific outcomes such as nucleosome spacing or positioning[11,24,25,27,28].

Conformational changes within the ATPase domain

How do the conformational changes within the ATPase domain relate to previously reported structural changes in related enzymes? The catalytic domain of the distant relative *Sulfolobus* Sso1653 was crystallized with and without bound DNA[35]. The two structures showed only minor differences well inside the ATPase core and therefore are unlikely to account for the increased exposure of peripheral arginines upon DNA binding. In conflict with the crystallographic data but in better agreement with our results, a FRET study using the same *Sulfolobus* protein concluded that DNA binding leads to a major structural rearrangement between the two ATPase lobes[37].

Additional crystallographic evidence supports a high degree of flexibility between the two ATPase lobes. The ATPase lobes of relatives of ISWI crystallized in a multitude of very different orientations[31,35,53,54]. Conformational changes between the two ATPase lobes may be functionally important for these enzymes, for example, for translocation on DNA or regulation of enzyme activity[5,44]. Conceivably, multiple orientations of ISWI's ATPase lobes coexist in solution, accounting for the different enzyme species detected by our ATPase experiments[32]. DNA may preferentially stabilize a subset of these states, thereby aligning the composite catalytic site formed at the cleft between both lobes[5]. As motifs of both ATPase lobes are thought to contact ATP[35], a proper alignment of the lobes might increase the affinity for ATP, explaining our biochemical data.

The increased exposure of peripheral arginines upon DNA binding also suggests that these regions undergo structural changes. Trypsin cleaved DNA-bound ISWI adjacent to a conserved acidic motif in the NTR (**Supplementary Fig. 3**). Despite a lack of sequence similarity, the NTR of Chd1 also contains a highly acidic motif, which was suggested to act as a pseudosubstrate and compete with DNA for binding to lobe 2. The authors proposed that, in excellent agreement with our proteolytic results, DNA binding would force a structural rearrangement in Chd1 in which the NTR undocks from lobe 2 (ref. 31). The NTRs of both enzymes may therefore fulfill similar roles and gate the entrance to the nucleic acid–binding site.

On the C-terminal side, trypsin cut the polypeptide chain within the 'brace' motif of lobe 2 (ref. 4). The brace is in close contact with lobe 1 and is directly followed by a stretch of amino acids that folds back to form a bridge between both ATPase lobes[31,32]. We suggest that the brace or bridge may hold the ATPase lobes in a configuration that is not fully competent for ATP hydrolysis and that binding of nucleic acids relieves this inhibition. These results reinforce the notion that the ATPase domain represents an autonomous remodeling engine, which is optimized and modulated by the evolution of accessory domains and subunits.

METHODS

Methods and any associated references are available in the online version of the paper.

Note: Supplementary information is available in the online version of the paper.

ACKNOWLEDGMENTS

We are grateful to C. Müller (European Molecular Biology Laboratory, Heidelberg, Germany) and D. Rhodes (Nanyang Technological University, Singapore) for the donation of plasmids and to the following colleagues at Ludwig-Maximilians-Universität, Munich, Germany, for materials: N. Hepp for 13-mer nucleosomal arrays, C. Boenisch for 197-bp 601 DNA, V.K. Maier and C. Regnard for recombinant histone octamers. We thank R. Mentele for the Edman digest, I. Forné for performing the LC-MS/MS experiment and Z. Ökten for comments on the manuscript. H.K. acknowledges support by the Elite Network of Bavaria. This work was supported by grants of the Deutsche Forschungsgemeinschaft to P.B.B. (SFB 594 TP A6 and Be 1140/6-1).

AUTHOR CONTRIBUTIONS

F.M.-P., H.K. and J.L. performed experiments. All authors interpreted results and contributed to writing.

COMPETING FINANCIAL INTERESTS

The authors declare no competing financial interests.

Published online at http://www.nature.com/doifinder/10.1038/nsmb.2457.
Reprints and permissions information is available online at http://www.nature.com/reprints/index.html.

1. Hargreaves, D.C. & Crabtree, G.R. ATP-dependent chromatin remodeling: genetics, genomics and mechanisms. *Cell Res.* **21**, 396–420 (2011).
2. Clapier, C.R. & Cairns, B.R. The biology of chromatin remodeling complexes. *Annu. Rev. Biochem.* **78**, 273–304 (2009).
3. Hota, S.K. & Bartholomew, B. Diversity of operation in ATP-dependent chromatin remodelers. *Biochim. Biophys. Acta* **1809**, 476–487 (2011).
4. Flaus, A. & Owen-Hughes, T. Mechanisms for ATP-dependent chromatin remodelling: the means to the end. *FEBS J.* **278**, 3579–3595 (2011).
5. Hauk, G. & Bowman, G.D. Structural insights into regulation and action of SWI2/SNF2 ATPases. *Curr. Opin. Struct. Biol.* **21**, 719–727 (2011).
6. Flaus, A., Martin, D.M., Barton, G.J. & Owen-Hughes, T. Identification of multiple distinct Snf2 subfamilies with conserved structural motifs. *Nucleic Acids Res.* **34**, 2887–2905 (2006).
7. Dechassa, M.L. *et al.* Disparity in the DNA translocase domains of SWI/SNF and ISW2. *Nucleic Acids Res.* 4412–4421 (2012).
8. Fan, H.Y., Trotter, K.W., Archer, T.K. & Kingston, R.E. Swapping function of two chromatin remodeling complexes. *Mol. Cell* **17**, 805–815 (2005).
9. Saha, A., Wittmeyer, J. & Cairns, B.R. Chromatin remodeling through directional DNA translocation from an internal nucleosomal site. *Nat. Struct. Mol. Biol.* **12**, 747–755 (2005).

10. Zofall, M., Persinger, J., Kassabov, S.R. & Bartholomew, B. Chromatin remodeling by ISW2 and SWI/SNF requires DNA translocation inside the nucleosome. *Nat. Struct. Mol. Biol.* **13**, 339–346 (2006).
11. McKnight, J.N., Jenkins, K.R., Nodelman, I.M., Escobar, T. & Bowman, G.D. Extranucleosomal DNA binding directs nucleosome sliding by Chd1. *Mol. Cell. Biol.* **31**, 4746–4759 (2011).
12. Richmond, T.J. & Davey, C.A. The structure of DNA in the nucleosome core. *Nature* **423**, 145–150 (2003).
13. Suto, R.K. *et al.* Crystal structures of nucleosome core particles in complex with minor groove DNA-binding ligands. *J. Mol. Biol.* **326**, 371–380 (2003).
14. Makde, R.D., England, J.R., Yennawar, H.P. & Tan, S. Structure of RCC1 chromatin factor bound to the nucleosome core particle. *Nature* **467**, 562–566 (2010).
15. Ferreira, H., Flaus, A. & Owen-Hughes, T. Histone modifications influence the action of Snf2 family remodelling enzymes by different mechanisms. *J. Mol. Biol.* **374**, 563–579 (2007).
16. Gangaraju, V.K., Prasad, P., Srour, A., Kagalwala, M.N. & Bartholomew, B. Conformational changes associated with template commitment in ATP-dependent chromatin remodeling by ISW2. *Mol. Cell* **35**, 58–69 (2009).
17. Clapier, C.R., Langst, G., Corona, D.F., Becker, P.B. & Nightingale, K.P. Critical role for the histone H4 N terminus in nucleosome remodeling by ISWI. *Mol. Cell. Biol.* **21**, 875–883 (2001).
18. Dang, W., Kagalwala, M.N. & Bartholomew, B. Regulation of ISW2 by concerted action of histone H4 tail and extranucleosomal DNA. *Mol. Cell. Biol.* **26**, 7388–7396 (2006).
19. Hamiche, A., Kang, J.G., Dennis, C., Xiao, H. & Wu, C. Histone tails modulate nucleosome mobility and regulate ATP-dependent nucleosome sliding by NURF. *Proc. Natl. Acad. Sci. USA* **98**, 14316–14321 (2001).
20. Whitehouse, I., Stockdale, C., Flaus, A., Szczelkun, M.D. & Owen-Hughes, T. Evidence for DNA translocation by the ISWI chromatin-remodeling enzyme. *Mol. Cell. Biol.* **23**, 1935–1945 (2003).
21. Zhang, Y. *et al.* DNA translocation and loop formation mechanism of chromatin remodeling by SWI/SNF and RSC. *Mol. Cell* **24**, 559–568 (2006).
22. Bowman, G.D. Mechanisms of ATP-dependent nucleosome sliding. *Curr. Opin. Struct. Biol.* **20**, 73–81 (2010).
23. Grüne, T. *et al.* Crystal structure and functional analysis of a nucleosome recognition module of the remodeling factor ISWI. *Mol. Cell* **12**, 449–460 (2003).
24. Dang, W. & Bartholomew, B. Domain architecture of the catalytic subunit in the ISW2-nucleosome complex. *Mol. Cell. Biol.* **27**, 8306–8317 (2007).
25. Yamada, K. *et al.* Structure and mechanism of the chromatin remodelling factor ISW1a. *Nature* **472**, 448–453 (2011).
26. Gangaraju, V.K. & Bartholomew, B. Dependency of ISW1a chromatin remodeling on extranucleosomal DNA. *Mol. Cell. Biol.* **27**, 3217–3225 (2007).
27. Yang, J.G., Madrid, T.S., Sevastopoulos, E. & Narlikar, G.J. The chromatin-remodeling enzyme ACF is an ATP-dependent DNA length sensor that regulates nucleosome spacing. *Nat. Struct. Mol. Biol.* **13**, 1078–1083 (2006).
28. Ryan, D.P., Sundaramoorthy, R., Martin, D., Singh, V. & Owen-Hughes, T. The DNA-binding domain of the Chd1 chromatin-remodelling enzyme contains SANT and SLIDE domains. *EMBO J.* **30**, 2596–2609 (2011).
29. Corona, D.F. *et al.* ISWI is an ATP-dependent nucleosome remodeling factor. *Mol. Cell* **3**, 239–245 (1999).
30. Cairns, B.R. Chromatin remodeling: insights and intrigue from single-molecule studies. *Nat. Struct. Mol. Biol.* **14**, 989–996 (2007).
31. Hauk, G., McKnight, J.N., Nodelman, I.M. & Bowman, G.D. The chromodomains of the Chd1 chromatin remodeler regulate DNA access to the ATPase motor. *Mol. Cell* **39**, 711–723 (2010).
32. Forne, I., Ludwigsen, J., Imhof, A., Becker, P.B. & Mueller-Planitz, F. Probing the conformation of the ISWI ATPase domain with genetically encoded photoreactive crosslinkers and mass spectrometry. *Mol Cell Proteomics* **11**, M111.012088 (2012).
33. Racki, L.R. *et al.* The chromatin remodeller ACF acts as a dimeric motor to space nucleosomes. *Nature* **462**, 1016–1021 (2009).
34. Singleton, M.R., Dillingham, M.S. & Wigley, D.B. Structure and mechanism of helicases and nucleic acid translocases. *Annu. Rev. Biochem.* **76**, 23–50 (2007).
35. Dürr, H., Korner, C., Muller, M., Hickmann, V. & Hopfner, K.P. X-ray structures of the *Sulfolobus solfataricus* SWI2/SNF2 ATPase core and its complex with DNA. *Cell* **121**, 363–373 (2005).
36. Sharma, A., Jenkins, K.R., Heroux, A. & Bowman, G.D. Crystal structure of the chromodomain helicase DNA-binding protein 1 (Chd1) DNA-binding domain in complex with DNA. *J. Biol. Chem.* **286**, 42099–42104 (2011).
37. Lewis, R., Durr, H., Hopfner, K.P. & Michaelis, J. Conformational changes of a Swi2/Snf2 ATPase during its mechano-chemical cycle. *Nucleic Acids Res.* **36**, 1881–1890 (2008).
38. Fersht, A. *Structure and Mechanism in Protein Science: A Guide to Enzyme Catalysis and Protein Folding* (W.H. Freeman, 1999).
39. Boyer, L.A., Latek, R.R. & Peterson, C.L. The SANT domain: a unique histone-tail-binding module? *Nat. Rev. Mol. Cell Biol.* **5**, 158–163 (2004).
40. Clapier, C.R., Nightingale, K.P. & Becker, P.B. A critical epitope for substrate recognition by the nucleosome remodeling ATPase ISWI. *Nucleic Acids Res.* **30**, 649–655 (2002).
41. Längst, G., Bonte, E.J., Corona, D.F. & Becker, P.B. Nucleosome movement by CHRAC and ISWI without disruption or trans-displacement of the histone octamer. *Cell* **97**, 843–852 (1999).
42. Maier, V.K., Chioda, M., Rhodes, D. & Becker, P.B. ACF catalyses chromatosome movements in chromatin fibres. *EMBO J.* **27**, 817–826 (2008).
43. Logie, C. & Peterson, C.L. Catalytic activity of the yeast SWI/SNF complex on reconstituted nucleosome arrays. *EMBO J.* **16**, 6772–6782 (1997).
44. Dürr, H., Flaus, A., Owen-Hughes, T. & Hopfner, K.P. Snf2 family ATPases and DExx box helicases: differences and unifying concepts from high-resolution crystal structures. *Nucleic Acids Res.* **34**, 4160–4167 (2006).
45. Kagalwala, M.N., Glaus, B.J., Dang, W., Zofall, M. & Bartholomew, B. Topography of the ISW2-nucleosome complex: insights into nucleosome spacing and chromatin remodeling. *EMBO J.* **23**, 2092–2104 (2004).
46. Hall, M.A. *et al.* High-resolution dynamic mapping of histone-DNA interactions in a nucleosome. *Nat. Struct. Mol. Biol.* **16**, 124–129 (2009).
47. Mihardja, S., Spakowitz, A.J., Zhang, Y. & Bustamante, C. Effect of force on mononucleosomal dynamics. *Proc. Natl. Acad. Sci. USA* **103**, 15871–15876 (2006).
48. Lorch, Y., Maier-Davis, B. & Kornberg, R.D. Mechanism of chromatin remodeling. *Proc. Natl. Acad. Sci. USA* **107**, 3458–3462 (2010).
49. Strohner, R. *et al.* A 'loop recapture' mechanism for ACF-dependent nucleosome remodeling. *Nat. Struct. Mol. Biol.* **12**, 683–690 (2005).
50. Blosser, T.R., Yang, J.G., Stone, M.D., Narlikar, G.J. & Zhuang, X. Dynamics of nucleosome remodelling by individual ACF complexes. *Nature* **462**, 1022–1027 (2009).
51. Fyodorov, D.V. & Kadonaga, J.T. Dynamics of ATP-dependent chromatin assembly by ACF. *Nature* **418**, 897–900 (2002).
52. Eberharter, A., Vetter, I., Ferreira, R. & Becker, P.B. ACF1 improves the effectiveness of nucleosome mobilization by ISWI through PHD-histone contacts. *EMBO J.* **23**, 4029–4039 (2004).
53. Thomä, N.H. *et al.* Structure of the SWI2/SNF2 chromatin-remodeling domain of eukaryotic Rad54. *Nat. Struct. Mol. Biol.* **12**, 350–356 (2005).
54. Caruthers, J.M., Johnson, E.R. & McKay, D.B. Crystal structure of yeast initiation factor 4A, a DEAD-box RNA helicase. *Proc. Natl. Acad. Sci. USA* **97**, 13080–13085 (2000).

ONLINE METHODS

Enzyme expression and purification. pPROEX-HTb–based expression plasmids with genes encoding *Drosophila* $ISWI_{FL}$, $ISWI_{FL}$ E257Q, $ISWI_{26–648}$ and $ISWI_{1–697}$ were kindly provided by C. Müller (EMBL, Heidelberg, Germany). All genes were fused N terminally to a His_6-TEV tag . The E257Q mutation was introduced into $ISWI_{26–648}$ by QuikChange mutagenesis (Stratagene). Expression and purification was performed as described[32]. The His_6-TEV tag was cleaved off by TEV protease for $ISWI_{FL}$ and $ISWI_{1–697}$. For $ISWI_{26–648}$, experiments were carried out in the presence of the tag. ATPase parameters of $ISWI_{26–648}$ with and without tag were quantitatively the same (data not shown).

Enzyme assays and enzyme ligands. Unless otherwise stated, reactions were performed at 28 °C in a buffer containing 25 mM HEPES-KOH, pH 7.6, 100 mM potassium acetate, 1.5 mM magnesium acetate, 0.1 mM EDTA, 10% glycerol, 10 mM β-mercaptoethanol. As indicated, some ATPase assays were performed in a buffer with an increased buffering capacity (250 mM HEPES-KOH, pH 7.6) and excess Mg^{2+} ions (100 mM magnesium acetate) to prevent high concentrations of ATP from substantially altering the pH and the concentration of free unchelated Mg^{2+} ions. Both buffers yielded comparable ATPase parameters (**Table 1** and **Supplementary Table 1**). Remodeling was followed in 25 mM HEPES-KOH, pH 7.6, 50 mM NaCl, 1 mM MgCl, 0.1 mM EDTA, 10% glycerol and 1 mM DTT at 26 °C. All remodeling reactions contained an ATP-regenerating system consisting of phosphoenolpyruvate (3–6 mM) and a pyruvate kinase-lactate dehydrogenase mixture (15.5 U/ml; Sigma). Nucleotides were always added as stoichiometric complexes with Mg^{2+}. ADP and AMPPNP were purified before use[55]. ATP was purified if used at concentrations exceeding 3 mM or if no ATP regenerating system was used.

HPLC-purified oligopeptides and DNA oligonucleotides were purchased (Peptide Specialty Laboratories and Biomers, respectively; **Supplementary Table 2**). Short DNA duplexes were created by annealing. The 147-bp DNA used for NCP reconstitution was purified from SmaI digests of a plasmid harboring derivatives of the Widom-601 sequence with terminal SmaI sites. 197-bp DNA was generated by AvaI digests of a pUC derivative containing 25 repeats of the Widom-601 sequence (kindly provided by D. Rhodes, NTU, Singapore). During nucleosome assembly, it is expected that the 147-bp and 197-bp DNA form 0-N-2 and 29-N-23 nucleosomes, respectively[14,56]. DNA used for 13-mer nucleosomal arrays was gene synthesized (Genscript). It contained 197-bp repeats of Widom-601 derivatives with a KpnI site at position −32 relative to the dyad axis of the central nucleosome.

Mono- and polynucleosomes were reconstituted with recombinant *Drosophila* histones by salt-gradient dialysis as described[57,58]. H4 tail–deleted arrays lacked the 19 N-terminal amino acids of histone H4. Nucleosomal arrays were purified by Mg^{2+} precipitation (25-mer arrays, 3.5 mM; 13-mer WT-H4 arrays, 5 mM; 13-mer H4 tail–deleted arrays, 8.5 mM)[42,58]. The 13-mer arrays were subsequently dialyzed into 10 mM Tris, pH 7.7, 0.1 mM EDTA, pH 8, 1 mM DTT. Mononucleosomes used in the TLC ATPase assay were purified over a glycerol gradient (10% to 30%) and buffer exchanged into reaction buffer by ultrafiltration. The concentration of nucleosomal DNA was determined by measuring its DNA content by UV absorbance at 260 nm. The indicated concentrations of nucleosomal arrays refer to the concentration of individual nucleosomes. Unless otherwise noted, nucleosomes with WT-H4 were used.

Steady-state ATP hydrolysis assays. Two different ATPase assays were employed. A thin-layer chromatography (TLC)–based assay was used to follow hydrolysis of [γ-^{32}P]ATP in reactions that required the use of subsaturating ATP concentrations (**Fig. 3a–c** and **Supplementary Fig. 4**). All other ATPase data were collected by a coupled ATP-hydrolysis assay in 384-well plates as described[32]. For the TLC assay, reactions were initiated by addition of trace amounts of [γ-^{32}P]ATP supplemented with 1 μm purified, nonradioactive ATP. Three time points (in addition to a 'zero' time point from a reaction that lacked enzyme) were collected by stopping the reaction with three volumes of 2 mM EDTA, 0.3 M NaH_2PO_4, 1 M LiCl. Control experiments showed that ISWI was fully quenched on time scales that were much faster than the experiments required. Reactions were spotted on PEI cellulose F (Merck) and developed in 0.3 M NaH_2PO_4, 1 M LiCl. After autoradiography, signals were quantified, and a line was fit through the data points of each time course. $k_{cat}/K_{m,obs}$ values were obtained from the slopes by normalizing for the enzyme concentration. When the enzyme and ATP concentrations were varied four- and five-fold, respectively, measured rates deviated less than two-fold.

Partial proteolysis assays. If not specified otherwise, $ISWI_{26–648}$ (2.5 μM) was partially proteolyzed with trypsin (20 nM; Promega), LysC (38 nM; Roche) or ArgC (21 nM; Roche). The reaction was stopped by addition of two volumes of SDS sample buffer and immediate incubation at 95 °C for 10 min. Samples were separated by SDS-PAGE (12%) and stained by Coomassie Blue.

Double-filter DNA-binding assay. 39-bp DNA was 5′ labeled with [γ-^{32}P]ATP by polynucleotide kinase. Trace amounts of labeled DNA were incubated for 10 min with varying ISWI concentrations. The mixture was then applied on a membrane sandwich composed of a protein-binding (Protran-BA85, Whatman) and a DNA-binding membrane (Hybond-N+, Amersham) as described[59].

Nucleosome-sliding assays. For mononucleosome sliding, centrally positioned mononucleosomes (197-bp DNA; 160 nM) were incubated with ATP (0.5 mM), $ISWI_{FL}$ (30 nM) or $ISWI_{26–648}$ (300 nM). Time points were quenched by apyrase (2.5 U/μl) and excess linearized plasmid DNA (0.4 mg/ml). Native PAGE (4.5%) was performed with 0.2 μg mononucleosomal DNA.

For polynucleosome sliding, 25-mer regular nucleosomal arrays (30 nM) were incubated with ATP (100 μM) and $ISWI_{FL}$ (10 nM) or $ISWI_{26–648}$ (300 nM). Remodeling was quenched after 6 h with apyrase (2.5 U/μl). The arrays were then digested with AvaI (1.2 U/μl) for 3 h at 26 °C. Samples were deproteinized and analyzed as described below. Exhaustive digests with high concentrations of AvaI overnight gave analogous results.

Restriction enzyme accessibility assay. 25-mer nucleosomal arrays (100 nM) were incubated for 1 h with wild-type or E257Q mutant $ISWI_{26–648}$ (both 5 μM), ATP (50 μM) and the indicated restriction enzymes (AluI, 0.5 U/μl; BsrBI, 0.5 U/μl; BsiWI, 1 U/μl; BanI, 2 U/μl). The reactions were stopped with EDTA (20–40 mM) and SDS (0.4%). Samples were deproteinized, and DNA was ethanol precipitated, resolved by agarose gel electrophoresis and visualized by ethidium bromide staining.

To quantitate remodeling, 13-mer arrays (20 or 100 nM) were incubated with $ISWI_{FL}$ or $ISWI_{26–648}$, respectively, ATP (1 mM) and KpnI (2 U/μl). Reactions were quenched and analyzed as above. Negligible accessibility (<5%) was seen when the reaction was simultaneously initiated and quenched or when ISWI was omitted. Controls showed that the ATP-regenerating system was not depleted throughout the assay. k_{obs} for remodeling was obtained by fitting the time courses to a single exponential function (equation (1)). The maximal remodeling velocities ($k_{obs,max}$) were obtained by fitting the data to standard or inverse binding isotherms (equation (2)).

$$y = 100 * (1 - e^{-k_{obs} * t}) \quad (1)$$

$$y = k_{obs,max} - \left(amp * \frac{[E]}{K_{1/2} + [E]} \right) \quad (2)$$

Observed remodeling rates were proportionally faster for $ISWI_{26–648}$ (but not $ISWI_{FL}$) when the KpnI concentration was raised from 2 U/μl to 5 U/μl. This rate enhancement was independent of the $ISWI_{26–648}$ concentration between 0.3 and 30 μM. Reported rates, including the maximal remodeling rate constant $k_{obs,max}$, are therefore lower estimates for $ISWI_{26–648}$. The reported deleterious effect of the HSS deletion on remodeling is consequently an upper estimate.

Kinetic and thermodynamic modeling and data fitting. Modeling was performed in Mathematica (Wolfram Research). Data were fit with Matlab (The Mathworks) or KaleidaGraph (Synergy Software). The biphasic ATPase data were fit to equation (3) (**Fig. 1a**,**b**). As saturation with ATP was not achieved, the second phase was represented only by the linear term m*[ATP]. m possesses a complex dependence on the rate and equilibrium constants in the reaction scheme (**Supplementary Fig. 1a**) and was not interpreted further.

$$v = k_{cat,obs,Phase\ 1} * [ATP] / (K_{m,obs,Phase\ 1} + [ATP]) + m * [ATP] \quad (3)$$

doi:10.1038/nsmb.2457

55. Horst, M., Oppliger, W., Feifel, B., Schatz, G. & Glick, B.S. The mitochondrial protein import motor: dissociation of mitochondrial hsp70 from its membrane anchor requires ATP binding rather than ATP hydrolysis. *Protein Sci.* **5**, 759–767 (1996).
56. Vasudevan, D., Chua, E.Y. & Davey, C.A. Crystal structures of nucleosome core particles containing the '601' strong positioning sequence. *J. Mol. Biol.* **403**, 1–10 (2010).
57. Dyer, P.N. *et al.* Reconstitution of nucleosome core particles from recombinant histones and DNA. *Methods Enzymol.* **375**, 23–44 (2004).
58. Huynh, V.A., Robinson, P.J. & Rhodes, D. A method for the *in vitro* reconstitution of a defined "30 nm" chromatin fibre containing stoichiometric amounts of the linker histone. *J. Mol. Biol.* **345**, 957–968 (2005).
59. Wong, I. & Lohman, T.M. A double-filter method for nitrocellulose-filter binding: application to protein-nucleic acid interactions. *Proc. Natl. Acad. Sci. USA* **90**, 5428–5432 (1993).

Supplementary Material

The ATPase domain of ISWI is an autonomous remodeling machine

Mueller-Planitz et al., *Nature Structural and Molecular Biology*, 20, 82-89 (2013)

Supplementary Figures

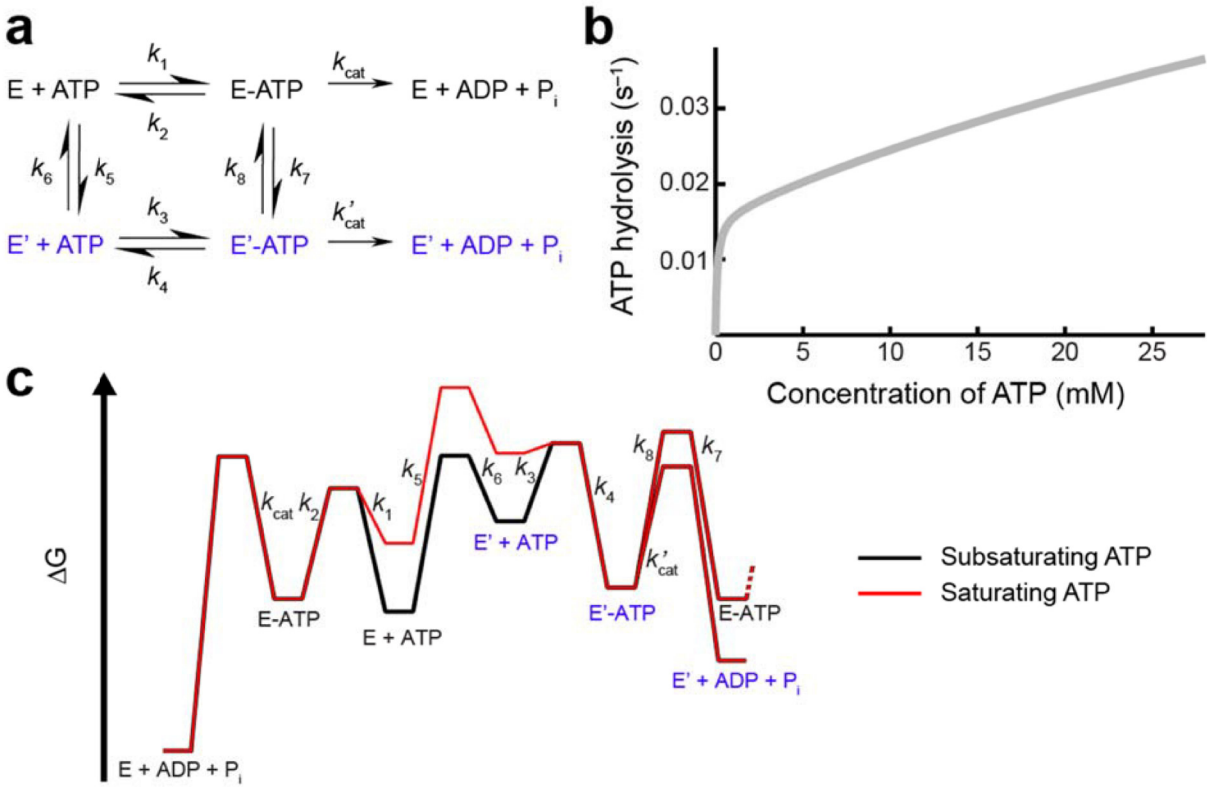

Supplementary Figure 1: The presence of two ISWI conformations can result in a biphasic ATP concentration dependence of ATP hydrolysis. (**a**) A simple reaction scheme in which the enzyme exists in two conformations, E and E', each being able to bind and hydrolyze ATP with different rate constants. (**b**) Modeling of the scheme in **a** showed that a biphasic ATP concentration dependence closely resembling the data shown in Figure 1a could be obtained (k_{cat} = 0.015 s^{-1}, k'_{cat} = 1 s^{-1}, k_1 = 10^5 M^{-1} s^{-1}, k_2 = 10 s^{-1}, k_3 = 10^9 M^{-1} s^{-1}, k_4 = 10^{-2} s^{-1}, k_5 = 10^{-3} s^{-1}, k_6 = 10^5 s^{-1}, k_7 = 10^{-4} s^{-1}, k_8 = 10^{-3} s^{-1}). Shown is an example in which both enzyme conformations had strongly different affinities for ATP. Note that many solutions resulted in biphasic behavior, not all of which required different ATP affinities (to produce a biphasic ATP concentration dependence, the ATP affinities of E and E' may or may not be similar to each other, E and E' may or may not have similar ATP turnover rates - k_{cat} or k'_{cat} may even become zero -, the ATP binding rate constants k_1 and k_3 may or may not assume similar values and the equilibration between E <=> E' and E-ATP <=> E'-ATP may or may not be similarly fast). Solutions that produce biphasic curves, however, required the four species E, E', E-ATP and E'-ATP to be present and to interconvert (mathematical derivation not shown). All solutions that produced a biphasic ATP response exhibited an ATP-concentration dependent change in the flux through the reaction scheme, i.e., different intermediates were populated due to a change in the rate limiting step (illustrated exemplary in the next panel). (**c**) Free energy profiles using the rate constants from the previous panel. With subsaturating concentrations of ATP (black line), E + ATP is the ground state of the reaction. E and ATP react to E-ATP, and ISWI then hydrolyzes ATP via k_{cat}. With saturating concentrations of ATP (red line), E + ATP quickly reacts to E-ATP. Since k_{cat} is too slow to hydrolyze all ATP immediately, some of the E-ATP reacts via k_7 to E'-ATP from where ATP is quickly hydrolyzed via k'_{cat}.

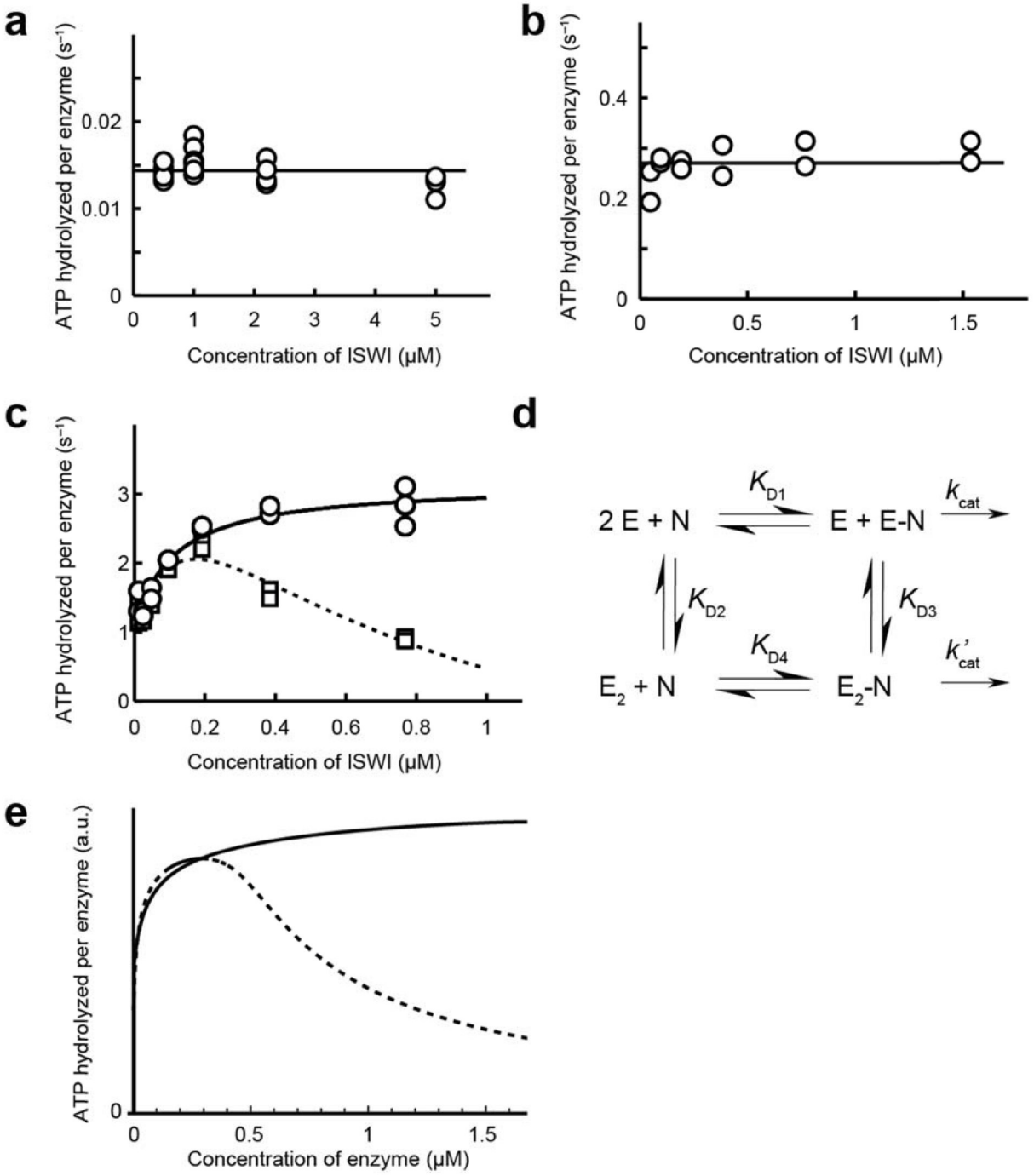

Supplementary Figure 2: Enzyme concentration dependence of ATP hydrolysis by $ISWI_{FL}$. (**a**) ATP hydrolysis by ligand-free $ISWI_{FL}$ was independent of the enzyme concentration between 0.5 and 5 μM. The biphasic ATP concentration dependence (**Fig. 1a**) therefore could not be caused by possible multimerization of ISWI. The assay was performed with 7 mM ATP in 100 mM Mg^{2+}. (**b**) ATP hydrolysis of DNA-bound $ISWI_{FL}$ remained constant between 0.05 to 1.5 μM enzyme, demonstrating that the ATPase signal was independent of possible enzyme multimerization. The assay was performed with saturating concentrations of 59-bp DNA and 3 mM ATP in 1.5 mM free Mg^{2+}. (**c**) The chromatin-stimulated reaction showed a pronounced dependence on the $ISWI_{FL}$ concentration. Two concentrations of chromatinized plasmid DNA were used (dashed line: 0.02 mg/mL, solid line: 0.1

mg/mL, referring to the DNA content). Increasing ATPase rates between 0 and 0.2 µM $ISWI_{FL}$ were consistent with enzyme dimerization on nucleosomes and subsequent enzyme activation[2]. The decreasing activity observed for the lower chromatin concentration above 0.2 µM $ISWI_{FL}$ was well explained by out-titration of available ISWI binding sites on chromatin. The data were collected with 3 mM ATP and 1.5 mM free Mg^{2+}. (**d**) Simple reaction scheme to explain the data shown in **c**. A single enzyme (E) bound to a nucleosome (N) hydrolyzes ATP with a different rate constant (k_{cat}) than an enzyme dimer (k'_{cat}). (**e**) *In silico* modeling of the reaction scheme in **d** recapitulated the features of the curves in **c**. Simulations were run for two nucleosome concentrations (0.2 µM, dashed line; 1 µM, solid line) with $K_{D1} = 10^{-1}$ µM, $K_{D2} = 10$ µM, $K_{D3} = 10^{-2}$ µM, $K_{D4} = 10^{-4}$ µM and $k'_{cat} = 4\ k_{cat}$.

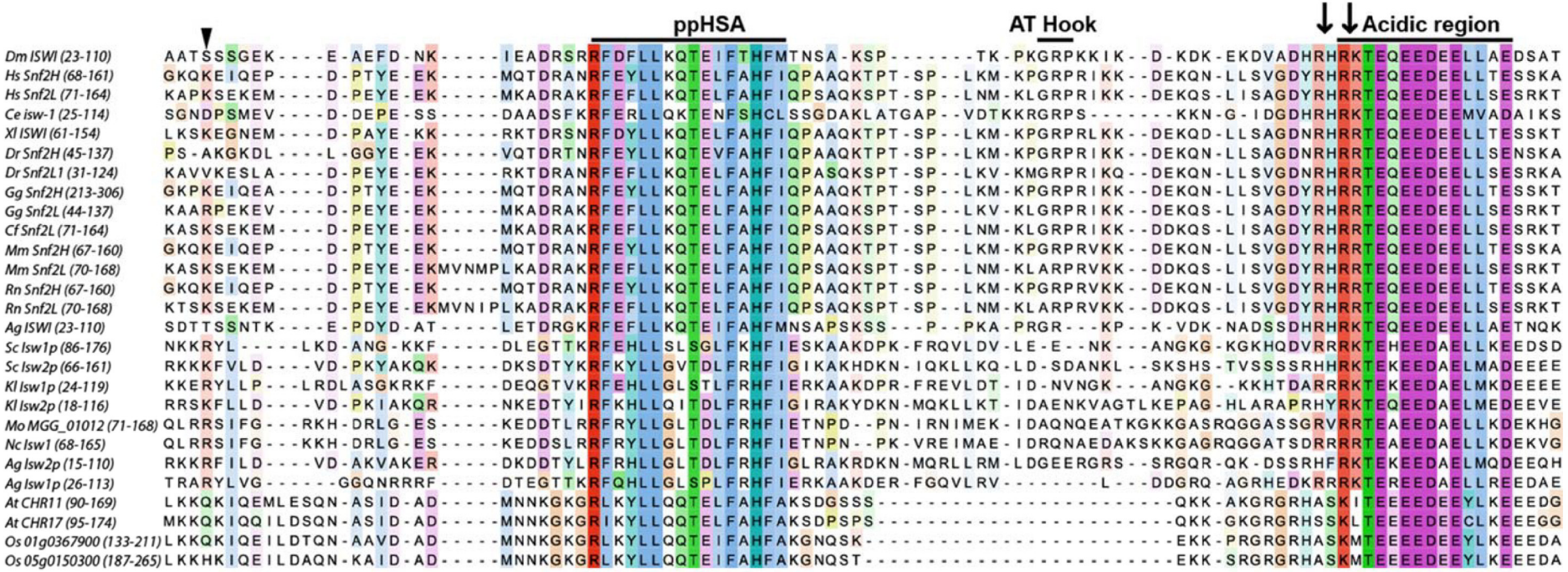

Supplementary Figure 3: Alignment of the N-terminal region of ISWI homologs from various organisms. Two highly conserved motifs exist: an acidic motif and the ppHSA motif, named so because it shares homology with the region after the post-HSA domain found in other family of remodelers (data not shown)[1]. The alignment is cut off at the C-terminal side before 'motif Q' of Snf2-type ATPases begins[3]. An AT hook ('GRP') has been previously described[4], but it is comparatively poorly conserved. The arrowhead points to the first amino acid included in $ISWI_{26–648}$. Arrows indicate tryptic cleavage sites obtained specifically in the DNA-bound conformation (**Fig. 3a**). *Dm: Drosophila melanogaster, Hs: Homo sapiens, Ce: Caenorhabditis elegans, Xl: Xenopus laevis, Dr: Danio rerio, Gg: Gallus gallus, Cf: Canis familiaris, Mm: Mus musculus, Rn: Rattus norvegicus, Ag: Anopheles gambiae, Sc: Saccharomyces cerevisiae, Kl: Kluyveromyces lactis, Mo: Magnaporthe oryzae, Nc: Neurospora crassa, Ag: Ashbya gossypii, At: Arabidopsis thaliana, Os: Oryza sativa.* Amino acid numbers are given in parenthesis. The color intensity is indicative of the level of conservation. The alignment was performed with T-Coffee (www.ebi.ac.uk/Tools/msa/tcoffee/), and the figure was prepared with Jalview 2.7 (www.jalview.org/).

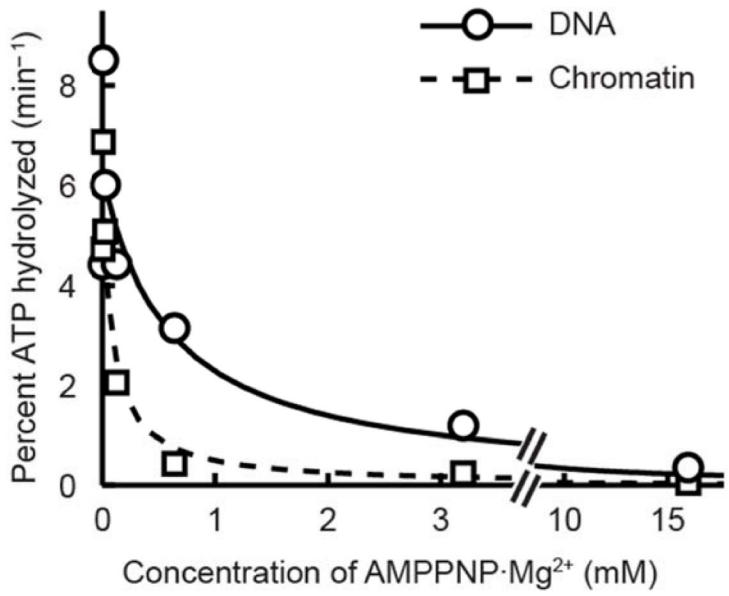

Supplementary Figure 4: The nucleotide affinity increased six-fold if ISWI was bound to chromatin instead of DNA. The affinity of the non-hydrolyzable ATP analog AMPPNP was measured in a competition experiment using ATP hydrolysis as readout. Saturating concentrations of 39-bp duplex DNA (20 µM) or chromatinized plasmid DNA (0.08 mg/mL) were incubated with $ISWI_{FL}$ (80 nM or 10 nM, respectively) and varying concentrations of AMPPNP. The reaction was initiated with 1 µM ATP. The data were fit to a binding isotherm and yielded K_i values of 570 µM (solid line) and 90 µM (dashed line). The affinity for ADP was similarly increased (data not shown). The ~six-fold effect on the K_i was larger than the ~two-fold effect on $K_{M,obs}$ (**Suppl. Table 1**). This discrepancy indicated that the $K_{M,obs}$ values did not directly reflect the affinity for ATP.

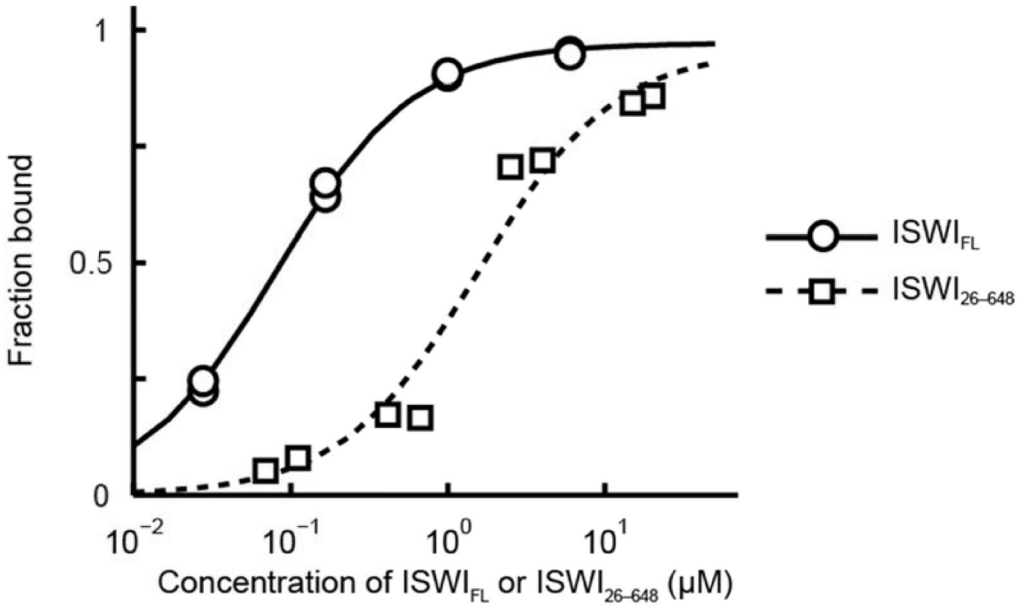

Supplementary Figure 5: Deletion of the HSS domain led to a decreased DNA affinity but did not abolish DNA binding. Binding of trace amounts of duplex DNA to $ISWI_{FL}$ or $ISWI_{26–648}$ was followed in a double-filter DNA binding assay[5]. Lines are fits of the data to a simple binding isotherm yielding K_D = 0.08 μM (solid line) and K_D = 1.6 μM (dashed line).

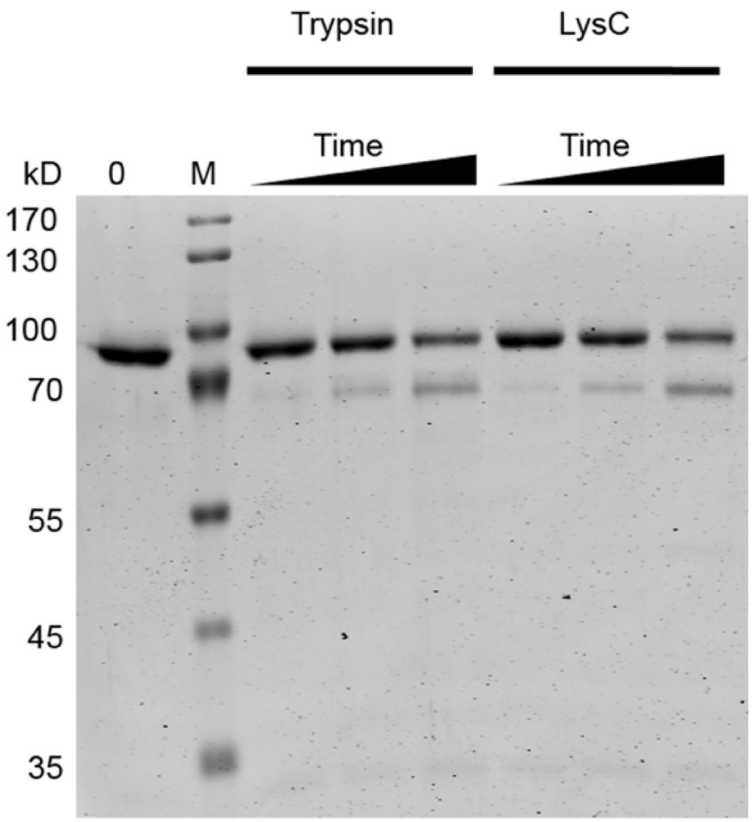

Supplementary Figure 6: Trypsin and LysC cleaved the same residues in DNA-free $ISWI_{26–648}$. Proteolytic fragments of $ISWI_{26–648}$ generated by trypsin and LysC (20 nM and 17 nM, respectively) after 5, 15 and 60 min were separated by SDS-PAGE and stained with Coomassie Blue. The identical mobility of the predominant cleavage products suggested that trypsin cleaved DNA-free $ISWI_{26–648}$ next to a lysine, not an arginine residue. 0: Undigested sample. M: Molecular weight marker.

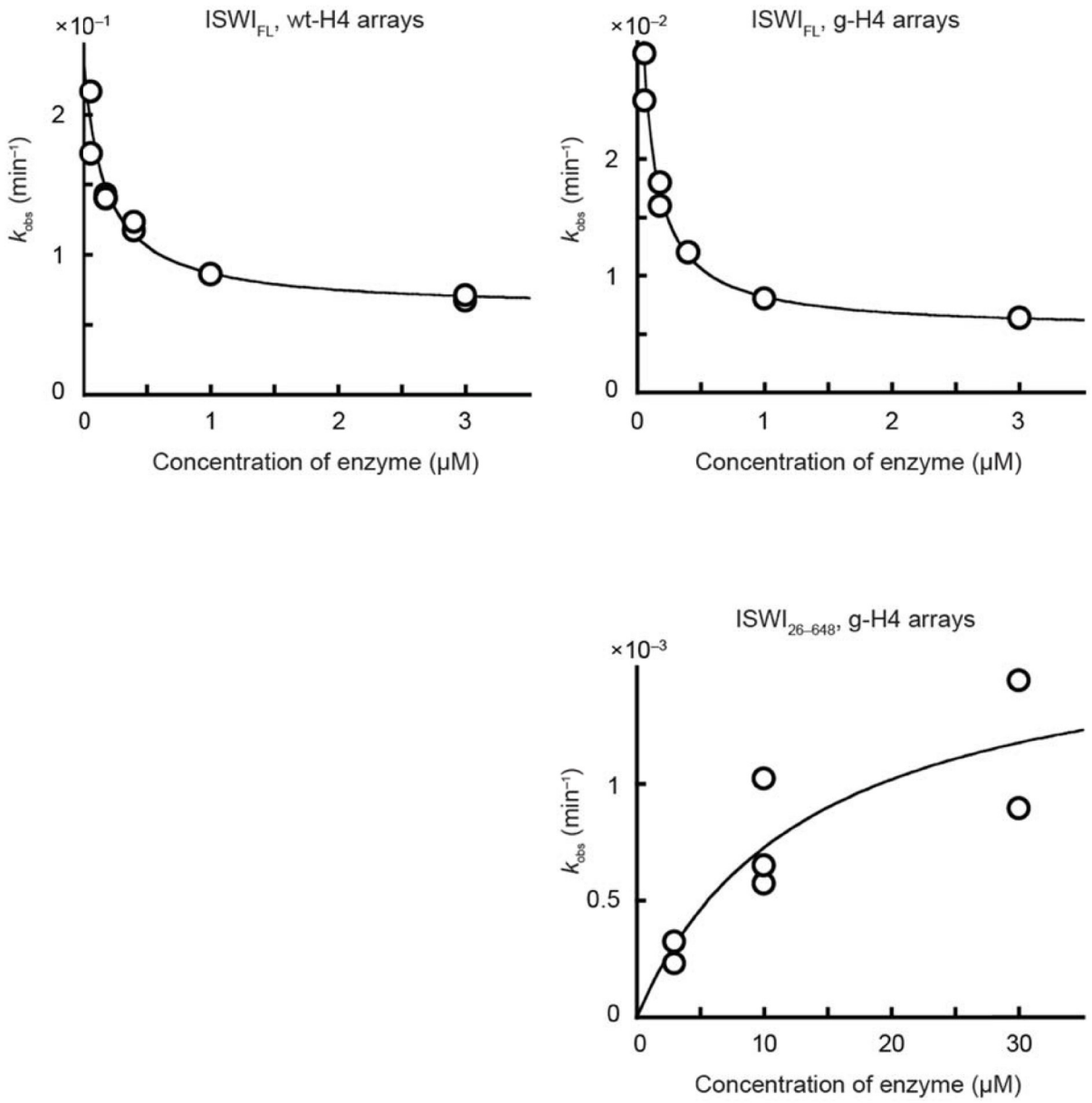

Supplementary Figure 7: Determination of the maximal remodeling velocities of ISWI$_{FL}$ and ISWI$_{26–648}$ on wt-H4 and g-H4 arrays. As described by others, the remodeling activities *decreased* with increasing enzyme concentration for ISWI$_{FL}$ (http://www.epigenesys.eu/; Protocol PROT24). To obtain the maximal remodeling velocities ($k_{obs,max}$) for ISWI$_{FL}$, we corrected for this decrease by fitting the data to inverse binding isotherms (see Methods), extrapolating back to (low) enzyme concentrations where this effect was not present. $k_{obs,max}$ for ISWI$_{26–648}$ remodeling of g-H4 arrays was determined as before (**Fig. 6d**). Data points within each graph were from multiple independent experiments.

Supplementary Tables

Supplementary Table 1: ATPase parameters of $ISWI_{FL}$ and $ISWI_{26–648}$ [a]

		TLC assay	NADH ox. coupled assay		
		$k_{cat}/K_{M,obs}$	$k_{cat}/K_{M,obs}$	$k_{cat,\,obs}$	$K_{M,obs}$
		($M^{-1}\,s^{-1}$)	($M^{-1}\,s^{-1}$)	(s^{-1})	(mM)
$ISWI_{FL}$	DNA	$(3.2 \pm 0.8)\times10^3$	$(1.5 \pm 0.4)\times10^3$	0.22 ± 0.04	0.12 ± 0.03
	NCP	$(5 \pm 2)\times10^4$*	N.d.[b]	1.9 ± 0.8	0.04 ± 0.03[c]
	Chromatin	$(3 \pm 1)\times10^4$	$(3.7 \pm 0.1)\times10^4$	1 to 3[d]	0.05 ± 0.02

		$k_{cat}/K_{M,obs}$[e]
		($M^{-1}\,s^{-1}$)
$ISWI_{26–648}$	DNA	$(4.1 \pm 0.6)\times10^3$
	NCP	$(9 \pm 4)\times10^4$*
	Chromatin	$(7 \pm 5)\times10^4$

[a]: Compared to Table 1 in the main text, a reaction buffer containing a lower Mg^{2+} concentration (1.5 mM) was used to prevent aggregation of chromatin. All reported values were obtained with saturating ligand concentrations. DNA reactions contained a 39-bp DNA duplex (NADH oxidation coupled assay) or 147-bp DNA (TLC assay), NCP reactions nucleosome core particles assembled on the 147-bp Widom-601 sequence, and chromatin reactions 25-mer nucleosomal arrays (TLC assay) or polynucleosomes assembled on plasmid DNA (NADH assay). Where indicated (asterisk), errors are min and max values of two independent measurements. Otherwise, errors are standard deviations of at least three independent measurements.
[b]: N.d.: Not determined.
[c]: Value calculated from $k_{cat,obs}$ and $k_{cat}/K_{M,obs}$.
[d]: Values varied with the enzyme concentration (**Suppl. Fig. 2c**).
[e]: All values measured by the TLC ATPase assay.

Supplementary Table 2: (a) Oligonucleotides[a]; (b) oligopeptides used in the study[b]

	Name	Sequence
a	39-bp DNA duplex	5'-TGCATGTATTGAACAGCGACTCGGGTTATGTGATGGACC
	59-bp DNA duplex	5'-ATACATCCTGTGCATGTATTGAACAGCGACTCGGGTTATGTGATGGACCCTATACGCGG
b	H4 tail peptide	TGRGKGGKGLGKGGAKRHRKVLRD
	Scrambled peptide 1	BGARLDGRKGHGGRLKGKVRGGKK
	Scrambled peptide 2	KLRRGGXGDVKTGKLGGRKAGRGH

[a]: Sequences of only one of the two strands per DNA duplex are shown.
[b]: X indicates an acetylated lysine residue. B stands for the unnatural amino acid *p*-benzoyl-*p*-phenylalanine, which connects to the neighbouring amino acids via a regular peptide bond.

Supplementary Note

Additional scenarios explaining a biphasic ATP concentration dependence of ATP hydrolysis

1) *"ISWI is mostly dimerized in solution under assay conditions and each subunit has a different K_M for ATP."*

   This possibility is ruled out by the observation that DNA-free ISWI is in a monomeric state in solution as measured by multiple angle light scattering by us (data not shown) and by analytical ultracentrifugation by others[2].

2) *"A small fraction of ISWI is dimerized in solution under assay conditions, and the monomer and the dimer have different K_M values for ATP."*

   One would expect that more dimer forms with increasing enzyme concentrations and that the observed reaction velocity would consequently change as well. This expectation is not consistent with experimental results (**Suppl. Fig. 2a,b**).

3) *"ISWI preparations contain contaminating DNA. DNA-free and the DNA-bound ISWI have a different K_M for ATP."*

   Treatment with nucleases and extensive purification of $ISWI_{FL}$ using five consecutive chromatography steps (including size exclusion chromatography in 2 M salt) did not abolish the biphasic behavior seen in Figure 1a. Moreover, we did not observe changes of the biphasic shape upon a jump in the ionic strength of the buffer (from 1.5 mM to 100 mM Mg^{2+}), which should drastically weaken protein-DNA interactions (data not shown). Finally, $ISWI_{1–697}$ and $ISWI_{26–648}$ also exhibited a biphasic response to the ATP concentration (**Fig. 1b** and data not shown) although they intrinsically bound DNA with much weaker affinity than $ISWI_{FL}$ (**Suppl. Fig. 5**).

4) *"Proteolysis fragments of ISWI are present, and they have a different K_M for ATP."*

   The extensive purification discussed above argued against this possibility. Moreover, constructs lacking the entire C-terminus ($ISWI_{1–697}$ and $ISWI_{26–648}$) still showed the biphasic response to variation of the ATP concentration, making it unlikely that the same contaminants were present in all enzyme preparations (**Fig. 1b** and data not shown).

5) *"ISWI possesses a second, allosteric binding site for ATP."*

   Neither structural nor biochemical evidence exists for ISWI or related enzymes to support a second, allosteric binding site.

6) *"A fraction of ISWI is misfolded and therefore nearly inactive".*

   Active site titration experiments with 39-bp long DNA duplexes refuted the possibility that a majority of $ISWI_{26–648}$ was misfolded to the extent that DNA could not bind and stimulate ATP hydrolysis (data not shown). Our active site titration experiments were, however, not sensitive enough to detect a minor fraction of misfolded protein. If this minor fraction were responsible for one or the other catalytic phase of the biphasic ATPase curve, its specific ATPase activity would however be considerable as the following consideration shows. In the biphasic ATPase curve, the

first phase contributed 0.014 s^{-1} and the second phase >0.046 s^{-1} to the amplitude (**Table 1**). If, for example, 10% misfolded, nearly inactive protein were present, its specific activity would be 0.14 s^{-1} (= 10 × 0.014 s^{-1}) or >0.46 s^{-1} (= 10 × 0.046 s^{-1}). These values approach the DNA-stimulated $k_{cat,obs}$ of 0.51s^{-1}. The hypothetical misfolded fraction can therefore not be considered "nearly inactive".

Why can $ISWI_{26–648}$ not distinguish nucleosomes from free DNA in presence of saturating ATP?

The $k_{cat}/K_{M,obs}$ of $ISWI_{26–648}$ was markedly (17- to 23-fold) stimulated by NCPs and nucleosomal arrays relative to DNA (**Fig. 3a,b**) whereas the $k_{cat,obs}$ apparently was not (data not shown). Two scenarios could explain these observations. The first scenario is discussed in the main text. In this scenario, $ISWI_{26–648}$ would recognize the DNA component of the nucleosome, leading to DNA-like stimulation, but most enzyme molecules - at steady-state - would not find the proper site at SHL2. Support for this scenario came from the observation that $ISWI_{26–648}$ could only poorly discriminate between free DNA and nucleosomes even under subsaturating ATP concentrations. $ISWI_{FL}$, on the other hand, was much less prone to unproductive binding because the HSS domain strongly increased the specificity for nucleosomes (**Fig. 3c**).

The second scenario, in contrast, posits that all $ISWI_{26–648}$ molecules bind productively at SHL2 of the nucleosome. Lack of stimulation of $k_{cat,obs}$ therefore cannot be explained by unproductive binding elsewhere on nucleosomal DNA in this model. If true, $K_{M,obs}$ for $ISWI_{26–648}$ would have to decrease by 17- to 23-fold, such that $k_{cat,obs}$ devided by $K_{M,obs}$ would yield a value that is 17- to 23-fold larger relative to DNA. Evidence against this scenario came from steady-state ATPase parameters of $ISWI_{FL}$. The $K_{M,obs}$ of $ISWI_{FL}$ was only modestly decreased (two- to three-fold; **Suppl. Table 1**). Given the high similarity of the ATPase parameters of $ISWI_{FL}$ and $ISWI_{26–648}$, the second scenario seemed unlikely.

Supplementary References

1. Szerlong, H. et al. The HSA domain binds nuclear actin-related proteins to regulate chromatin-remodeling ATPases. *Nat Struct Mol Biol* **15**, 469-76 (2008).
2. Racki, L.R. et al. The chromatin remodeller ACF acts as a dimeric motor to space nucleosomes. *Nature* **462**, 1016-21 (2009).
3. Flaus, A., Martin, D.M., Barton, G.J. & Owen-Hughes, T. Identification of multiple distinct Snf2 subfamilies with conserved structural motifs. *Nucleic Acids Res* **34**, 2887-905 (2006).
4. Aravind, L. & Landsman, D. AT-hook motifs identified in a wide variety of DNA-binding proteins. *Nucleic Acids Res* **26**, 4413-21 (1998).
5. Wong, I. & Lohman, T.M. A double-filter method for nitrocellulose-filter binding: application to protein-nucleic acid interactions. *Proc Natl Acad Sci U S A* **90**, 5428-32 (1993).

2.2 No need for a power stroke in ISWI-mediated nucleosome sliding

Johanna Ludwigsen[1], Henrike Klinker[1,2] and Felix Mueller-Planitz[1]

[1]Adolf Butenandt Institute and [2]Center for Integrated Protein Science Munich,

Ludwig-Maximilians-Universität, Munich, Germany

Published in *EMBO reports*, 14, 1092-1097 (2013);

doi: 10.1038/embor.2013.160

Declaration of contributions

This study was conceived by F. Müller-Planitz and me. I performed all experiments except for the nucleosome sliding experiment shown in Figure 4, which was done by H. Klinker. She also wrote the corresponding materials and methods section and revised the figure legend. The manuscript was written by Felix-Mueller-Planitz and me. Furthermore, I prepared all figures and figure legends.

EMBO reports

TRANSPARENT PROCESS

scientific report

No need for a power stroke in ISWI-mediated nucleosome sliding

Johanna Ludwigsen[1], *Henrike Klinker*[1,2] *& Felix Mueller-Planitz*[1+]

[1]Adolf-Butenandt-Institute, Ludwig-Maximilians-Universität and [2]Center for Integrated Protein Science Munich, Munich, Germany

Nucleosome remodelling enzymes of the ISWI family reposition nucleosomes in eukaryotes. ISWI contains an ATPase and a HAND-SANT-SLIDE (HSS) domain. Conformational changes between these domains have been proposed to be critical for nucleosome repositioning by pulling flanking DNA into the nucleosome. We inserted flexible linkers at strategic sites in ISWI to disrupt this putative power stroke and assess its functional importance by quantitative biochemical assays. Notably, the flexible linkers did not disrupt catalysis. Instead of engaging in a power stroke, the HSS module might therefore assist DNA to ratchet into the nucleosome. Our results clarify the roles had by the domains and suggest that the HSS domain evolved to optimize a rudimentary remodelling engine.

Keywords: ISWI; chromatin remodelling; nucleosome sliding

EMBO *reports* (2013) **14,** 1092–1097. doi:10.1038/embor.2013.160

INTRODUCTION

Nucleosomes are the basic packaging units of chromatin in eukaryotes. By binding tightly to ~146 bp of DNA, they act as physical barriers for the cellular machinery that needs to access the underlying DNA, for example, during transcription, DNA replication and DNA repair. The cell must precisely control the genomic location of nucleosomes to allow for a regulated use of the genetic material in response to different environmental and developmental stimuli.

Mobilizing the nucleosomes is a challenge for the cell as they are inherently stable particles. Dozens of DNA-histone contacts must be broken to rearrange nucleosomes. The cell thus employs dedicated enzymes, so called ATP-dependent nucleosome remodelling factors, to shift the position of nucleosomes along DNA [1]. Remodelling factors of the ISWI and several other families can move nucleosomes along DNA in a process that is termed nucleosome sliding. Elucidating the molecular mechanisms of remodelling enzymes remains a pressing goal.

[1]Adolf-Butenandt-Institute, Ludwig-Maximilians-Universität, Schillerstrasse 44, 80336 Munich, Germany
[2]Center for Integrated Protein Science Munich, Ludwig-Maximilians-Universität, Munich, Germany
[+]Corresponding author. Tel: +089 2180 75 431; Fax: +089 2180 75 425;
E-mail: felix.mueller-planitz@med.uni-muenchen.de

Received 23 July 2013; revised 4 September 2013; accepted 16 September 2013; published online 11 October 2013

Early mechanistic clues came from the observation that all remodelling factors contain ATPase engines that are evolutionary related to DNA helicases [2]. Indeed, many remodellers can translocate on DNA much like helicases do [3–5]. However, unlike helicases, they do not separate the DNA strands. Remarkably, the ATPase domains of several remodellers localize to DNA well within the nucleosome, two helical turns away from the nucleosomal dyad, suggesting that helicase-like translocation of DNA takes place inside the nucleosome [5–9].

DNA translocation within the nucleosome begs the question how DNA enters the nucleosome in the first place. For remodelling by ISWI enzymes, it has been proposed that a conformational change mechanically pulls flanking DNA into the nucleosome [10–13]. The energy required for this conformational change would come from hydrolysis of ATP. A step that uses chemical energy to perform mechanical work is often called a power stroke, a terminology that we adopt herein. The carboxy-terminal DNA-binding domain (DBD) of ISWI, which comprises the HAND, SANT and SLIDE (HSS) domains, would be intimately involved in such a power stroke, as it binds to the DNA that flanks the nucleosome [14]. Notably, recent models propose that the power stroke takes place only after the first 7 bp of DNA have been extruded already from the nucleosome's exit site through the translocase activity of the ATPase domain. The size of the proposed power stroke has been measured to be ≤3 bp [11].

Other data appear to be in conflict but can be reconciled with the power stroke model. We and others have shown that ISWI can remodel nucleosomes even if the HSS module is missing [15,16]. Similarly, the C-terminal DBD of Chd1, composed of a related SANT-SLIDE module [17], is also not required for remodelling [18,19]. Nevertheless, the remodelling activity of ISWI decreases an order of magnitude on deletion or mutation of the HSS module [10,15]. This drop in activity could potentially be attributed to a missing power stroke in the deletion mutants.

Other scenarios, however, can also explain the drop in activity incurred by deletion of the HSS module without invoking a power stroke. As the HSS domain is the nucleosome recognition module [15,20], the ATPase domain lacks sufficient specificity to dock productively to its binding site on the nucleosome. Lack of specificity can result in lower observed ATPase and remodelling activity. This problem becomes especially apparent with saturating concentrations of ATP [15]. In addition, the

removal of the HSS module might allow a polypeptide motif at the C-terminal end of the ATPase domain known as 'bridge' or 'NegC' to inhibit the enzyme by holding the ATPase domain in a catalytically less active conformation [15,16].

Here we explore whether a power stroke operating between the ATPase and HSS module constitutes an important part of the catalytic strategy of *Drosophila* ISWI. As rigidity in the force-transducing regions of the protein is necessary during a power stroke, one can test the functional relevance of the putative power stroke by artificially increasing the flexibility of these enzyme regions [21,22]. To this end, we inserted glycine-serine rich linkers at several strategic locations in the protein. These linkers act like random coils with a high degree of flexibility [23,24]. Surprisingly, ISWI enzymes with these artificial, flexible hinges showed no defect in ATPase, restriction enzyme accessibility-based remodelling and nucleosome sliding assays. These results strongly argue against the power stroke model. We instead conclude that the HSS module assumes a more passive role during catalysis in that it mainly increases the time the ATPase engine can productively engage with the proper binding site on the nucleosome. With regards to how DNA enters the nucleosome, we propose that DNA ratchets into the nucleosome once the tension that builds up by extruding base pairs (bp) from the exit site becomes too large.

RESULTS

To probe for the importance of the putative ATP-dependent power stroke, we inserted glycine- and serine-rich flexible linkers [23,24] into regions of ISWI that could conceivably transmit the force. The 'brace' and 'bridge' at the C-terminal end of the ATPase domain could be such elements, because they intimately contact both ATPase lobes and thus could directly react to the ATPase cycle [2,15,16,19,25]. The connection between the ATPase and HSS modules is another prime candidate, as the force generated by the ATPase domain must reach the HSS module. Force transmitted from the HAND-SANT to the SLIDE domain would have to go through the connecting spacer helix, as no tertiary contacts between SANT and SLIDE exist [20]. We chose altogether four insertion points (Fig 1A). Linker lengths varied between 10 and 20 amino acids. When fully extended, these linkers can reach ~4–8 nm, a significant range considering the size of the proposed power stroke (≤3 bp, equivalent to ≤1 nm; [11]). All ISWI preparations (Fig 1B) were monodisperse as judged by size exclusion chromatography (supplementary Fig S1 online). The monodispersity attests to the overall structural integrity of the enzymes.

The HSS domain has been proposed to communicate to the ATPase domain and modulate its ATP hydrolysis. Mutations in the SLIDE domain, for instance, can allosterically affect ATP hydrolysis [10]. Moreover, nucleosomes no longer stimulate ATP hydrolysis better than naked DNA when the HSS domain is removed with saturating, although not with sub-saturating, concentrations of ATP [15]. We therefore tested if the ISWI derivatives that have a more flexible link between the ATPase and C-terminal domains could efficiently hydrolyse ATP. We used saturating ATP concentrations to measure ATP turnover, and in fact throughout this study, as defects in the function of the HSS domain become maximally apparent under these conditions [15].

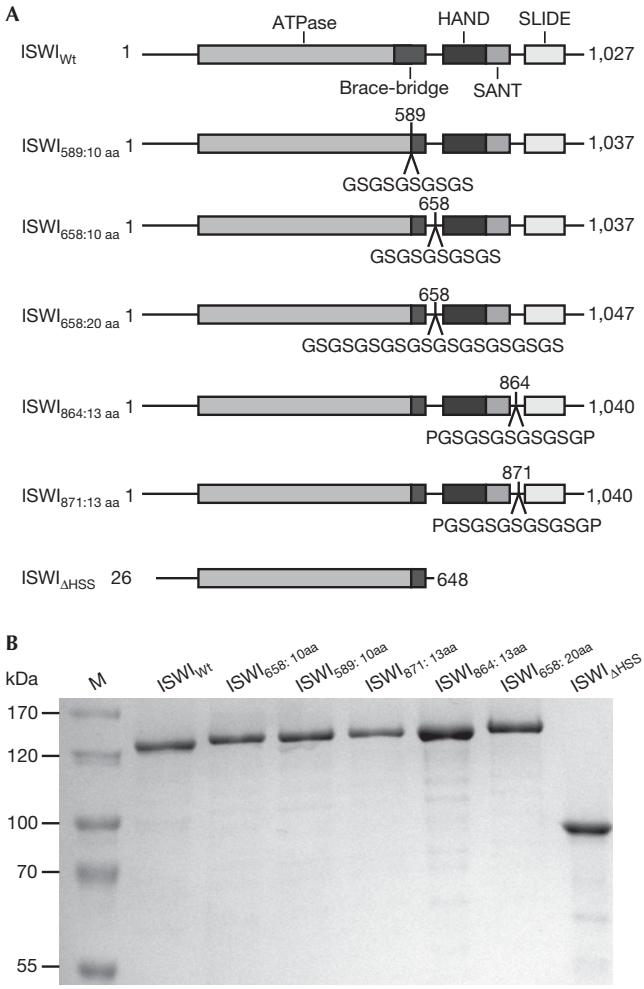

Fig 1 | ISWI derivatives used in this study. (**A**) Schematic representation of ISWI derivatives. Glycine-rich inserts were introduced behind the indicated amino-acid positions. Numbers in subscript refer to the insertion position and the size of the insert. ISWI$_{\Delta HSS}$ spans the amino acids 26–648 and lacks the C-terminal HSS domains. (**B**) Coomassie-stained SDS–PAGE gel showing the purified ISWI derivatives from A. aa, amino acid; HSS, HAND, SANT and SLIDE; SDS–PAGE, SDS–polyacrylamide gel electrophoresis; WT, wild type.

DNA-stimulated ATPase rates of all mutants were indistinguishable from wild-type ISWI (ISWI$_{Wt}$), deviating no more than 1.3-fold (Fig 2). All mutants, just as the wild type, hydrolysed ATP an order of magnitude faster when bound to nucleosomes than to DNA. Importantly, absolute rates for the nucleosome stimulated reaction varied by no more than 1.8-fold between ISWI$_{Wt}$ and all its derivatives. As ATPase rates were largely unaffected, we conclude that the artificial flexible joints did not disrupt the putative communication between the domains and suggest that force transduction is not necessary for efficient ATP hydrolysis. In addition, we conclude that all mutants were properly folded and recognized DNA and nucleosomes like their wild-type counterpart. Indeed, similar concentrations of DNA and nucleosomes saturated the wild type and insertion mutants. For comparison, an order of magnitude higher concentrations

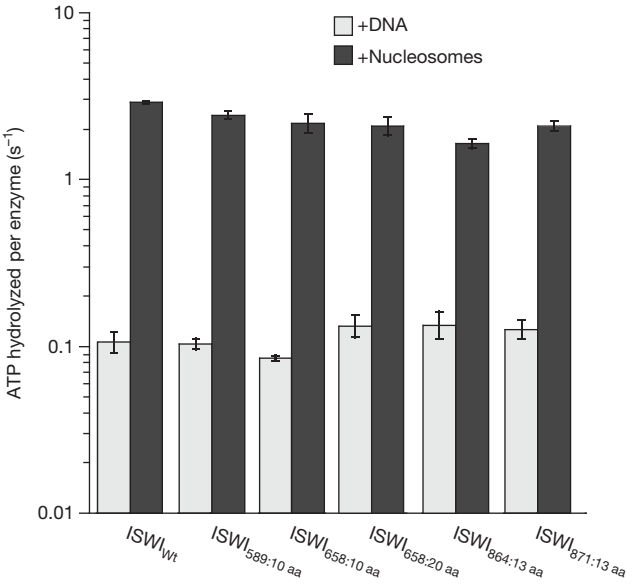

Fig 2 | Insertion of flexible polypeptide linkers does not disrupt DNA- and nucleosome-stimulated ATP hydrolysis. ATPase rates were measured in the presence of saturating concentrations of ATP, DNA or nucleosomes. Errors are s.d. for ISWI$_{Wt}$ ($n=3$) and minimal and maximal values of two independent measurements for all other enzyme derivatives. ATPase rates in the absence of DNA were $<0.02\,s^{-1}$ under otherwise identical conditions (data not shown). ISWI$_{Wt}$, wild-type ISWI.

had to be used to saturate ISWI that completely lacked the HSS domain (ISWI$_{\Delta HSS}$; [15] and data not shown).

The ATPase results do not favour but also do not rule out the power stroke hypothesis. For example, even though the insertion mutants efficiently hydrolysed ATP, a power stroke might be necessary to couple hydrolysis to remodelling. To test this scenario, we performed remodelling assays.

Remodelling leads to exposure of nucleosomal DNA to solvent and can be detected with restriction endonucleases that cut the exposed DNA. We used a quantitative assay that monitors exposure of a unique KpnI site that is occluded by the central nucleosome in a 13-mer nucleosomal array [15]. Rate constants for remodelling (k_{obs}) were determined by measuring exposure of the KpnI site over time and fitting the data to single exponential functions (Fig 3A). Several remodeller concentrations were used to control for possible differences in binding affinities between the ISWI derivatives and the known property of full-length ISWI to inhibit its own catalysis at higher concentrations (Fig 3B) [15].

Unexpectedly, none of the ISWI derivatives containing flexible linkers showed remodelling defects. Used at the same concentration, they all exposed the KpnI site as efficiently as ISWI$_{Wt}$, with k_{obs} differing by no more than a factor of 1.3. For comparison, ISWI$_{\Delta HSS}$ exposed nucleosomal DNA an order of magnitude more slowly (Fig 3C), confirming previous results [15].

As exposed nucleosomal DNA might be an early intermediate during nucleosome sliding, it was important to test if formation of these intermediates was successfully coupled to nucleosome sliding. We monitored sliding in the context of nucleosomal arrays. Each linker DNA contained an exposed AvaI restriction site that became protected upon sliding (Fig 4A) [15].

Surprisingly, but in accordance with the results shown above, all insertion mutants were able to slide nucleosomes over the AvaI sites (Fig 4B). In fact, time courses showed that ISWI$_{Wt}$ and all insertion mutants moved nucleosomes with similar efficiency. As shown before [15], also ISWI$_{\Delta HSS}$ relocated nucleosomes, although higher concentrations and longer incubation times were necessary.

DISCUSSION AND CONCLUSIONS

According to recent mechanistic models, the ATPase engine of ISWI is bound to DNA well within the nucleosome and starts the remodelling process by translocating single bp of DNA in the direction of the exit side of the nucleosome. ATP hydrolysis is required for the transport of each bp. Only after the initial 7 bp of DNA have exited the nucleosome will fresh DNA enter from the opposite side of the nucleosome [10,11]. How DNA enters the nucleosome is unclear.

Prominent models favor a power stroke as a mechanism for how DNA enters the nucleosome [10–13]. At this stage of remodelling, hydrolysis of ATP does not fuel transport of DNA according to these models. Instead, ATP hydrolysis would be coupled to a conformational change between the HSS and ATPase modules. This conformational change exerts force onto the HSS domain and the DNA at the entry site bound by it. Three bp thereby enter the nucleosome (Fig 5A). Subsequently, the ATPase engine resumes transporting single bp toward the exit site [10,11].

In striking opposition to predictions derived from the power stroke model, none of the glycine-rich flexible insertions caused any detectable catalytic defects. Apparently, ISWI can tolerate considerable flexibility between individual domains. Notably, the Bowman lab came to very similar conclusions in a recent study that focused on the related remodelling enzyme Chd1 [26]. We note that inherent flexibility in the remodellers might allow the DBD and ATPase domain of one enzyme molecule to simultaneously contact two neighbouring nucleosomes, a situation that has recently been suggested to be important for remodelling by ISWI enzymes [27].

We were particularly surprised that the 10–20 amino acid long insertions on either side of the brace–bridge polypeptide did not hamper catalysis, as this polypeptide makes intimate contacts with the ATPase domain and was proposed to regulate the enzyme [15,16,19,25]. Depending on whether or not the structure of the brace and bridge is disrupted by the insertions, we can either conclude that this region might be of lesser importance for remodelling than previously hypothesized [16] or that build-up of force is not necessary for proper function of the brace–bridge polypeptide.

If not by a power stroke, how else can flanking DNA enter the nucleosome? We propose that the HSS and ATPase domains work independently of each other with no need for direct coordination during catalysis (Fig 5B). The HSS domain is an important recognition module for the nucleosome [15,20] and is expected to anchor the enzyme to the nucleosome. Anchoring increases the chance for the ATPase engine to productively engage the nucleosome and start with the translocation of DNA. After the first seven translocation steps, the structure of the nucleosome becomes highly strained, particularly around the DNA delimited by the ATPase and HSS module, such that translocation stalls.

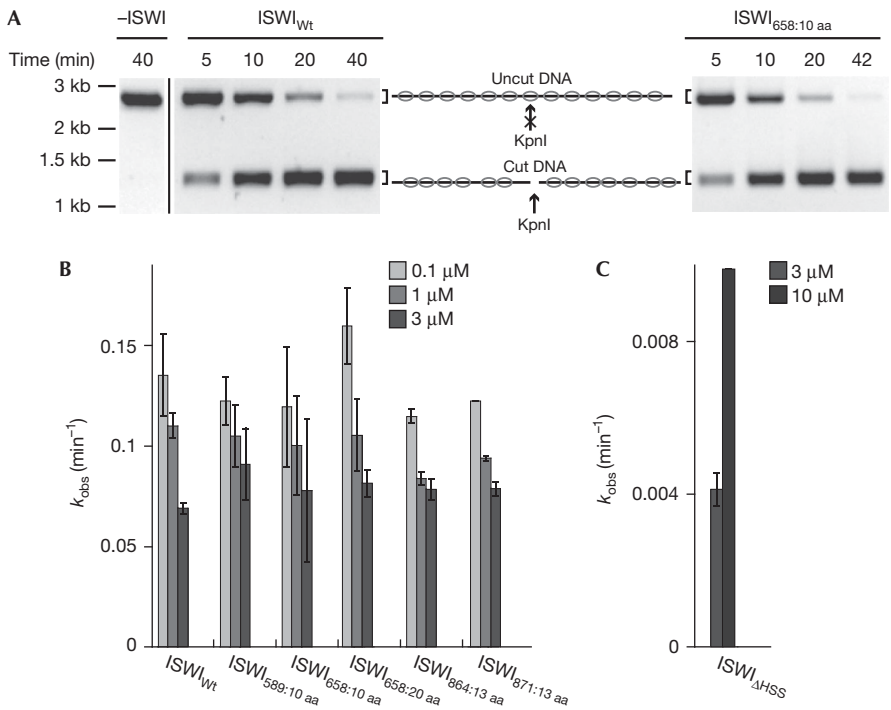

Fig 3 | Insertion of flexible polypeptide linkers does not disrupt nucleosome remodelling. (**A**) Remodelling activity was probed by following the accessibility of a unique, central KpnI restriction site in a 13-mer nucleosomal array (see schematic). Exemplary time courses for remodelling by ISWI$_{Wt}$ and ISWI$_{658:10\ aa}$ (both 3 μM). In mock-treated samples (− ISWI), the KpnI site was not accessible. The original unspliced gel picture containing the mock-treated sample and the ISWI$_{Wt}$ time-course is provided as supplementary Fig S2 online. (**B**,**C**) The observed rate constants for remodelling, k_{obs}, were determined for ISWI derivatives at the indicated concentrations by fitting time courses as in **A** to single exponential functions. Errors are s.d. for ISWI$_{589:10\ aa}$ and ISWI$_{658:10\ aa}$ ($n = 4$ for 0.1 μM and 1 μM; $n = 3$ for 3 μM) and 1 μM ISWI$_{Wt}$ ($n = 3$). In all other instances, minimal and maximal values of two independent measurements are shown. aa, amino acid; ISWI$_{Wt}$, wild-type ISWI; kb, kilobases.

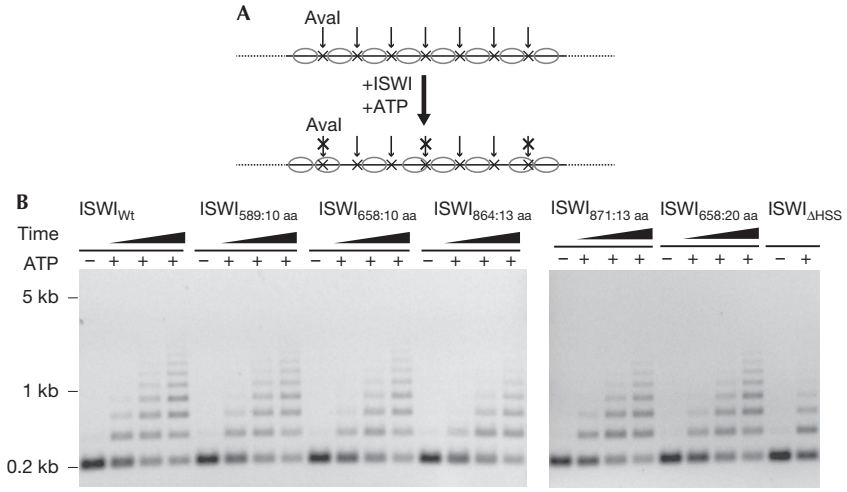

Fig 4 | Insertion of flexible polypeptide linkers does not compromise nucleosome sliding. (**A**) Schematic depiction of the nucleosome sliding assay. 25-mer nucleosomal arrays containing exposed AvaI restriction sites in the linker DNA were used to follow nucleosome sliding. Accessibility to AvaI (arrows) changes upon remodelling. Nucleosomes (ovals) and AvaI sites (x) are indicated. (**B**) ISWI$_{Wt}$ and the insertion mutants were incubated with nucleosomal arrays for 3, 13 and 48 min, whereas ISWI$_{ΔHSS}$ was incubated for 6 h. Control reactions (−) were depleted of ATP with apyrase before addition of ISWI and incubated for 6 h (ISWI$_{ΔHSS}$) or 48 min (all other enzymes). ISWI$_{Wt}$, wild-type ISWI.

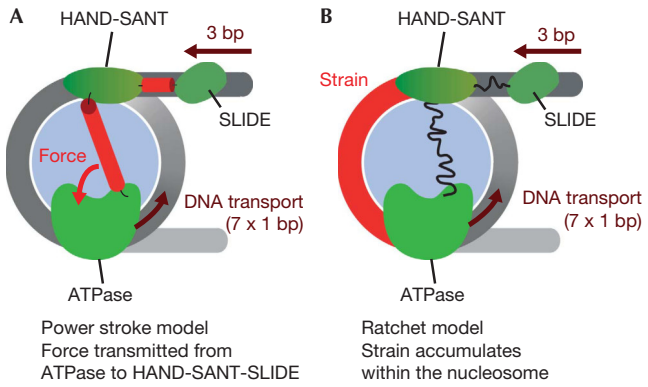

Fig 5 | Models for nucleosome remodelling by ISWI. (**A**) Power stroke model. First, the ATPase engine of ISWI translocates 7 bp of DNA. The ATPase and HSS domains then undergo a power stroke that exerts force on the HSS domains. The power stroke pulls 3 bp of flanking DNA into the nucleosome. Hypothetical force-transducing elements are coloured red. (**B**) Ratchet model. As in **A**, the ATPase engine translocates 7 bp. This translocation strains the structure of the nucleosome, in particular the DNA delimitated by the ATPase and HSS domains (red). When the strain on the nucleosome structure becomes too large, 3 bp of DNA ratchet into the nucleosome. No direct coordination between the HSS and ATPase domain is required for this mechanism and flexible linkage between individual domains (curved lines) does not affect remodelling. Histones are light blue; DNA is grey.

Eventually, the HSS domain loses its grip on the DNA flanking the nucleosome, allowing 3 bp to ratchet in.

Although not part of a power stroke, the HSS module clearly evolved to carry out important functions that collectively optimize remodelling by an order of magnitude [10,15]. Besides established functions such as anchoring the remodeller to the nucleosome and increasing the processivity [10,15], we hypothesize that the HSS module improves catalysis by changing the structure of the nucleosome around the DNA entry site, perhaps by locally separating the DNA from the histone surface [13,28]. Other remodelling subfamilies that do not interact with flanking DNA and therefore cannot engage in a power stroke in the first place might in fact use a similar mechanism [29], pointing to an unified remodelling strategy shared between several remodeller subfamilies.

METHODS

Protein expression and purification. pPROEX-HTb-based expression plasmids with genes encoding *Drosophila melanogaster* $ISWI_{Wt}$ and $ISWI_{\Delta HSS}$ were kindly provided by C. Müller (EMBL, Heidelberg, Germany). All genes were fused amino-terminally to a His_6-TEV tag. Flexible linkers were introduced into $ISWI_{Wt}$ by polymerase incomplete primer extension at the appropriate positions [30]. All ISWI derivatives were fully sequenced. Expression and purification were performed as described [25]. The His_6-TEV tag was cleaved off by TEV protease for all ISWI constructs except for $ISWI_{\Delta HSS}$. Catalytic parameters of $ISWI_{\Delta HSS}$ are unaffected by the presence of the tag [15].

Enzyme assays and enzyme ligands. All assays were performed in 25 mM HEPES-KOH, pH 7.6, 50 mM NaCl, 1 mM $MgCl_2$, 0.1 mM EDTA, 10% glycerol, 0.2 g/l BSA and 1 mM DTT at 26 °C in the presence of an ATP-regenerating system as described [15]. Nucleosomes were reconstituted with recombinant *Drosophila melanogaster* histones by salt-gradient dialysis [31]. The concentration of nucleosomal DNA was determined by measuring its UV absorption at 260 nm. For nucleosomal arrays, concentrations refer to the concentration of individual nucleosomes.

ATP hydrolysis assays. ATP hydrolysis was monitored using an NADH-coupled assay as described [25]. Saturating concentrations of ATP-Mg^{2+} (1 mM), linearized plasmid DNA (pT7blue derivative; 0.2 mg/ml) and nucleosomes reconstituted on the same plasmid DNA (0.1 mg/ml) were used. Saturation was controlled in all cases by titration of the ligand at least over a 16-fold range.

Nucleosome remodelling assay. Remodelling activity was probed as previously described [15] by incubating 13-mer nucleosomal arrays (100 nM) with ISWI derivatives at the indicated concentrations, ATP-Mg^{2+} (1 mM) and KpnI (2 U/μl). Reactions were quenched with SDS (0.4%) and EDTA (20 mM) before the samples were deproteinized and analysed as described [15].

Nucleosome sliding assay. Nucleosome sliding was performed as described [15] by incubation of 25-mer nucleosomal arrays (30 nM) with ATP-Mg^{2+} (0.2 mM) and the respective ISWI derivative ($ISWI_{\Delta HSS}$: 300 nM; all other enzymes: 5 nM). After quenching the reaction with apyrase (2.5 U/μl), arrays were digested with AvaI (1.1 U/μl) at 26 °C for 3–3.5 h. The AvaI digest was terminated with EDTA (40 mM) and SDS (0.4%) before the samples were deproteinized and analysed as described [15].

Supplementary information is available at EMBO *reports* online (http://www.emboreports.org).

ACKNOWLEDGEMENTS

We are grateful to Nadine Harrer for collecting preliminary data, Katharina Braunger and Franziska Henze for help with protein purification, Nicola Hepp for preparation of 13-mer nucleosomal DNA and Gregory D. Bowman and Peter B. Becker for discussions and comments. J.L. thanks the Ernst Schering foundation for granting a predoctoral fellowship. H.K. was supported by a grant of the 'Center for Integrated Protein Science Munich' available to Peter B. Becker. This research was supported by the Deutsche Forschungsgemeinschaft by grant MU3613/1-1 available to F.M.-P.

Author contributions: J.L. and H.K. performed all experiments, interpreted the results and contributed to the manuscript. F.M.-P. conceived the study, interpreted the results and wrote the manuscript.

CONFLICT OF INTEREST

The authors declare that they have no conflict of interest.

REFERENCES

1. Clapier CR, Cairns BR (2009) The biology of chromatin remodeling complexes. *Annu Rev Biochem* **78:** 273–304
2. Flaus A, Martin DM, Barton GJ, Owen-Hughes T (2006) Identification of multiple distinct Snf2 subfamilies with conserved structural motifs. *Nucleic Acids Res* **34:** 2887–2905
3. Saha A, Wittmeyer J, Cairns BR (2002) Chromatin remodeling by RSC involves ATP-dependent DNA translocation. *Genes Dev* **16:** 2120–2134
4. Whitehouse I, Stockdale C, Flaus A, Szczelkun MD, Owen-Hughes T (2003) Evidence for DNA translocation by the ISWI chromatin-remodeling enzyme. *Mol Cell Biol* **23:** 1935–1945
5. Zofall M, Persinger J, Kassabov SR, Bartholomew B (2006) Chromatin remodeling by ISW2 and SWI/SNF requires DNA translocation inside the nucleosome. *Nat Struct Mol Biol* **13:** 339–346
6. Saha A, Wittmeyer J, Cairns BR (2005) Chromatin remodeling through directional DNA translocation from an internal nucleosomal site. *Nat Struct Mol Biol* **12:** 747–755

7. Schwanbeck R, Xiao H, Wu C (2004) Spatial contacts and nucleosome step movements induced by the NURF chromatin remodeling complex. *J Biol Chem* **279:** 39933–39941
8. Dang W, Kagalwala MN, Bartholomew B (2006) Regulation of ISW2 by concerted action of histone H4 tail and extranucleosomal DNA. *Mol Cell Biol* **26:** 7388–7396
9. Dechassa ML, Zhang B, Horowitz-Scherer R, Persinger J, Woodcock CL, Peterson CL, Bartholomew B (2008) Architecture of the SWI/SNF-nucleosome complex. *Mol Cell Biol* **28:** 6010–6021
10. Hota SK, Bhardwaj SK, Deindl S, Lin YC, Zhuang X, Bartholomew B (2013) Nucleosome mobilization by ISW2 requires the concerted action of the ATPase and SLIDE domains. *Nat Struct Mol Biol* **20:** 222–229
11. Deindl S, Hwang WL, Hota SK, Blosser TR, Prasad P, Bartholomew B, Zhuang X (2013) ISWI remodelers slide nucleosomes with coordinated multi-base-pair entry steps and single-base-pair exit steps. *Cell* **152:** 442–452
12. Langst G, Becker PB (2001) ISWI induces nucleosome sliding on nicked DNA. *Mol Cell* **8:** 1085–1092
13. Strohner R, Wachsmuth M, Dachauer K, Mazurkiewicz J, Hochstatter J, Rippe K, Langst G (2005) A 'loop recapture' mechanism for ACF-dependent nucleosome remodeling. *Nat Struct Mol Biol* **12:** 683–690
14. Dang W, Bartholomew B (2007) Domain architecture of the catalytic subunit in the ISW2-nucleosome complex. *Mol Cell Biol* **27:** 8306–8317
15. Mueller-Planitz F, Klinker H, Ludwigsen J, Becker PB (2013) The ATPase domain of ISWI is an autonomous nucleosome remodeling machine. *Nat Struct Mol Biol* **20:** 82–89
16. Clapier CR, Cairns BR (2012) Regulation of ISWI involves inhibitory modules antagonized by nucleosomal epitopes. *Nature* **492:** 280–284
17. Ryan DP, Sundaramoorthy R, Martin D, Singh V, Owen-Hughes T (2011) The DNA-binding domain of the Chd1 chromatin-remodelling enzyme contains SANT and SLIDE domains. *EMBO J* **30:** 2596–2609
18. McKnight JN, Jenkins KR, Nodelman IM, Escobar T, Bowman GD (2011) Extranucleosomal DNA binding directs nucleosome sliding by Chd1. *Mol Cell Biol* **31:** 4746–4759
19. Hauk G, McKnight JN, Nodelman IM, Bowman GD (2010) The chromodomains of the Chd1 chromatin remodeler regulate DNA access to the ATPase motor. *Mol Cell* **39:** 711–723
20. Grune T, Brzeski J, Eberharter A, Clapier CR, Corona DF, Becker PB, Muller CW (2003) Crystal structure and functional analysis of a nucleosome recognition module of the remodeling factor ISWI. *Mol Cell* **12:** 449–460
21. Yildiz A, Tomishige M, Gennerich A, Vale RD (2008) Intramolecular strain coordinates kinesin stepping behavior along microtubules. *Cell* **134:** 1030–1041
22. Hackney DD, Stock MF, Moore J, Patterson RA (2003) Modulation of kinesin half-site ADP release and kinetic processivity by a spacer between the head groups. *Biochemistry* **42:** 12011–12018
23. Evers TH, van Dongen EM, Faesen AC, Meijer EW, Merkx M (2006) Quantitative understanding of the energy transfer between fluorescent proteins connected via flexible peptide linkers. *Biochemistry* **45:** 13183–13192
24. Sahoo H, Roccatano D, Zacharias M, Nau WM (2006) Distance distributions of short polypeptides recovered by fluorescence resonance energy transfer in the 10 A domain. *J Am Chem Soc* **128:** 8118–8119
25. Forne I, Ludwigsen J, Imhof A, Becker PB, Mueller-Planitz F (2012) Probing the conformation of the ISWI ATPase domain with genetically encoded photoreactive crosslinkers and mass spectrometry. *Mol Cell Proteomics* **11:** M111 012088
26. Nodelman IM, Bowman GD (2013) Nucleosome sliding by Chd1 does not require rigid coupling between DNA-binding and ATPase domains. *EMBO Rep* **14:** 1098–1103
27. Yamada K, Frouws TD, Angst B, Fitzgerald DJ, DeLuca C, Schimmele K, Sargent DF, Richmond TJ (2011) Structure and mechanism of the chromatin remodelling factor ISW1a. *Nature* **472:** 448–453
28. Gangaraju VK, Prasad P, Srour A, Kagalwala MN, Bartholomew B (2009) Conformational changes associated with template commitment in ATP-dependent chromatin remodeling by ISW2. *Mol Cell* **35:** 58–69
29. Lorch Y, Maier-Davis B, Kornberg RD (2010) Mechanism of chromatin remodeling. *Proc Natl Acad Sci USA* **107:** 3458–3462
30. Klock HE, Lesley SA (2009) The polymerase incomplete primer extension (PIPE) method applied to high-throughput cloning and site-directed mutagenesis. *Methods Mol Biol* **498:** 91–103
31. Dyer PN, Edayathumangalam RS, White CL, Bao Y, Chakravarthy S, Muthurajan UM, Luger K (2004) Reconstitution of nucleosome core particles from recombinant histones and DNA. *Methods Enzymol* **375:** 23–44

Supplementary Material

No need for a power-stroke in ISWI-mediated nucleosome sliding

Ludwigsen et al., *EMBO reports*, 14, 1092-1097 (2013)

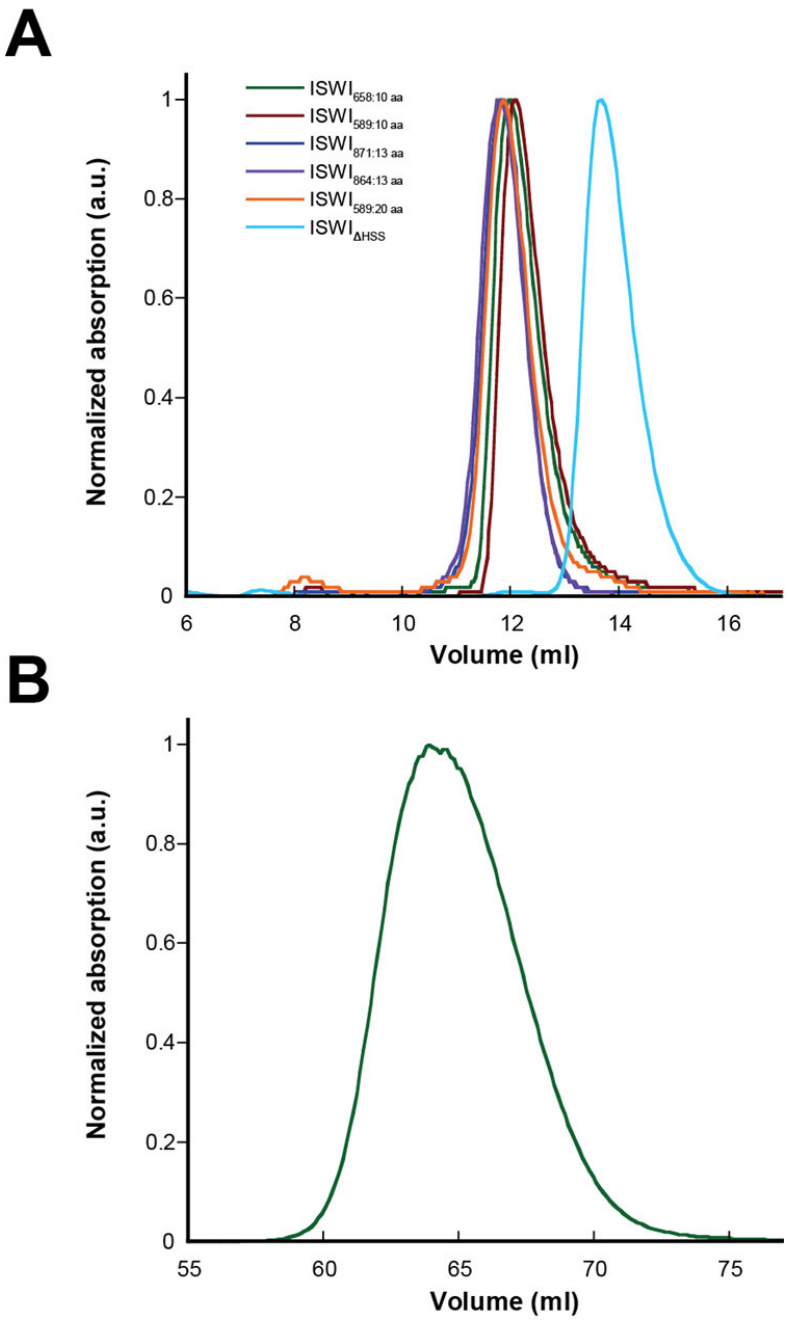

Supplementary Figure 1: Proteins of this study analyzed by size exclusion chromatography (SEC). All proteins were purified by metal affinity and ion exchange chromatography prior to SEC (see Methods). (**A**) ISWI mutants (1 to 1.6 mg of insertion mutants and 3.4 mg of $ISWI_{\Delta HSS}$) were separated over a Superdex 200 10/300 GL column (GE Healthcare). UV absorption was measured at 280 nm except for $ISWI_{\Delta HSS}$ (254 nm) to prevent saturation of the UV detector. (**B**) $ISWI_{Wt}$ (7 mg) was separated over a HiLoad 16/600 Superdex 200 column (GE Healthcare). Absorption was measured at 280 nm. The mobile phase contained 50 mM Hepes-KOH pH 7.6, 0.2 mM EDTA, 200 mM potassium acetate and 1 mM dithiothreitol for all insertion mutants and $ISWI_{Wt,}$ and 25 mM Hepes-KOH pH 7.6, 1.5 mM magnesium acetate, 0.1 mM EDTA, 100 mM potassium chloride, 10% glycerol and 10 mM beta-mercaptoethanol for $ISWI_{\Delta HSS}$.

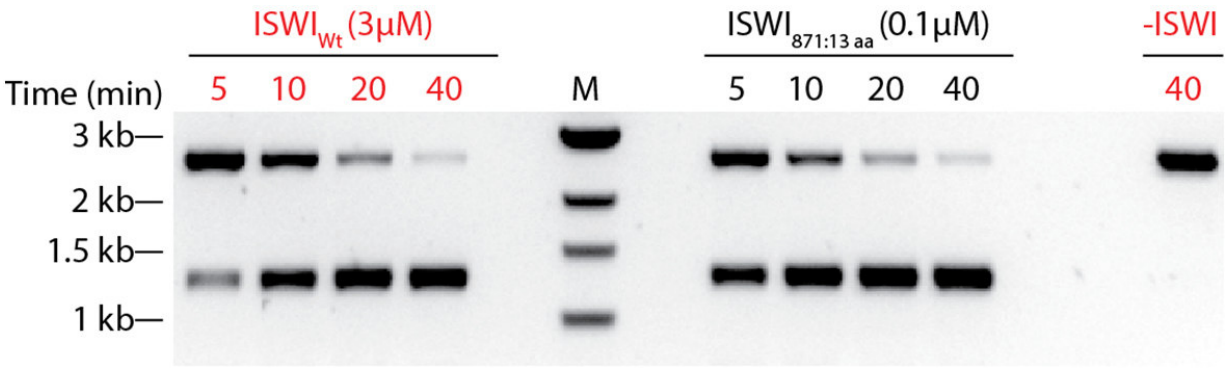

Supplementary Figure 2: Original agarose gel used to generate Figure 3A. Remodeling time courses were obtained for ISWI$_{Wt}$ and ISWI$_{871:13\ aa}$ as explained in Figure 3. Mock-treated sample (-ISWI) served as a control. Red labeled lanes are shown in Figure 3A. M: molecular weight marker; kb: kilobases.

2.3 Concerted regulation of ISWI by an autoinhibitory domain and the H4 N-terminal tail

Johanna Ludwigsen[1], Sabrina Pfennig[1], Ashish Singh[1], Christina Schindler[2,3], Nadine Harrer[1], Ignasi Forné[1], Martin Zacharias[2,3], Felix Mueller-Planitz[1]

[1]Biomedical Center, Ludwig-Maximilians-Universität München, Germany; [2]Technische Universität München, Germany; [3]Center for Integrated Protein Science Munich, Germany

Published in eLife, 6:e21477 (2017)

doi: 10.7554/eLife.21477

Declaration of contributions

This study was conceived by F. Müller-Planitz and me. I performed experiments, analyzed data and prepared the figures with the exceptions listed below. All yeast experiments were performed by A. Singh (Figure 2 and Figure 2 – Figure supplement 1). S. Pfennig crosslinked nucleosomes containing benzophenone-labeled H4 to ISWI and performed the corresponding control experiments (Figure 5A–D, Figure 5 – Figure supplement 1G–J, Figure 5 – Figure supplement 2B,C). C. Schindler performed all *in silico* docking studies (Figure 4F, Figure 4 – Figure supplement 3A–C, Figure 5E). I. Forné performed mass spectrometry measurements and helped with data analysis. N. Harrer helped preparing Figure 7 and all figures involving spectra obtained from mass spectrometry. N. Harrer also helped to analyze mass spectrometry data. The manuscript was written and revised by F. Mueller-Planitz and me. The materials and methods sections were written by the author, who performed the corresponding experiment.

eLIFE elifesciences.org

RESEARCH ARTICLE

Concerted regulation of ISWI by an autoinhibitory domain and the H4 N-terminal tail

Johanna Ludwigsen[1], Sabrina Pfennig[1], Ashish K Singh[1], Christina Schindler[2,3], Nadine Harrer[1], Ignasi Forné[1], Martin Zacharias[2,3], Felix Mueller-Planitz[1]*

[1]Biomedical Center, Ludwig-Maximilians-Universität München, Munich, Germany; [2]Physics Department (T38), Technische Universität München, Munich, Germany; [3]Center for Integrated Protein Science Munich, Munich, Germany

Abstract ISWI-family nucleosome remodeling enzymes need the histone H4 N-terminal tail to mobilize nucleosomes. Here we mapped the H4-tail binding pocket of ISWI. Surprisingly the binding site was adjacent to but not overlapping with the docking site of an auto-regulatory motif, AutoN, in the N-terminal region (NTR) of ISWI, indicating that AutoN does not act as a simple pseudosubstrate as suggested previously. Rather, AutoN cooperated with a hitherto uncharacterized motif, termed AcidicN, to confer H4-tail sensitivity and discriminate between DNA and nucleosomes. A third motif in the NTR, ppHSA, was functionally required in vivo and provided structural stability by clamping the NTR to Lobe 2 of the ATPase domain. This configuration is reminiscent of Chd1 even though Chd1 contains an unrelated NTR. Our results shed light on the intricate structural and functional regulation of ISWI by the NTR and uncover surprising parallels with Chd1.

DOI: 10.7554/eLife.21477.001

***For correspondence:** felix.mueller-planitz@med.uni-muenchen.de

Competing interests: The authors declare that no competing interests exist.

Funding: See page 21

Received: 13 September 2016
Accepted: 20 January 2017
Published: 21 January 2017

Reviewing editor: Jerry L Workman, Stowers Institute for Medical Research, United States

Introduction

Eukaryotic cells package their DNA into chromatin. Chromatin organization allows cells to compact, protect and regulate their genomes. Nucleosomes are the primary building blocks of chromatin. These particles consist of ~150 bp of DNA that wrap almost twice around an octamer of histones. Nucleosomal DNA, however, is not accessible to most nuclear factors. Nature therefore evolved ATP-dependent nucleosome remodeling complexes that can alter the position or the structure of nucleosomes as necessary.

Numerous remodeling complexes with distinct activities are active in any cell. Some move nucleosomes along DNA, eject histones or exchange them for histone variants, and some can even perform several of these activities (***Zhou et al., 2016***). How the various remodelers are regulated in response to cellular needs is not well understood. Several remodelers, for instance, respond to post-translational modifications present on histones (***Swygert and Peterson, 2014***). Others are directly regulated by post-translational modifications (***Kim et al., 2010***) or react to small signaling molecules (***Zhao et al., 1998***). Cells also adjust the subunit composition of remodeling complexes during development (***Lessard et al., 2007***). All these examples indicate exquisite levels of controls exerted over remodeling complexes. The fact that mutations in subunits of human remodeling factors strongly associate with and in some cases drive cancers underscores the necessity to regulate remodeler activity (***Kadoch and Crabtree, 2015***; ***Garraway and Lander, 2013***).

Remodelers of the ISWI family – like most other remodelers – can reposition nucleosomes along DNA in a process termed nucleosome sliding. ISWI's activity is directly regulated by the histone H4 N-terminal tail and by DNA that flanks the nucleosome, so called linker DNA. The regulation

eLife digest In the cells of animals, plants and other eukaryotes, DNA wraps tightly around proteins called histones to form structures known as nucleosomes that resemble beads on a string. When nucleosomes are sufficiently close to each other they interact and clump together, which compacts the DNA and prevents the genes in that stretch of DNA being activated.

But how do cells mobilize their nucleosomes? A nucleosome remodeling enzyme called ISWI can slide nucleosomes along DNA. ISWI becomes active when it interacts with a 'tail' region of a histone protein called H4. However, the H4 tail prefers to interact with neighboring nucleosomes instead of with ISWI. Therefore when ISWI slides a nucleosome close to another one, the H4 tail of the nucleosome binds instead to its new neighbor so that ISWI cannot continue to slide. By this mechanism, ISWI is proposed to pile up nucleosomes, which subsequently compact, leading to the inactivation of this part of the genome.

To investigate how ISWI recognizes the H4 tail, Ludwigsen et al. mapped where the H4 tail binds to ISWI by combining the biochemical methods of cross-linking and mass spectrometry. In addition, mutagenesis experiments identified a new motif in the enzyme that is essential for recognizing the H4 tail. In the absence of the nucleosome, this motif – called AcidicN – works with a neighboring motif called AutoN to keep ISWI in an inactive state. The two motifs also work together to enable ISWI to distinguish between nucleosomes and DNA. Further evidence suggests that other remodeling enzymes have similar regulation mechanisms; therefore this method of controlling nucleosome remodeling may have been conserved throughout evolution.

Further studies are now needed to detect the shape changes that occur in ISWI as it recognizes the histone tail and work out how this leads to nucleosome remodeling. Inside cells, ISWI is usually found within large complexes that consist of many proteins. It therefore also remains to be discovered whether the proteins in these complexes impose additional layers of regulation and complexity on the activity of ISWI.

DOI: 10.7554/eLife.21477.002

imposed by these epitopes has direct consequences for the biological output of ISWI remodelers. By measuring the length of linker DNA, ISWI can generate arrays of evenly spaced nucleosomes (***Lieleg et al., 2015***; ***Yang et al., 2006***; ***Yamada et al., 2011***), a characteristic feature of chromatin. Arrays of nucleosomes can further compact. In the compacted state, the histone H4 N-terminal tail of one nucleosome contacts the acidic patch formed by H2A and H2B of a neighboring nucleosome (***Luger et al., 1997***; ***Dorigo et al., 2004***). This interaction sequesters the H4 tail, which now is no longer available for binding to and stimulating the activity of ISWI. Thus, ISWI's activity on the compacted chromatin would decrease, ensuring the unidirectionality of the reaction. This process is in line with the importance of some ISWI complexes in heterochromatin biology (***Bozhenok et al., 2002***).

How ISWI senses the H4 tail is largely unknown. Evidence points to the ATPase domain of ISWI directly binding the H4 tail (***Racki et al., 2014***; ***Mueller-Planitz et al., 2013***), consistent with the tail directly influencing catalytic reaction steps (***Clapier et al., 2001***; ***Dang et al., 2006***). However, a domain at the C-terminal side of ISWI, the HAND-SANT-SLIDE (HSS) domain, has been implicated in binding the H4 tail as well (***Boyer et al., 2004***; ***Grüne et al., 2003***). Another layer of regulation is imposed by the non-catalytic subunit termed ACF1, which associates with ISWI and sequesters the H4 tail under certain conditions (***Hwang et al., 2014***).

ISWI recognizes amino acids $R_{17}H_{18}R_{19}$ within the H4 tail, which are part of a stretch of amino acids called basic patch (***Fazzio et al., 2005***; ***Hamiche et al., 2001***; ***Clapier et al., 2002***). Notably, ISWI contains an identical motif, here called AutoN. Mutation of AutoN's two arginines to alanines (referred to as 2RA) increased the DNA-stimulated ATPase activity and nucleosome sliding, and suppressed the dependence of ISWI's ATPase and sliding activities on the H4 tail. According to the current model, AutoN directly binds to and blocks the H4-tail binding site, acting as a gatekeeper for the H4 tail. This model necessitates a conformational change of the NTR to allow binding of H4 (***Hwang et al., 2014***; ***Clapier and Cairns, 2012***). Indeed, a conformational change could be traced to AutoN upon nucleic acid binding (***Mueller-Planitz et al., 2013***). Of note, the 2RA mutation

diminished but did not abolish the H4-tail dependency, implicating also other regions in the H4 recognition process (**Clapier and Cairns, 2012**).

The AutoN motif is embedded in a structurally and functionally poorly characterized domain referred to as the N-terminal region (NTR). Besides AutoN, the NTR contains additional motifs: an acidic region that we termed AcidicN, the 'post-post-helicase-SANT-associated' (ppHSA) motif, so named because it follows the post-HSA motif in remodelers of the Snf2 family (**Mueller-Planitz et al., 2013**; **Szerlong et al., 2008**), and a weakly conserved AT-hook (**Mueller-Planitz et al., 2013**; **Aravind and Landsman, 1998**). Their functions remain unknown.

Here, we systematically interrogated the functions of all conserved motifs within the NTR by mutagenesis and a series of quantitative biochemical assays in vitro and in vivo. We paid particular attention to probe for possible crosstalk between these motifs and the H4 tail to understand its recognition process. Using protein crosslinking followed by mass spectrometry and protein structural modeling we obtained information about the general structural architecture of the NTR-ATPase module. With similar approaches, we mapped the H4-tail binding site. We interpret our results within a unified structural and functional framework for the combined inhibition of ISWI by the NTR and recognition of the histone H4 tail. Contrary to current models, we propose that AutoN does not occlude the binding pocket of the H4 tail and that inhibition by AutoN involves a more elaborate mechanism than simple mimicry of the H4 basic patch.

Results

The NTR contains conserved motifs

Multiple sequence alignment of ISWI homologs revealed several sequence motifs in the NTR of ISWI (**Mueller-Planitz et al., 2013**). To assess their degree of conservation we queried the UniProt database for ISWI homologs (**Figure 1—figure supplement 1**). Sequence alignment of these candidates showed conservation of AutoN (**Clapier and Cairns, 2012**) but also indicated that two other motifs, termed ppHSA and AcidicN, were at least as conserved (**Figure 1**). In contrast, an AT-hook (**Aravind and Landsman, 1998**) was poorly conserved. Of note, a separate PSI-BLAST of the NTR of ISWI revealed conservation of ppHSA across multiple families of remodelers, including Snf2, Lsh and Ino80, suggesting shared function (**Figure 1F**). ppHSA and AcidicN have not been characterized so far.

The ppHSA motif is important for structural stability

To study its physiological role, we serially truncated the NTR of Isw1 in *Saccharomyces cerevisiae* (**Figure 2A**) and tested whether these truncation variants complemented a previously characterized growth defect of a yeast triple knockout (TKO) strain lacking three remodelers (*ΔISW1, ΔISW2, ΔCHD1*) at elevated temperatures (**Tsukiyama et al., 1999**). To assess whether complementation was dependent on the expression level, the alleles were placed under the control of synthetic promoters of varying strengths (**Blazeck et al., 2012**). Protein expression levels were measured by Western blot analysis (**Figure 2—figure supplement 1E**).

Expression of none of the N-terminal truncation variants fully complemented the growth phenotype, indicating functional relevance of the NTR in vivo. In contrast, the TKO strain that was complemented with full-length Isw1 grew essentially as well as the *ΔISW2, ΔChd1* double knockout strain (DKO; **Figure 2B**, **Figure 2—figure supplement 1A**). Isw1 variants that lacked the AutoN-AcidicN region in addition to ppHSA grew modestly better than $Isw1_{\Delta ppHSA}$, in line with the general inhibitory nature of AcidicN and AutoN (compare rows 1 and 2 of **Figure 2—figure supplement 1B,C** to the same rows in D; see also below).

We noted a pronounced toxicity of all Isw1 mutants as indicated by slow growth at elevated expression levels (for instance, compare row four with row five in **Figure 2—figure supplement 1B, C,D**). Full-length Isw1, on the other hand, was not toxic at comparable expression levels (**Figure 2—figure supplement 1A**).

Toxicity at high expression levels could be caused by structural instability of the N-terminally truncated Isw1 variants. Indeed, analogous ISWI derivatives from *Drosophila melanogaster* proved difficult to purify (see below), supporting the notion that mutations in the NTR destabilize ISWI structure.

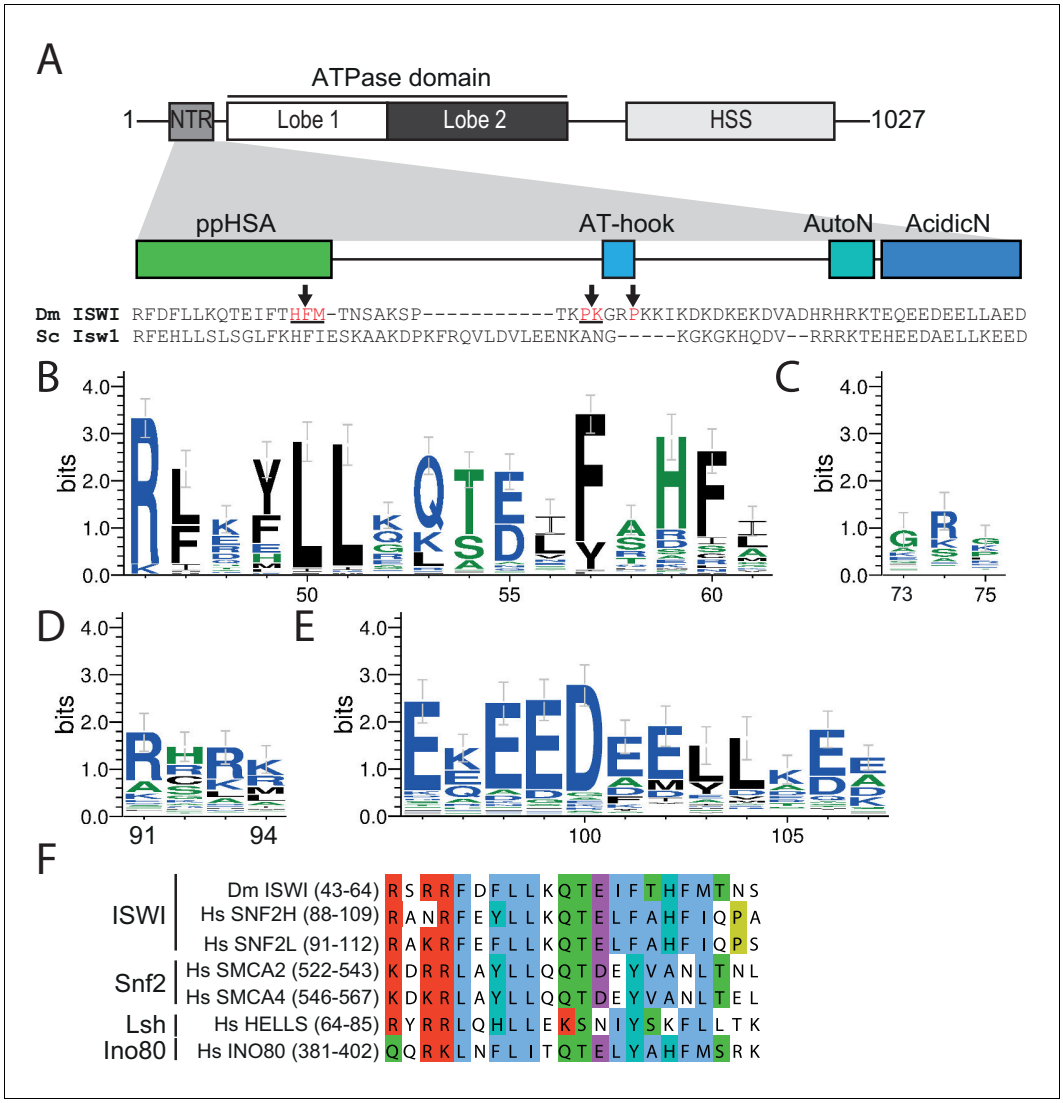

Figure 1. The NTR of ISWI contains several conserved sequence motifs. (**A**) Schematic representation of the ISWI domain composition. The grey inset shows the sequence and motifs of the NTR. Arrows indicate amino acids within the NTR of *Drosophila* ISWI that crosslinked to Lobe 2 of the ATPase domain (***Table 1***). HSS, HAND-SANT-SLIDE domain. (**B–E**) Sequence logos showing the sequence conservation of (**B**) ppHSA, (**C**) AT-hook, (**D**) AutoN, and (**E**) AcidicN. X-Axis values are amino acid positions in *D. melanogaster* ISWI. See ***Figure 1—figure supplement 1*** for full alignment. (**F**) Alignment of the ppHSA motif of *Drosophila* (Dm) ISWI with the human (Hs) ISWI homologs SNF2H and SNF2L and representatives of unrelated remodeler families.

DOI: 10.7554/eLife.21477.003

The following figure supplement is available for figure 1:

Figure supplement 1. Alignment of ISWI homologs from various organisms.

DOI: 10.7554/eLife.21477.004

The ppHSA motif does not substantially contribute to catalysis

Toxicity of the Isw1 NTR deletions precluded a detailed analysis in vivo. Importantly, the in vivo results left open the possibility that NTR-deleted Isw1 was catalytically inactive. We therefore continued to study the function of the NTR motifs in vitro using purified *Drosophila* ISWI proteins.

Although ISWI variants carrying mutations or deletions in the NTR generally expressed well, we failed to purify them using standard protocols. For each ISWI variant, we screened through a variety of expression and purification strategies to improve the yield of soluble protein. The strategies that

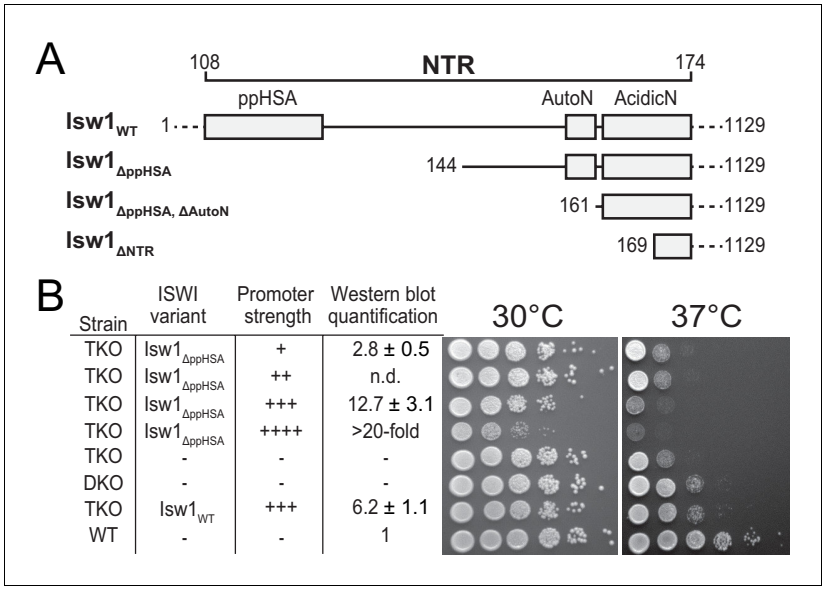

Figure 2. Functional importance of the NTR of yeast Isw1 in vivo. (**A**) Successive N-terminal truncation mutants of Isw1. Note that $Isw1_{\Delta NTR}$ lacked the entire N-terminus up to the first seven residues of AcidicN (***Figure 1E***). (**B**) Complementation assay with $Isw1_{\Delta ppHSA}$. A yeast strain lacking *ISW1, ISW2 and CHD1* (TKO) was transformed with Isw1 derivatives under control of promoters of varying strengths. In comparison to a strain lacking only *ISW2* and *CHD1* (DKO), $Isw1_{WT}$ fully complemented the growth phenotype at elevated temperatures (37˚C). In contrast, $Isw1_{\Delta ppHSA}$ did not complement at any expression level. Results for other Isw1 variants can be found in ***Figure 2—figure supplement 1***. Growth was assessed by spotting tenfold serial dilutions of liquid cultures.

DOI: 10.7554/eLife.21477.005

The following figure supplement is available for figure 2:

Figure supplement 1. Complementation assay with N-terminal truncation variants of Isw1.

DOI: 10.7554/eLife.21477.006

we employed included fusion to solubility tags (Z_2, GB1, NusA, TrxA), fusion to or co-expression of chaperones (trigger factor, GroES/GroEL, DnaK/DnaJ/GrpE) and inclusion of protease sites (3C) at three locations in the NTR to cleave off parts of the N-terminus after purification. The strategies that proved successful are summarized schematically in ***Figure 3—figure supplement 1*** and ***Figure 6—figure supplement 1***.

We first benchmarked the DNA- and chromatin-stimulated ATPase activities of ISWI that lacked ppHSA ($ISWI_{\Delta ppHSA}$) or both ppHSA and AT-hook ($ISWI_{\Delta ppHSA;\ \Delta AT\text{-}hook}$) against the activity of wild-type ISWI ($ISWI_{WT}$). We used saturating ATP and nucleic acid concentrations as indicated by control experiments with varying levels of ligands (***Figure 3—figure supplement 2***). DNA- and chromatin-stimulated ATPase rates of the truncation mutants varied by no more than 1.8-fold from $ISWI_{WT}$ (***Figure 3A,B***) indicating that ppHSA and AT-hook were largely dispensable for ATP hydrolysis and for proper recognition of chromatin.

To evaluate whether ppHSA and AT-hook were required to efficiently couple ATP hydrolysis to nucleosome remodeling, we employed a quantitative remodeling assay. This assay monitors remodeling of a single nucleosome in the context of a 25-mer nucleosomal array by measuring the remodeling-dependent exposure of a unique restriction enzyme site originally occluded by the nucleosome (***Mueller-Planitz et al., 2013***). Time courses of the remodeling reaction were fit to single exponential functions to extract the observed remodeling rate constant k_{obs} (***Figure 3C***; ***Figure 3—figure supplement 3***), which provided us with a quantitative measure to compare the remodeling activities of ISWI and its derivatives.

Remodeling was affected only modestly by deletion of parts of the NTR (3.3- and 1.4-fold for $ISWI_{\Delta ppHSA}$ and $ISWI_{\Delta ppHSA,\ \Delta AT\text{-}hook}$, respectively; ***Figure 3C***). In conclusion, ATPase and remodeling data suggested that both ppHSA and AT-hook are not absolutely required for catalysis in vitro. The

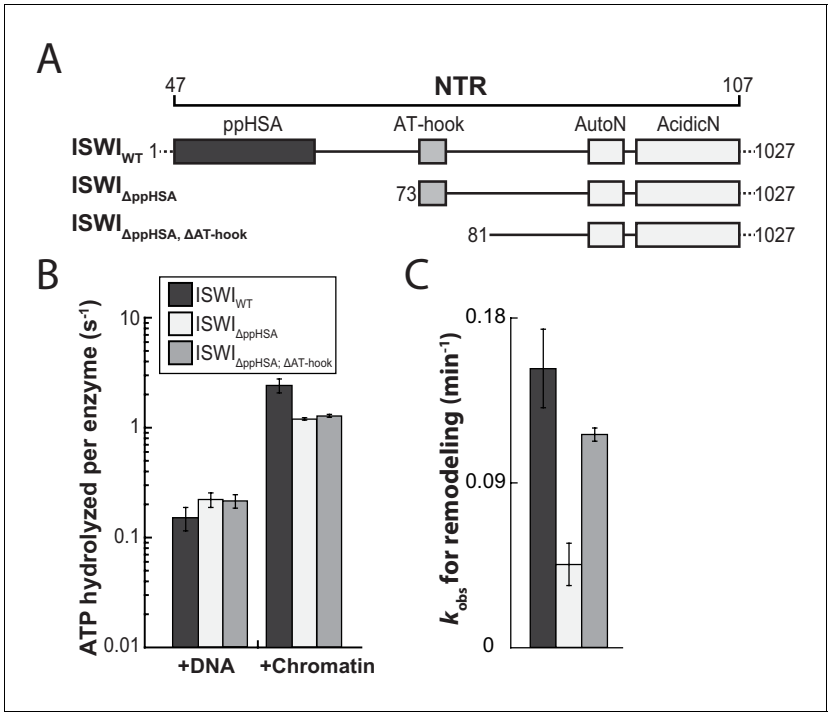

Figure 3. The ppHSA motif is largely dispensable for catalysis. (**A**) N-terminal truncation mutants of *Drosophila* ISWI. (**B**) DNA- and nucleosome-stimulated ATP turnover. ATPase rates were measured in the presence of saturating concentrations of ATP (1 mM), DNA (0.2 g/l) or nucleosomes (0.1 g/l). Errors for nucleosome-stimulated rates of ISWI deletion mutants are minimal and maximal values of two independent measurements, and s.d. for all other measurements ($n \geq 4$). ATPase rates in absence of nucleic acids were <0.022 s^{-1} for all ISWI variants (data not shown). (**C**) Remodeling activity was determined by measuring the accessibility changes of a unique KpnI restriction site in a 25-mer nucleosomal array (100 nM nucleosomes, 300 nM enzyme). Errors are s.d. ($n \geq 3$) except for ISWI$_{\Delta ppHSA; \Delta AT\text{-}hook}$ for which minimal and maximal values of two independent measurements are shown. Raw data of the remodeling assay can be found in ***Figure 3—figure supplement 3***. Color code as in panel **B**.

DOI: 10.7554/eLife.21477.007

The following figure supplements are available for figure 3:

Figure supplement 1. Cloning and purification of N-terminal truncation variants of *Drosophila* ISWI.

DOI: 10.7554/eLife.21477.008

Figure supplement 2. Saturation controls for ISWI$_{WT}$ and ISWI$_{\Delta ppHSA}$ in ATPase assays.

DOI: 10.7554/eLife.21477.009

Figure supplement 3. Determination of the rate constants for remodeling (k_{obs}; ***Figure 3C***) for ISWI$_{WT}$ and N-terminal truncation mutants of ISWI.

DOI: 10.7554/eLife.21477.010

modest decreases in remodeling activities could be due to lower stability of these enzymes (see above).

The NTR contacts Lobe 2 of the ATPase domain

We speculated that the NTR might stabilize the structure of ISWI by adopting a similar configuration as the two chromo domains of the related remodeler Chd1. Like the NTR, the chromo domains are located directly N-terminal to the ATPase module. Notably, they bridge over and pack against the second ATPase lobe, presumably locking the ATPase in an inactive state (***Figure 4A***) (***Hauk et al., 2010***).

To explore, we first determined the binding interface of the chromo domains (amino acids 239–284) on Lobe 2 of the ATPase module using the PISA algorithm (www.ebi.ac.uk/pdbe/pisa/) and visualized the analogous surface on a homology model of ISWI (***Figure 4B***; cyan). We then site-specifically inserted the UV-crosslinking amino acid *p*-benzoyl-*p*-phenylalanine (abbreviated Bpa or B)

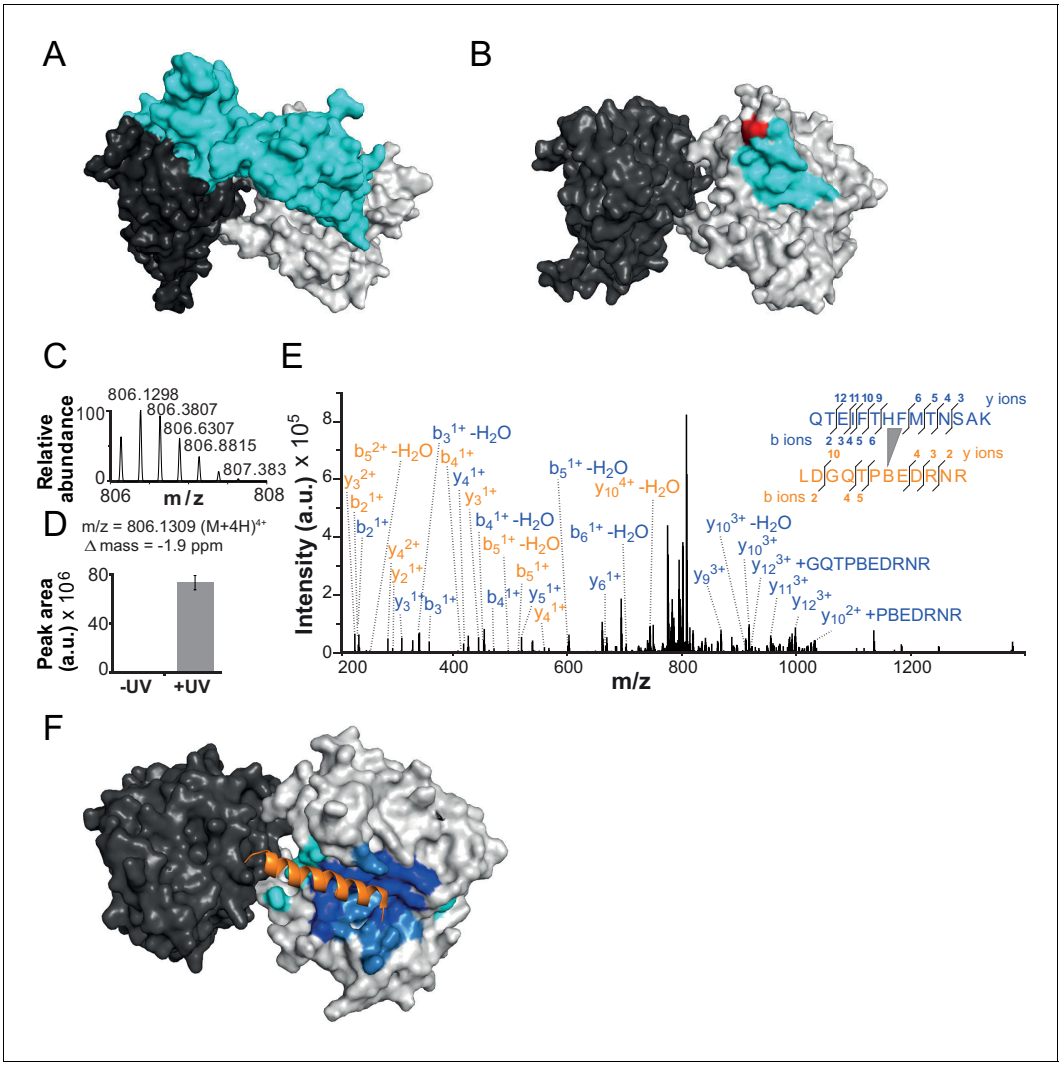

Figure 4. The NTR contacts Lobe 2 of the ATPase domain. (**A**) Surface representation of the Chd1 crystal structure (PDB code 3MWY) (***Hauk et al., 2010***). ATPase Lobe 1 and 2 are colored dark and light grey, respectively, and the N-terminal chromo domains cyan. (**B**) Homology model of the ISWI ATPase domain (***Forné et al., 2012***). Cyan: hypothetical binding interface of the ISWI NTR (see main text), red: position of Bpa substitution (H483). (**C–E**) Mass spectrometric validation of the crosslink XL1 (***Table 1***) formed between Bpa at position 483 and an NTR peptide. (**C**) Isotopic distribution of the crosslinked peptide. (**D**) UV-dependent increase of the signal for the crosslinked peptide. Extracted ion chromatograms of the ions were used for the quantification. (**E**) High resolution, high accuracy MS2 fragmentation spectrum. Top right: summary of observed product ions mapped onto the sequence of the crosslinked peptide. B: Bpa. (**F**) Predicted docking interface of AcidicN (blue and dark blue), AutoN (cyan and dark blue) and overlapping regions (dark blue) in the structural model of ISWI. The predicted interface for AcidicN overlaps with the interface for the acidic helix of the N-terminal chromo domains of Chd1 (orange) (***Hauk et al., 2010***).

DOI: 10.7554/eLife.21477.011

The following figure supplements are available for figure 4:

Figure supplement 1. The effect of the H483B mutation on chromatin remodeling.

DOI: 10.7554/eLife.21477.012

Figure supplement 2. Validation of additional crosslinks detected in the $ISWI_{H483B}$ dataset.

DOI: 10.7554/eLife.21477.013

Figure supplement 3. Structural predictions of NTR elements.

DOI: 10.7554/eLife.21477.014

into this hypothetical binding interface in ISWI (H483B; ***Figure 4B***, red) using established strategies (***Forné et al., 2012***; ***Chin et al., 2002***).

We first tested whether mutagenesis of H483 impacted catalysis. The H483B mutation diminished the DNA- and chromatin-stimulated ATPase activity of full-length ISWI by fourfold each, a result that may not be surprising given that the mutation is located in the conserved 'block D' of Snf2 ATPases (***Flaus et al., 2006***) (***Figure 6—figure supplement 4***). Importantly, the remodeling activity of $ISWI_{H483B}$ was reduced to a similar degree (threefold), indicating that the efficiency of remodeling per hydrolyzed ATP was unchanged (***Figure 4—figure supplement 1***). We conclude that $ISWI_{H483B}$, albeit hydrolyzing ATP more slowly than $ISWI_{WT}$, efficiently coupled ATP hydrolysis to chromatin remodeling, which suggested that the mutant remained structurally largely intact. Also, auto-regulation of $ISWI_{H483B}$ by its NTR was unperturbed because mutagenesis of the NTR had analogous effects on $ISWI_{WT}$ and $ISWI_{H483B}$ (see below), further justifying the use of $ISWI_{H483B}$ for crosslinking experiments.

Crosslinking of full-length $ISWI_{H483B}$ was induced by UV irradiation, and the crosslinks were mapped by high accuracy mass spectrometry (MS) (***Forné et al., 2012***; ***Mueller-Planitz, 2015***). Remarkably, $ISWI_{H483B}$ crosslinked to several positions in the NTR within or adjacent to the ppHSA motif (***Figure 1A***, arrows; ***Figure 4C–E***; ***Figure 4—figure supplement 2***; ***Table 1***). We independently replicated these crosslinking results with a truncated form of ISWI ($ISWI_{26\text{-}648}$), which lacked the HSS domain and non-conserved N-terminal amino acids (data not shown).

In our previous work, we incorporated Bpa in a variety of places on Lobes 1 and 2 of the ATPase domain but never observed crosslinks to the NTR (***Forné et al., 2012***; ***Mueller-Planitz, 2015***). We therefore suggest that the ppHSA motif specifically docked to a location in proximity of amino acid 483 in Lobe 2. Docking of the NTR against Lobe 2 may be necessary for the structural integrity of ISWI-type remodelers (see above). The presence of ppHSA in other remodelers (Snf2, Lsh and Ino80; ***Figure 1F***) predicts similar functions beyond the ISWI family.

If the NTR is structurally close to Lobe 2 of the ATPase module, AutoN and the neighboring AcidicN motif may also be able to contact Lobe 2. To explore this idea, we performed in silico docking studies to predict the binding site of AutoN and AcidicN. We carried out three independent docking runs to model the interaction of Lobe 2 with AutoN, AcidicN and AutoN-AcidicN, respectively (see Materials and methods for details). All three *ab initio* docking runs yielded a large cluster of models that identified the preferred binding site for AutoN and AcidicN (***Figure 4F***; ***Figure 4—figure supplement 3A***). Docking of scrambled peptides as a control partially diminished the preference for this binding pocket (data not shown). Docking of AutoN-AcidicN against a homology model comprising both ATPase lobes gave very similar results, suggesting specificity of the motifs for binding to Lobe 2 (***Figure 4—figure supplement 3B***). We validated the docking results by mutagenesis further below.

Strikingly, AcidicN, which is predicted to be α-helical (***Figure 4—figure supplement 3C,D***), contacted Lobe 2 precisely where an acidic helix of the chromo domains of Chd1 bound (***Hauk et al., 2010***), which suggested conservation of this binding mode. Based on our results, we propose the

Table 1. Overview of crosslinks formed by $ISWI_{H483B}$.

			Bpa peptide		Target peptide	
ID	Mass (D a)	Error (ppm)	Sequence[*,†]	Site	Sequence[†]	Site
XL1	3220.4946	−1.9	LDGQTPBEDRNR	483	QTEIFTHFM^{ox}TNSAK[‡]	59–60
XL2	3204.5056	−3.7	LDGQTPBEDRNR	483	QTEIFTHFMTNSAK[‡]	60–61
XL3	2950.3474	−1.0	LDGQTPBEDR	483	QTEIFTHFM^{ox}TNSAK[‡]	55–59
XL4	2934.3571	−2.6	LDGQTPBEDR	483	QTEIFTHFMTNSAK[‡]	59–61
XL5	2207.0968	+0.2	LDGQTPBEDRNR	483	SPTKPK[‡]	69–72
XL6	1936.9645	−6.1	LDGQTPBEDR	483	SPTKPK[‡]	71–72
XL7	1736.8594	−6.1	LDGQTPBEDR	483	GRPK	75

[*]B symbolizes Bpa.

[†]Crosslinked amino acids are underlined; [ox]indicates oxidized methionine (+15.9949 Da).

[‡]Precise attachment sites not distinguishable from data.

DOI: 10.7554/eLife.21477.015

NTR to adopt a structural architecture akin to the chromo domains of Chd1 (***Figure 4A***) despite complete lack of sequence conservation between the two.

The H4 tail binds Lobe 2 adjacent to AutoN-AcidicN

Due to sequence similarity, the H4 tail and AutoN may compete for the same binding site (***Hwang et al., 2014***; ***Clapier and Cairns, 2012***). We thus set out to identify the H4-tail binding pocket within ISWI and compare it to the predicted AutoN interaction surface.

We adopted two complementary crosslinking approaches. First, we used two different H4-tail peptides, which carried a Bpa moiety either at amino acid 1 or 10 (T1B and L10B peptides, respectively), and bound these peptides to $ISWI_{26-648}$ in the presence of DNA (***Mueller-Planitz et al., 2013***). After irradiation, a lower-mobility band was detected by SDS-PAGE, which suggested successful crosslinking (***Figure 5—figure supplement 1A,E***). We mapped several crosslinks of the H4 peptides to Lobe 2 by MS (***Figure 5—figure supplement 1A–F***; ***Table 2***). Control experiments showed that the T1B H4 peptide stimulated the ATPase activity like a wild-type H4 peptide (***Figure 5—figure supplement 2A***).

Because the peptides may not exclusively bind ISWI in the physiological binding pocket, we pursued a second approach. We reconstituted entire nucleosomes bearing a photo-reactive benzophenone on the N-terminal tail of H4. Benzophenone labeling was achieved by chemical modification of single cysteine mutants of H4 (T1C and L10C). These nucleosomes bound to full-length ISWI and stimulated its ATPase activity like wild-type nucleosomes (***Figure 5—figure supplement 2B,C***) suggesting that they were properly recognized by the remodeler. UV-irradiation of full-length ISWI bound to benzophenone-labeled T1C nucleosomes retarded the mobility of the remodeler during SDS-PAGE, indicative of successful crosslinking (***Figure 5A***). MS analysis mapped a crosslink to Lobe 2 of ISWI (***Figure 5B–D***). We repeated these crosslinking experiments with the human ISWI homolog SNF2H. Both T1C- and L10C-labeled nucleosomes crosslinked to Lobe 2 of SNF2H (***Figure 5—figure supplement 1G–J***). In summary, two very different crosslinking approaches, one employing Bpa-containing peptides and one using benzophenone-derivatized nucleosomes, consistently yielded crosslinks between the H4 tail and Lobe 2 of the ATPase domain. ***Table 2*** lists all crosslink candidates, classified in terms of their reliability (see Materials and methods). Notably, methionine residues were overrepresented as targets of the photo-crosslinking approach, consistent with the known preference of benzophenones for methionine (***Wittelsberger et al., 2006***). In summary, our data strongly indicated the H4-tail binding site to reside on or close to Lobe 2.

To identify the H4-tail binding pocket we turned to crosslink-guided in silico docking of the H4-tail peptide. We only used the five crosslinks for this analysis that passed stringent quality controls (***Table 2***, high reliability; see also Materials and methods). The predicted docking interface is

Table 2. Overview of H4-tail mediated crosslinks.

						H4 peptide		Remodeler peptide	
ID	Reliability	H4	Remodeler construct	Mass (Da)	Error (ppm)	Sequence*	Site	Sequence†	Site
XL11	high	nucleosomal	$ISWI_{WT}$	2034.8571	−0.2	XGR	1	QIQEFN<u>M</u>DNSAK	495
XL12	high	nucleosomal	SNF2H	2251.9753	−0.4	GXGK	10	VLDILEDYC<u>M</u>WR	520
XL13a	high	peptide	$ISWI_{26-648}$	1648.7601	−0.4	BGR	1	LDGQT<u>P</u>HEDR	482
XL13b	high	peptide	$ISWI_{26-648}$	1918.9052	−0.9	BGR	1	LDGQT<u>P</u>HEDRNR	482
XL13c	high	peptide	$ISWI_{26-648}$	3340.5374	−2.8	BGR	1	LDGQT<u>P</u>HEDRNRQIQEFNMDNSAK	482
XL14	medium	nucleosomal	SNF2H	2222.9624	−1.5	XGR	1	VLDILEDY<u>CMWR</u>‡	519–22
XL15	medium	peptide	$ISWI_{26-648}$	1257.6261	+2.3	BGR	1	<u>M</u>VIQGGR	578
XL16	medium	peptide	$ISWI_{26-648}$	1424.7832	−3.9	BGR	1	IVE<u>R</u>AEVK	568
XL17	medium	peptide	$ISWI_{26-648}$	1453.7998	−4.6	GBGK	10	IVE<u>R</u>AEVK	568

*B symbolizes Bpa; X symbolizes Benzophenone-labeled cysteine.

†Crosslinked amino acids are underlined.

‡Precise attachment sites not distinguishable from data.

DOI: 10.7554/eLife.21477.016

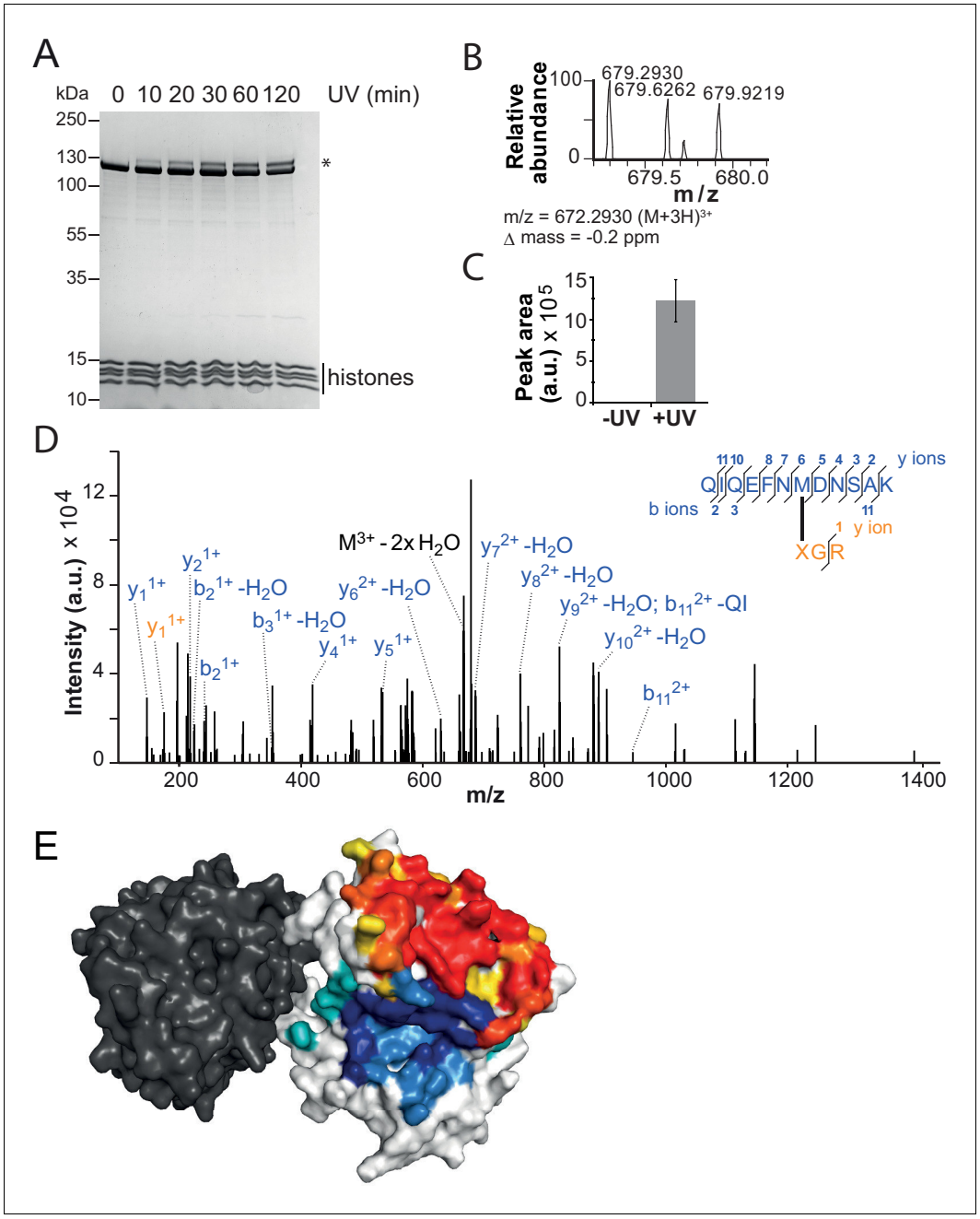

Figure 5. The binding sites of the NTR and the H4-tail on Lobe 2 are proximal. (**A–D**) Crosslinking of nucleosomes containing benzophenone-labeled H4 to ISWI. (**A**) Crosslinking time course analyzed by SDS-PAGE and Coomassie staining. The asterisk marks a UV-irradiation dependent band of lower mobility containing the crosslink mapped in **B–D**. (**B–D**) Mapping and validation of a crosslink (XL11; ***Table 2***) formed in the upshifted band in **A**. Isotopic distribution of the crosslinked peptide, MS2 spectrum and quantification as in ***Figure 4***. (**E**) Crosslink-guided in silico docking of an H4 peptide (amino acids 1–20) to ISWI. The predicted docking interface of the H4 tail on Lobe 2 is illustrated in a yellow and red color scale, which indicates low to high contact probabilities between the docked H4 tail and Lobe 2. The contact probabilities were calculated from a family of 383 docked structures (see Materials and methods). For comparison, the predicted docking interface of the NTR is shown in shades of blue (see ***Figure 4F***).

DOI: 10.7554/eLife.21477.017

The following figure supplements are available for figure 5:

Figure 5 continued on next page

Figure 5 continued

Figure supplement 1. Additional crosslinks between the H4 tail and ISWI or SNF2H.
DOI: 10.7554/eLife.21477.018

Figure supplement 2. Controls for possible adversary effects of covalent modifications of the H4 tail.
DOI: 10.7554/eLife.21477.019

Figure supplement 3. Surfaces on Lobe 2 that were sampled by selected amino acids in the H4 tail during crosslink-guided structural docking.
DOI: 10.7554/eLife.21477.020

visualized in ***Figure 5E*** and ***Figure 5—figure supplement 3***. Note that not all lower quality crosslinks were compatible with this binding mode, possibly because the H4-tail peptide bound flexibly or in multiple binding modes (***Racki et al., 2014***). Some of these modes may not be strongly populated or functionally active as crosslinking can in principle trap fleeting intermediates. We also cannot rule out false positives among the lower quality candidates.

AcidicN helps ISWI to recognize chromatin

Interestingly, the predicted docking interface of AcidicN was in close proximity to the H4-tail interface. This prompted us to investigate the function of AcidicN and – in the following section – its potential involvement in the H4-tail recognition process.

To study its function, we replaced three or six negatively charged amino acids in AcidicN by uncharged ones using conservative E to Q and D to N mutations. These mutants were denoted $ISWI_{+3}$ and $ISWI_{+6}$ respectively (***Figure 6A***). To improve solubility, $ISWI_{+6}$ was fused to a solubility tag (Z_2-tag; ***Figure 6—figure supplement 1***). Control experiments ruled out interference of the Z_2-tag on catalytic properties of ISWI (***Figure 6—figure supplement 2A,B***).

Of note, the +3 and+6 mutants had a strongly deregulated ATPase, hydrolyzing ATP markedly faster than $ISWI_{WT}$ when presented with saturating amounts of naked DNA. In fact, DNA-stimulated ATPase rates of $ISWI_{+6}$ reached values of nucleosome-stimulated $ISWI_{WT}$ rates. Also its basal ATPase activity was strongly (20-fold) upregulated compared to $ISWI_{WT}$ (***Figure 6B***; ***Figure 6—figure supplement 3A,B***). To rule out that co-purifying contaminating ATPases overwhelm the ATPase signal, we combined the +6 mutation with a point mutation in the ATPase that abrogates ATPase activity (E257Q). ATP hydrolysis and remodeling were negligible for $ISWI_{+6;\ E257Q}$, providing strong evidence against this possibility (***Figure 6—figure supplement 2B,C***).

In contrast to the DNA-stimulated reaction, nucleosome-stimulated ATPase and remodeling activities were comparable between the AcidicN mutants and $ISWI_{WT}$ (***Figure 6B,C***). Taken together, these results indicated that the AcidicN mutants were not simply hyperactive, but misregulated instead. More specifically, mutation of AcidicN prevented ISWI from properly recognizing whether chromatin was bound and led to futile ATP hydrolysis in the absence of chromatin.

To independently test this conclusion and to further validate the usefulness of the H483B mutant used further above, we combined the H483B and AcidicN mutations (***Figure 6—figure supplement 4***). DNA-stimulated ATP hydrolysis was strongly upregulated in the $ISWI_{+3;\ H483B}$ and $ISWI_{+6;\ H483B}$ double mutants relative to the $ISWI_{H483B}$ single mutant and reached levels of the chromatin-stimulated reaction. These data closely paralleled and therefore independently validated our results obtained with $ISWI_{+3}$ and $ISWI_{+6}$. We conclude that AcidicN regulates $ISWI_{WT}$ and $ISWI_{H483B}$ in a very similar fashion, further justifying the use of $ISWI_{H483B}$ for crosslinking experiments above.

To validate the predicted binding interface of AcidicN on Lobe 2 and to further probe the functionality of this interaction, we introduced mutations in Lobe 2. We selected three positively charged residues for mutagenesis, K403, R458 and R508, which are predicted to participate in docking to the negatively charged AcidicN motif (***Figure 7A***; ***Figure 7—figure supplement 1***). Charge-reversal of these residues would be expected to weaken docking of AcidicN to Lobe2 and – in the simplest case – phenocopy the effects of the mutation of AcidicN. Indeed, the interface mutants had a strongly upregulated DNA-stimulated ATPase activity whereas chromatin-stimulated ATP turnover and nucleosome remodeling were largely unaffected (***Figure 7B,C***; ***Figure 7—figure supplement 2***). The interface mutants therefore behaved just like the AcidicN mutants discussed above. A control mutant ($ISWI_{R486;\ 488D}$), carrying amino acid substitutions just outside of the predicted AcidicN binding interface, however, retained its ability to discriminate chromatin over DNA in the ATP hydrolysis

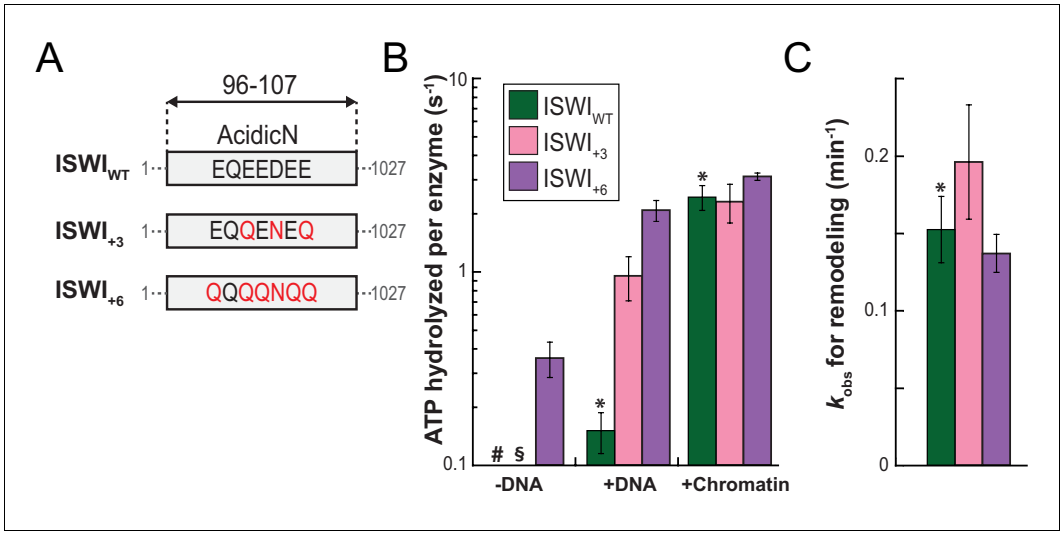

Figure 6. AcidicN is a strong negative regulator of the ATPase. (**A**) Design of AcidicN derivatives of ISWI (see also ***Figure 6—figure supplement 1A***). (**B**) Effects of AcidicN mutation on ATP hydrolysis in absence or presence of saturating concentrations of DNA and chromatin. In absence of DNA, ATPase activities of ISWI$_{WT}$ (#) and ISWI$_{+3}$ (§) were $\leq$0.06 s^{-1}. Errors are s.d. ($n \geq 4$). (**C**) Effects of AcidicN mutation on the remodeling activities. Nucleosomal arrays containing wild-type H4 were used. Errors are s.d. ($n \geq 3$) except for ISWI$_{+3}$ for which minimal and maximal values of two independent measurements are shown. Color code as in panel (**B**). Raw data of the remodeling assay can be found in ***Figure 8—figure supplement 1***. Results for ISWI$_{WT}$ (*) are replotted for comparison from ***Figure 3B,C***.

DOI: 10.7554/eLife.21477.021

The following figure supplements are available for figure 6:

Figure supplement 1. AcidicN and AutoN mutants.

DOI: 10.7554/eLife.21477.022

Figure supplement 2. Comparison of ATPase and remodeling activities of ISWI control variants used in this study.

DOI: 10.7554/eLife.21477.023

Figure supplement 3. Saturation controls for ISWI$_{+6}$ in ATPase assays.

DOI: 10.7554/eLife.21477.024

Figure supplement 4. AcidicN mutations upregulate the ATPase activity of ISWI$_{H483B}$.

DOI: 10.7554/eLife.21477.025

assay (***Figure 7B***). These data support the notion that AcidicN interacts with Lobe 2 at the predicted interface and that this interaction is functionally important to discriminate whether chromatin is bound to the enzyme.

AcidicN and AutoN cooperate during recognition of chromatin and H4 tail

To explore whether AcidicN takes part in H4-tail recognition, we measured the dependence of AcidicN mutants on the H4 tail in remodeling assays. Strikingly, the +3 and+6 ISWI derivatives lost most of their reliance on the H4 tail during remodeling (***Figure 8A***). In contrast, ISWI$_{\Delta ppHSA}$ and ISWI$_{\Delta ppHSA;\ \Delta AT\text{-}hook}$ retained a strong H4-tail dependence, which indicated that ppHSA had little involvement in H4-tail recognition.

Two AcidicN interface mutants described above (K403D and R458D) also depended less on the H4 tail during remodeling than ISWI$_{WT}$ (***Figure 8A***). The third mutant (R508D) and the control mutant (R485; 488D) were apparently still sensitive towards loss of the H4 tail. These two mutants, however, were not saturated with tail-less chromatin so that the calculated values represented upper limits for the H4-tail dependence (<24 fold and <15 fold, respectively; ***Figure 8—figure supplement 1E*** and data not shown).

Lack of the H4-tail dependence of AcidicN mutants was reminiscent of the phenotype previously described for the ISWI$_{2RA}$ mutation in AutoN (***Clapier and Cairns, 2012***). The 2RA mutation

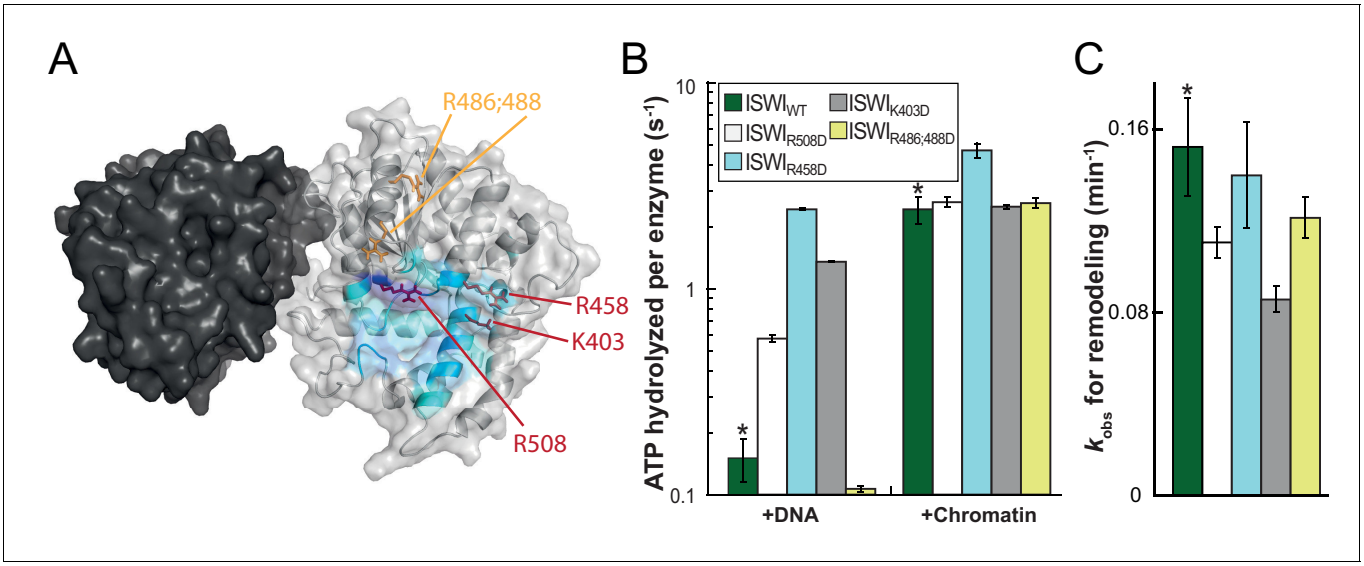

Figure 7. Validation of the predicted binding interface of AcidicN on Lobe 2. (**A**) Homology model of the ISWI ATPase domain. Dark and light grey, ATPase lobes 1 and 2, respectively; blue, hypothetical binding interface of AcidicN as in ***Figure 4—figure supplement 3A***. Positively charged residues selected for mutagenesis are shown in red (AcidicN interface mutant) and orange (control mutant). (**B**) Mutation of the AcidicN interface (K403D, R458D and R508D) strongly upregulated DNA-stimulated ATP hydrolysis relative to $ISWI_{WT}$, whereas the nucleosome-stimulated ATP turnover was similar. In contrast, a control mutation (R486; 488D) had little effect on ATP hydrolysis. Saturating concentrations of DNA and chromatin were used. Errors are s.d. for $ISWI_{WT}$ and minimal and maximal values of two independent measurements for all other constructs. (**C**) AcidicN interface variants of ISWI robustly remodeled nucleosomes within twofold of $ISWI_{WT}$. Nucleosomal arrays containing wild-type H4 were used. Errors are s.d. ($n \geq 3$) for $ISWI_{WT}$ and minimal and maximal values of two independent measurements for all other constructs. Raw data of the remodeling assay can be found in ***Figure 7—figure supplement 2***. Color code as in (**B**). Results for $ISWI_{WT}$ (*) were replotted for comparison from ***Figure 3B,C***.

DOI: 10.7554/eLife.21477.026

The following figure supplements are available for figure 7:

Figure supplement 1. Coomassie-stained SDS-PAGE of purified recombinant ISWI constructs analyzed in ***Figure 7***.

DOI: 10.7554/eLife.21477.027

Figure supplement 2. Determination of rate constants for remodeling of AcidicN interface mutants.

DOI: 10.7554/eLife.21477.028

(***Figure 6—figure supplement 1***) suppressed the dependence on the H4 tail also in our experiments, albeit our quantitative analysis showed an even more robust reduction than previously seen (***Figure 8A***). $ISWI_{2RA}$ was catalytically fully active, as was an AcidicN and AutoN double mutant ($ISWI_{+6;\ 2RA}$; ***Figure 8—figure supplement 1***). Like the respective single mutants, $ISWI_{+6;\ 2RA}$ barely relied on the presence of the H4 tail (***Figure 8A***; ***Figure 8—figure supplement 1***).

Compared to the respective single mutants, the $ISWI_{+6;\ 2RA}$ double mutant hydrolyzed ATP even faster in the absence of any ligand (***Figure 8B***). This result suggested that both motifs contributed to repression of the basal ATPase activity. In contrast, DNA- and chromatin-stimulated ATP turnover rates were not further perturbed by the double mutation (***Figure 8B***), consistent with both motifs cooperating during discrimination of chromatin from DNA.

Discussion

Dozens of ATP-dependent chromatin remodeling factors are at work in any eukaryotic cell. Their activities impact every process that involves the cell's genetic material, including transcription, replication, DNA repair and recombination. Dysfunction and improper regulation of these complexes may have dire consequences for human health (***Kadoch and Crabtree, 2015***; ***Garraway and Lander, 2013***). Perhaps as a consequence, remodelers across many families independently evolved intricate mechanisms for autoregulation (***Clapier and Cairns, 2012***; ***Hauk et al., 2010***; ***Wang et al., 2014***; ***Clapier et al., 2016***; ***Gottschalk et al., 2009***).

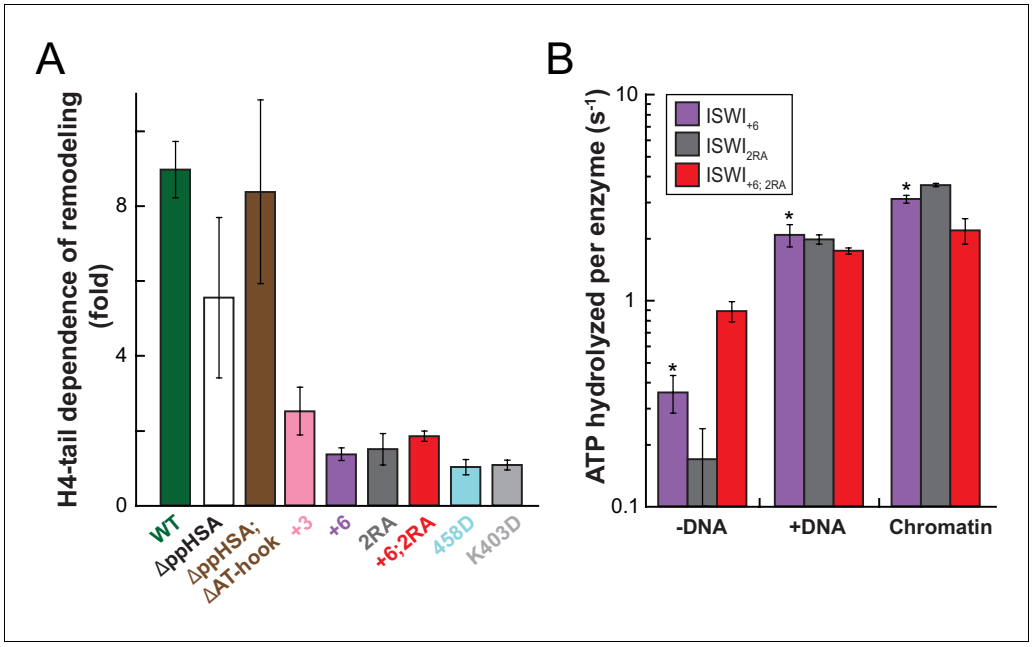

Figure 8. Mutation of AcidicN, the AcidicN binding interface or AutoN suppresses dependence on the H4-tail. (**A**) H4-tail dependence of the remodeling activities of ISWI variants. Values were calculated from the observed remodeling rate constants obtained for WT and tail-less H4 chromatin (***Figure 8—figure supplement 1E***). (**B**) ATP hydrolysis measurements of $ISWT_{+6}$, $ISWI_{2RA}$ and $ISWI_{+6;\ 2RA}$ in absence or presence of saturating concentrations of DNA and chromatin.

DOI: 10.7554/eLife.21477.029

The following figure supplement is available for figure 8:

Figure supplement 1. Raw data of the remodeling assays.

DOI: 10.7554/eLife.21477.030

It has been known for many years that the activity of ISWI remodelers is regulated by the H4 tail (***Clapier et al., 2001***). Regulation by the H4 tail was later also discovered for remodelers of the Chd1 (***Ferreira et al., 2007***) and Alc1 families (***Ahel et al., 2009***). The molecular mechanism of H4-tail recognition and regulation has remained elusive, not least because the tail's binding site had not been mapped. Using crosslinking-MS, we found the H4 tail to bind to the conserved Lobe 2 of the ATPase module. Direct binding to the ATPase domain explains regulation of otherwise divergent remodeler families and explains the influence of the H4 tail on catalytic, as opposed to purely binding steps (***Clapier et al., 2001***; ***Dang et al., 2006***). Our data do not rule out additional binding sites on other domains and on ISWI's partner subunit ACF1 as proposed earlier (***Boyer et al., 2004***; ***Grüne et al., 2003***; ***Hwang et al., 2014***).

ISWI and Chd1 proteins have evolved a complex autoregulatory mechanism. This mechanism involves an autoinhibitory domain N-terminal to the ATPase. Inhibition by this domain is countered in an unknown fashion by H4-tail binding. Two limiting scenarios can explain the data (***Figure 9***).

The first model has been proposed earlier (***Clapier and Cairns, 2012***) and posits that AutoN acts as a pseudosubstrate by mimicking part of the basic patch of the H4 tail. In fact, AutoN (amino acids 'RHRK', which are present in many but not all ISWI proteins; ***Figure 1D*** and ***Figure 1—figure supplement 1***) was initially discovered by way of its resemblance to the amino acids '$R_{17}H_{18}R_{19}K_{20}$' on histone H4 (***Clapier and Cairns, 2012***). In this model, the basic patch of the H4 tail must compete with AutoN for the same binding site on the ATPase domain, such that AutoN and possibly the entire NTR is displaced upon tail binding (***Clapier and Cairns, 2012***; ***Hauk et al., 2010***). This model is supported by the observations that the NTR can in principle undergo conformational changes (***Mueller-Planitz et al., 2013***) and that the chromo domains of Chd1 must rearrange before the ATPase domain assumes a catalytically active conformation (***Hauk et al., 2010***). Direct experimental support for a shared binding site of AutoN and H4 basic patch has been lacking, however, and the

resemblance of the two motifs may be purely coincidental in principle. Of the four amino acids that resemble the H4 tail, only three ($R_{17}H_{18}R_{19}$) were found to be functionally important for ISWI enzymes (***Fazzio et al., 2005***; ***Clapier et al., 2002***; ***Clapier and Cairns, 2012***). Recent crystallographic evidence also did not support the molecular mimicry hypothesis (see below) (***Yan et al., 2016***).

We favor a second, simpler model, which does not invoke molecular mimicry (***Figure 9***). In this model, the AutoN and the H4-tail binding sites are not identical, possibly allowing simultaneous binding of both to Lobe 2 at least temporarily. This scenario is fully compatible with our suggestion that the docking sites for the H4 tail and AutoN-AcidicN are adjacent to each other but not overlapping (***Figure 5E***). Conceivably, the negatively charged AcidicN motif may even promote binding of the basic H4 tail to a neighboring site. A structural rearrangement of the NTR upon H4 tail binding is compatible with but not required in this model. Similarly, conformational changes of the NTR upon DNA binding (***Mueller-Planitz et al., 2013***; ***Hauk et al., 2010***) or during other steps of the reaction cycle are also fully consistent with it.

Intriguing parallels between ISWI's NTR and Chd1's chromo domains become apparent. Our crosslinking results indicate that the NTR of ISWI docks against Lobe 2 of the ATPase domain in a very similar fashion as the chromo domains of Chd1, and docking appears to involve an acidic motif in both cases (***Hauk et al., 2010***). Thus, the overall conformational architecture of ISWI's ATPase module may be shared with Chd1. Moreover, both domains are known to inhibit the ATPase, both are predicted to undergo conformational changes upon substrate binding (***Mueller-Planitz et al., 2013***; ***Clapier and Cairns, 2012***) and both confer sensitivity towards the histone H4 tail (***Clapier and***

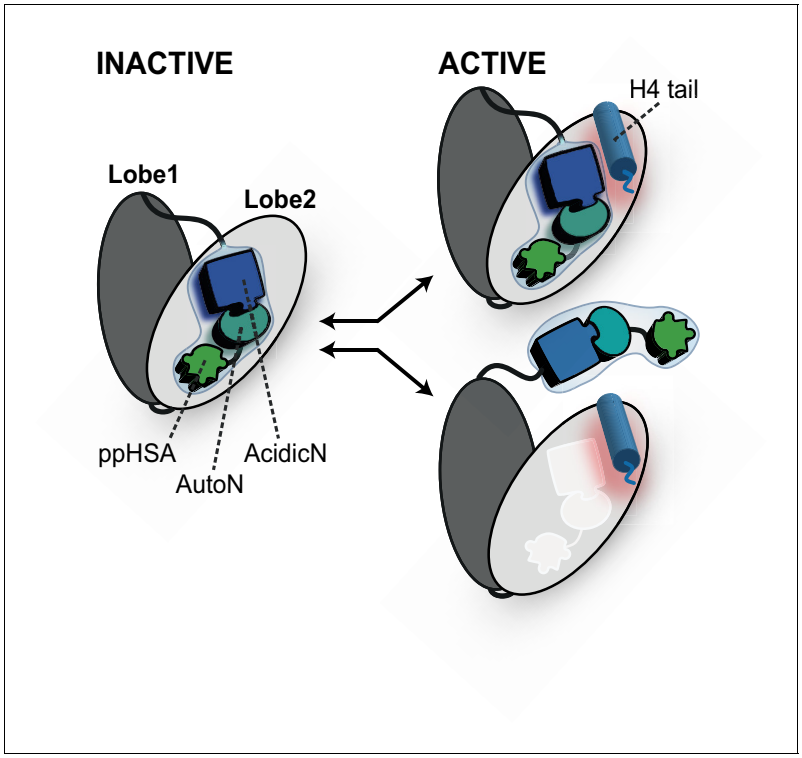

Figure 9. Proposed models for autoregulation imposed by the NTR and the recognition process of the H4 tail. The ppHSA motif, AcidicN and AutoN dock against Lobe 2 of the ATPase domain, promoting an overall structural architecture of the ATPase module that is reminiscent of Chd1 (***Figure 4A***). AcidicN and AutoN functionally collaborate in the H4 tail recogniton process. The docking site of AutoN-AcidicN is adjacent to the H4 tail potentially allowing simultaneous binding (top). Alternatively, the H4 tail may displace the NTR as suggested previously (bottom) (***Clapier and Cairns, 2012***).

DOI: 10.7554/eLife.21477.031

Cairns, 2012; *Hauk et al., 2010*). Thus, despite complete lack of sequence conservation between both domains, they appear to have evolved very similar functionalities.

The NTR of ISWI contains several conserved motifs whose functions have mostly remained unexplored so far. Because the ppHSA motif and adjacent regions crosslinked to the ATPase lobe 2, we suggest that it is important for docking the NTR against the ATPase domain. Consistent with such a structural role of this motif, we found that $ISWI_{\Delta ppHSA}$ is destabilized in vitro and in vivo. Of note, the ppHSA motif is present in a wide variety of unrelated remodelers, including Ino80, Lsh, and Snf2, suggesting that their ATPases, too, might bind the ppHSA motif and assemble into a structurally analogous architecture.

In this study, we functionally characterized AcidicN, a novel motif in the NTR. ISWI with a mutated AcidicN had a deregulated, hyperactive ATPase activity. Notably, this mutant hydrolyzed ATP with comparable velocities when bound to either DNA or nucleosomes, indicating that it lost its ability to discriminate between them. In particular, it lost its H4-tail dependence. This phenotype is reminiscent of mutations in the acidic helix in Chd1 (*Hauk et al., 2010*), underscoring the functional parallels between the NTR and chromo domains discussed above. The effects of AcidicN mutations were also remarkably similar to AutoN mutations (*Clapier and Cairns, 2012*), which suggested that they work together. The mechanism of autoinhibition by the NTR therefore may involve more than simple mimicry of H4's basic patch by AutoN (*Clapier and Cairns, 2012*). Supporting its functional importance, AcidicN is at least as conserved as AutoN in our alignments.

During the revision of this manuscript, a crystal structure of the ATPase module of ISWI from a thermophilic fungus became available (*Yan et al., 2016*). Even though both studies relied on different approaches, they arrived at very similar conclusions. As suggested by our crosslinking and modeling data, the NTR packed against the ATPase domain in the structure of the thermostable ISWI. We correctly predicted the AcidicN binding pocket on Lobe 2 (*Figure 4—figure supplement 3A*), and our crosslinks between Lobe 2 and the NTR were fully supported by the structure as well. Finally, the authors succeeded in co-crystallizing a histone H4-tail peptide with Lobe 2 of the ATPase. Even though only the basic patch of the tail peptide was visible in the structure, its location overlapped well with the position of the modeled H4 basic patch (*Figure 5—figure supplement 3C*). AutoN crystallized in closer proximity to the interaction site of the basic patch than suggested by modeling, but molecular mimicry of AutoN with the basic patch was not supported by the structure.

Sensitive biophysical assays will be instrumental in the future for resolving conformational changes that may occur during H4-tail recognition and for understanding their functional importance in ISWI complexes. Moreover, ascertaining the predicted role of H4-tail recognition for the formation or maintenance of compact heterochromatic regions remains an important goal.

Materials and methods

Amino acid sequence alignments and sequence logos

Search for homologous proteins of full-length *Drosophila* ISWI and alignment of sequences were done using HHblits with standard settings. Sequence logos of conserved NTR motifs were derived with WebLogo three from this alignment (*Schneider and Stephens, 1990*). Proteins containing the ppHSA motif were identified by PSI-BLAST against the 120 N-terminal amino acids of ISWI. The alignment was done using T-Coffee. Sequence alignments were visualized using Jalview 2.9.

Spotting assays

S. cerevisiae Isw1 alleles were cloned into selected destination vectors of a galactose-inducible hybrid promoter library (generously provided by Dr. Hal Alper, UT Austin, USA) (*Blazeck et al., 2012*). The following destination vectors were used, sorted according to increasing promoter strength: Gal4pBS2-P_{leum} (denoted '+' in *Figure 2B*; *Figure 2—figure supplement 1*), Gal4pBS4-P_{leum} ('++'), UAS_{gal}-A9-P_{cyc} ('+++'), and UAS_{gal}-P_{gal} ('++++'). Destination vectors were XbaI and ClaI digested and gel purified. Isw1 derivatives were PCR-amplified from yeast genomic DNA, gel purified and ligated into the destination vectors by Gibson assembly. All spotting assays employed untagged Isw1 variants. All constructs were sequence verified before transformation. As an empty vector control, the UAS promoter, coding and terminator sequences were removed from the Gal4pBS2-P_{leum} plasmid by AscI and MluI digest and subsequent self-ligation.

YTT227 (TKO), YTT225 (DKO) and W1588-4c (wild-type; **Table 3**) were transformed with indicated plasmids via a standard transformation protocol. Single colonies were picked and grown overnight in Synthetic complete (SC)-Ura + Glucose (2%) media. The culture was then diluted to OD 0.05 in SC-Ura Galactose media (2%) and grown for 24 hr. Cells were diluted again to OD 0.1 in Galactose media and grown for another 24 hr before spotting. Cells were diluted to OD 1.0, and tenfold serial dilutions were spotted on galactose media and incubated at 30°C, 37°C or 38.5°C for 72 hr. At least two replicates were performed on different days with a single transformant of a sequence-verified clone.

Western analysis

For Western analysis, Isw1 variants were C-terminally tagged by fusion to a cassette containing a $(GGS)_2$ linker, a 3C cleavage site, a $(GGS)_5$ linker and a TAP tag. YTT227 that expressed TAP-tagged Isw1 variants was induced with galactose as above, diluted to OD 0.1 and grown to OD 1.0 in 10 ml SC-Ura + Galactose media. YFMP047 (**Table 3**), containing a genomically TAP-tagged Isw1 allele, was grown as a control in YPAD media. Cells were harvested, washed twice with cold water and dissolved in 200 µl Extraction buffer (40 mM Hepes-KOH pH 7.5, 10% Glycerol, 350 mM NaCl, 0.1% Tween-20, 1 µg/ml Pepstatin, 2 µg/ml Leupeptin, 2 µg/ml Aprotinin, 1 mM PMSF. Glass beads (200 µl) were added, and the suspension was vortexed for 10 min with a 30 s on/off cycle on ice. After centrifugation (13,000 rpm, 20 min 4°C), supernatants were harvested, aliquoted (50 µl), flash frozen, and stored at −80°C for subsequent use. Supernatants were thawed on ice and 50 µg of each extract was loaded on a 10% SDS gel. Anti-TAP antibody (CAB1001, ThermoFisher; 1:5000 dilution) was used to detect TAP-tagged ISW1 mutants and anti-H3 antibody (ab1791, Abcam; 1:20,000 dilution) was used as a loading control. Membranes were scanned using the LI-COR Odyssey IR imaging system (ODY-0853) and bands were quantified using Image Studio Lite v5.2.5. Expression levels were normalized to the signal of genomically integrated TAP-tagged Isw1. Two technical replicates were performed.

Construct design and cloning of *Drosophila* ISWI variants

A pPROEX-HTb–based expression plasmid with the gene encoding *Drosophila* $ISWI_{WT}$ (kindly provided by C. Müller; EMBL, Heidelberg, Germany) served as the template for all ISWI variants. An overview over cloned ISWI variants is presented in **Figure 3—figure supplement 1A** and **Figure 6—figure supplement 1A**. All ISWI genes were fused N-terminally to a His_6-tag. To generate $ISWI_{\Delta ppHSA}$ and $ISWI_{\Delta ppHSA;\ \Delta AT\text{-}hook}$, a 3C cleavage site was introduced at the desired site by QuikChange mutagenesis or polymerase incomplete primer extension. The trigger factor gene was amplified from pTf16 (Takara Bio Inc.) and fused to the $ISWI_{WT}$ gene by Gibson assembly. $ISWI_{+6}$ was subcloned into the pET-Z2 plasmid (kindly provided by Dr. Arie Geerlof, Helmholtz Zentrum, Munich, Germany).

Protein expression and purification of ISWI variants

Expression and purification of His_6-tagged $ISWI_{WT}$ and its derivatives was performed essentially as described (**Forné et al., 2012**) with the following variations. Tags or parts of the NTR were cleaved off by specific proteases (TEV and 3C, respectively) as indicated (**Figure 3—figure supplement 1A**; **Figure 6—figure supplement 1A**). $ISWI_{H483B}$ was expressed and purified as described (**Forné et al., 2012**). During its purification, the UV light of the FPLC remained switched off to protect the Bpa residue. All ISWI variants were purified once except $ISWI_{+3}$ and Z_2-$ISWI_{+6}$, which were purified twice.

Table 3. Yeast strains used in this study.

Strain	Genotype	Reference
W1588-4C	*MAT***a** *ade2-1 his3-11,15 leu2-3,112 trp1-1 ura3-1 can1-100* but *RAD5*	**Tsukiyama et al. (1999)**
YTT227	*MAT***a** *ade2-1 his3-11,15 leu2-3,112 trp1-1 ura3-1 can1-100* but *RAD5 isw1::ADE2 isw2::LEU2 chd1::TRP1*	**Tsukiyama et al. (1999)**
YTT225	*MAT***a** *ade2-1 his3-11,15 leu2-3,112 trp1-1 ura3-1 can1-100* but *RAD5 isw2::LEU2 chd1::TRP1*	**Tsukiyama et al. (1999)**
YFMP047	*MAT***a** *his3Δ1 leu2Δ0 met15Δ0 ura3Δ0 ISW1-TAP::HIS3MX6*	*Open Biosystems*

DOI: 10.7554/eLife.21477.032

The independent preparations were indistinguishable in ATPase assays ($ISWI_{+3}$ and Z_2-$ISWI_{+6}$). Whereas $ISWI_{+3}$ preparations were not directly compared, independent Z_2-$ISWI_{+6}$ preparations also yielded same results in remodeling assays.

Expression and purification of SNF2H

A pBH4-based expression plasmid encoding full-length human SNF2H (kindly provided by G. Narlikar; UCSF, San Francisco) was transformed into Rosetta competent *E. coli* cells. Protein expression was performed in 2x YT medium (20 g/l tryptone, 10 g/l yeast extract, 10 g/l NaCl) supplemented with 34 mg/l chloramphenicol and 100 mg/l ampicillin. Expression of SNF2H was induced by addition of 0.4 mM IPTG at 18°C for approximately 18 hr. Bacteria cells were resuspended in 20 ml lysis buffer per 1 l culture (25 mM HEPES pH 8.0, 300 mM KCl, 7.5 mM imidazole, 10% glycerol, 1 mM DTT) supplemented with protease inhibitors (1 mM PMSF, 1 mg/l Aprotinin, 1 mg/l Leupeptin, 0.7 mg/l Pepstatin) per 1 l culture, and lysed by French Press (Thermo Spectronic) and ultrasonication (Branson). Per 1 l lysed bacteria culture, 1000 U Benzonase (Merck Millipore) were added. The lysate was clarified by centrifugation (30 min, SS34 rotor). The N-terminal His_6-tagged SNF2H was purified by nickel affinity chromatography (HisTrap HP, 5 ml; GE Healthcare). An elution gradient was applied with 25 mM HEPES pH 7.0, 300 mM KCl and 400 mM Imidazole and enzyme-containing fractions were pooled. Contaminating DNA was removed by passing the sample over an anion exchange column (Mono Q 5/50 GL ion exchange column; GE Healthcare) that was pre-equilibrated in SEC buffer (25 mM HEPES pH 7.5, 300 mM KCl, 1 mM DTT). The flow-through of the column was collected. The protein sample was concentrated to 0.5–1 ml per 1 l of original *E. coli* culture in centrifugal filters (Amicon Ultra-4, 30 kDa MWCO; Millipore). TEV protease (prepared in-house) was added to a final concentration of 0.075–0.15 mg/ml and the concentrated protein sample was dialyzed against 1 l SEC buffer overnight in dialysis tubing (6000–8000 Da MWCO; Sectra/Por). The protein sample was loaded onto a size exclusion chromatography column (Superdex 200 HiLoad 16/60, 120 ml; GE Healthcare) pre-equilibrated in SEC buffer. Elution fractions were pooled according to purity and, as necessary, concentrated and dialyzed into storage buffer (25 mM HEPES pH 7.5, 210 mM KCl, 15% glycerol, 1 mM DTT) for at least 16 hr.

Nucleosome reconstitution

Drosophila histones were purified as described (***Klinker et al., 2014***; ***Luger et al., 1999***). The 187 bp long Widom-601 derivative used for end-positioned mononucleosomes (0N40) was excised from pFMP151 with SmaI (NEB) and PAGE purified. DNA for 25-mer nucleosomal arrays used in remodeling assays was excised from pFMP233 with EcoRI HF, HincII and AseI (NEB) and purified by phenol/chloroform extraction and ethanol precipitation. Polynucleosomes used in ATP-hydrolysis assays were assembled on linearized plasmid DNA (pT7 blue derivative). Histone octamers, mononucleosomes and polynucleosomes, including 25-mer nucleosomal arrays, were prepared by salt-gradient dialysis as described (***Mueller-Planitz et al., 2013***; ***Luger et al., 1999***). Mononucleosomes were further purified by glycerol gradient ultracentrigation. Nucleosomal arrays were purified further by Mg^{2+} precipitation (3.5 mM for WT-H4 arrays, 8.5 mM for H4-tail deleted arrays) (***Mueller-Planitz et al., 2013***). The concentration of nucleosomal DNA was determined by measuring its UV absorption at 260 nm. For nucleosomal arrays, concentrations refer to the concentration of individual nucleosomes.

Enzyme assays

Remodeling and ATPase assays were performed in 25 mM HEPES-KOH, pH 7.6, 50 mM NaCl, 1 mM $MgCl_2$, 0.1 mM EDTA, 10% glycerol, 0.2 g/l BSA and 1 mM DTT at 26°C in the presence of a ATP regenerating system as described (***Mueller-Planitz et al., 2013***).

ATP hydrolysis was monitored by an NADH-coupled ATP hydrolysis assay (***Mueller-Planitz et al., 2013***; ***Forné et al., 2012***). Saturating concentrations of ATP-Mg^{2+} (1 mM) and of nucleic acids ligands were used (0.2 mg/ml of linearized pT7blue and 0.1 mg/ml of chromatin assembled on the same DNA, respectively). Saturation of DNA and chromatin was controlled by varying the concentration of the ligands at least 16-fold (***Figure 3—figure supplement 2***; ***Figure 6—figure supplement 3***). Occasional occurrence of air bubbles in ATPase experiments precluded accurate measurements; affected samples were excluded from the analysis. In no other assays were outliers excluded.

Remodeling activity was probed by a restriction enzyme accessibility assay (**Mueller-Planitz et al., 2013**). A 25-mer nucleosomal array with a 197 bp nucleosomal repeat length was used. The 19th nucleosome of this array occluded a unique KpnI site at position −32 relative to its dyad (**Mueller-Planitz et al., 2013**). Arrays (100 nM) were incubated with ISWI derivatives at the indicated concentrations, ATP-Mg^{2+} (1 mM) and KpnI (2 U/ml). Reactions were quenched with SDS (0.4%) and EDTA (20 mM) before the samples were deproteinized, ethanol precipitated and resolved by agarose gel electrophoresis (**Mueller-Planitz et al., 2013**). k_{obs} for remodeling was obtained by fitting time courses to a single exponential function. When the enzyme concentration was varied ≥threefold, typically between 100 nM and 300 nM, similar values for k_{obs} were obtained with a few exceptions, suggesting that arrays were generally saturated (**Figure 3—figure supplement 3**; **Figure 4—figure supplement 1**; **Figure 7—figure supplement 2**; **Figure 8—figure supplement 1A–D** and data not shown). The exceptions comprised $ISWI_{\Delta ppHSA;\ \Delta AT\text{-}hook}$, $ISWI_{+3}$ and $ISWI_{H483B}$ on WT-arrays and $ISWI_{+3}$, $ISWI_{R508D}$ and $ISWI_{R486;\ 488D}$ on tail-less H4 arrays.

UV crosslinking

To site-specifically attach a UV-reactive benzophenone residue to full-length histone H4, single cysteines were introduced into the histone H4 tail by site directed mutagenesis at the indicated positions. 4-(N-Maleimido)benzophenone (Sigma) was dissolved to 100 mM in N,N-Dimethylformamide (DMF) and added to a final concentration of 3 mM to denatured single cysteine variants of H4 (1 mg/ml) in 20 mM Tris/HCl pH 7.1, 7 M Guanidine-HCl, 5 mM EDTA, 2 mM TCEP for 2 hr at room temperature. After a 3 hr incubation in the dark, the labeling reaction was stopped by adding 20 mM DTT for 20 min.

UV-Crosslinking was performed in uncoated 384-well plates or 96-well plates (Greiner) on ice using the 365 nm irradiation of a BioLink UV-Crosslinker (Peqlab) for the indicated durations. Crosslinking between benzophenone-labeled nucleosomes (0N40; 1 µM) and stoichiometric amounts of ISWI or SNF2H was performed in 20 mM Tris/HCl, pH 7.7, 100 mM KCl, 0.1 mM EDTA, 3 mM DTT. Crosslinking between $ISWI_{26\text{-}648}$ (0.1 mg/ml) and a histone H4 peptide comprising the 24 N-terminal amino acids of H4 carrying a Bpa substitution at position 1 or 10 was carried out in the presence of 13 µM 59 bp DNA duplex in 25 mM HEPES-KOH, pH 7.6, 50 mM NaCl, 1 mM MgCl2, 0.1 mM EDTA, 10% glycerol and 1 mM DTT for 3 hr as above. Samples were subsequently digested with benzonase before further processing. Crosslinking between Bpa variants of ISWI (H483B) was carried out as described (**Forné et al., 2012**).

UV-irradiated samples and unirradiated control samples were separated by SDS-PAGE and Coomassie stained. Protein bands were excised and trypsin digested for subsequent mass spectrometry as described (**Forné et al., 2012**; **Wilm et al., 1996**).

Mapping of crosslinks by LC-MS/MS

For LC-MS/MS, 5 µl were injected in either an Ultimate 3000 system (Thermo) and desalted on-line in a C18 micro column (75 µm i.d. x 15 cm, packed with C18 PepMap, 3 µm, 100 Å by LC Packings) or desalted offline using C18 Stagetip and injected in an Ultimate 3000 RSLCnano system (Thermo). Desalted sample was then separated in a 15 cm analytical C18 micro column (75 µm i.d. packed with C18 PepMap, 3 µm, 100 Å by LC Packings or homepacked 75 µm ID with ReproSil-Pur C18-AQ 2.4 µm from Dr. Maisch) with a 40 to 60 min gradient from 5% to 60% acetonitrile in 0.1% formic acid. The effluent from the HPLC was directly electrosprayed into an LTQ-Orbitrap XL as described before (**Forné et al., 2012**) or a Q Exactive HF MS (Thermo). The Q Exactive HF MS was operated in a data-dependent mode. Survey full scan MS spectra (from m/z 375–1600) were acquired with resolution R = 60,000 at m/z 400 (AGC target of 3×10^6). The ten most intense peptide ions with charge states between 3 and 5 were sequentially isolated to a target value of 1×10^5, and fragmented at 27% normalized collision energy. Typical mass spectrometric conditions were: spray voltage, 1.5 kV; no sheath and auxiliary gas flow; heated capillary temperature, 250˚C; ion selection threshold, 33.000 counts.

Each Thermo binary raw file was converted to a dta file using Decon2LS (**Zimmer et al., 2006**) or to an mgf file using Proteome Discoverer 1.4 (Thermo) and -as needed- recalibrated with the Post-Search Recalibrator Node. Crosslinks were mapped by Crossfinder (**Forné et al., 2012**; **Mueller-**

Planitz, 2015). Typical error windows were ±10 ppm for MS1 searches and ±15 ppm for MS2 searches. All amino acid residues were regarded as potential sites of crosslinking.

Crosslink candidates were independently validated by the authors J.L., S.P., N.H. and F.M.-P. and rated as high, medium and low confidence. The validation comprised a general assessment of the spectrum quality, removal of wrong product ion assignments, and evaluation of the actual evidence for the presence of the two peptides within the crosslink. The mass spectrometry data have been deposited to the ProteomeXchange Consortium via the PRIDE partner repository with the dataset identifier PXD005831.

In silico docking studies

Interactions between NTR motifs and the histone H4 tail with Lobe 2 were modeled using the fully blind peptide-protein docking protocol pepATTRACT (*Schindler et al., 2015a*) in the ATTRACT docking engine (*de Vries et al., 2015*) (www.attract.ph.tum.de/peptide.html). The termini of the motifs ('peptides') were left uncharged, other parameters were set to the default values as described (*Schindler et al., 2015a*). Briefly, for each motif three idealized peptide conformations (extended, α-helical and poly-proline) were generated from sequence and this peptide ensemble was docked rigidly against the protein domain using the ATTRACT coarse-grained force field (*Zacharias, 2003*). The top-ranked 1000 structures were subjected to two stages of atomistic refinement using the flexible interface refinement method iATTRACT (*Schindler et al., 2015b*) and a short molecular dynamics simulation in implicit solvent with the AMBER program (*Case et al., 2014*). The pepATTRACT protocol requires neither knowledge about the peptide binding site nor of the bound peptide conformation and is therefore suitable for predicting complexes between proteins and motifs from intrinsically unstructured regions.

The structure of ISWI ATPase Lobe 2 (residues 352–637) was modeled by homology from the structure of Chd1 (PDB 3MWY) using MODELLER (*Webb and Sali, 2016*). We performed three docking runs modeling the potential binding site for the AutoN motif (residues 89–97; DHRHRKTEQ), the AcidicN motif (residues 96–104; EQEEDEELL) and the full module AutoN+AcidicN (residues 89–104; DHRHRKTEQEEDEELL) separately. During the first two runs, we modeled the peptide ensemble from the sequence as described above. For the third run, we used PEP-FOLD2 (*Shen et al., 2014*), PEP-FOLD3 (*Lamiable et al., 2016*) and I-TASSER (*Yang et al., 2015*) servers to predict the structure of the module. We used the resulting 13 conformations for ensemble docking to Lobe 2. To test the specificity of the docking solutions, we also modeled Lobe 2 binding to scrambled sequences of AutoN (HRQHKDERT), AcidicN (LEDELQEEE) and AutoN-AcidicN (HLREQLDTHE REDEKE). Docking of AutoN-AcidicN against the homology model comprising both ATPase lobes was done as described above.

During docking of the histone H4 tail (residues 1–20) to Lobe 2, we used the five high confidence crosslinks (*Table 3*), which – due to redundancy – provided three unique amino acid linkages. These linkages were used as upper harmonic distance restraints with a maximum distance of 20 Å to guide the modeling (pepATTRACT-local protocol) (*Schindler et al., 2015a*). After molecular dynamics refinement (see above), which did not apply crosslinking restraints for technical reasons, models were filtered for those that still satisfied the distance restraints provided by the crosslinks, yielding 383 models. All figures were created using PyMOL (www.pymol.org).

Acknowledgements

We thank Geeta Narlikar (UC San Francisco, USA), Hal Alper (UT Austin, USA) and Arie Geerlof (Helmholtz Center, Munich, Germany) for plasmids and protocols, Axel Imhof (LMU, Munich, Germany) for access to MS machines, Silvia Härtel for technical help and Philipp Korber (LMU, Munich, Germany) and Peter Becker (LMU, Munich, Germany) for discussions. JL and AKS are grateful to the Schering Stiftung and the DAAD, respectively, for predoctoral fellowships. This work was funded by DFG grants MU 3613/1–1, MU 3613/3–1 and SFB 1064/1 TP-A07 awarded to FMP and the Center of Integrated Protein Science Munich (CIPSM) to MZ, respectively.

Additional information

Funding

Funder	Grant reference number	Author
Ernst Schering Foundation		Johanna Ludwigsen
Deutscher Akademischer Austauschdienst		Ashish K Singh
Deutsche Forschungsgemeinschaft	CIPSM	Martin Zacharias
Deutsche Forschungsgemeinschaft	MU 3613/1-1	Felix Mueller-Planitz
Deutsche Forschungsgemeinschaft	MU 3613/3-1	Felix Mueller-Planitz
Deutsche Forschungsgemeinschaft	SFB 1064/1TP-A07	Felix Mueller-Planitz

The funders had no role in study design, data collection and interpretation, or the decision to submit the work for publication.

Author contributions

JL, Conceptualization, Investigation, Visualization, Writing—original draft, Writing—review and editing; SP, Investigation, Visualization, Writing—review and editing; AKS, Investigation, Visualization, Writing—review and editing; CS, Software, Investigation, Visualization, Writing—review and editing; NH, Formal analysis, Validation, Visualization; IF, Visualization, Methodology; MZ, Conceptualization, Software, Supervision, Funding acquisition, Project administration; FM-P, Conceptualization, Software, Supervision, Funding acquisition, Investigation, Writing—original draft, Project administration, Writing—review and editing

Author ORCIDs

Felix Mueller-Planitz, http://orcid.org/0000-0001-8273-6473

Additional files

Major datasets

The following dataset was generated:

Author(s)	Year	Dataset title	Dataset URL	Database, license, and accessibility information
Johanna Ludwigsen, Sabrina Pfennig, Ashish K Singh, Christina Schindler, Nadine Harrer, Ignasi Forné, Martin Zacharias, Felix Mueller-Planitz	2017	Concerted regulation of ISWI by an autoinhibitory domain and the H4 N-terminal tail	http://www.ebi.ac.uk/pride/archive/projects/PXD005831	Publicly available at the PRIDE Archive (accession no. PXD005831)

References

Ahel D, Horejsí Z, Wiechens N, Polo SE, Garcia-Wilson E, Ahel I, Flynn H, Skehel M, West SC, Jackson SP, Owen-Hughes T, Boulton SJ. 2009. Poly(ADP-ribose)-dependent regulation of DNA repair by the chromatin remodeling enzyme ALC1. *Science* **325**:1240–1243. doi: 10.1126/science.1177321, PMID: 19661379

Aravind L, Landsman D. 1998. AT-hook motifs identified in a wide variety of DNA-binding proteins. *Nucleic Acids Research* **26**:4413–4421. doi: 10.1093/nar/26.19.4413, PMID: 9742243

Blazeck J, Garg R, Reed B, Alper HS. 2012. Controlling promoter strength and regulation in Saccharomyces cerevisiae using synthetic hybrid promoters. *Biotechnology and Bioengineering* **109**:2884–2895. doi: 10.1002/bit.24552, PMID: 22565375

Boyer LA, Latek RR, Peterson CL. 2004. The SANT domain: a unique histone-tail-binding module? *Nature Reviews Molecular Cell Biology* **5**:158–163. doi: 10.1038/nrm1314, PMID: 15040448

Bozhenok L, Wade PA, Varga-Weisz P. 2002. WSTF-ISWI chromatin remodeling complex targets heterochromatic replication foci. *The EMBO Journal* **21**:2231–2241. doi: 10.1093/emboj/21.9.2231, PMID: 11980720

Case DA, Babin V, Berryman JT, Betz RM, Cai Q, Cerutti DS, Cheatham TE, Darden TA, Duke RE, Gohlke H, Goetz AW, Gusarov S, Homeyer N, Janowski P, Kaus J, Kolossváry I, Kovalenko A, Lee TS, LeGrand S, Luchko T, et al. 2014. *Amber 14*. University of California, San Francisco. http://ambermd.org/

Chin JW, Martin AB, King DS, Wang L, Schultz PG. 2002. Addition of a photocrosslinking amino acid to the genetic code of Escherichiacoli. *PNAS* **99**:11020–11024. doi: 10.1073/pnas.172226299, PMID: 12154230

Clapier CR, Cairns BR. 2012. Regulation of ISWI involves inhibitory modules antagonized by nucleosomal epitopes. *Nature* **492**:280–284. doi: 10.1038/nature11625, PMID: 23143334

Clapier CR, Kasten MM, Parnell TJ, Viswanathan R, Szerlong H, Sirinakis G, Zhang Y, Cairns BR. 2016. Regulation of DNA translocation efficiency within the chromatin remodeler RSC/Sth1 Potentiates Nucleosome Sliding and Ejection. *Molecular Cell* **62**:453–461. doi: 10.1016/j.molcel.2016.03.032, PMID: 27153540

Clapier CR, Längst G, Corona DF, Becker PB, Nightingale KP. 2001. Critical role for the histone H4 N terminus in nucleosome remodeling by ISWI. *Molecular and Cellular Biology* **21**:875–883. doi: 10.1128/MCB.21.3.875-883.2001, PMID: 11154274

Clapier CR, Nightingale KP, Becker PB. 2002. A critical epitope for substrate recognition by the nucleosome remodeling ATPase ISWI. *Nucleic Acids Research* **30**:649–655. doi: 10.1093/nar/30.3.649, PMID: 11809876

Dang W, Kagalwala MN, Bartholomew B. 2006. Regulation of ISW2 by concerted action of histone H4 tail and extranucleosomal DNA. *Molecular and Cellular Biology* **26**:7388–7396. doi: 10.1128/MCB.01159-06, PMID: 17015471

de Vries SJ, Schindler CE, Chauvot de Beauchêne I, Zacharias M, Beauchene Cde. 2015. A web interface for easy flexible protein-protein docking with ATTRACT. *Biophysical Journal* **108**:462–465. doi: 10.1016/j.bpj.2014.12.015, PMID: 25650913

Dorigo B, Schalch T, Kulangara A, Duda S, Schroeder RR, Richmond TJ. 2004. Nucleosome arrays reveal the two-start organization of the chromatin fiber. *Science* **306**:1571–1573. doi: 10.1126/science.1103124, PMID: 15567867

Fazzio TG, Gelbart ME, Tsukiyama T. 2005. Two distinct mechanisms of chromatin interaction by the Isw2 chromatin remodeling complex in vivo. *Molecular and Cellular Biology* **25**:9165–9174. doi: 10.1128/MCB.25.21.9165-9174.2005, PMID: 16227570

Ferreira H, Flaus A, Owen-Hughes T. 2007. Histone modifications influence the action of Snf2 family remodelling enzymes by different mechanisms. *Journal of Molecular Biology* **374**:563–579. doi: 10.1016/j.jmb.2007.09.059, PMID: 17949749

Flaus A, Martin DM, Barton GJ, Owen-Hughes T. 2006. Identification of multiple distinct Snf2 subfamilies with conserved structural motifs. *Nucleic Acids Research* **34**:2887–2905. doi: 10.1093/nar/gkl295, PMID: 16738128

Forné I, Ludwigsen J, Imhof A, Becker PB, Mueller-Planitz F. 2012. Probing the conformation of the ISWI ATPase domain with genetically encoded photoreactive crosslinkers and mass spectrometry. *Molecular & Cellular Proteomics* **11**:M111.012088. doi: 10.1074/mcp.M111.012088, PMID: 22167269

Garraway LA, Lander ES. 2013. Lessons from the cancer genome. *Cell* **153**:17–37. doi: 10.1016/j.cell.2013.03.002, PMID: 23540688

Gottschalk AJ, Timinszky G, Kong SE, Jin J, Cai Y, Swanson SK, Washburn MP, Florens L, Ladurner AG, Conaway JW, Conaway RC. 2009. Poly(ADP-ribosyl)ation directs recruitment and activation of an ATP-dependent chromatin remodeler. *PNAS* **106**:13770–13774. doi: 10.1073/pnas.0906920106, PMID: 19666485

Grüne T, Brzeski J, Eberharter A, Clapier CR, Corona DF, Becker PB, Müller CW. 2003. Crystal structure and functional analysis of a nucleosome recognition module of the remodeling factor ISWI. *Molecular Cell* **12**:449–460. doi: 10.1016/S1097-2765(03)00273-9, PMID: 14536084

Hamiche A, Kang JG, Dennis C, Xiao H, Wu C. 2001. Histone tails modulate nucleosome mobility and regulate ATP-dependent nucleosome sliding by NURF. *PNAS* **98**:14316–14321. doi: 10.1073/pnas.251421398, PMID: 11724935

Hauk G, McKnight JN, Nodelman IM, Bowman GD. 2010. The chromodomains of the Chd1 chromatin remodeler regulate DNA access to the ATPase motor. *Molecular Cell* **39**:711–723. doi: 10.1016/j.molcel.2010.08.012, PMID: 20832723

Hwang WL, Deindl S, Harada BT, Zhuang X. 2014. Histone H4 tail mediates allosteric regulation of nucleosome remodelling by Linker DNA. *Nature* **512**:213–217. doi: 10.1038/nature13380, PMID: 25043036

Kadoch C, Crabtree GR. 2015. Mammalian SWI/SNF chromatin remodeling complexes and Cancer: mechanistic insights gained from human genomics. *Science Advances* **1**:e1500447. doi: 10.1126/sciadv.1500447, PMID: 26601204

Kim JH, Saraf A, Florens L, Washburn M, Workman JL. 2010. Gcn5 regulates the dissociation of SWI/SNF from chromatin by acetylation of Swi2/Snf2. *Genes & Development* **24**:2766–2771. doi: 10.1101/gad.1979710, PMID: 21159817

Klinker H, Haas C, Harrer N, Becker PB, Mueller-Planitz F. 2014. Rapid purification of recombinant histones. *PLoS One* **9**:e104029. doi: 10.1371/journal.pone.0104029, PMID: 25090252

Lamiable A, Thévenet P, Rey J, Vavrusa M, Derreumaux P, Tufféry P. 2016. PEP-FOLD3: faster de novo structure prediction for linear peptides in solution and in complex. *Nucleic Acids Research* **44**:W449–W454. doi: 10.1093/nar/gkw329, PMID: 27131374

Lessard J, Wu JI, Ranish JA, Wan M, Winslow MM, Staahl BT, Wu H, Aebersold R, Graef IA, Crabtree GR. 2007. An essential switch in subunit composition of a chromatin remodeling complex during neural development. *Neuron* **55**:201–215. doi: 10.1016/j.neuron.2007.06.019, PMID: 17640523

Lieleg C, Ketterer P, Nuebler J, Ludwigsen J, Gerland U, Dietz H, Mueller-Planitz F, Korber P. 2015. Nucleosome spacing generated by ISWI and CHD1 remodelers is constant regardless of nucleosome density. *Molecular and Cellular Biology* **35**:1588–1605. doi: 10.1128/MCB.01070-14, PMID: 25733687

Luger K, Mäder AW, Richmond RK, Sargent DF, Richmond TJ. 1997. Crystal structure of the nucleosome core particle at 2.8 A resolution. *Nature* **389**:251–260. doi: 10.1038/38444, PMID: 9305837

Luger K, Rechsteiner TJ, Richmond TJ. 1999. Expression and purification of recombinant histones and nucleosome reconstitution. *Methods in Molecular Biology* **119**:1–16. doi: 10.1385/1-59259-681-9:1, PMID: 10804500

Mueller-Planitz F, Klinker H, Ludwigsen J, Becker PB. 2013. The ATPase domain of ISWI is an autonomous nucleosome remodeling machine. *Nature Structural & Molecular Biology* **20**:82–89. doi: 10.1038/nsmb.2457, PMID: 23202585

Mueller-Planitz F. 2015. Crossfinder-assisted mapping of protein crosslinks formed by site-specifically incorporated crosslinkers. *Bioinformatics* **31**:2043–2045. doi: 10.1093/bioinformatics/btv083, PMID: 25788624

Racki LR, Naber N, Pate E, Leonard JD, Cooke R, Narlikar GJ. 2014. The histone H4 tail regulates the conformation of the ATP-binding pocket in the SNF2h chromatin remodeling enzyme. *Journal of Molecular Biology* **426**:2034–2044. doi: 10.1016/j.jmb.2014.02.021, PMID: 24607692

Schindler CE, de Vries SJ, Zacharias M. 2015a. Fully blind Peptide-Protein docking with pepATTRACT. *Structure* **23**:1507–1515. doi: 10.1016/j.str.2015.05.021, PMID: 26146186

Schindler CE, de Vries SJ, Zacharias M. 2015b. iATTRACT: simultaneous global and local interface optimization for protein-protein docking refinement. *Proteins: Structure, Function, and Bioinformatics* **83**:248–258. doi: 10.1002/prot.24728, PMID: 25402278

Schneider TD, Stephens RM. 1990. Sequence logos: a new way to display consensus sequences. *Nucleic Acids Research* **18**:6097–6100. doi: 10.1093/nar/18.20.6097, PMID: 2172928

Shen Y, Maupetit J, Derreumaux P, Tufféry P. 2014. Improved PEP-FOLD approach for peptide and miniprotein structure prediction. *Journal of Chemical Theory and Computation* **10**:4745–4758. doi: 10.1021/ct500592m, PMID: 26588162

Swygert SG, Peterson CL. 2014. Chromatin dynamics: interplay between remodeling enzymes and histone modifications. *Biochimica et Biophysica Acta (BBA) - Gene Regulatory Mechanisms* **1839**:728–736. doi: 10.1016/j.bbagrm.2014.02.013, PMID: 24583555

Szerlong H, Hinata K, Viswanathan R, Erdjument-Bromage H, Tempst P, Cairns BR. 2008. The HSA domain binds nuclear actin-related proteins to regulate chromatin-remodeling ATPases. *Nature Structural & Molecular Biology* **15**:469–476. doi: 10.1038/nsmb.1403, PMID: 18408732

Tsukiyama T, Palmer J, Landel CC, Shiloach J, Wu C. 1999. Characterization of the imitation switch subfamily of ATP-dependent chromatin-remodeling factors in Saccharomyces cerevisiae. *Genes & Development* **13**:686–697. doi: 10.1101/gad.13.6.686, PMID: 10090725

Wang L, Limbo O, Fei J, Chen L, Kim B, Luo J, Chong J, Conaway RC, Conaway JW, Ranish JA, Kadonaga JT, Russell P, Wang D. 2014. Regulation of the Rhp26ERCC6/CSB chromatin remodeler by a novel conserved leucine latch motif. *PNAS* **111**:18566–18571. doi: 10.1073/pnas.1420227112, PMID: 25512493

Webb B, Sali A. 2016. Comparative protein structure modeling using MODELLER. *Current protocols in bioinformatics* **54**:5.6.1–5.6.5. doi: 10.1002/0471250953.bi0506s47

Wilm M, Shevchenko A, Houthaeve T, Breit S, Schweigerer L, Fotsis T, Mann M. 1996. Femtomole sequencing of proteins from polyacrylamide gels by nano-electrospray mass spectrometry. *Nature* **379**:466–469. doi: 10.1038/379466a0, PMID: 8559255

Wittelsberger A, Thomas BE, Mierke DF, Rosenblatt M. 2006. Methionine acts as a "magnet" in photoaffinity crosslinking experiments. *FEBS Letters* **580**:1872–1876. doi: 10.1016/j.febslet.2006.02.050, PMID: 16516210

Yamada K, Frouws TD, Angst B, Fitzgerald DJ, DeLuca C, Schimmele K, Sargent DF, Richmond TJ. 2011. Structure and mechanism of the chromatin remodelling factor ISW1a. *Nature* **472**:448–453. doi: 10.1038/nature09947, PMID: 21525927

Yan L, Wang L, Tian Y, Xia X, Chen Z. 2016. Structure and regulation of the chromatin remodeller ISWI. *Nature* **540**:466–469. doi: 10.1038/nature20590

Yang J, Yan R, Roy A, Xu D, Poisson J, Zhang Y. 2015. The I-TASSER suite: protein structure and function prediction. *Nature Methods* **12**:7–8. doi: 10.1038/nmeth.3213, PMID: 25549265

Yang JG, Madrid TS, Sevastopoulos E, Narlikar GJ. 2006. The chromatin-remodeling enzyme ACF is an ATP-dependent DNA length sensor that regulates nucleosome spacing. *Nature Structural & Molecular Biology* **13**:1078–1083. doi: 10.1038/nsmb1170, PMID: 17099699

Zacharias M. 2003. Protein-protein docking with a reduced protein model accounting for side-chain flexibility. *Protein Science* **12**:1271–1282. doi: 10.1110/ps.0239303, PMID: 12761398

Zhao K, Wang W, Rando OJ, Xue Y, Swiderek K, Kuo A, Crabtree GR. 1998. Rapid and phosphoinositol-dependent binding of the SWI/SNF-like BAF complex to chromatin after T lymphocyte receptor signaling. *Cell* **95**:625–636. doi: 10.1016/S0092-8674(00)81633-5, PMID: 9845365

Zhou CY, Johnson SL, Gamarra NI, Narlikar GJ. 2016. Mechanisms of ATP-Dependent chromatin remodeling motors. *Annual Review of Biophysics* **45**:153–181. doi: 10.1146/annurev-biophys-051013-022819, PMID: 27391925

Zimmer JS, Monroe ME, Qian WJ, Smith RD. 2006. Advances in proteomics data analysis and display using an accurate mass and time tag approach. *Mass Spectrometry Reviews* **25**:450–482. doi: 10.1002/mas.20071, PMID: 16429408

Figures and figure supplements

Concerted regulation of ISWI by an autoinhibitory domain and the H4 tail

Ludwigsen et al., eLife, 6:e21477 (2017)

eLIFE elifesciences.org

RESEARCH ARTICLE

Figures and figure supplements

Concerted regulation of ISWI by an autoinhibitory domain and the H4 N-terminal tail

Johanna Ludwigsen *et al*

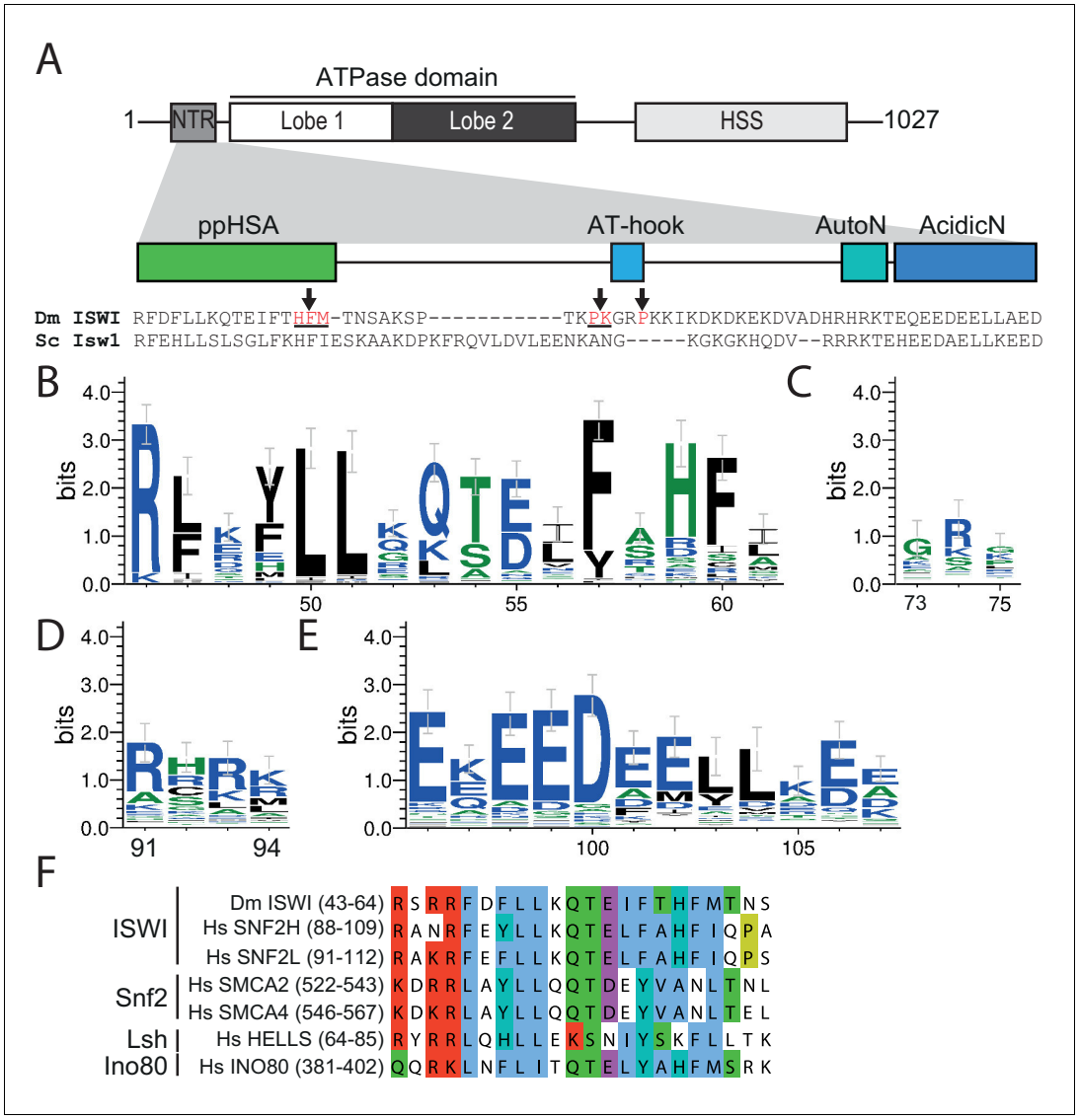

Figure 1. The NTR of ISWI contains several conserved sequence motifs. (**A**) Schematic representation of the ISWI domain composition. The grey inset shows the sequence and motifs of the NTR. Arrows indicate amino acids within the NTR of *Drosophila* ISWI that crosslinked to Lobe 2 of the ATPase domain (***Table 1***). HSS, HAND-SANT-SLIDE domain. (**B–E**) Sequence logos showing the sequence conservation of (**B**) ppHSA, (**C**) AT-hook, (**D**) AutoN, and (**E**) AcidicN. X-Axis values are amino acid positions in *D. melanogaster* ISWI. See ***Figure 1—figure supplement 1*** for full alignment. (**F**) Alignment of the ppHSA motif of *Drosophila* (Dm) ISWI with the human (Hs) ISWI homologs SNF2H and SNF2L and representatives of unrelated remodeler families.

DOI: 10.7554/eLife.21477.003

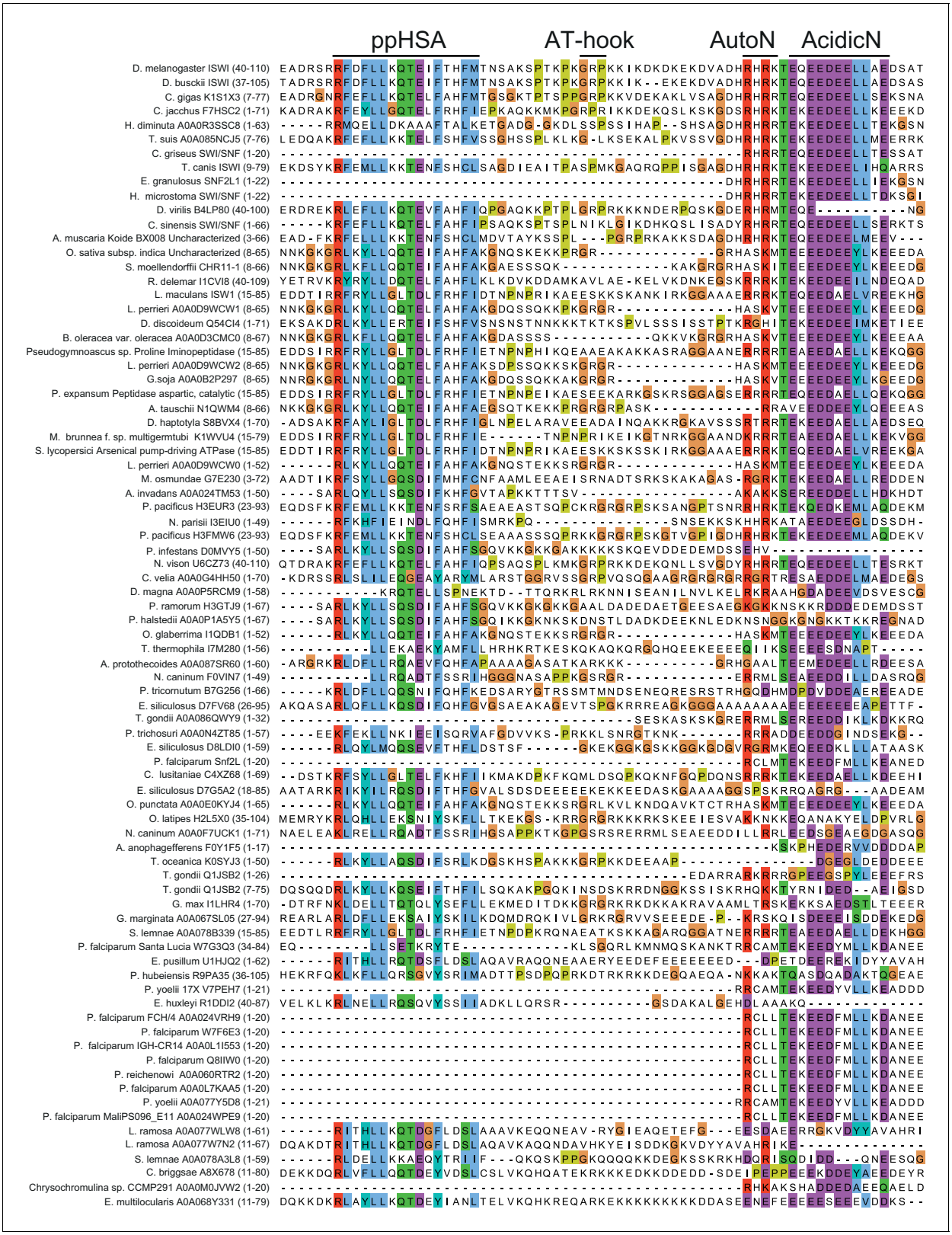

Figure 1—figure supplement 1. Alignment of ISWI homologs from various organisms. Search for homologous proteins and alignment was done using HHblits (toolkit.tuebingen.mpg.de/hhblits). 26 Sequences lacking an NTR were manually deleted from the alignment.

Figure 1—figure supplement 1 continued on next page

Figure 1—figure supplement 1 continued

DOI: 10.7554/eLife.21477.004

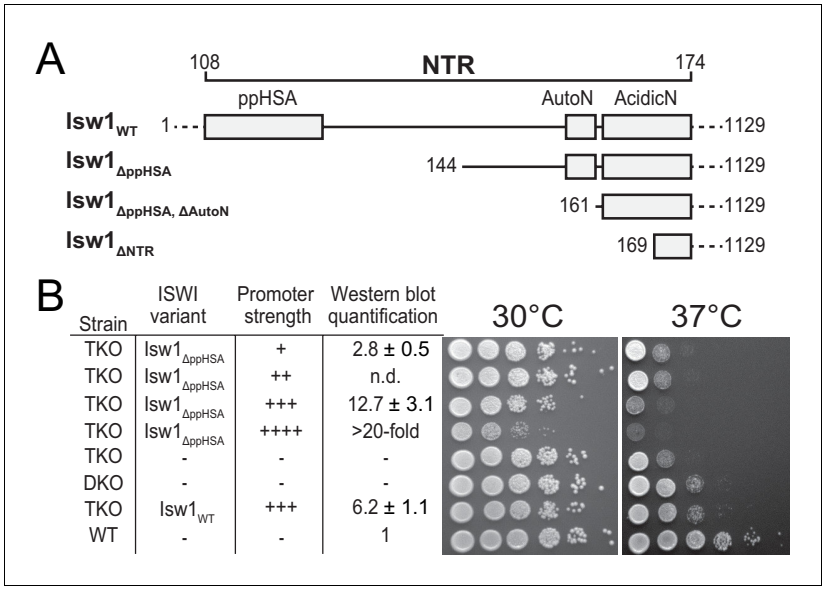

Figure 2. Functional importance of the NTR of yeast Isw1 in vivo. (**A**) Successive N-terminal truncation mutants of Isw1. Note that $Isw1_{\Delta NTR}$ lacked the entire N-terminus up to the first seven residues of AcidicN (***Figure 1E***). (**B**) Complementation assay with $Isw1_{\Delta ppHSA}$. A yeast strain lacking *ISW1, ISW2 and CHD1* (TKO) was transformed with Isw1 derivatives under control of promoters of varying strengths. In comparison to a strain lacking only *ISW2* and *CHD1* (DKO), $Isw1_{WT}$ fully complemented the growth phenotype at elevated temperatures (37°C). In contrast, $Isw1_{\Delta ppHSA}$ did not complement at any expression level. Results for other Isw1 variants can be found in ***Figure 2—figure supplement 1***. Growth was assessed by spotting tenfold serial dilutions of liquid cultures.

DOI: 10.7554/eLife.21477.005

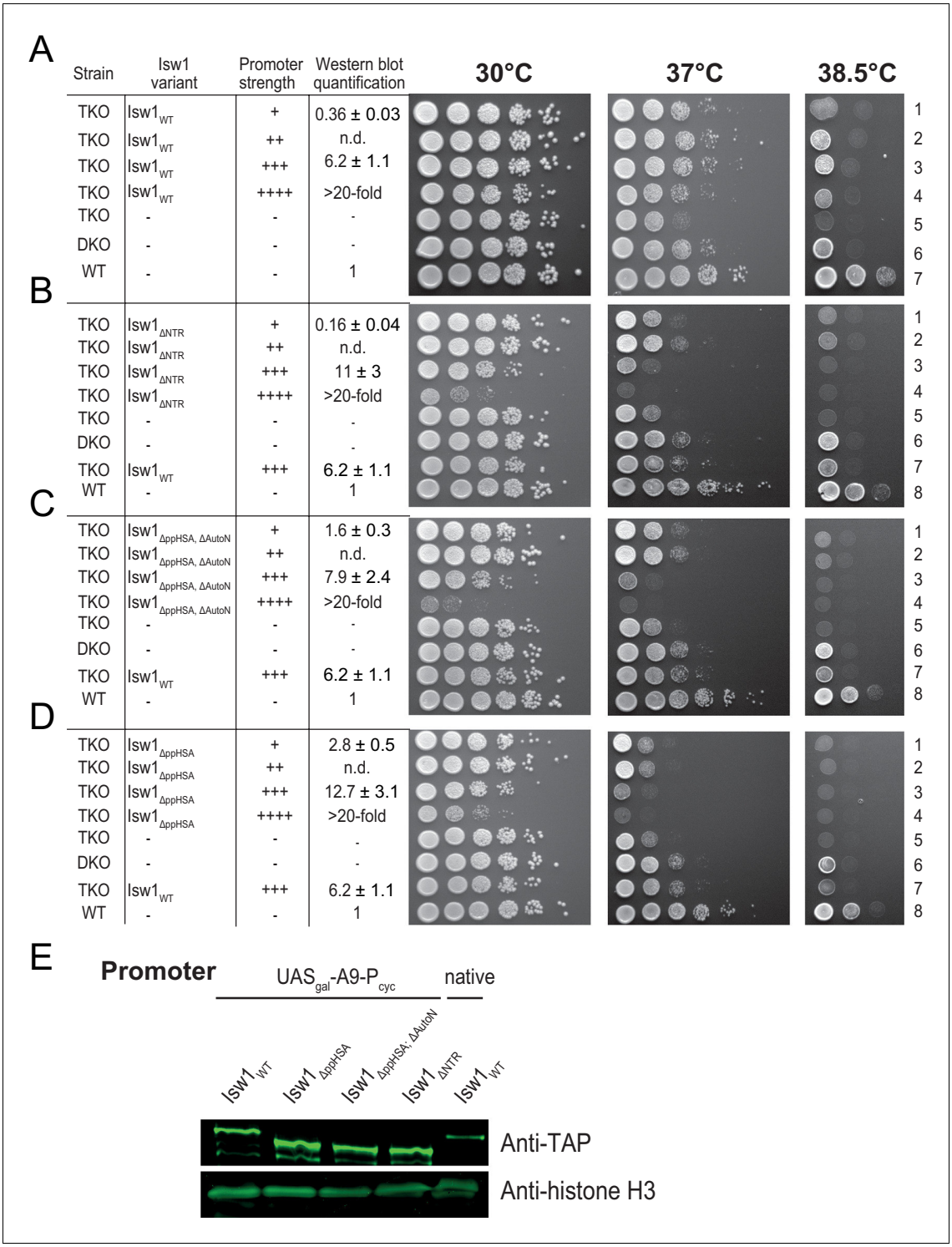

Figure 2—figure supplement 1. Complementation assay with N-terminal truncation variants of Isw1. (**A–D**) Growth assays as in ***Figure 2B***. Expression levels were estimated by Western analysis (see panel **E**). Results in **D** (30˚C and 37˚C) are replotted from ***Figure 2***. (**E**) Exemplary Western blot to determine relative expression levels (tabulated in **A–D**) using an Anti-TAP antibody. TAP-tagged Isw1 variants under control of the indicated promoter were expressed. Their expression level was normalized against genomically TAP-tagged wild-type Isw1. Errors are minimal and maximal values of two technical replicates. H3 served as a loading control.

DOI: 10.7554/eLife.21477.006

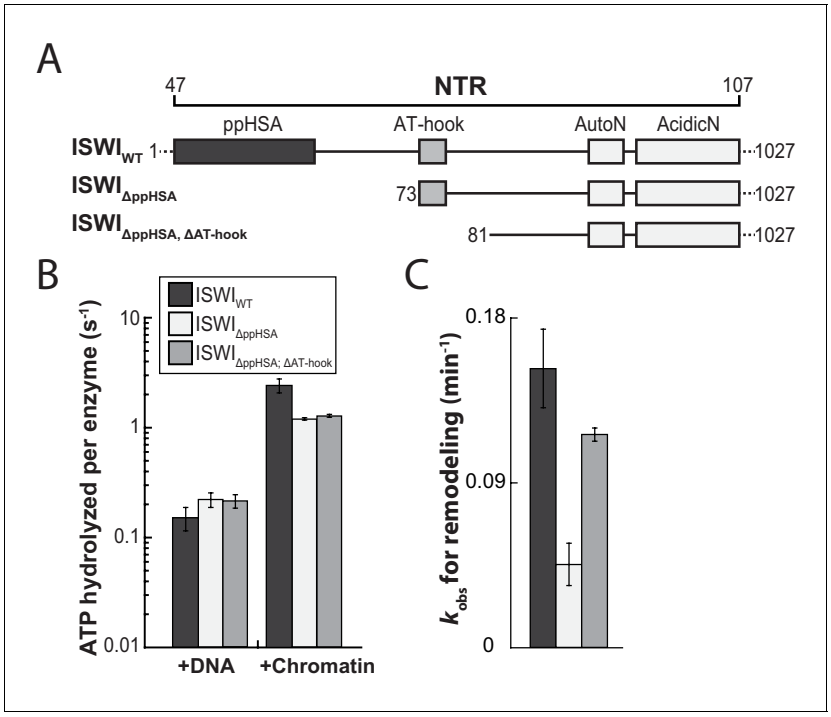

Figure 3. The ppHSA motif is largely dispensable for catalysis. (**A**) N-terminal truncation mutants of *Drosophila* ISWI. (**B**) DNA- and nucleosome-stimulated ATP turnover. ATPase rates were measured in the presence of saturating concentrations of ATP (1 mM), DNA (0.2 g/l) or nucleosomes (0.1 g/l). Errors for nucleosome-stimulated rates of ISWI deletion mutants are minimal and maximal values of two independent measurements, and s.d. for all other measurements ($n \geq 4$). ATPase rates in absence of nucleic acids were <0.022 s^{-1} for all ISWI variants (data not shown). (**C**) Remodeling activity was determined by measuring the accessibility changes of a unique KpnI restriction site in a 25-mer nucleosomal array (100 nM nucleosomes, 300 nM enzyme). Errors are s.d. ($n \geq 3$) except for ISWI$_{\Delta ppHSA; \Delta AT\text{-}hook}$ for which minimal and maximal values of two independent measurements are shown. Raw data of the remodeling assay can be found in ***Figure 3—figure supplement 3***. Color code as in panel **B**.
DOI: 10.7554/eLife.21477.007

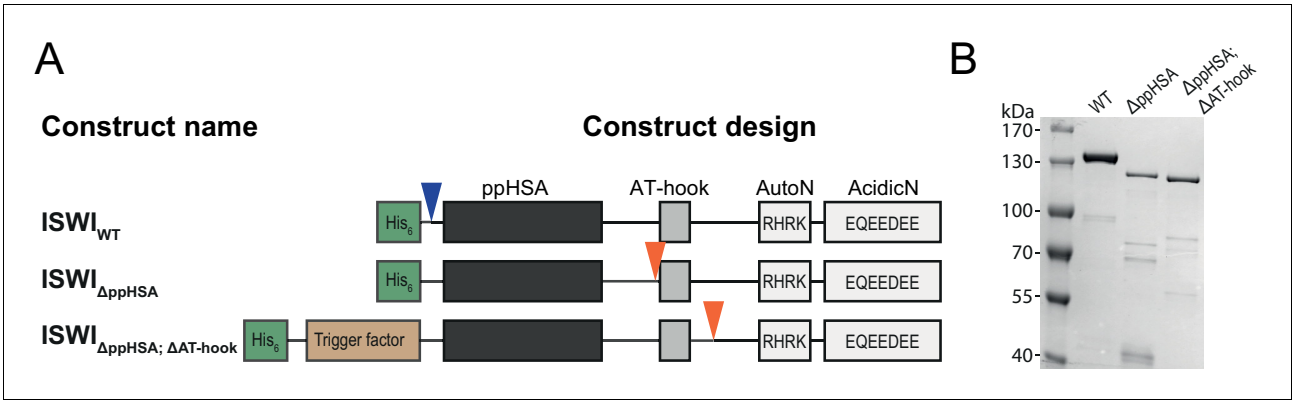

Figure 3—figure supplement 1. Cloning and purification of N-terminal truncation variants of *Drosophila* ISWI. (**A**) Construct design. Only the NTR region and N-terminally fused affinity (His_6) and solubility tags (Trigger factor) are shown (not to scale). Blue arrowheads indicate a TEV cleavage site, orange arrowheads indicate a 3C protease cleavage site that were used to cleave off the tag. (**B**) Coomassie stained SDS-PAGE of purified recombinant ISWI variants.

DOI: 10.7554/eLife.21477.008

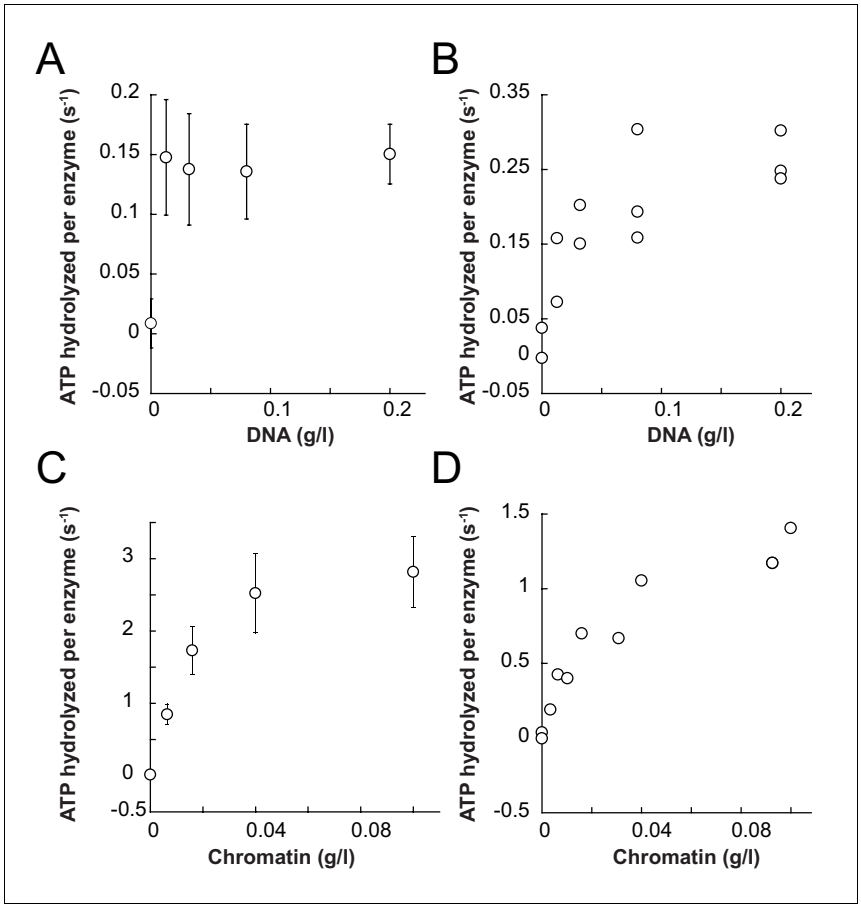

Figure 3—figure supplement 2. Saturation controls for $ISWI_{WT}$ and $ISWI_{\Delta ppHSA}$ in ATPase assays. (**A**,**B**) Linearized pT7blue DNA was titrated over a 16-fold range. 0.2 mg/ml were saturating for $ISWI_{WT}$. (**A**) and $ISWI_{\Delta ppHSA}$ (**B**). (**C**, **D**) Titration of chromatin assembled on linearized pT7blue DNA. 0.1 mg/ml were close to saturation for $ISWI_{WT}$ (**C**) and $ISWI_{\Delta ppHSA}$ (**D**). Errors are s.d. ($n \geq 7$).

DOI: 10.7554/eLife.21477.009

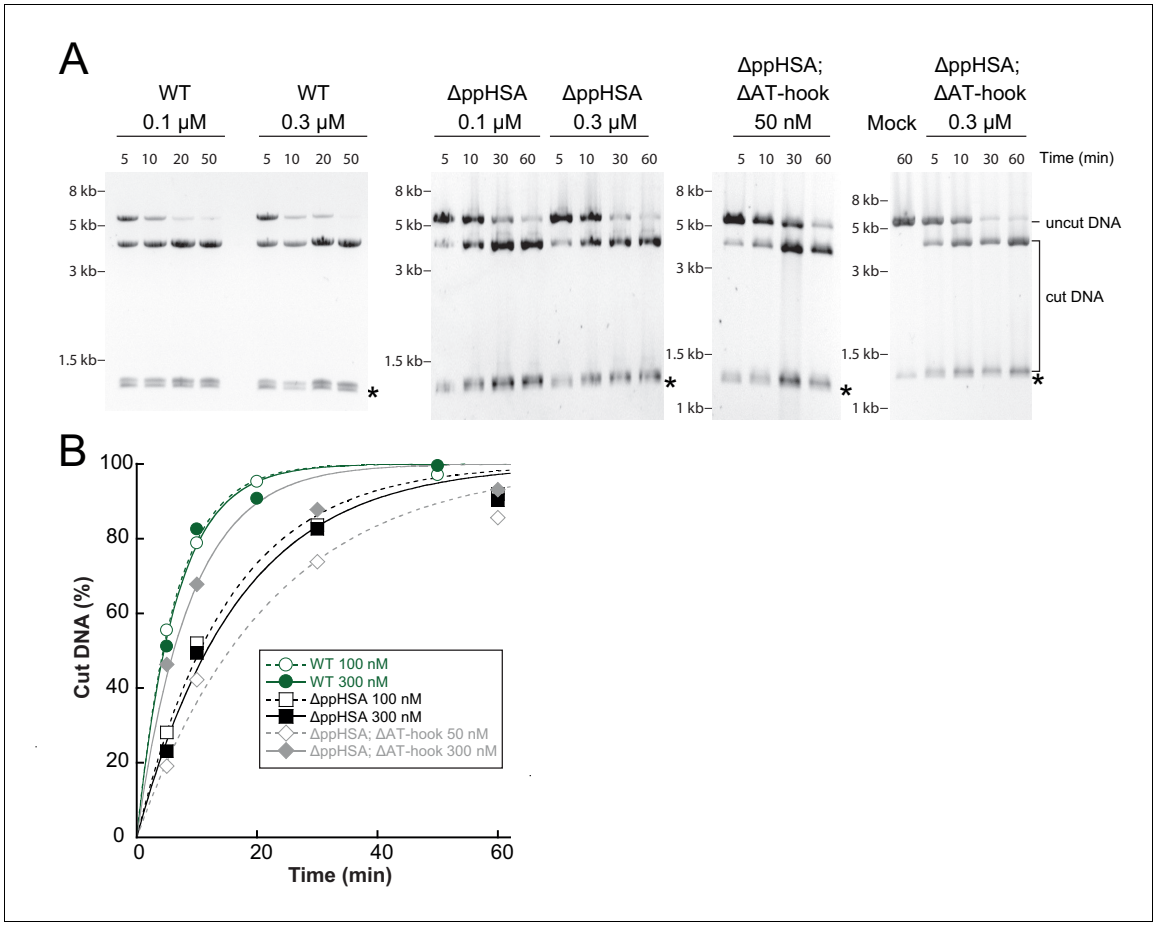

Figure 3—figure supplement 3. Determination of the rate constants for remodeling (k_{obs}; ***Figure 3C***) for $ISWI_{WT}$ and N-terminal truncation mutants of ISWI. (**A**) Exemplary remodeling time courses for $ISWI_{WT}$, $ISWI_{\Delta ppHSA}$ and $ISWI_{\Delta ppHSA;\ \Delta AT\text{-}hook}$. Asterisks mark a contaminating non-nucleosomal DNA (competitor DNA) that was not completely removed during preparation of nucleosomal arrays. Mock: Sample lacking ISWI. (**B**) Quantification of time courses shown in (**A**). Data were fit to a single exponential function to extract the rate constant k_{obs}. The reactions progressed similarly fast when 100 nM and 300 nM enzyme were employed, suggesting saturation of chromatin. Because $ISWI_{\Delta ppHSA;\ \Delta AT\text{-}hook}$ at 50 nM was substoichiometric to nucleosomes (100 nM), it remodeled noticeably more slowly than at 300 nM.

DOI: 10.7554/eLife.21477.010

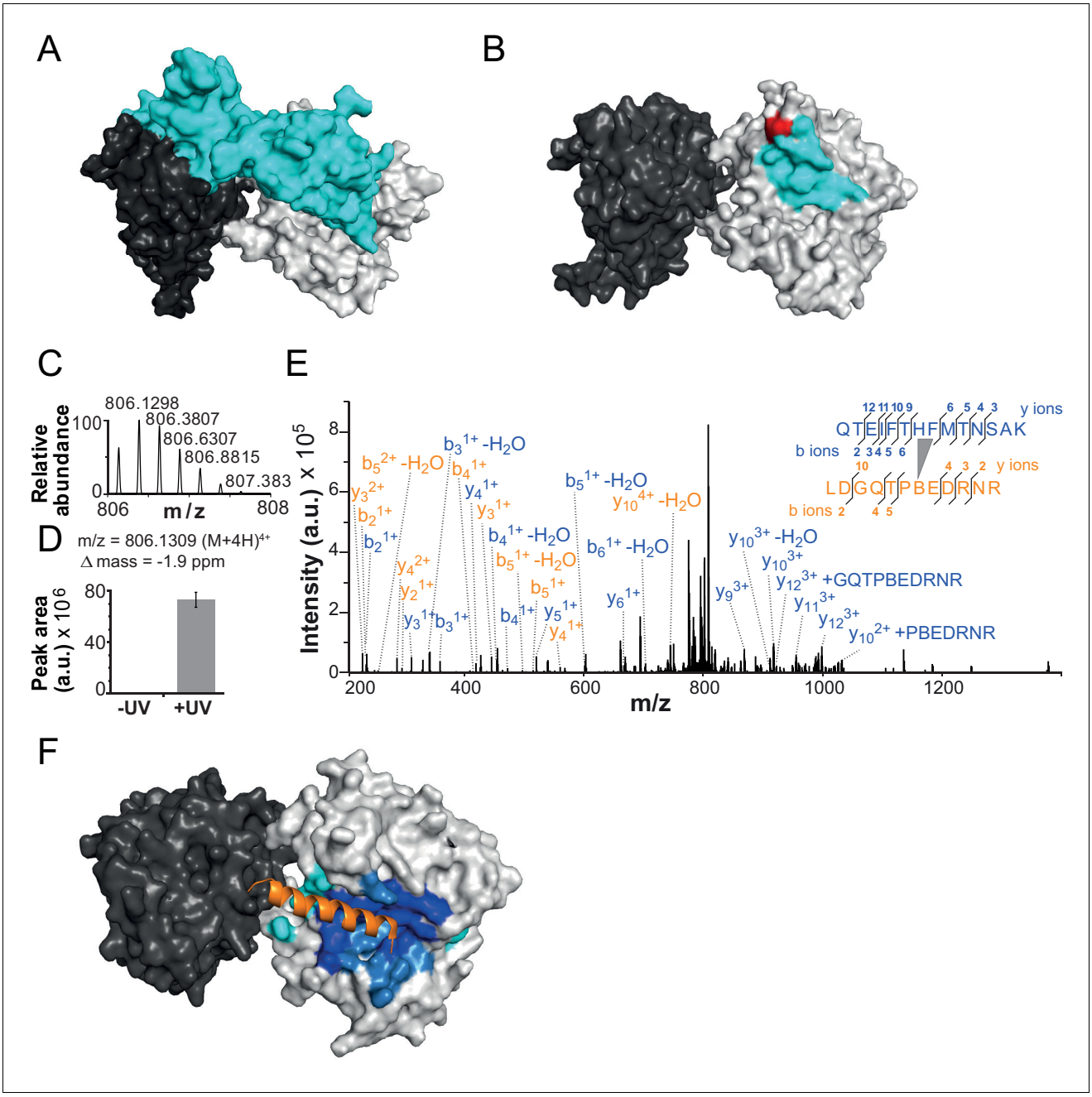

Figure 4. The NTR contacts Lobe 2 of the ATPase domain. (**A**) Surface representation of the Chd1 crystal structure (PDB code 3MWY) (***Hauk et al., 2010***). ATPase Lobe 1 and 2 are colored dark and light grey, respectively, and the N-terminal chromo domains cyan. (**B**) Homology model of the ISWI ATPase domain (***Forné et al., 2012***). Cyan: hypothetical binding interface of the ISWI NTR (see main text), red: position of Bpa substitution (H483). (**C–E**) Mass spectrometric validation of the crosslink XL1 (***Table 1***) formed between Bpa at position 483 and an NTR peptide. (**C**) Isotopic distribution of the crosslinked peptide. (**D**) UV-dependent increase of the signal for the crosslinked peptide. Extracted ion chromatograms of the ions were used for the quantification. (**E**) High resolution, high accuracy MS2 fragmentation spectrum. Top right: summary of observed product ions mapped onto the sequence of the crosslinked peptide. B: Bpa. (**F**) Predicted docking interface of AcidicN (blue and dark blue), AutoN (cyan and dark blue) and overlapping regions (dark blue) in the structural model of ISWI. The predicted interface for AcidicN overlaps with the interface for the acidic helix of the N-terminal chromo domains of Chd1 (orange) (***Hauk et al., 2010***).

DOI: 10.7554/eLife.21477.011

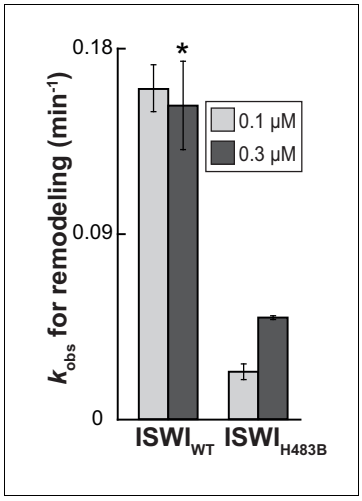

Figure 4—figure supplement 1. The effect of the H483B mutation on chromatin remodeling. With 0.3 µM enzyme, the observed rate constant for remodeling (k_{obs}) was ~threefold affected by the mutation. Note, however, that ISWI$_{H483B}$, in contrast to ISWI$_{WT}$, was not fully saturating at this concentration, as suggested by the saturation control (0.1 µM enzyme). Error bars are s. d. ($n \geq 3$) for ISWI$_{WT}$ and minimal and maximal values of two independent measurements for ISWI$_{H483B}$. Data marked with an asterisk (*) was replotted from ***Figure 3C***.

DOI: 10.7554/eLife.21477.012

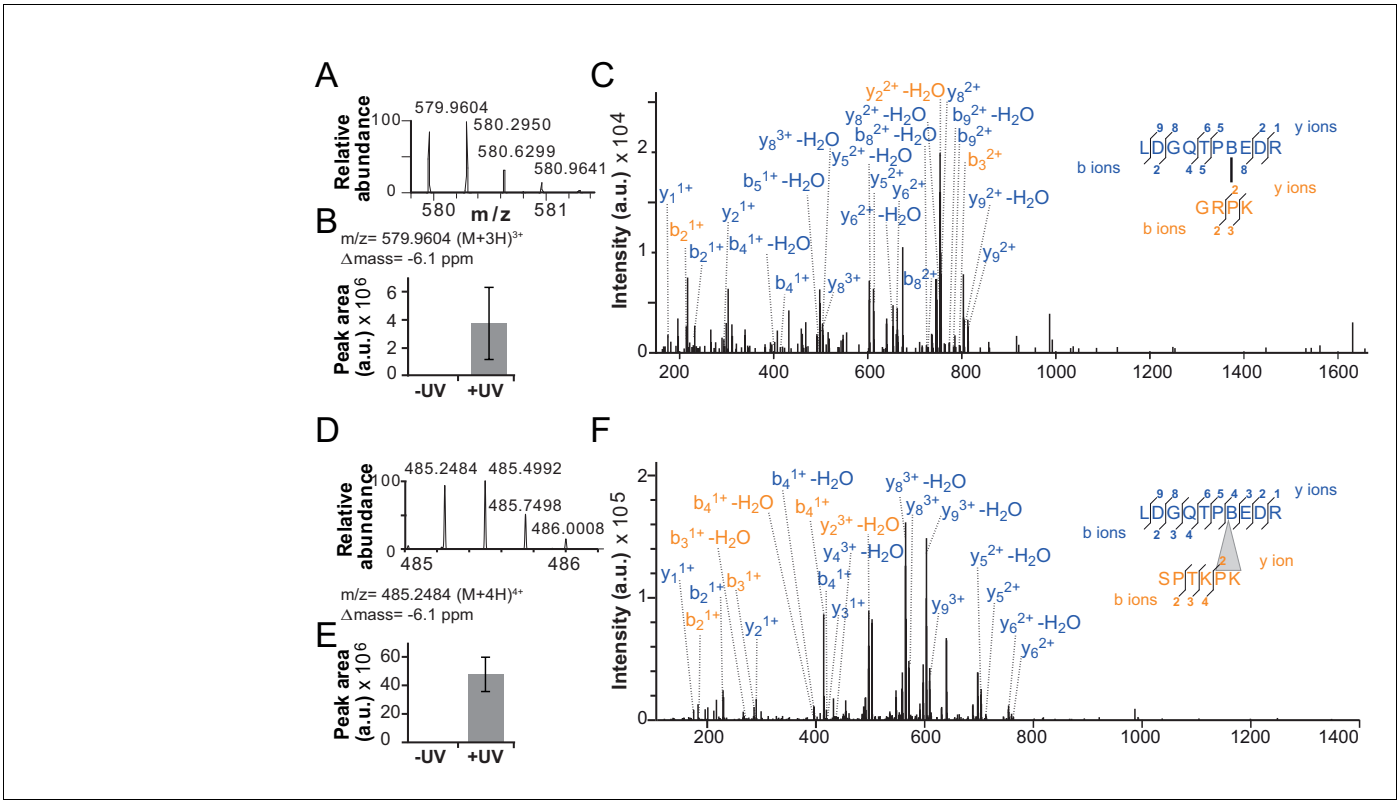

Figure 4—figure supplement 2. Validation of additional crosslinks detected in the $ISWI_{H483B}$ dataset. (**A–C**) Crosslink XL7 (***Table 1***) to P_{75}. (**D–F**) Crosslink XL6 to $P_{71}K_{72}$. For description of data, see ***Figure 4***.

DOI: 10.7554/eLife.21477.013

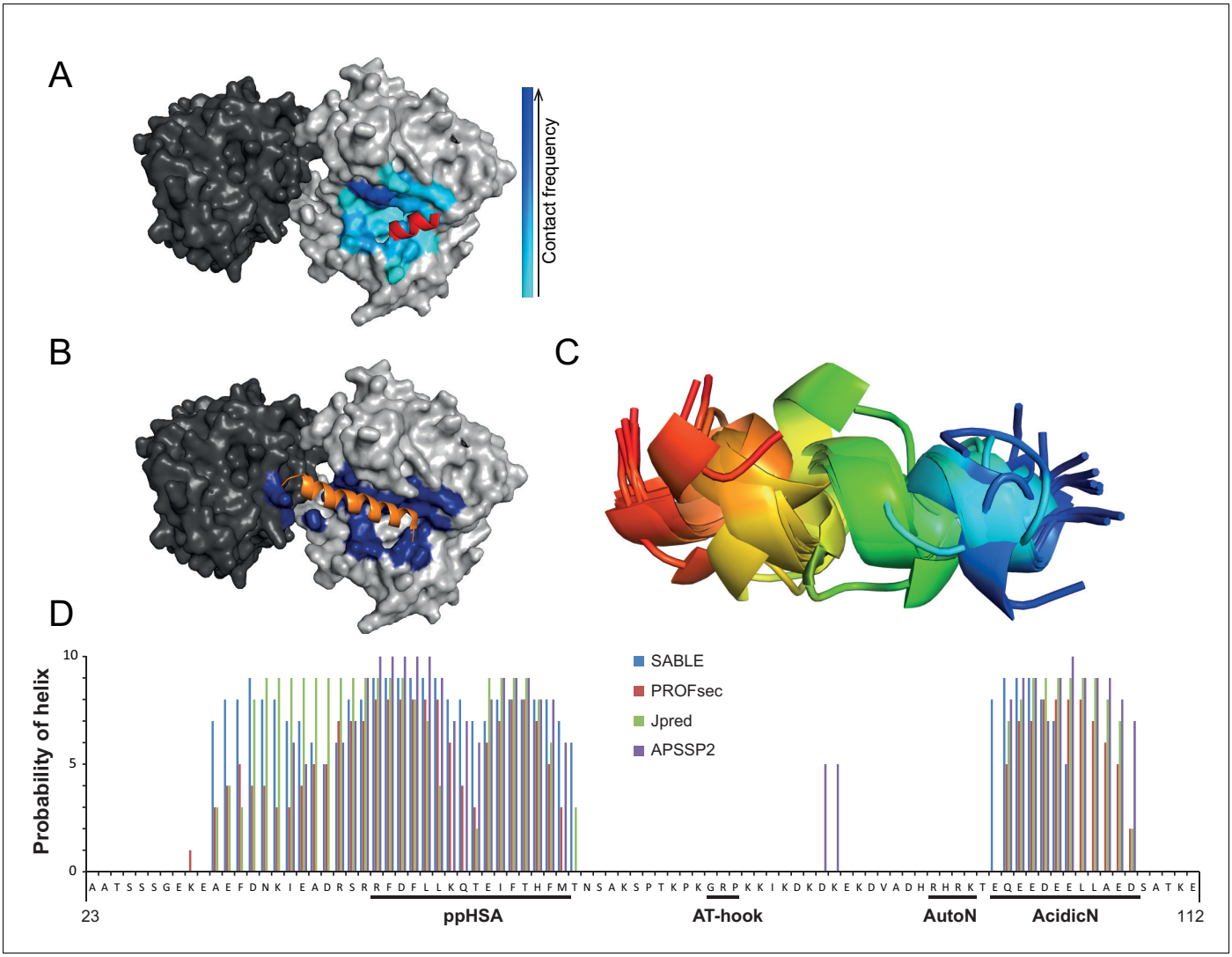

Figure 4—figure supplement 3. Structural predictions of NTR elements. (**A**) Predicted docking interface of AcidicN. The cyan to blue color scale denotes low to high contact probabilities. The location of AcidicN in the MtISWI crystal structure (PDB 5JXR), which became available during the revision of this study, is shown in red. (**B**) Predicted docking interface (blue) of the AutoN-AcidicN peptide in the structural model of ISWI. During docking, both Lobe 1 and Lobe 2 were present (cf. the docking interface shown in ***Figure 4F***). The acidic helix of the N-terminal chromo domains of Chd1 is shown in orange for reference. (**C**) Structure prediction of a peptide comprising AutoN and AcidicN (DHRHRKTEQEEDEELL) by PEP-FOLD and I-TASSER. (**D**) Helical Propensity of amino acids 23–112 of ISWI predicted by four different algorithms (see legend).

DOI: 10.7554/eLife.21477.014

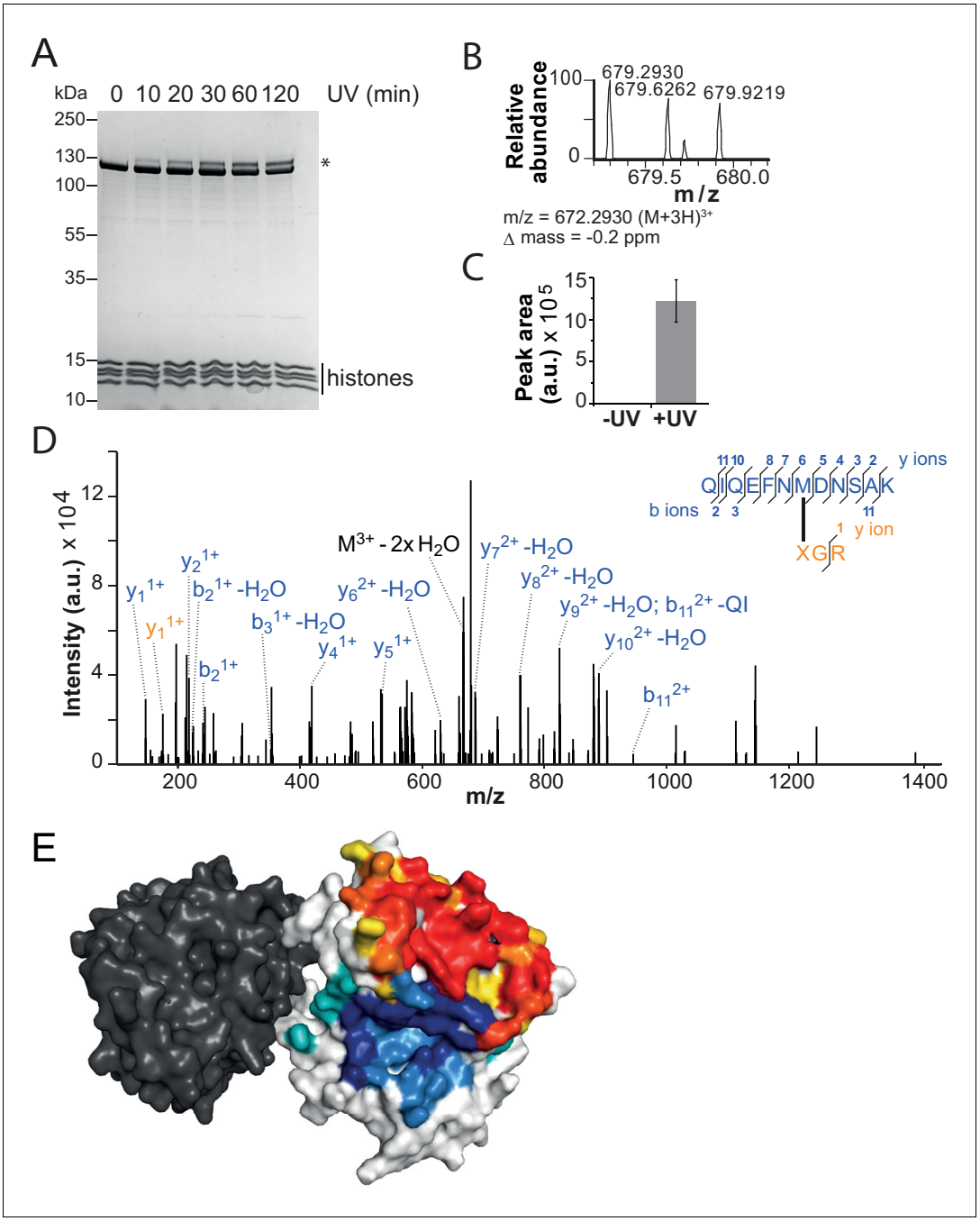

Figure 5. The binding sites of the NTR and the H4-tail on Lobe 2 are proximal. (**A–D**) Crosslinking of nucleosomes containing benzophenone-labeled H4 to ISWI. (**A**) Crosslinking time course analyzed by SDS-PAGE and Coomassie staining. The asterisk marks a UV-irradiation dependent band of lower mobility containing the crosslink mapped in **B–D**. (**B–D**) Mapping and validation of a crosslink (XL11; ***Table 2***) formed in the upshifted band in **A**. Isotopic distribution of the crosslinked peptide, MS2 spectrum and quantification as in ***Figure 4***. (**E**) Crosslink-guided in silico docking of an H4 peptide (amino acids 1–20) to ISWI. The predicted docking interface of the H4 tail on Lobe 2 is illustrated in a yellow and red color scale, which indicates low to high contact probabilities between the docked H4 tail and Lobe 2. The contact probabilities were calculated from a family of 383 docked structures (see Materials and methods). For comparison, the predicted docking interface of the NTR is shown in shades of blue (see ***Figure 4F***).
DOI: 10.7554/eLife.21477.017

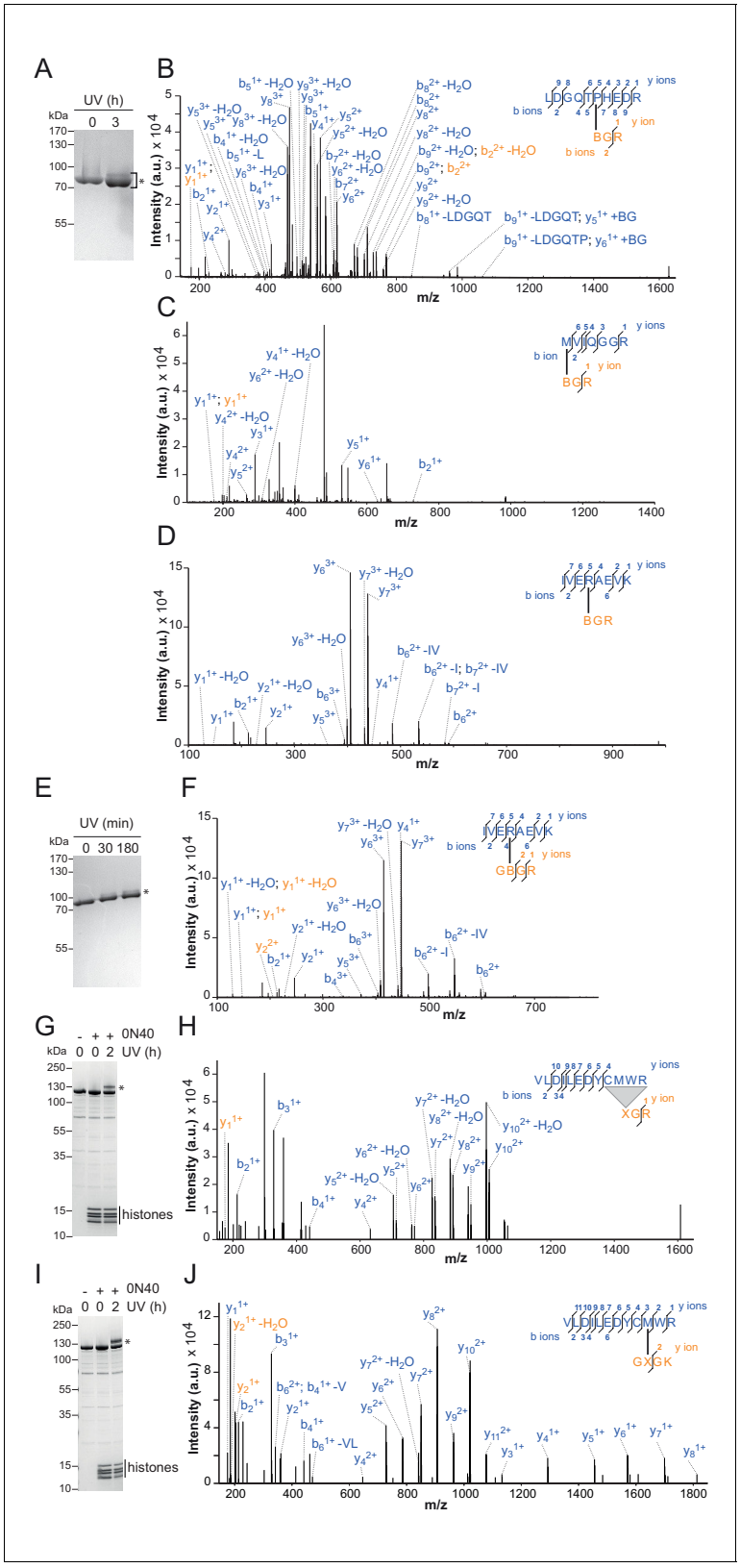

Figure 5—figure supplement 1. Additional crosslinks between the H4 tail and ISWI or SNF2H. (**A–D**) SDS-PAGE analysis and MS mapping of crosslinks formed between a synthetic H4 tail peptide containing Bpa at amino acid

Figure 5—figure supplement 1 continued on next page

Figure 5—figure supplement 1 continued

one to the following amino acids in $ISWI_{26-648}$: H482 (**A**; XL13a in ***Table 2***); M578 (**B**; XL15); R568 (**C**; XL16). (**E–F**) MS mapping and SDS-PAGE analysis of crosslinks formed between a synthetic H4 tail peptide containing Bpa at amino acid 10 to R568 of $ISWI_{26-648}$ (XL17). Asterisks next to SDS gels mark upshifted bands indicative of successful crosslinking. (**G**,**H**) SDS-PAGE analysis and MS mapping of crosslinks formed by benzophenone-labeled T1C nucleosomes to $C_{519}M_{520}W_{521}R_{522}$ of SNF2H (XL14). (**I**,**J**) SDS-PAGE analysis and MS mapping of crosslinks formed by benzophenone-labeled L10C nucleosomes to position 520 of SNF2H (XL12). B: Bpa, X: Benzophenone-labeled cysteine, 0N40: Mononucleosomes with 40 bp of DNA flanking one side of the nucleosome.
DOI: 10.7554/eLife.21477.018

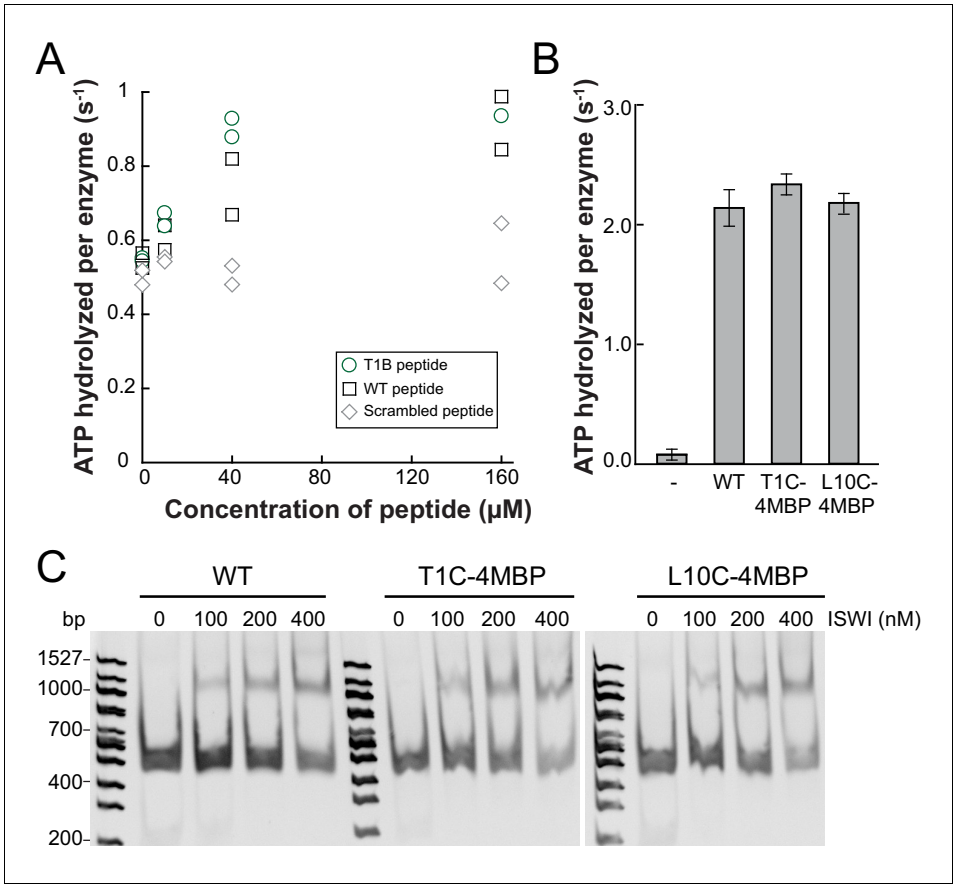

Figure 5—figure supplement 2. Controls for possible adversary effects of covalent modifications of the H4 tail. (**A**) H4 tail peptides (amino acid 1–24) carrying a T1B substitution stimulated the ATPase of $ISWI_{WT}$ (0.5 μM) activity similarly well as WT tail peptides in the presence of 1.2 g/l salmon sperm DNA. In contrast, a scrambled sequence with a Bpa moiety at position one did not noticeably stimulate the ATPase. The ATP concentration was 1 mM. Scrambled and WT peptide data were replotted from ref. 15. (**B**) T1C and L10C mononucleosomes labeled with 4-(N-Maleimido)benzophenone (4MBP) stimulated the ATPase activity of $ISWI_{WT}$ similarly well as WT nucleosomes. A reaction without nucleosomes (–) served as a control. (**C**) WT and 4MBP-labeled T1C and L10C mononucleosomes (200 nM) bound $ISWI_{WT}$ (0 to 400 nM) similarly well in an electrophoretic mobility shift assay. Samples were resolved on a 5% native polyacrylamide gel.

DOI: 10.7554/eLife.21477.019

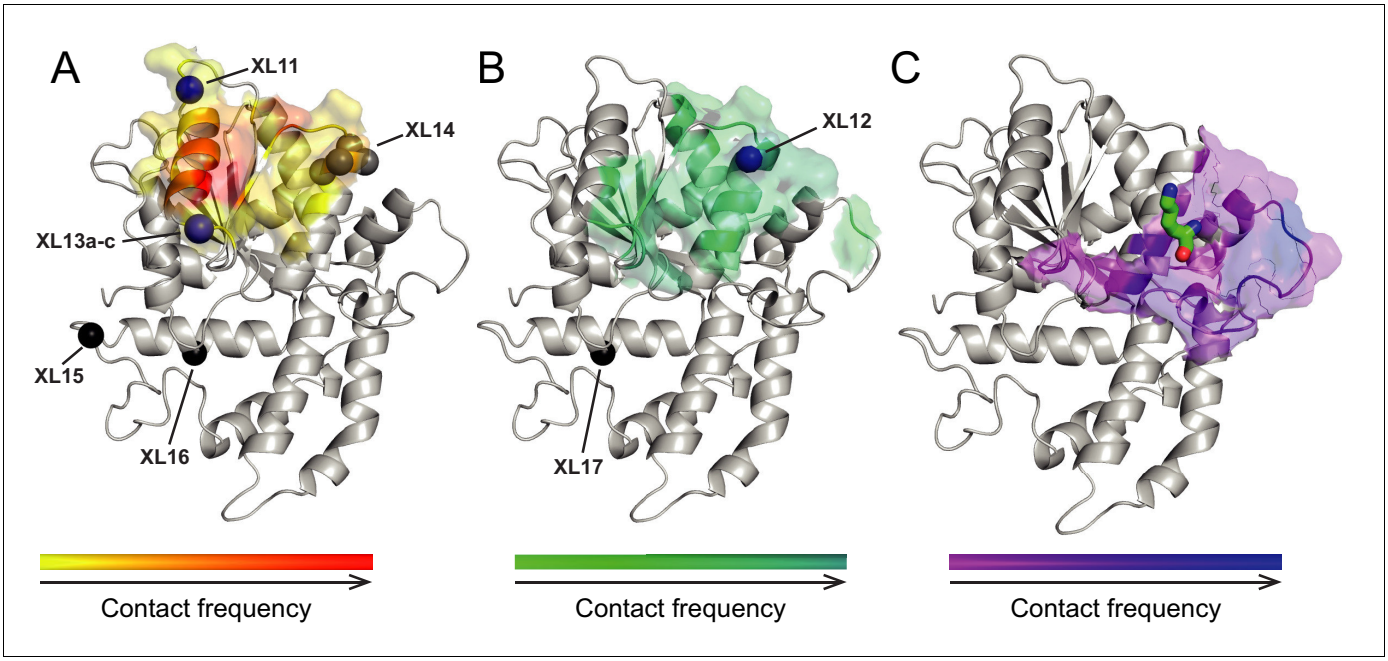

Figure 5—figure supplement 3. Surfaces on Lobe 2 that were sampled by selected amino acids in the H4 tail during crosslink-guided structural docking. (**A**) Interaction surface of histone H4 T1 on Lobe 2 of ISWI. Crosslinked amino acids (***Table 2***) are shown as spheres. Blue, high confidence crosslink positions used for modeling; black and grey, lower confidence crosslink positions. Precise attachment sites are not available for XL14 (grey). (**B**) Interaction surface of H4 L10. Coloring of spheres as in (**A**). (**C**) Predicted interaction surface of H4 K16. H4 K16 from the crystal structure of MtISWI Lobe 2 in complex with an H4 peptide (PDB 5JXT) is shown as stick representation for reference. The color scales indicate contact probabilities between individual amino acids in the H4 tail and Lobe 2 across a family of 383 structural models.

DOI: 10.7554/eLife.21477.020

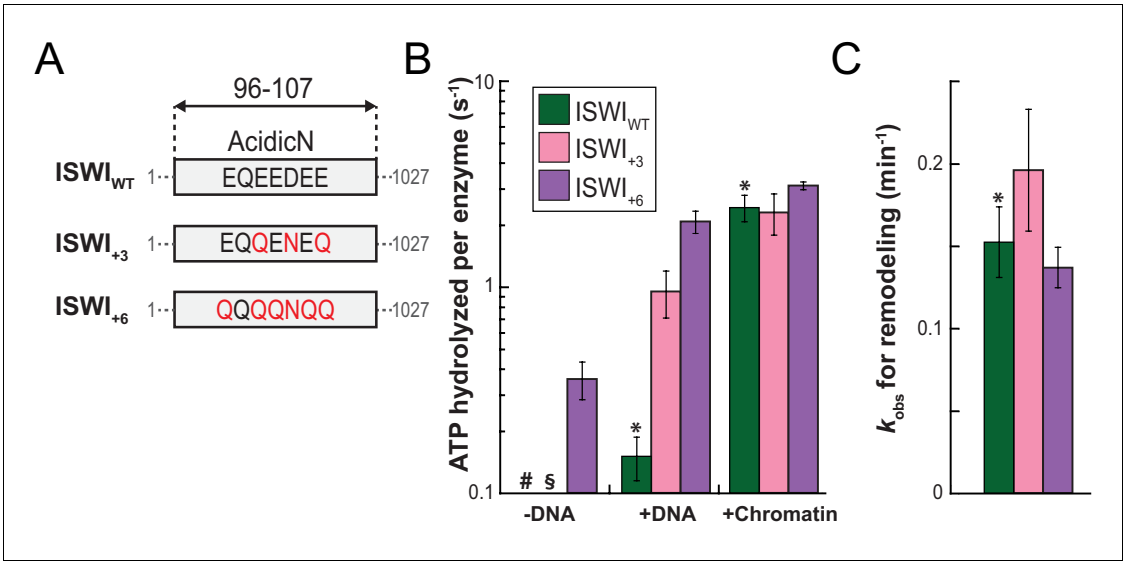

Figure 6. AcidicN is a strong negative regulator of the ATPase. (**A**) Design of AcidicN derivatives of ISWI (see also ***Figure 6—figure supplement 1A***). (**B**) Effects of AcidicN mutation on ATP hydrolysis in absence or presence of saturating concentrations of DNA and chromatin. In absence of DNA, ATPase activities of ISWI$_{WT}$ (#) and ISWI$_{+3}$ (§) were $\leq$0.06 s^{-1}. Errors are s.d. (n $\geq$ 4). (**C**) Effects of AcidicN mutation on the remodeling activities. Nucleosomal arrays containing wild-type H4 were used. Errors are s.d. (n $\geq$ 3) except for ISWI$_{+3}$ for which minimal and maximal values of two independent measurements are shown. Color code as in panel (**B**). Raw data of the remodeling assay can be found in ***Figure 8—figure supplement 1***. Results for ISWI$_{WT}$ (*) are replotted for comparison from ***Figure 3B,C***.

DOI: 10.7554/eLife.21477.021

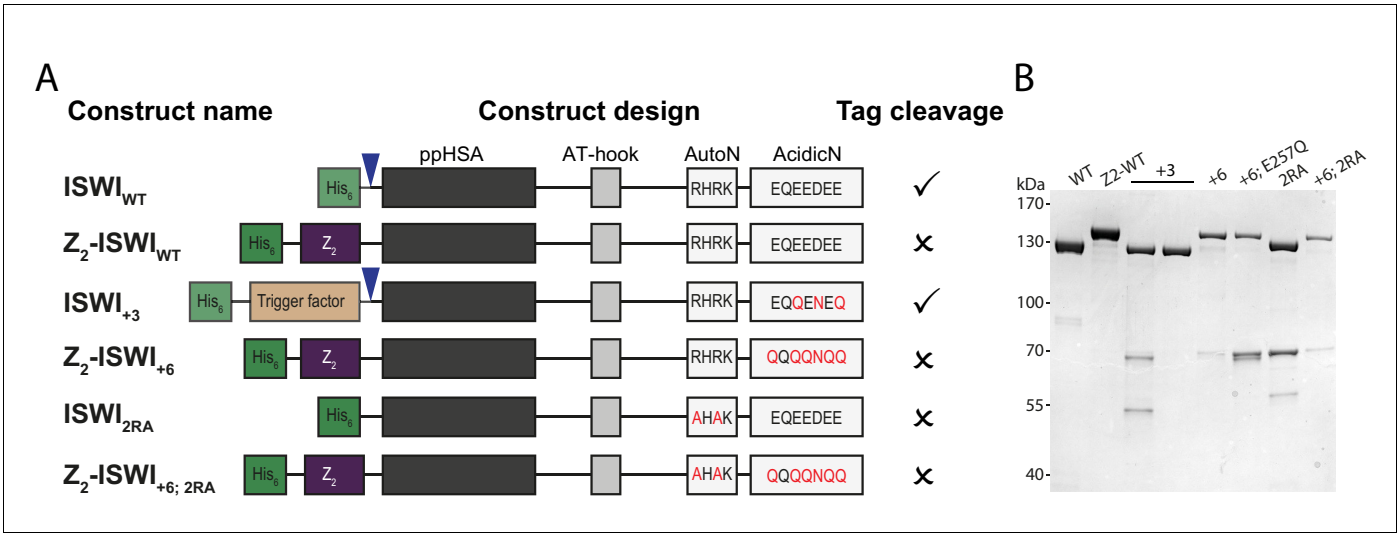

Figure 6—figure supplement 1. AcidicN and AutoN mutants. (**A**) Construct design. Only the NTR region of ISWI including affinity and solubility tags are shown (not to scale). Blue arrowheads indicate a TEV cleavage site. Tags were removed by protease cleavage as indicated. (**B**) Coomassie-stained SDS-PAGE of purified recombinant proteins.

DOI: 10.7554/eLife.21477.022

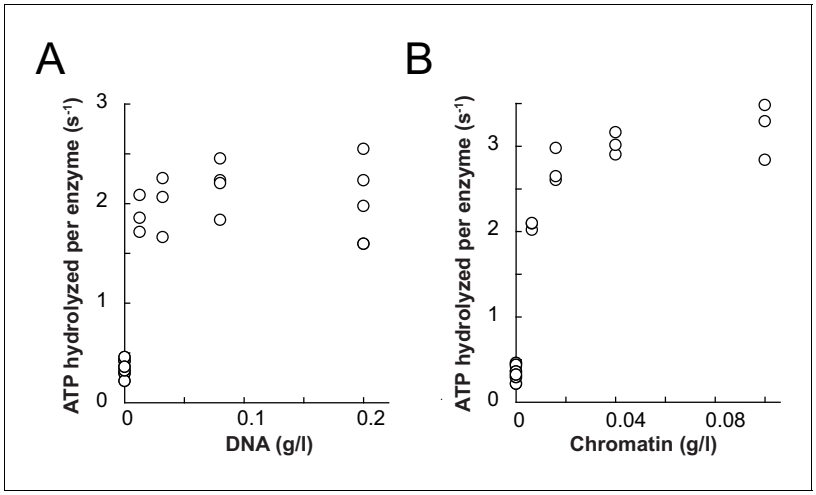

Figure 6—figure supplement 2. Comparison of ATPase and remodeling activities of ISWI control variants used in this study. (**A**) The Z_2 solubility tag did not interfere with DNA- and chromatin-stimulated ATPase activities. Saturating amounts of nucleic acid ligands (0.2 mg/ml **of** linearized pT7blue and 0.1 mg/ml of chromatin assembled on the same DNA, respectively) and ATP (1 mM) were used. The unstimulated basal activity was $\leq$0.05 s^{-1}. Errors are s.d. ($n \geq 3$). (**B**) The Z_2 solubility tag did not interfere with remodeling rates on wild-type H4 containing chromatin and tail-less H4 chromatin. Z_2-tagged $ISWI_{+6;\ E257Q}$, which contained a point mutation in the ATPase domain rendering it catalytically inactive, was included as a control. Its activity on tail-less H4 arrays was undetectable (§). Errors are s.d. ($n \geq 3$) except for the ATPase-dead construct ($ISWI_{+6;\ E257Q}$), which was tested once. (**C**) DNA- and chromatin-stimulated ATP hydrolysis rates of the ATPase dead double mutant $ISWI_{+6;\ E257Q}$ were negligible ($\leq$0.04 s^{-1}). Errors are s.d. ($n \geq 3$) for $ISWI_{WT}$ and minimal and maximal values of two independent measurements for $ISWI_{+6;\ E257Q}$. The asterisks (*) mark data that were replotted for comparison from ***Figure 3B,C***.
DOI: 10.7554/eLife.21477.023

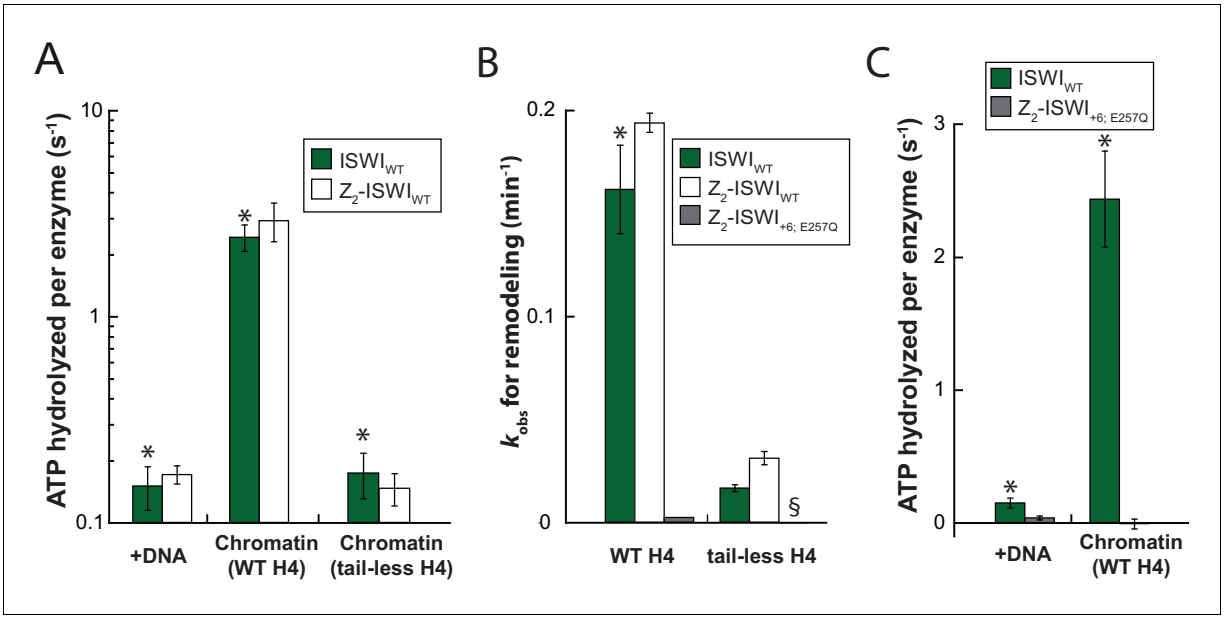

Figure 6—figure supplement 3. Saturation controls for $ISWI_{+6}$ in ATPase assays. (**A**) Linearized pT7blue DNA was titrated over a 16-fold range. 0.2 mg/ml were saturating. (**B**) Titration of chromatin assembled on linearized pT7blue DNA. 0.1 mg/ml were close to saturation.
DOI: 10.7554/eLife.21477.024

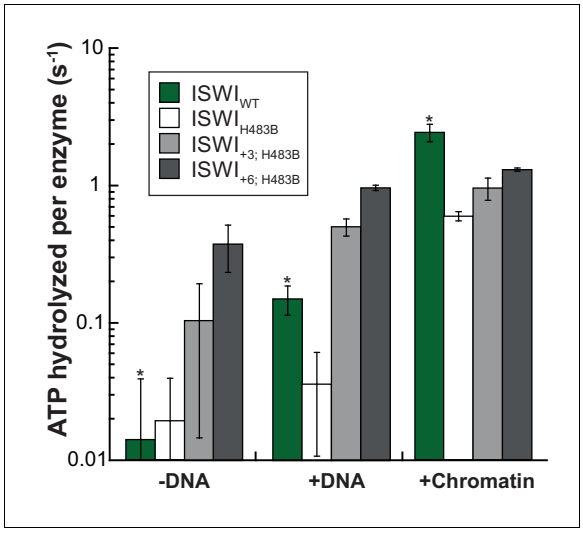

Figure 6—figure supplement 4. AcidicN mutations upregulate the ATPase activity of $ISWI_{H483B}$. Relative to $ISWI_{WT}$, $ISWI_{H483B}$ had a ~fourfold diminished DNA- and chromatin-stimulated ATPase activity. Additional mutation of AcidicN (+3; +6) strongly activated both DNA- and chromatin-stimulated ATP turnover. Errors are s.d. for $ISWI_{WT}$ and minimal and maximal values of two independent measurements for all other constructs. Data for $ISWI_{WT}$ (*) were replotted for comparison from ***Figure 3B***.

DOI: 10.7554/eLife.21477.025

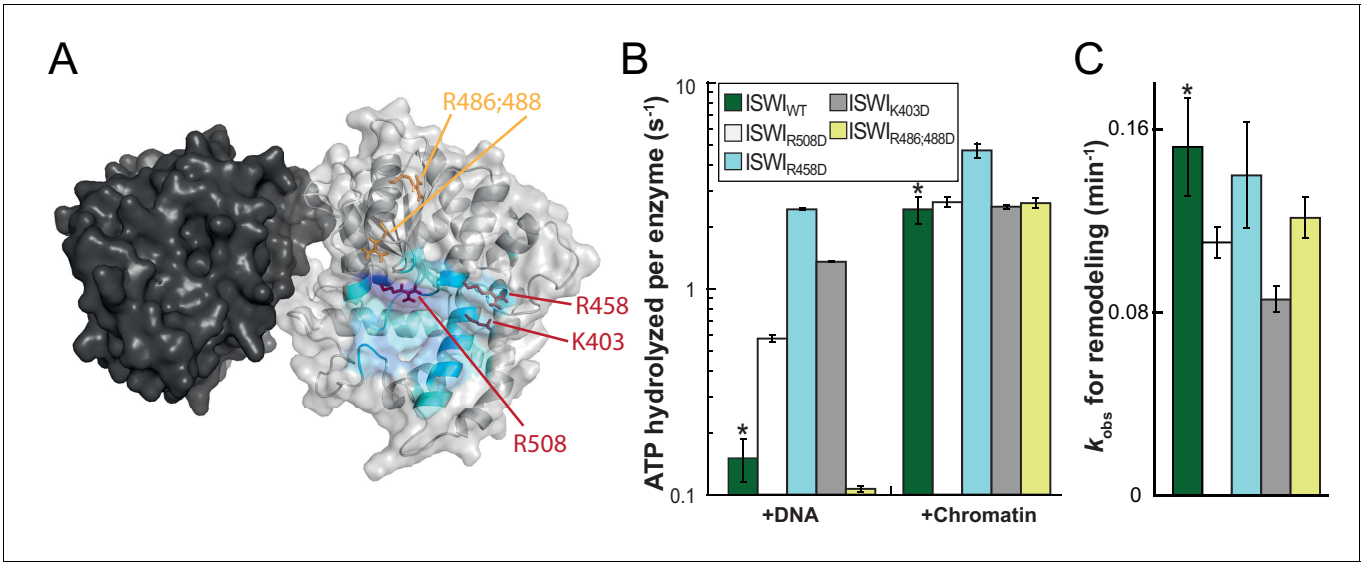

Figure 7. Validation of the predicted binding interface of AcidicN on Lobe 2. (**A**) Homology model of the ISWI ATPase domain. Dark and light grey, ATPase lobes 1 and 2, respectively; blue, hypothetical binding interface of AcidicN as in ***Figure 4—figure supplement 3A***. Positively charged residues selected for mutagenesis are shown in red (AcidicN interface mutant) and orange (control mutant). (**B**) Mutation of the AcidicN interface (K403D, R458D and R508D) strongly upregulated DNA-stimulated ATP hydrolysis relative to $ISWI_{WT}$, whereas the nucleosome-stimulated ATP turnover was similar. In contrast, a control mutation (R486; 488D) had little effect on ATP hydrolysis. Saturating concentrations of DNA and chromatin were used. Errors are s.d. for $ISWI_{WT}$ and minimal and maximal values of two independent measurements for all other constructs. (**C**) AcidicN interface variants of ISWI robustly remodeled nucleosomes within twofold of $ISWI_{WT}$. Nucleosomal arrays containing wild-type H4 were used. Errors are s.d. ($n \geq 3$) for $ISWI_{WT}$ and minimal and maximal values of two independent measurements for all other constructs. Raw data of the remodeling assay can be found in ***Figure 7—figure supplement 2***. Color code as in (**B**). Results for $ISWI_{WT}$ (*) were replotted for comparison from ***Figure 3B,C***.

DOI: 10.7554/eLife.21477.026

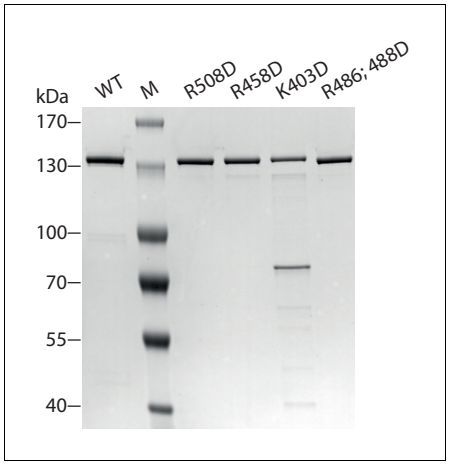

Figure 7—figure supplement 1. Coomassie-stained SDS-PAGE of purified recombinant ISWI constructs analyzed in ***Figure 7***.
DOI: 10.7554/eLife.21477.027

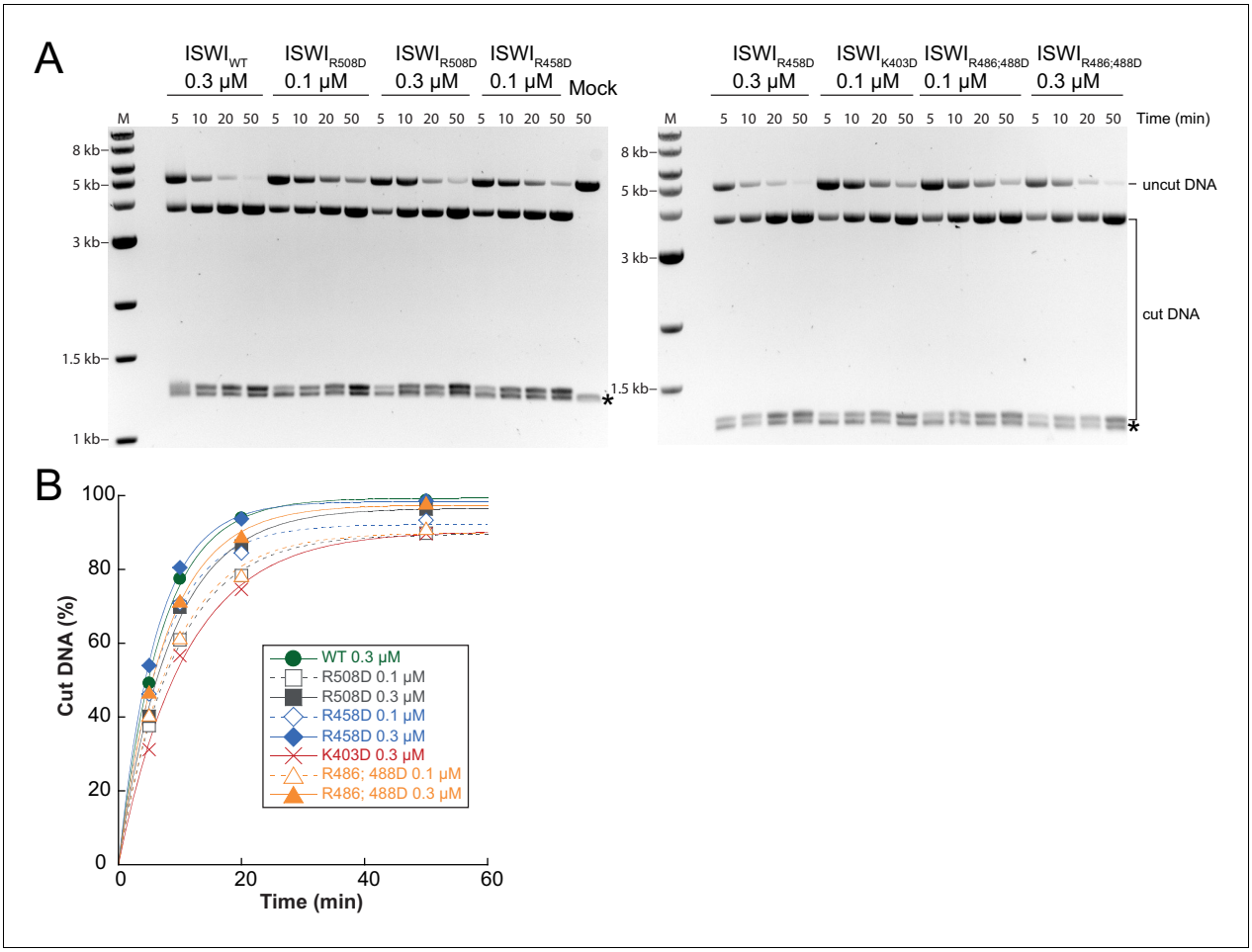

Figure 7—figure supplement 2. Determination of rate constants for remodeling of AcidicN interface mutants. (**A**) Exemplary remodeling time courses on WT H4-arrays for interface mutants. Asterisks mark a contaminating non-nucleosomal DNA (competitor DNA) that was not completely removed during preparation of nucleosomal arrays. Mock: Sample lacking ISWI. (**B**) Quantification of time courses shown in (**A**). Data were fit to a single exponential function to extract k_{obs} (see ***Figure 7C***).

DOI: 10.7554/eLife.21477.028

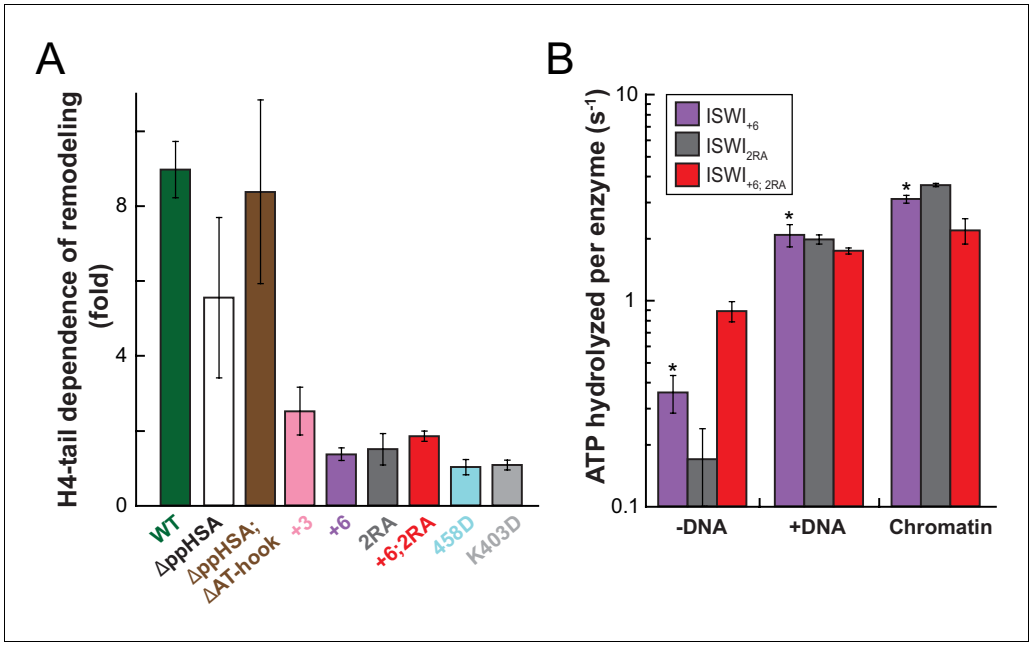

Figure 8. Mutation of AcidicN, the AcidicN binding interface or AutoN suppresses dependence on the H4-tail. (**A**) H4-tail dependence of the remodeling activities of ISWI variants. Values were calculated from the observed remodeling rate constants obtained for WT and tail-less H4 chromatin (***Figure 8—figure supplement 1E***). (**B**) ATP hydrolysis measurements of $ISWT_{+6}$, $ISWI_{2RA}$ and $ISWI_{+6;\ 2RA}$ in absence or presence of saturating concentrations of DNA and chromatin.

DOI: 10.7554/eLife.21477.029

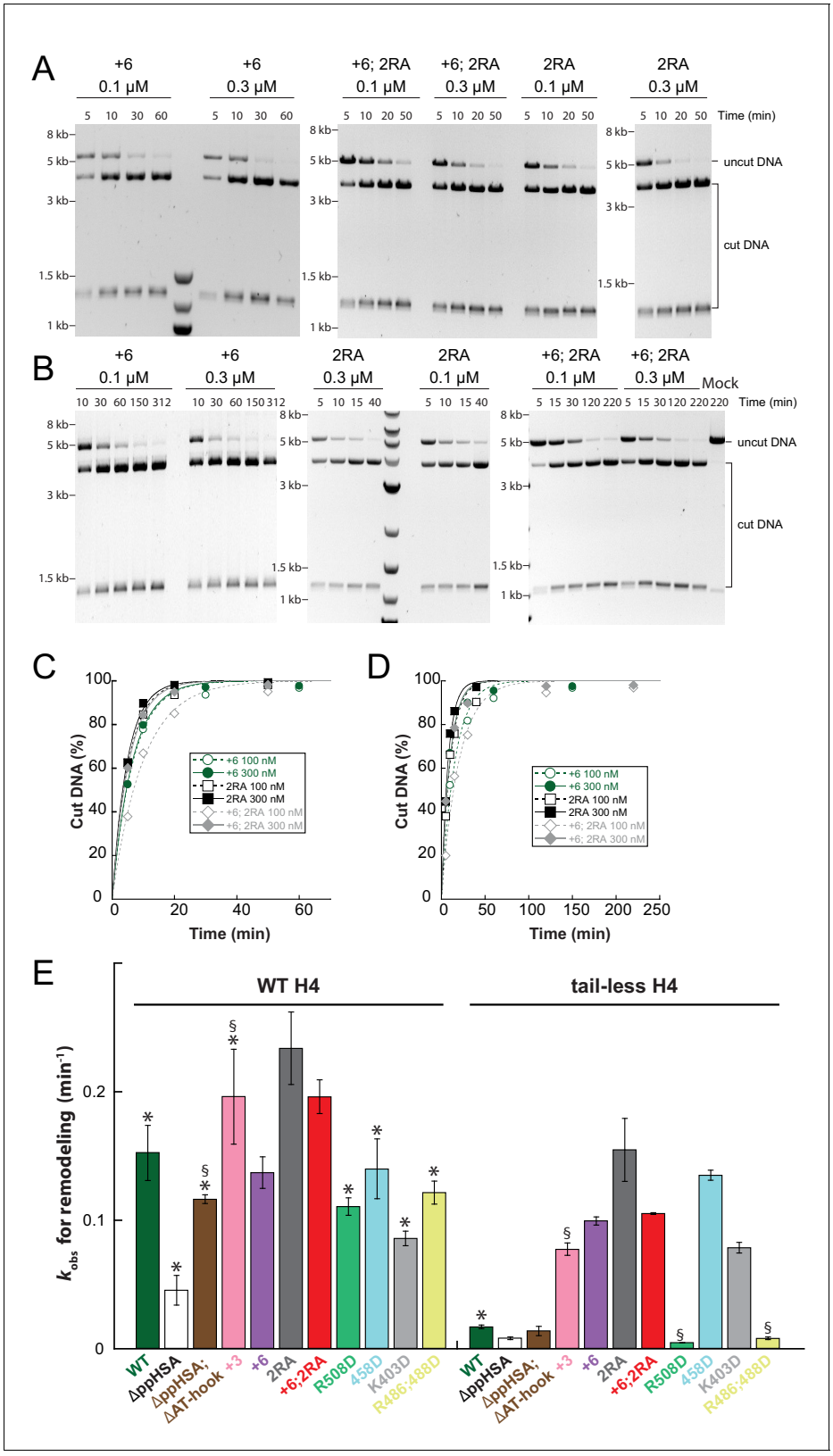

Figure 8—figure supplement 1. Raw data of the remodeling assays. (**A–D**) Determination of rate constants (k_{obs}) from remodeling assays for $ISWI_{+6}$, $ISWI_{2RA}$ and $ISWI_{+6;\ 2RA}$. Shown are exemplary time courses on nucleosomal

Figure 8—figure supplement 1 continued on next page

Figure 8—figure supplement 1 continued

arrays containing wild-type (**A**,**C**) and tail-less H4 (**B**,**D**). Data were fit to a single exponential function to extract the rate constant k_{obs}. (**E**) Rate constants for remodeling of ISWI variants used in this study (all 300 nM). Errors are s.d. ($n \geq 3$) for $ISWI_{WT}$, $ISWI_{\Delta ppHSA}$, and $ISWI_{+6}$ and minimal and maximal values of two independent measurements for all other variants. Samples, in which the enzyme concentration was not saturating, are indicated (§). Data marked with asterisks (*) were replotted from previous figures for better overview.

DOI: 10.7554/eLife.21477.030

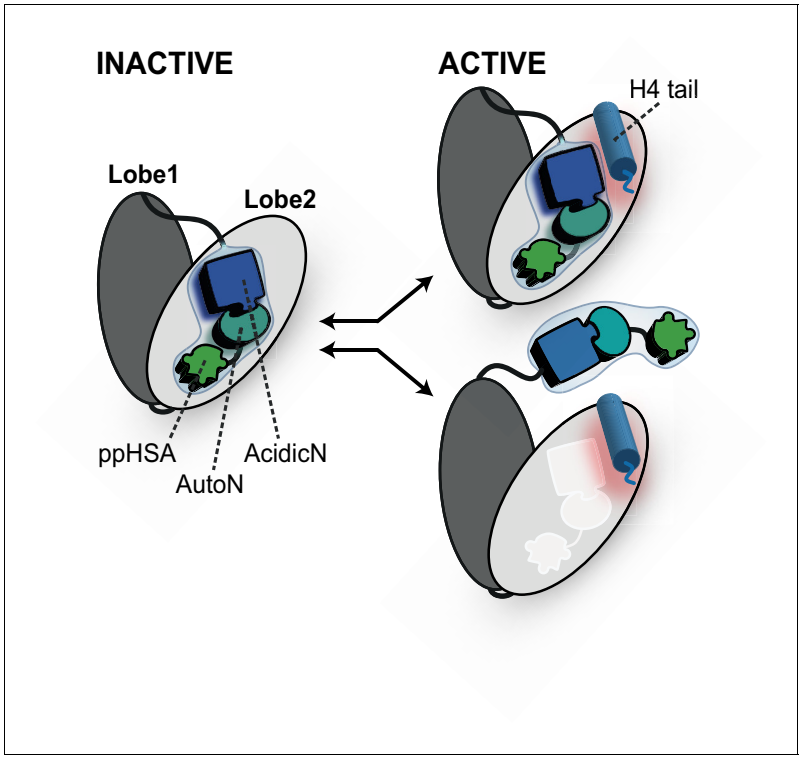

Figure 9. Proposed models for autoregulation imposed by the NTR and the recognition process of the H4 tail. The ppHSA motif, AcidicN and AutoN dock against Lobe 2 of the ATPase domain, promoting an overall structural architecture of the ATPase module that is reminiscent of Chd1 (***Figure 4A***). AcidicN and AutoN functionally collaborate in the H4 tail recogniton process. The docking site of AutoN-AcidicN is adjacent to the H4 tail potentially allowing simultaneous binding (top). Alternatively, the H4 tail may displace the NTR as suggested previously (bottom) (***Clapier and Cairns, 2012***).

DOI: 10.7554/eLife.21477.031

2.4 Remodeling and repositioning of nucleosomes in nucleosomal arrays

Johanna Ludwigsen[1,2], Nicola Hepp[1,2], Henrike Klinker[1], Sabrina Pfennig[1]

and Felix Mueller-Planitz[1]

[1]Biomedical Center, Ludwig-Maximilians-University, 82152 Martinsried, Germany

[2]These authors contributed equally to this work

Methods in Molecular Biology series (Springer), Molecular Motors volume

in revision

Declaration of contributions

N. Hepp and I contributed equally to this work. N. Hepp designed and prepared all materials and developed the original protocol for the quantitative polynucleosome remodeling assay (sections 2.2, 3.1). H. Klinker developed the polynucleosome repositioning assay (sections 2.3, 3.2). I applied and optimized the protocols. Moreover, I wrote the first draft of the manuscript and developed the enclosed version together with F. Mueller-Planitz, N. Hepp and H. Klinker. S. Pfennig helped writing the introduction and prepared Figure 1. I prepared all remaining figures.

Remodeling and repositioning of nucleosomes in nucleosomal arrays

Johanna Ludwigsen[1,2], Nicola Hepp[1,2], Henrike Klinker[1], Sabrina Pfennig[1]

and Felix Mueller-Planitz[1,*]

[1]Biomedical Center, Ludwig-Maximilians-University, 82152 Martinsried, Germany

[2]These authors contributed equally to this work

*Correspondence: Felix.Mueller-Planitz@med.uni-muenchen.de

I. Abstract

ATP-dependent nucleosome remodeling factors sculpt the nucleosomal landscape of eukaryotic chromatin. They deposit or evict nucleosomes or reposition them along DNA in a process termed nucleosome sliding. Remodeling has traditionally been analyzed using mononucleosomes as a model substrate. *In vivo*, however, nucleosomes form extended arrays with regular spacing. Here, we describe how regularly spaced nucleosomal arrays can be reconstituted *in vitro* and how these arrays can be used to dissect remodeling in the test tube. We outline two assays. The first assay senses various structural changes to a specific nucleosome within the nucleosomal array whereas the second assay is specific towards detecting repositioning of nucleosomes within the array. Both assays exploit changes to the accessibility of DNA to restriction enzymes during the remodeling reaction.

II. Key words

a. ATP-dependent nucleosome remodeling
b. Nucleosome remodeling/sliding/repositioning
c. Nucleosomal arrays
d. ISWI
e. Snf2-family ATPase
f. Chromatin remodeling enzyme

1 INTRODUCTION

In the nucleus of eukaryotic cells, the DNA is organized together with proteins in a highly ordered structure called chromatin. The smallest unit of chromatin is the nucleosome, which consists of approximately 147 bp of DNA that is spooled around an octamer of histones. The nucleosome represents a physical barrier for many nuclear processes including transcription, replication, DNA methylation and DNA repair. To overcome the barrier imposed by nucleosomes, cells have evolved a class of factors called nucleosome remodeling enzymes. These factors keep chromatin dynamic allowing the cells to rapidly adapt to environmental or developmental cues (1, 2). During the remodeling process, the energy of ATP-hydrolysis is used to weaken or disrupt DNA–histone contacts and facilitate assembly, disassembly or repositioning of entire nucleosomes or the exchange of certain histones for histone variants. Chromatin remodeling enzymes all belong to the Snf2-family of helicase-related proteins with ISWI, Snf2h and Chd1 belonging to the best studied representatives (3, 4).

To study the enzymatic activities of remodeling enzymes *in vitro*, a number of remodeling assays have been devised over the years. Initially, most assays relied on mononucleosomes as model substrates (5, 6). Since nucleosomes occur in form of large assemblies *in vivo*, remodeling assays that employed arrays of nucleosomes were later developed to better mimic the physiological situation (7, 8).

Here we describe two assays to study structural changes of 25-mer nucleosomal arrays during the remodeling process. The term 'remodeling' comprises many structural modifications of the nucleosomal organization imposed by ATP-dependent chromatin remodeling enzymes (Figure 1). For example, nucleosome remodelers may physically slide nucleosomes along DNA, they may evict or *de novo* assemble nucleosomes or they may locally unwrap DNA from the nucleosome (2).

The first assay we describe exploits unique restriction sites that are occluded by nucleosomes before the remodeling process. As soon as the nucleosomal organization of the array is changed, the restriction sites become accessible to restriction enzymes (RE). Cleavage of the DNA is detected by gel electrophoresis. Quantitative kinetic parameters can be derived from this assay. By choosing unique restriction sites that are occluded by specific nucleosomes, remodeling of these nucleosomes can be directly isolated (Figure 1) (9-11).

The second assay specifically visualizes nucleosome repositioning within nucleosomal arrays. Arrays that harbor restriction sites within the linker DNA region are used in this assay (Figure 1). Repositioning of nucleosomes by ATP-dependent chromatin remodeling enzymes leads to occlusion of these sites and to a change in the restriction fragment pattern (9, 10).

Both assays employ canonical *Drosophila* histones and ISWI as the remodeling enzyme. The assays are however readily adaptable to study other remodeling enzymes, and the effects of mutant histones or histone variants. To follow the protocols described below, a stock of purified histone octamers and remodeling enzyme is required. They are available commercially or can be prepared as described previously (12-14).

2 MATERIALS

2.1 Standard molecular biology materials

- TE buffer: 10 mM Tris–HCl pH 8, 0.1 mM EDTA pH 8
- 5× TBE buffer pH 8.3: 445 mM Tris base, 445 mM boric acid, 10 mM EDTA pH 8
- 5× TB buffer pH 8.3: 25 mM Tris base, 445 mM boric acid
- Ethidium bromide (10 mg/ml)
- Agarose, e.g. Universal agarose (Bio&Sell)
- 3 M sodium acetate pH 5.2
- Ethanol (absolute)
- Siliconized, low-retention microcentrifuge tubes, e.g. Micro tube 1.5 ml low binding (Sarstedt)
- Agarose gel electrophoresis equipment

2.2 Quantitative polynucleosome remodeling assay

2.2.1 Preparation of the DNA fragment

- Plasmid pFMP233
- Giga-format plasmid DNA purification Kit, e.g. Nucleobond® PC 10000 (Macherey-Nagel)
- Restriction enzymes: EcoRI HF, HincII, AseI and CutSmart Buffer (NEB)
- Optional: MaXtract High density 2 ml (Qiagen)
- Ultrapure Phenol:Chloroform:Isoamylalcohol 25:24:1 (v/v) (Invitrogen)

2.2.2 Assembly of nucleosomal arrays

2.2.2.1 Salt gradient dialysis

- High salt buffer: 10 mM Tris–HCl pH 7.6, 2 M NaCl, 1 mM EDTA pH 8, 0.01% NP-40, 1 mM DTT
- No salt buffer: 10 mM Tris–HCl pH 7.6, 1 mM EDTA pH 8, 0.01% NP-40, 1 mM DTT
- Low salt buffer: 10 mM Tris–HCl pH 7.6, 50 mM NaCl, 1 mM EDTA pH 8, 0.01% NP-40, 1 mM DTT
- Peristaltic pump and tubing
- Slide-A-Lyzer Mini dialysis device MWCO 7K, 0.1 ml or conventional dialysis bags.

2.2.2.2 $MgCl_2$ precipitation

- Precipitation buffer: 10 mM Tris–HCl pH 7.6, 7 mM $MgCl_2$
- Storage buffer (optional): 25 mM Hepes–KOH pH 7.6, 0.1 mM EDTA pH 8, 50 mM NaCl, 10% glycerol, 0.2 mg/ml BSA, 1 mM DTT

2.2.2.3 Quality controls

- EX50 buffer: 10 mM Hepes–KOH pH 7.6, 50 mM KCl, 1.5 mM $MgCl_2$, 0.5 mM EGTA
- 1× remodeling buffer: 25 mM Hepes–KOH pH 7.6, 0.1 mM EDTA, 50 mM NaCl, 10% glycerol, 0.2 mg/ml BSA, 1 mM DTT
- 0.5 M EDTA pH 8
- 20% SDS solution
- 10 mM Tris–HCl pH 8
- Restriction enzymes: NotI, BsiWI (NEB)
- Proteinase K (10 mg/ml, Bioline) (note 1)
- High quality agarose for native agarose gels, e.g. LE GP Agarose (Biozym)
- 0.2× TB buffer diluted from 5× stock see section 2.1
- 0.5× TBE buffer diluted from 5× stock, see section 2.1
- 6× blue gel loading buffer: 0.1% bromophenol blue, 60% glycerol in TE buffer
- 6× orange G gel loading buffer: 0.1% orange G, 60% glycerol in TE buffer

2.2.3 Performing the remodeling Assay

- Quenching solution: 0.4% SDS, 20 mM EDTA
- 20× regenerating system: 120 mM phosphoenolpyruvate (Molekula), 310 U/ml pyruvate kinase–lactate dehydrogenase mixture (Sigma), 20 mM DTT, prepare freshly and keep on ice.

- 5× remodeling buffer stock: 125 mM Hepes–KOH pH 7.6, 5 mM $MgCl_2$, 0.5 mM EDTA, 250 mM NaCl, 50% glycerol. Can be stored for months at -20°C.
- 1× remodeling buffer: diluted from 5× remodeling buffer stock supplemented with 1 mM DTT and 0.2 g/l BSA shortly before use
- Appropriate restriction enzyme, e.g. KpnI (NEB) (for selection of restriction enzyme, see Figure 2b)
- 25-mer nucleosomal array with unique restriction enzyme sites (section 3.1.3)
- 50 mM Mg^{2+}-ATP (note 2).
- Purified nucleosome remodeling enzyme, e.g. *Drosophila* ISWI (15)
- Proteinase K (10 mg/ml), for preparation, see note 1
- 10 mM Tris–HCl pH 8

2.2.4 Quantification and evaluation

- 6× blue gel loading buffer (see section 2.2.2.3)
- 0.7% agarose gel in 0.5× TBE containing 0.5 µg/ml ethidium bromide
- Running buffer: 0.5× TBE containing 0.5 µg/ml ethidium bromide
- AIDA image analyzer software (Raytest) or a similar software

2.3 Polynucleosome repositioning assay

2.3.1 Preparation of the DNA fragment

- pUC18-based plasmid containing ~25 consecutive repeats of a 197-bp Widom-601 sequence (Figure 5a; kind gift of D. Rhodes)
- Restriction enzymes: EcoRI HF, HincII, DraI (NEB)
- NEB Buffer 2, NEB Buffer 4 (NEB) or CutSmart Buffer (NEB)
- All materials listed in section 2.1.1

2.3.2 Assembly of nucleosomal arrays

- All materials listed in section 2.1.3
- For quality controls AvaI and AluI (NEB)

2.3.3 Performing the polynucleosome repositioning assay

- 5× remodeling buffer stock and 1× remodeling buffer as described in section 2.1.4
- 50 mM Mg^{2+}-ATP (note 2)
- 25-mer nucleosomal array from section 2.2.2
- Apyrase, 50 U/µl (NEB)
- AvaI (NEB)
- Purified nucleosome remodeling enzyme, e.g. *Drosophila* ISWI (15)
- 1.2% agarose gel in 0.5× TBE containing 0.5 µg/ml ethidium bromide
- 6× orange gel loading buffer

3 METHODS

3.1 Quantitative polynucleosome remodeling assay

This section describes a polynucleosome remodeling assay that can be applied to quantitatively study the activity of nucleosome remodeling enzymes. The assay makes use of an *in vitro* reconstituted nucleosomal array consisting of 25 nucleosomes (Figure 2b). Each histone octamer protects the DNA that is wrapped around it from cleavage by a restriction endonuclease. Upon remodeling of the array by remodeling enzymes, nucleosomal DNA becomes accessible to endonucleases. Cleavage of the DNA therefore indicates remodeling. By monitoring DNA cleavage over time, observed rate constants for remodeling (k_{obs}) can be determined (9).

3.1.1 Plasmid digest

A DNA fragment containing 25 consecutive copies of a modified 197-bp Widom-601 nucleosome positioning sequence is cut out of the plasmid pFMP233 using appropriate restriction enzymes (Figure 2). The vector backbone is subsequently cut into smaller fragments. During assembly of nucleosomes, these fragments will bind histones with a lower affinity than the 601 array and thereby protect the array from over-assembly with excess histones. These fragments are referred to as competitor DNA below.

1. Prepare at least 3 mg of the plasmid pFMP233 using a Giga-format plasmid DNA purification kit.
2. Digest pFMP233 (1 g/l) with EcoRI HF (0.25 U/µg DNA) and HincII (0.6 U/µg DNA) in CutSmart Buffer at 37°C for 3 h.
3. Check completeness of digest on a 0.7% agarose gel. The two resulting fragments have a size of 4930 bp and 2653 bp (Figure 2a,c).
4. When the digest is deemed complete, heat–inactivate restriction enzymes by incubation at 65°C for 20 min.
5. Put tubes on ice before adding AseI to a final concentration of 0.5 U/µg plasmid. Incubate at 37°C for 4 h.
6. Check completeness of digest on a 0.7% agarose gel. The resulting fragments have a size of 4930 bp, 1230 bp and 130 bp. The 2650-bp fragment from step 2 should completely be digested before continuing (Figure 2a,c)
7. Perform a standard phenol/chloroform extraction to purify the DNA from contaminants. We often use MaXtract High Density tubes (Qiagen) to aid in the phase separation.
8. Precipitate DNA by addition of 1/10 vol. of 3 M sodium acetate pH 5.2 and 2.5 volumes ethanol (absolute). Freeze at -20°C for at least 1 h. Spin down at 4°C for 30 min in a SS-34 rotor at 19000 rpm and take off the supernatant without disturbing the DNA pellet. Air-dry pellet for 15 min and then resuspend DNA in TE buffer to a final concentration of 2 g/l.
9. Store DNA at -20°C until further use.

3.1.2 Preparation of histones and histone octamers

Detailed protocols for expression and purification of histones and for the reconstitution of histone octamers can be found elsewhere (12-14). We recommend storing histone octamers in 50 µg aliquots in 10 mM Tris–HCl pH 7.5, 2 M NaCl, 1 mM EDTA, 5 mM β-mercaptoethanol at -80°C.

3.1.3 Assembly of nucleosomal arrays by salt gradient dialysis

Histone octamers and digested plasmid DNA (containing the array and competitor DNA; section 3.1.1) are mixed in a buffer containing 2 M NaCl (16-18). Under these conditions, the octamer is unable to bind DNA. By gradually decreasing the salt concentration of the buffer, nucleosomes assemble on the DNA.

The optimal stoichiometry between octamers and DNA has to be determined in small-scale test assemblies. Following preparative nucleosome assembly, nucleosomal arrays are separated from competitor DNA by $MgCl_2$ precipitation (16, 19). This section concludes with a number of controls that assess the quality of the arrays.

3.1.3.1 Test assembly

Perform all steps at 4–8°C on ice or in a cold room. Use siliconized microcentrifuge tubes.

1. Assemble Slide-A-Lyzer MINI dialysis devices MWCO 7 kDa, 0.1 ml, into a foam float, and place the float into the high salt buffer to prewet their membranes.
2. Flush tubing for the peristaltic pump with high salt buffer.
3. Prepare four test assemblies in which the molar ratio of octamer to 601-sites is varied between 0.7 and 1.7. To this end, mix a constant concentration of digested plasmid DNA (0.1 mg/ml of the 25-mer fragment, corresponding to 0.15 mg/ml of digested plasmid DNA from section 3.1.1) and varying concentrations of octamers in 2 M NaCl, 10 mM Tris–HCl pH 7.6 (final concentrations). Minimal recommended volume is 50 µl, which is sufficient to perform all quality controls described in section 2.2.2.3 (note 3).
4. Transfer test assembly reactions to dialysis tubes.
5. Put the foam float carefully into a glass beaker containing 0.2 l of high salt buffer and a magnetic stir bar (note 4).
6. Pump in 1.8 l of no salt buffer into the beaker over a time period of at least 24 h. Start with a slow flow rate (1 ml/min) to prevent the salt concentration from dropping too fast in the beginning and increase the velocity after 6 hours to 1.4 ml/min. Make sure that the buffers mix well during the assembly using the magnetic stirrer (note 5).
7. After the gradient is finished, transfer the tubes into a beaker containing 1 l of low salt buffer and dialyse for another 2 h.
8. Transfer the test assemblies into a fresh tube.
9. Proceed with step 3.1.3.3 to decide which octamer to DNA ratio is to be used for a preparative assembly.

3.1.3.2 Preparative assembly

Perform all steps at 4–8°C on ice or in a cold room. Use siliconized microcentrifuge tubes.

1. Assemble Slide-A-Lyzer MINI dialysis devices MWCO 7K, 0.1 ml, into a foam float, and place the float into the high salt buffer to prewet their membranes.
2. Choose the octamer:DNA ratio that yielded best results in the test assembly (section 3.1.3.1).
3. Mix the digested plasmid DNA, which contains the 601 array and competitor DNA (0.1 mg/ml of the 25-mer fragment) and octamers in a final concentration of 2 M NaCl and 10 mM Tris–HCl pH 7.6.
4. Transfer the mixture into Slide-A-Lyzer MINI dialysis devices. The maximum volume for these dialysis tubes should not exceed 100 µl per device. Use larger devices or conventional dialysis bags when scaling further up.

5. Put the foam float carefully into a glass beaker containing 1 l of high salt buffer and a magnetic stir bar (note 4).
6. Pump in 3 l of low salt buffer into the beaker over a time period of at least 24 h (flow rate of ~2 ml/min). In parallel, pump buffer out of the beaker with the same flow rate. This way the volume in the beaker should stay constant throughout the assembly. Make sure that the buffers are mixed well during the assembly using the magnetic stirrer. The experimental set-up is depicted in Figure 3a. Regarding flow rates, see note 5.
7. After the gradient is finished, transfer the tubes into a beaker containing 1 l of low salt buffer and dialyse for another 2 h.
8. Transfer the assembled arrays to a microcentrifuge tube.

3.1.3.3 Purification of nucleosomal arrays by $MgCl_2$ precipitation

To purify fully assembled nucleosomal arrays from partially assembled ones, free and chromatinized competitor DNA, magnesium ions are added, which precipitate nucleosomal arrays. In contrast, competitor DNA and nucleosomes assembled on competitor DNA remain soluble under these conditions (16, 19).

1. Remove any precipitates in the sample by centrifugation for 15 min at 4°C and maximum speed. Transfer the supernatant to a fresh, pre-weighed microcentrifuge tube. Weigh the tube again and determine the volume by subtracting the mass of the empty tube, assuming that 1 µg equals 1 µl.
2. Determine the concentration of nucleosomal array by measuring the absorption of their DNA content at 260 nm, assuming that 1 OD equals 50 µg/ml DNA (note 6).
3. Save 200 ng of arrays (input sample) for subsequent analysis on a native agarose gel described in section 3.1.3.4 (note 6).
4. Add 1 volume of precipitation buffer per volume of arrays (note 7).
5. Mix gently by tapping against the tube, but do not pipet up and down.
6. Incubate on ice for 15 min.
7. Pellet nucleosomal arrays by centrifugation at 4°C and maximum speed for 15 min. A transparent pellet may be visible after centrifugation.
8. Remove the supernatant carefully and as completely as possible. Save the supernatant and take an aliquot of the supernatant with twice the volume of the input-aliquot.
9. Do not let the pellet dry. Resuspend it immediately in TE buffer containing 0.1 mM DTT such that the final array concentration is between 200-300 ng/µl (as measured by its DNA content, see note 6).
10. Mix gently by tapping against the tube, but do not pipet up and down. Determine the DNA concentration by measuring the absorbance at 260 nm as above (note 9).
11. Take an aliquot containing 200 ng arrays (pellet sample).
12. Dialyse arrays against 1 l storage buffer overnight to remove residual traces of $MgCl_2$ (note 10).
13. Store nucleosomal arrays at 4°C. The 25-mer arrays described here are stable for approximately one year. Shelf-life may differ for other types of arrays (note 11).

3.1.3.4 Quality controls

To assess the saturation of arrays with histone octamers, we routinely perform three different controls. First, the efficiency of the $MgCl_2$ precipitation is an indicator of the saturation of the arrays because under-assembled arrays do not precipitate well. It can be directly monitored on a native agarose gel (Figure 3b). Arrays should be found exclusively in the pellet whereas competitor DNA

should stay in the supernatant after addition of $MgCl_2$. Another sign of sufficient assembly is if competitor DNA experienced a slight decrease in its electrophoretic mobility. Such a decreased mobility indicates that histones started to bind competitor DNA because array DNA was saturated.

The second control to assess the extent of saturation of the arrays uses a restriction enzyme that can cut in each linker DNA (NotI for arrays from Figure 2 and AvaI for arrays from Figure 5). This approach should liberate only mononucleosomes. If arrays are under- or over-saturated however, it will also generate naked 197-bp long DNA or di- and trinucleosomes, respectively. These species can easily be separated on a native agarose gel.

The third assay sensitively detects defects (if any) in the regular array of nucleosomes. To this end, a restriction enzyme (BsiWI) is used that recognizes sites that should be occluded by every nucleosome within the array. In case a BsiWI site is nucleosome-free, the enzyme can cleave the array at this site. After purification of the DNA, the DNA fragments are separated by agarose gel electrophoresis. Fully assembled arrays will remain uncut, whereas under-assembled arrays will generate a ladder of DNA fragments (Figure 3d).

3.1.3.4.1 Native gel of arrays

1. Prepare a ~10 cm long native 0.7% agarose gel in 0.2× TB buffer (note 12).
2. Load equal amounts (200 ng of input- and pellet-fractions) of the $MgCl_2$ precipitation onto the gel. Also load the corresponding volume of the supernatant-fraction (load twice the volume of the input). Use blue gel loading buffer for loading.
3. Run gel until blue dye front has almost run out of the gel.
4. Stain gel for 30 min in 0.2× TB buffer containing 5 µg/ml ethidium bromide.
5. Destain gel in 0.2× TB buffer or water for 15 min before visualization on a gel documentation system (note 13).

3.1.3.4.2 NotI digest

1. Digest 200 ng arrays with 2.3 µl NotI (20 U/µl) in EX50 buffer in a final volume of 15 µl for 3 h at 26°C.
2. Add 3 µl of 6× orange G gel loading buffer.
3. Load sample onto 1.1% native agarose gel (~10 cm) in 0.2× TB buffer (note 12).
4. Run gel until the loading dye has almost run out of the gel.
5. Stain gel for 30 min in 0.2× TB buffer containing 5 µg/ml ethidium bromide.
6. Destain gel in 0.2× TB buffer or water for 15 min before visualization on a gel documentation system.

3.1.3.4.3 BsiWI digest

1. Digest 250 ng arrays with 2 µl BsiWI (10 U/µl) in 1× remodeling buffer in a final volume of 20 µl for 1 h at 26°C
2. Add 1.2 µl SDS (10%), 1.2 µl EDTA (0.5 M) and 2 µl of Proteinase K (10 mg/ml), to digest proteins.
3. Digest proteins with Proteinase K in a final volume of 30 µl containing 0.4% SDS, 1 mg/ml proteinase K and 20 mM EDTA for 3 h at 37°C
4. Purify DNA by ethanol precipitation as described in section 3.1.1.
5. Air-dry pellet for 8 min.
6. Dissolve pellet in 8 µl 10 mM Tris–HCl pH 8.
7. Add 2 µl of 6× blue gel loading buffer.
8. Load sample onto 1% agarose gel (~10 cm long) in 0.5× TBE buffer containing 0.5 µg/ml ethidium bromide. Visualize DNA on a gel documentation system.

3.1.4 Performing the remodeling assay

Remodeling of nucleosomes in the 25-mer arrays leads to changes in the accessibility of restriction enzyme sites. Because 13 of the 25 nucleosomes occlude unique restriction sites (Figure 2b) remodeling of any of the nucleosomes can be visualized in isolation using the respective restriction enzyme. We optimized the assay following the accessibility changes of the KpnI restriction enzyme site upon remodeling by the ISWI remodeler (Figure 4). However, the assay can easily be adapted to other remodelers and to other restriction enzymes (20).

The assay is initiated by addition of the remodeling enzyme to a premix of nucleosomal arrays, the respective restriction enzyme, Mg^{2+}-ATP and an ATP-regenerating system. Aliquots are taken and immediately quenched at several time points during the reaction. Samples are then deproteinized, purified by ethanol precipitation and resolved on an agarose gel. The amount of cut DNA is then quantified by densitometry. Time-courses are fit to a single exponential function to extract rate constants for remodeling (k_{obs}).

1. Prepare a 20× ATP-regenerating system (note 14). For recipe, see section 2.2.3.
2. Prepare an appropriate number of quench tubes, one for each time point and each containing 8 µl of quenching solution.
3. Prepare reaction tubes on ice containing Mg^{2+}-ATP (note 15), 1× regenerating system, 2 U/µl KpnI and 12.5 ng/µl nucleosomal arrays (which corresponds to 4 nM arrays or 100 nM nucleosomes) in 1× remodeling buffer. A typical reaction volume is 55 µl, which is sufficient for five 10 µl time points. Use siliconized microcentrifuge tubes.
4. Let reactions equilibrate for 1–2 min to 26°C in a heat block.
5. Start the reaction by adding *Drosophila* ISWI (typical concentrations: 0.05 to 1 µM; note 16)
6. After appropriate incubation times, take aliquots by pipetting 10 µl of the reaction directly into the quench tube. Mix thoroughly. Suggested incubation times: 1, 4, 20, 60 and 180 min, but time points must be optimized such that at least two time points are collected before and two after the half-life of the reaction.
7. Keep quenched samples on ice until all reactions are quenched.
8. Heat tubes to 37°C for 2 min to dissolve precipitated SDS.
9. Add 2 µl proteinase K (10 mg/ml) to each aliquot and incubate for 3 h at 55°C or overnight at 37°C.
10. Purify DNA by ethanol precipitation as described in section 3.1.1.
11. Air-dry pellet for 8 min.
12. Dissolve pellet in 8 µl 10 mM Tris–HCl pH 8.

3.1.4.1 Quantification and evaluation

1. Add 2 µl of 6× blue gel loading buffer to each sample.
2. Load sample onto a ~17 cm long 0.7% agarose gel in 0.5× TBE buffer containing 0.5 µg/ml ethidium bromide. Add the same concentration of ethidium bromide also to the running buffer.
3. To separate cut DNA fragments from uncut fragments, run gel until blue dye front has almost run out of the gel.
4. Take a gel photo (Figure 4b). Make sure not to oversaturate DNA bands.
5. Quantify the amount of cut DNA at each time point using the AIDA Image Analyzer software (Raytest) or similar. Calculate the percentage of cut DNA for each gel lane.

6. Plot percentage of cut DNA versus time and fit data to a single exponential function (equation (1)) with KaleidaGraph (Synergy Software) or a similar software to extract the rate constant for remodeling k_{obs}.

$$y = 100 * (1 - e^{-k_{obs}*t}) \qquad (1)$$

3.1.4.2 Controls

1. Include a mock control lacking nucleosome remodeling enzyme to control for the stability of arrays during the time-period of the assay. Only negligible accessibility of the restriction enzyme site should be observed (<5%).
2. Include a control reaction lacking ATP to ensure that the observed effects are ATP-dependent.
3. Include a control that tests the efficiency of quenching by simultaneously adding remodeling enzyme and quenching solution to the reaction mix. Simultaneous pipetting can be achieved by aspirating both components into the same pipet tip while leaving a thin layer of air between them. If quenching is efficient, remodeling will be inhibited instantaneously and restriction enzyme sites will not become accessible.
4. Ensure that the velocity of DNA cleavage is not limited by the restriction enzyme by varying the concentration of the restriction enzyme at least threefold. This variation should not substantially affect the remodeling velocity.
5. Ensure that the ATP-regenerating system is not depleted throughout the assay for example by performing a Luciferase assay after taking the last time point (e.g. ENLITEN® ATP Assay system, Promega).
6. Ensure that the nucleosome remodeler is active throughout the assay. Incubate the nucleosome remodeler under assay conditions excluding nucleosomal arrays for the time-period of the assay. Then add nucleosomal arrays and verify that they are remodeled as efficiently as without an initial incubation of the enzyme.
7. Ensure that the observed activity is not due to contaminating proteins by employing an ATPase-dead mutant enzyme that should not be able to remodel nucleosomes.

3.2 Polynucleosome repositioning assay

The remodeling assay described above detects nucleosome eviction, nucleosome sliding and local structural changes inside the nucleosome (Figure 1). We now describe an assay that isolates the repositioning activity inside nucleosomal arrays. ISWI-type remodeling factors reposition nucleosomes by sliding them along DNA in *cis*(21, 22). Some remodeling factors, however, may also be able to evict and assemble nucleosomes such that nucleosomes are repositioned by two consecutive eviction-assembly cycles (Figure 1). Both of these activities are detectable by the assay described below. These two activities could in principle be differentiated by the addition of large amounts of naked DNA that would trap histones as soon as they are evicted from the nucleosomal array.

The assay makes use of an *in vitro* reconstituted regular nucleosomal array consisting of ~25 histone octamers assembled on a defined DNA fragment (Figure 5) (9, 10). Nucleosome repositioning is monitored by detecting changes in the accessibility of the AvaI restriction enzyme sites, which are located in the linker DNA connecting adjacent nucleosomes. Protection of the initially exposed AvaI sites is indicative of nucleosome repositioning. Whereas the remodeling assay presented above probes for exposure of nucleosomal DNA, the repositioning assay presented here detects protection of linker DNA upon remodeling.

3.3 Plasmid digest

The array DNA, comprising ~25 consecutive repeats of a 197-bp Widom-601 nucleosome positioning sequence is excised from a pUC18-based plasmid (kind gift from D. Rhodes) using appropriate restriction enzymes (Figure 5a). The vector backbone is fragmented further into pieces that serve as competitor DNA in the reconstitution reactions as described in section 3.1.1 (Figure 5b).

1. Prepare at least 3 mg of the plasmid carrying ~25 repeats of the Widom-601 sequence (Figure 5a).
2. Digest the purified plasmid (0.5 g/l) with EcoRI HF (0.4 U/µg DNA) and HincII (0.2 U/µg DNA) in NEB Buffer 2 or in CutSmart Buffer (NEB) at 37°C for 2 h.
3. Check completeness of digest on a 0.7% agarose gel. The two resulting fragments have a size of 4951 bp and 2655 bp (Figure 5b).
4. When the digest is deemed complete, EtOH precipitate the DNA as described in section 3.1.1. Dissolve the DNA pellet in TE buffer to a final concentration of 1 g/l.
5. Digest the DNA further with DraI (0.5 U/µg plasmid) in NEB Buffer 4 or in CutSmart Buffer. Incubate at 37°C for 4 h.
6. Check completeness of digest on a 0.7% agarose gel. The resulting fragments have a size of 4951 bp, 1115 bp, 829 bp and 692 bp. The 2655 bp fragment from step 2 should completely be digested before continuing (Figure 5b).
7. Precipitate the DNA as in step 4.
8. Perform a standard phenol/chloroform extraction to purify the DNA from contaminants. We often use MaXtract High Density tubes (Qiagen) to aid in the phase separation.
9. Precipitate the DNA as in step 4 and resuspend the DNA pellet in TE buffer to a final concentration of 2 g/l.
10. Store DNA at -20°C until further use.

3.3.1 Assembly and quality controls of nucleosomal arrays

Nucleosomal arrays are prepared as described in section 3.1.3. Quality controls are identical to the controls described in section 3.1.3.4 with the exception that different restriction enzymes are used. Digestion of arrays into mononucleosomes is achieved by addition of AvaI (15 U per 200 ng DNA) instead of NotI above. To control for saturation of arrays, accessibility of the AluI site (10 U per 250 ng DNA) is probed instead of the BsiWI site above (Figure 3b-d).

3.3.2 Performing the polynucleosome repositioning assay

1. Prepare a 20× regenerating system (note 14). For recipe, see section 2.2.3.
2. Prepare an appropriate number of quench tubes, one for each time point and each containing 5 µl of a 10 mU/µl apyrase quench solution.
3. Prepare reaction tubes on ice containing 3.75 ng/µl 25-mer regular nucleosomal arrays (which corresponds to 1.2 nM arrays and 30 nM nucleosomes), 100–200 µM Mg^{2+}-ATP and 1× regenerating system in 1× remodeling buffer (note 17). Use siliconized microcentrifuge tubes.
4. Let reactions equilibrate for 1–2 min to 26°C in a heat block.
5. Initiate the reaction by addition of a nucleosome remodeling enzyme (typical ISWI concentrations: 5–500 nM).
6. After appropriate incubation times, take aliquots by pipetting 20 µl of the reaction directly into the quench tube. Mix thoroughly and incubate for 15 min at 26°C. Suggested

incubation times for the repositioning reaction: 3, 15 and 60 min, but time points must be optimized to catch both early and late phases of the reaction.

7. Digest arrays with AvaI (1.2 U/µl) for 3–3.5 h at 26°C.
8. Terminate AvaI digestion by addition of 40 mM EDTA and 0.4% SDS.
9. Deproteinize samples and purify DNA by ethanol purification as described in section 3.1.4
7. Resolve DNA fragments on a ~17 cm long 1.2% agarose gel in 0.5× TBE buffer containing 0.5 µg/ml ethidium bromide. Use orange G loading dye and run gel until the dye has almost run out.
10. Visualize DNA on a gel documentation system (Figure 5d).

3.3.3 Controls

1. Include a mock control lacking nucleosome remodeling enzyme to verify that all AvaI sites are accessible for the restriction enzyme.
2. Include a control reaction lacking ATP to ensure that any observed effects in the presence of a nucleosome remodeler are ATP dependent.
3. Perform an apyrase quench control to ensure that the reaction is fully quenched after 15 min of incubation or to optimize quenching conditions. Before initiating the assay with a nucleosome remodeling enzyme, deplete ATP with apyrase for 15 min (or other chosen time points). In case ATP depletion is quantitative, no repositioning will be observed.
4. Make sure that the digestion with AvaI is complete by including a reaction with increased AvaI concentration and prolonged incubation time.
5. Include a reaction that is not digested with AvaI to ensure that none of the other components used in the assay contain a contaminant capable of cutting the array DNA.
6. Ensure that the occlusion of AvaI sites is not caused by binding of the nucleosome remodeling enzyme to the array. This can be achieved by addition of excess DNA or nucleosomes to the quenched samples before proceeding with the AvaI digest. The competitor must be at least tenfold in excess over nucleosomes in the array and considerably outnumber the enzyme in the sample. Include a control in which the competitor concentration is varied at least threefold to make sure that the competitor is not limiting. Incubate long enough (typically 10 min or more) such that the remodeling enzyme can dissociate from the array and bind the competitor. Incubation times must be adapted for each application. To check if the incubation was sufficiently long, vary incubation times at tenfold. To cleanly detect array DNA over competitor DNA, use a competitor that has a significantly different DNA length than fragments derived from the array.
7. Perform controls as described in steps 5–7 from section 3.1.4.2.

4 NOTES

1. Prepare a 10 mg/ml stock of Proteinase K in 50 mM Tris–HCl pH 8, 5 mM $CaCl_2$, 50% glycerol. Aliquot and store at -20°C.
2. Prepare first a 0.5 to 1 M ATP stock by quickly dissolving ATP (adenosine 5'-diphosphate sodium salt, Sigma) in ice-cold H_2O. Rapidly titrate with 10 M NaOH to neutrality (pH 6.5 to 7.5). The precise concentration of ATP in the stock is determined by UV absorption at 260 nm (ε = 15400 $M^{-1}cm^{-1}$). The 50 mM Mg^{2+}-ATP solution is obtained from the ATP stock by adding stoichiometric amounts of $MgCl_2$. Mix well and store in aliquots at -20°C.

3. When calculating the final salt concentration, take into account that octamers are stored in 2 M NaCl and therefore contribute significantly to the final salt concentration. Note, however, that modest variation of the final salt concentration is not expected to affect the results. Check for correct calibration of pipets before starting test assemblies as a precise titration of the octamer:DNA stoichiometry is critical.
4. Make sure there are no air bubbles underneath the membrane.
5. The flow rate of the pump may have to be manually measured before the assembly by weighing the amount of buffer pumped over a certain amount of time. Also note that the flow rate varies with the tubing used. The effective salt gradient applied here is steeper than in section 3.1.3.2, allowing for a faster protocol. Note, however, that a faster gradient may lead to more aggregation.
6. Throughout the protocol the concentration of nucleosomal arrays is estimated via their DNA content as determined by the absorption at 260 nm (1 OD_{260} = 50 µg/ml). The concentration of nucleosomal arrays can be well approximated by this approach as the contribution of histones to the absorption at 260 nm is negligible. All mass concentrations of arrays given in this protocol therefore refer to exclusively the DNA content of the arrays.
7. The $MgCl_2$ concentration necessary to specifically precipitate nucleosomal arrays has to be determined by titration for each type of array. Whereas a final concentration of 3.5 mM $MgCl_2$ is sufficient to precipitate a 25-mer array containing wild-type *Drosophila* histones, higher concentrations (8.5 mM) are needed to precipitate arrays whose nucleosomes lack the N-terminal tail of H4 for example.
8. Nucleosomal arrays readily stick to pipet tips and microcentrifuge tubes. Store nucleosomal arrays exclusively in siliconized microcentrifuge tubes.
9. We routinely store the arrays overnight at 4°C to allow the pellet to dissolve completely.
10. This step is optional.
11. If nucleosomal arrays are stored for an extended period of time, repeat the quality controls described in section 3.1.3.4.
12. It is important to use EDTA-free TB buffer here as EDTA acts as a chelating agent and sequesters Mg^{2+}.
13. Destaining reduces background fluorescence in the gel, but is not absolutely required.
14. The ATP-regenerating system should be prepared freshly.
15. The Mg^{2+}-ATP concentration used during the assay will depend on the specific needs. 1 mM Mg^{2+}-ATP is sufficient to saturate many enzymes and is therefore often used as the starting condition. If saturating concentrations are to be employed, verify that variation of the ATP concentration (at least threefold) does not significantly affect the remodeling velocity.
16. Required enzyme concentrations will depend on the specific needs. Fastest remodeling is expected if saturating conditions are chosen (enzyme concentration exceeds the nucleosome concentration and the dissociation constant (K_D) between enzyme and nucleosomes).
17. Higher ATP concentrations can in principle also be used. Higher apyrase concentrations or longer incubation with apyrase may however be required to efficiently quench the reaction. See section 3.1.4.2 for details how to perform a quench control.

5 Acknowledgements

J.L. thanks the Ernst Schering foundation for granting a predoctoral fellowship. This work was supported by the FöFoLe program of the LMU Munich (M18/2010 to N.H. and F.M.-P.) and the Deutsche Forschungsgemeinschaft (MU3613/1-1, MU3613/3-1 and SFB1064-A07 to F.M.-P).

6 References

1. D. C. Hargreaves, G. R. Crabtree, ATP-dependent chromatin remodeling: genetics, genomics and mechanisms. *Cell research* **21**, 396-420 (2011).
2. C. R. Clapier, B. R. Cairns, The biology of chromatin remodeling complexes. *Annual review of biochemistry* **78**, 273-304 (2009).
3. A. Flaus, T. Owen-Hughes, Mechanisms for ATP-dependent chromatin remodelling: the means to the end. *The FEBS journal* **278**, 3579-3595 (2011).
4. A. Flaus, D. M. Martin, G. J. Barton, T. Owen-Hughes, Identification of multiple distinct Snf2 subfamilies with conserved structural motifs. *Nucleic acids research* **34**, 2887-2905 (2006).
5. A. Eberharter, G. Langst, P. B. Becker, A nucleosome sliding assay for chromatin remodeling factors. *Method Enzymol* **377**, 344-353 (2004).
6. A. Eberharter, G. Langst, P. B. Becker, A nucleosome sliding assay for chromatin remodeling factors. *Methods Enzymol* **377**, 344-353 (2004).
7. V. K. Maier, M. Chioda, D. Rhodes, P. B. Becker, ACF catalyses chromatosome movements in chromatin fibres. *The EMBO journal* **27**, 817-826 (2008).
8. V. K. Maier, P. B. Becker, A defined in vitro system to study ATP-dependent remodeling of short chromatin fibers. *Methods in molecular biology* **833**, 255-270 (2012).
9. F. Mueller-Planitz, H. Klinker, J. Ludwigsen, P. B. Becker, The ATPase domain of ISWI is an autonomous nucleosome remodeling machine. *Nature structural & molecular biology* **20**, 82-89 (2013).
10. J. Ludwigsen, H. Klinker, F. Mueller-Planitz, No need for a power stroke in ISWI-mediated nucleosome sliding. *EMBO reports* **14**, 1092-1097 (2013).
11. C. Logie, C. L. Peterson, Catalytic activity of the yeast SWI/SNF complex on reconstituted nucleosome arrays. *The EMBO journal* **16**, 6772-6782 (1997).
12. H. Klinker, C. Haas, N. Harrer, P. B. Becker, F. Mueller-Planitz, Rapid purification of recombinant histones. *PloS one* **9**, e104029 (2014).
13. K. Luger, T. J. Rechsteiner, T. J. Richmond, Expression and purification of recombinant histones and nucleosome reconstitution. *Methods in molecular biology* **119**, 1-16 (1999).
14. K. Luger, T. J. Rechsteiner, T. J. Richmond, Preparation of nucleosome core particle from recombinant histones. *Methods in enzymology* **304**, 3-19 (1999).
15. I. Forne, J. Ludwigsen, A. Imhof, P. B. Becker, F. Mueller-Planitz, Probing the conformation of the ISWI ATPase domain with genetically encoded photoreactive crosslinkers and mass spectrometry. *Molecular & cellular proteomics : MCP* **11**, M111 012088 (2012).
16. V. A. Huynh, P. J. Robinson, D. Rhodes, A method for the in vitro reconstitution of a defined "30 nm" chromatin fibre containing stoichiometric amounts of the linker histone. *Journal of molecular biology* **345**, 957-968 (2005).
17. P. N. Dyer *et al.*, Reconstitution of nucleosome core particles from recombinant histones and DNA. *Methods in enzymology* **375**, 23-44 (2004).
18. K. M. Lee, G. Narlikar, Assembly of nucleosomal templates by salt dialysis. *Curr Protoc Mol Biol* **Chapter 21**, Unit 21 26 (2001).
19. P. M. Schwarz, J. C. Hansen, Formation and stability of higher order chromatin structures. Contributions of the histone octamer. *The Journal of biological chemistry* **269**, 16284-16289 (1994).

20. C. Lieleg *et al.*, Nucleosome spacing generated by ISWI and CHD1 remodelers is constant regardless of nucleosome density. *Molecular and cellular biology* **35**, 1588-1605 (2015).
21. G. Langst, E. J. Bonte, D. F. Corona, P. B. Becker, Nucleosome movement by CHRAC and ISWI without disruption or trans-displacement of the histone octamer. *Cell* **97**, 843-852 (1999).
22. A. Hamiche, R. Sandaltzopoulos, D. A. Gdula, C. Wu, ATP-dependent histone octamer sliding mediated by the chromatin remodeling complex NURF. *Cell* **97**, 833-842 (1999).
23. H. Klinker *et al.*, ISWI remodelling of physiological chromatin fibres acetylated at lysine 16 of histone H4. *PloS one* **9**, e88411 (2014).

7 FIGURE LEGENDS

Figure 1: Different outcomes of nucleosome remodeling. Remodeling comprises sliding, eviction and assembly of nucleosomes as well as local distortions of nucleosomal DNA. All these activities expose nucleosomal DNA (brown) which can be detected with appropriate restriction enzymes. Nucleosomes can be repositioned either by a sliding reaction, which occurs in *cis* (top), or by two consecutive ejection and assembly reactions (grey). Repositioning can be distinguished from other remodeling activities by monitoring occlusion of restriction sites located in the linker (red) upon remodeling.

Figure 2: Nucleosomal substrate for remodeling assay. (A) Vector map. (B) Schematic depiction of the 25-mer nucleosomal array. Each nucleosome consists of a 197-bp DNA fragment that harbors a variant of the Widom-601 nucleosome positioning sequence. Nucleosomes 1–12 (see magnification bottom left) assemble on identical DNA repeats whereas nucleosomes 13–25 (bottom right) assemble on bar-coded positioning sequences. The positions of common and unique RE sites in each of these repeats are indicated. Numbers designate the positions of the RE sites in basepairs relative to the nucleosomal dyad axis (0). (C) Restriction digest of the DNA vector for preparation of the nucleosomal array. Undigested vector DNA (-) was loaded as a control.

Figure 3: Reconstitution and quality controls of nucleosomal arrays. (A) Setup of salt gradient dialysis to reconstitute nucleosomal arrays (sections 3.1.3 and 3.3.1). (B) Purification of nucleosomal arrays by precipitation. Nucleosomal arrays, reconstituted with different octamer:DNA ratios, were precipitated by addition of $MgCl_2$ and analyzed on native agarose gels stained with ethidium bromide. Samples were taken of the unprecipitated arrays (I), and of the pellet (P) and supernatant (SN) after precipitation. Excess histone octamers led to nucleosome assembly on competitor DNA and a retardation of its mobility (ratio 1.6). Under-assembled arrays did not precipitate and can be found in the supernatant (ratio 0.9). (C and D) Quality controls of nucleosomal arrays. (C) Purified nucleosomal arrays from panel B were AvaI digested, then separated on a native agarose gel. DNA was visualized by ethidium bromide stain. Free 197-bp DNA was liberated from under-assembled arrays (ratio 0.9). (D) Nucleosomal arrays from panel B were AluI digested. The DNA was purified, separated on a native agarose gel and stained by ethidium bromide. Under-assembled arrays (ratio 0.9) were detected by a strong accessibility towards AluI. Panels b-d (adapted from ref. (23)) show quality controls for arrays prepared in section 3.3.1. Quality controls for arrays prepared in section 3.1.3 are analogous (see text).

Figure 4: Remodeling assay. (A) Schematic illustration of the assay. The nucleosome array contains a unique restriction site (X) that is occluded by a nucleosome (ovals). Upon remodeling, the restriction site becomes accessible and can be cleaved by the restriction enzyme. (B) Exemplary time course of a remodeling reaction. Reactions were quenched after the indicated time points, DNA was purified and separated by agarose gel electrophoresis. In a control reaction (-), ATP was omitted.

Figure 5: Polynucleosome repositioning assay. (A) Vector containing 25 identical repeats of a Widom-601 nucleosome position sequence with a repeat length of 197 bp. Each repeat contains an AluI site that is occluded by a nucleosome after assembly and an AvaI site in the linker DNA, as illustrated for the related array in Figure 2B, bottom left. (B) Restriction digest of the DNA vector to liberate the nucleosomal array. (C) Schematic illustration of the repositioning assay. AvaI can cleave within each linker DNA (X) in the unremodeled nucleosomal array. Nucleosome repositioning leads to occlusion of some AvaI sites. (B) Exemplary repositioning time course. Reactions were quenched after 3, 13 and 48 min before being subjected to an exhaustive AvaI digest. DNA was purified and separated by agarose gel electrophoresis. A reaction without ATP served as a negative control. Figure modified from ref. (10).

8 FIGURES

Figure 1

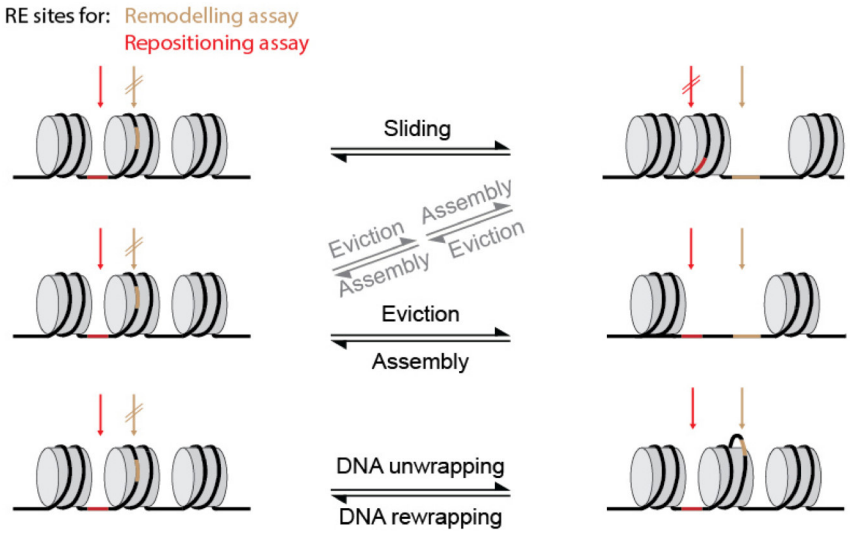

Figure 2

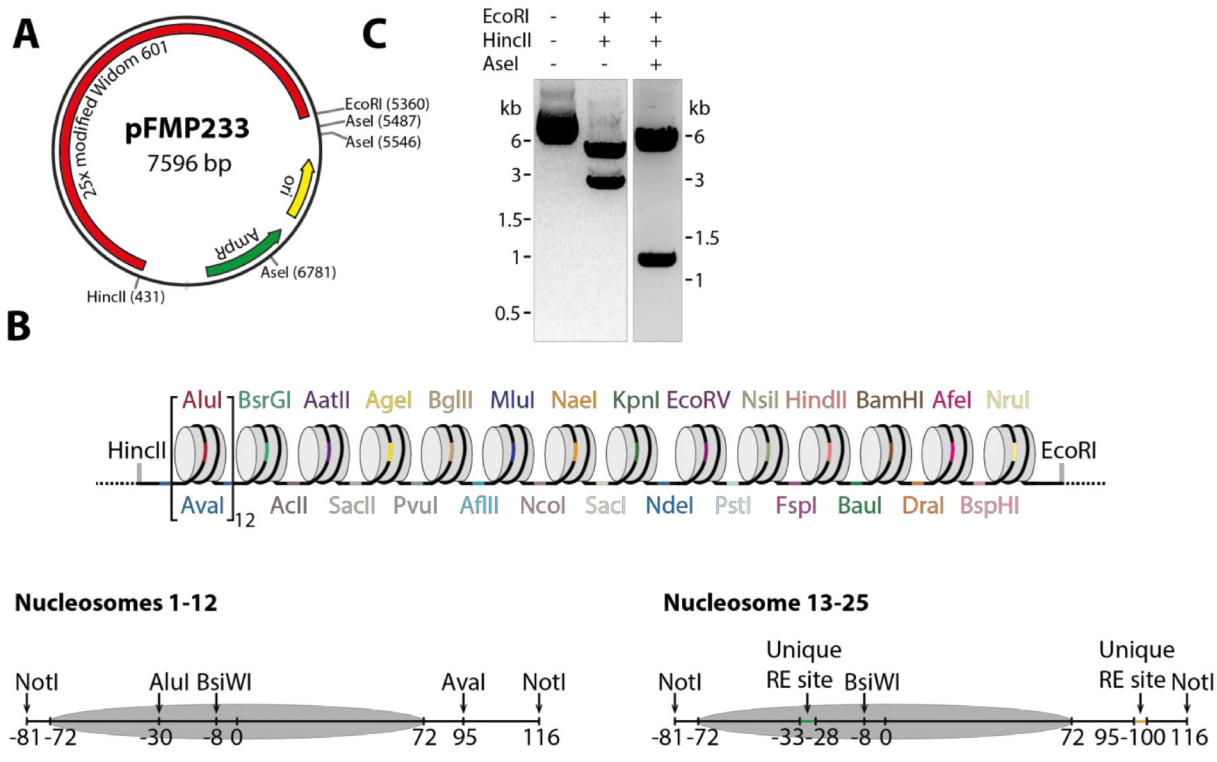

Figure 3

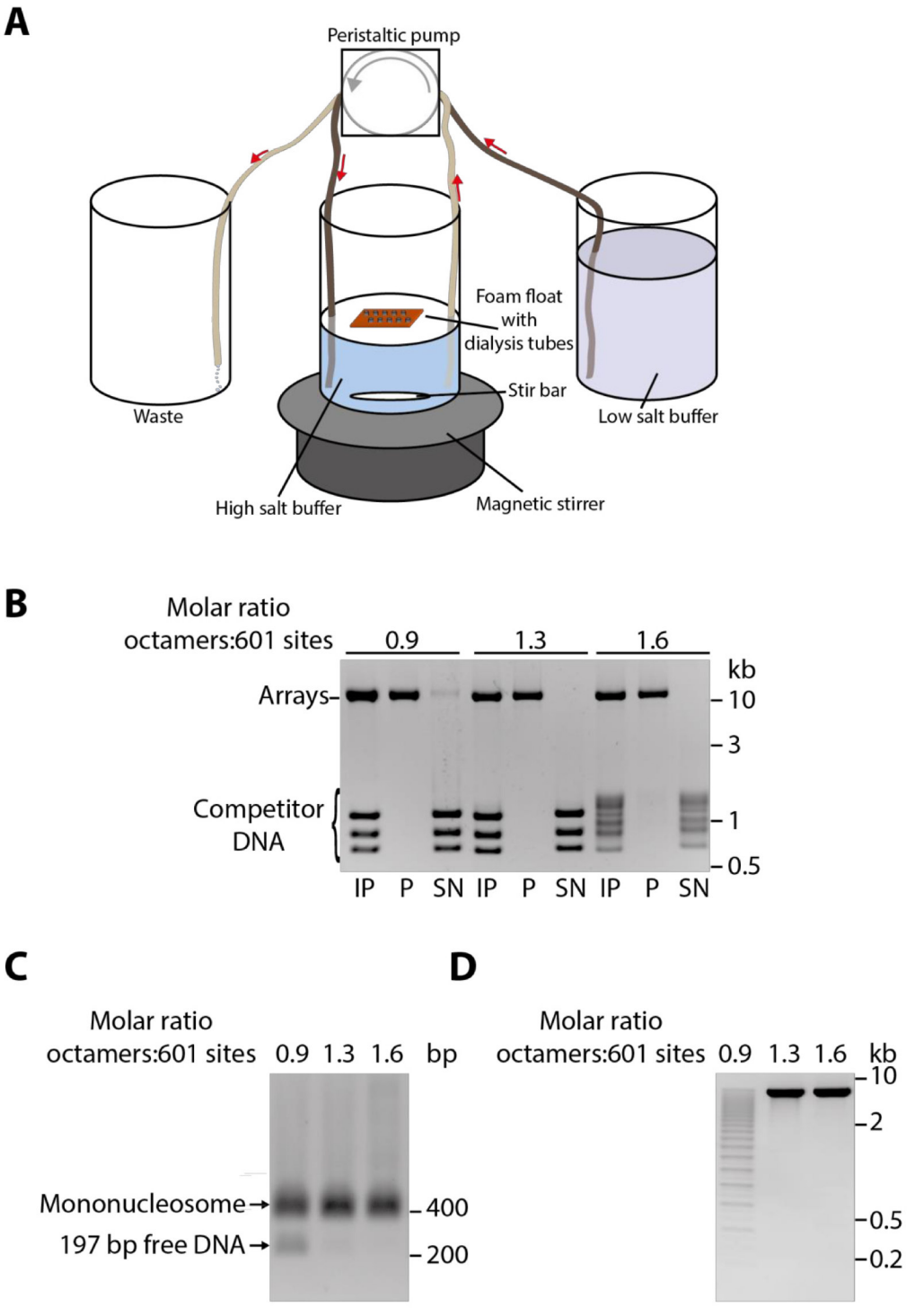
A
Peristaltic pump
Foam float with dialysis tubes
Stir bar
Waste
Low salt buffer
High salt buffer
Magnetic stirrer
B
Molar ratio octamers:601 sites
0.9
1.3
1.6
kb
Arrays
10
3
Competitor DNA
1
0.5
IP P SN IP P SN IP P SN
C
Molar ratio octamers:601 sites 0.9 1.3 1.6 bp
Mononucleosome
197 bp free DNA
400
200
D
Molar ratio octamers:601 sites 0.9 1.3 1.6 kb
10
2
0.5
0.2

Figure 4

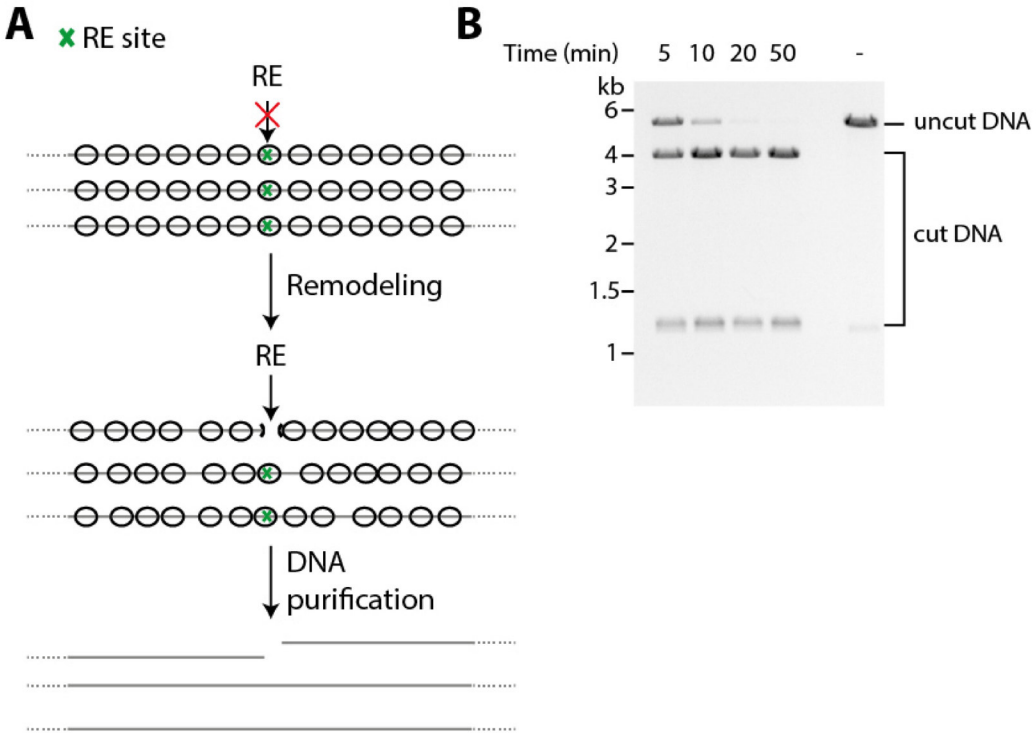

Figure 5

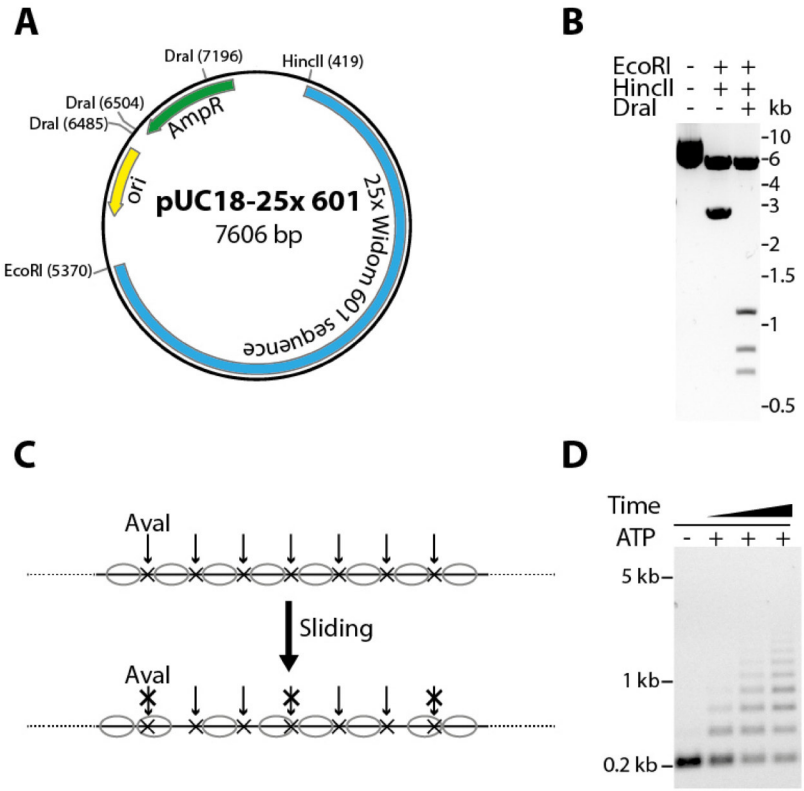

3. DISCUSSION

3.1 Role of the HSS domain during nucleosome sliding by ISWI

It is well established that the C-terminal HSS domain of ISWI constitutes a DNA binding module. Specifically, the HSS domain was shown to associate with extranucleosomal DNA flanking the nucleosome (157, 165, 206). Several recent models predict the HSS domain of ISWI to play an integral role during the sliding reaction.

Surprisingly, we found the HSS domain to be dispensable for nucleosome sliding. By studying a deletion mutant lacking the HSS domain ($ISWI_{26–648}$ or $ISWI_{\Delta HSS}$), we demonstrated that the HSS domain facilitated nucleosome sliding, but was by no means essential for the reaction. In fact, $ISWI_{26–648}$ retained all characteristics of a basic remodeling machine. The enzyme was able to associate with DNA and nucleosomes and exhibited DNA- and nucleosome-stimulated ATPase activity. Surprisingly, it even mobilized mononucleosomes and remodeled nucleosomal arrays, albeit with tenfold reduced velocity. Furthermore, like the wild-type enzyme, $ISWI_{26–648}$ was sensitive to deletion of the N-terminal tail of histone H4 (see section 2.1). Our results are in accordance with recent observations involving the nucleosome remodelers Chd1 (153, 176) and Chd2 (207). Like ISWI, both Chd-type remodelers retained the abilities to hydrolyze ATP and remodel nucleosomes upon deletion of their C-terminal DBD. Thus, all fundamental aspects of nucleosome sliding can be performed by the isolated ATPase motor.

In light of our observations, the role of the HSS domain during nucleosome sliding needs to be re-evaluated. Binding of the ISWI ATPase domain at SHL-2 and ATP-dependent translocation appears to be sufficient to induce nucleosome sliding. Possibly, translocation of the ATPase domain disturbs critical histone-DNA contacts within the nucleosome allowing mobilization of the octamer. Instead of playing an active mechanical role, we suggest the HSS domain to modulate and optimize nucleosome sliding for specialized tasks. Consistent with previous findings, we showed that the HSS domain considerably increases the affinity of ISWI to DNA. By tethering the remodeler to the nucleosome, the HSS domain may also increase the processivity. Conceivably, the HSS domain may align the ATPase domain on the nucleosome in an orientation that allows for productive DNA translocation. Furthermore, we found the HSS domain to form specific contacts to the nucleosome, which confer nucleosome specificity and help ISWI to reliably identify its correct substrate (see section 2.1).

Our results are in excellent agreement with several recent publications that revealed novel insight into the function of the HSS domain. Three studies from the Bowman laboratory demonstrated that the DNA-binding domain (DBD) of Chd1 is not only dispensable for nucleosome sliding, but can even be functionally substituted with foreign DBD's (176, 208). Interestingly, chimeric remodelers, where the native DBD was replaced with a foreign, sequence-specific DBD shifted nucleosomes towards their recognition sequence (176). Moreover, substitution of the DBD with streptavidin proved sufficient for sliding biotinylated nucleosomes (208). Sequence-specific nucleosome sliding was successfully achieved even *in vivo* by replacing the native DBD with the Ume6 repressor. The hybrid Chd1-Ume6 remodeler selectively modified the local nucleosome organization around URS1 target sites (209). The native DBD can apparently be substituted with any foreign DBD. It is thus conceivable that it does not form specific contacts to DNA, but rather passively tethers the

remodeler to the nucleosome. These findings further substantiate our hypothesis that the DBD's of ISWI and Chd1 are not required for the basic sliding reaction.

ISWI contains the autoregulatory NegC motif C-terminal to the ATPase domain (147) (see section 1.3.5). NegC was suggested to inhibit the coupling of ATP hydrolysis to productive nucleosome sliding. Association of the HSS domain with linker DNA was proposed to counteract the autoinhibition imposed by NegC. In line with these suggestions, deletion of NegC was shown to restore nucleosome sliding activity, which was reduced upon deletion of the HSS domain (147). The C-terminal deletion construct $ISWI_{26-648}$, which we analyzed, still contained NegC. Permanent NegC-mediated inhibition in the absence of the HSS domain may therefore account at least in part for the reduced sliding activity we observed for the $ISWI_{26–648}$ mutant (see section 2.1). Mechanistic details on how the HSS domain relieves NegC inhibition are currently not available. Notably, we showed that conformational changes in NegC upon DNA binding correlate with increased ATPase activity of ISWI (see section 2.1, Figure 2). Together, these results suggest that DNA binding relieves the autoinhibition provided by NegC.

A role of the HSS domain in sensing the length of linker DNA is well established (157, 165, 206). Thus, it does not come as a surprise that recent studies find the HSS domain to be critically involved in nucleosome spacing (141, 204, 210). Elegant single-molecule FRET measurements revealed a nucleotide state-dependent conformational rearrangement of the SNF2H HSS domain. A current model suggests that the HSS domain preferentially binds to linker DNA in the ADP-bound state. This state was suggested to correspond to a 'length-sensing' conformation of SNF2H not competent for DNA translocation. In this state NegC may block the coupling of ATP hydrolysis to translocation. Interestingly, replacement of NegC with a short linker prevented linker length sensing by SNF2H without disturbing overall sliding activity (204, 210). The mutant lacking NegC lost the ability to distinguish between core nucleosomes and nucleosomes containing linker DNA. Moreover, the linker length sensing defect also impaired the characteristic mononucleosome centering activity of SNF2H (204). Upon binding of ADP-BeF_x to the ATPase domain, the HSS domain engaged the nucleosome core relieving NegC inhibition and allowing for productive nucleosome sliding. This state was suggested to reflect the 'translocation-competent' state (204). These results are consistent with our findings and suggest the HSS domain to be a modulator of nucleosome sliding, but to be dispensable for the sliding reaction *per se*.

In vivo, the C-terminus of ISWI has yet additional functions and serves as a platform to recruit accessory subunits. In *D. melanogaster* a domain C-terminal to the HSS domain interacts with the accessory subunit Acf1 (139). In contrast, *S. cerivisiae* Isw1 and Isw2 require the SLIDE domain for recruitment of their complex partners (206, 211). As ISWI acts in the context of several remodeling factors inside the cell, deletion of the HSS domain may have diverse consequences *in vivo*.

In summary, we suggest the ISWI ATPase domain to constitute an autonomous remodeling machine. ATPase domains of nucleosome remodelers have evolved from ancestral helicases. We envision that domains flanking their ATPase domains including the HSS domain and N-terminal domains (see section 3.3.2) evolved to target and regulate the remodeler. To steer the remodeling reaction towards the desired outcome a multitude of accessory domains and subunits exist in different remodeler families.

3.2 Mechanism of nucleosome sliding by ISWI

Despite significant efforts by many researchers, molecular details of the basic sliding mechanism remain scarce. However, recent findings by us and others have considerably advanced the understanding of the reaction. An ATP-dependent conformational change termed 'power stroke' between the HSS and the ATPase domain was suggested to be required for pulling additional DNA into the nucleosome. According to the 'loop propagation' model (see section 1.3.4), excess DNA then forms a loop, which travels around the octamer towards the exit site. In contrast to wide-spread expectations, we showed that nucleosome sliding by ISWI does not require a power stroke (see section 2.2).

Even though we found the HSS domain of ISWI to be dispensable for nucleosome sliding, its deletion decreased the sliding activity of ISWI by tenfold. This could in principle be attributed to a missing power stroke in the deletion mutant where force transmission would not be possible. To probe for the existence of the postulated power stroke, we sought to artificially increase the flexibility at strategic positions between the ATPase and the HSS domain. As force-transducing elements are required to be rigid, flexibility would interfere with the build-up of intramolecular strain and thus prevent a power stroke (212, 213). To increase flexibility, we inserted glycine- and serine-rich polypeptide linkers, which have been shown to behave like random coils (214). Strikingly, ISWI derivatives carrying flexible insertions between ATPase and HSS domain showed no defects in neither ATPase nor nucleosome remodeling activities (see section 2.2). Our results strongly argue against the powers stroke hypothesis. Reassuringly, using a similar approach in the context of yeast Chd1, the Bowman laboratory came to a similar conclusion (215). They inserted up to 121 intrinsically disordered residues into the region connecting the Chd1 ATPase domain to the C-terminal DBD. The inserted linker only modestly affected the mononucleosome sliding activity of Chd1. In contrast, shortening the region between ATPase and DBD by 45 residues essentially blocked sliding. Collectively, these results suggest that a rigid connection between ATPase and DBD is not necessary. In fact, flexibility may even be an inherent property of the region connecting ATPase and DNA-binding domain.

A recent study provided exciting insight into the succession of ATP-dependent translocation steps occurring during nucleosome sliding (178). Using single-molecule FRET, Deindl et al. resolved single-base pair steps of several ISWI factors. Contrary to prior expectations, they demonstrated that DNA exits the nucleosome before additional DNA enters. According to their model, nucleosome sliding is initiated by translocation of the ISWI ATPase domain at SHL-2. This results in the extrusion of 7 bp of DNA out of the nucleosome before additional 3 bp enter. After these initial steps, another 3 bp exit the nucleosome allowing the 3 bp equivalent to be drawn in from the entry side. This cycle then proceeds until the remodeler dissociates from the nucleosome. The multi-bp steps were shown to comprise elementary step sizes of 1 bp, where step size is defined as the number of nucleotides translocated per ATP hydrolyzed (178). Single-bp steps have previously been observed for several SF1- and SF2-helicases including PcrA (216), UvrD (217), blood syndrome protein (BLM) (218) and non-structural protein 3 (NS3) (219) and appear to be conserved up to nucleosome remodelers.

The unforeseen observation that DNA leaves the nucleosome before additional DNA enters provides compelling evidence against formation of DNA loops during sliding. Quite the contrary, to accommodate the strain, DNA would rather have to stretch and unwind. Notably, even the RSC remodeler was reported to translocate DNA along the canonical wrapping path (220). This is

remarkable since Snf2-family remodelers are thought to disrupt DNA-histone contacts to a much higher degree compared to ISWI remodelers (221, 222). In the recently published ScSnf2-nucleosome structure the DNA around SHL-2 is indeed locally distorted, but is not extensively lifted off from the octamer surface (163). Thus, instead of pushing DNA inside the nucleosome, the HSS domain may act as a gate for DNA on the entry site. Until the initial 7 bp have exited the nucleosome, the HSS domain remains immobile and preserves the strain inside the nucleosome. Then, the accumulated strain is sufficient to trigger an action at the entry site. A conformational change in ISWI presumably forces the HSS domain to partially or completely loosen its grip on the entry site DNA allowing three additional bp to ratchet into the nucleosome.

The fact that the nucleosome constantly lacks several bp during remodeling raises the question how the nucleosome handles the strain. As the ATPase domain locally acts at SHL-2, the accumulated strain is probably not equally distributed over the entire nucleosome. Rather, the strain would be restricted to the region delimited by binding of the ATPase domain at SHL-2 and the HSS domain at the entry site (SHL-7) (see section 2.2, Figure 5). Possible ways to adapt the strain include the underwinding of DNA or an altered wrapping path on the surface of the histone octamer. Strikingly, a recent nuclear magnetic resonance (NMR) showed that also the histone octamer itself considerably deforms upon binding of SNF2H in the presence of ADP-BeF_x (223). In fact, the hydrophobic core of the H3-H4 histone fold dimer close to the dyad appears to be distorted. Changes were also detected within H2A, although these could not be assigned to a specific region. To test for the functional relevance of the conformational changes, site-specific disulfide bridges were introduced into the nucleosome to restrict octamer flexibility. Indeed, a crosslink close to the dyad interfered with mononucleosome centering by SNF2H (223). Hence, octamer deformation appears to be a critical step during nucleosome sliding and may allow the nucleosome to accommodate less DNA and prevent accumulation of strain.

In summary, we suggest that DNA does not translocate around the nucleosome in a wave-like manner involving DNA loops. Furthermore, we suggest that nucleosome sliding by ISWI-type remodelers does not require a power stroke between the HSS and the ATPase domain. Instead of taking part in a power stroke, the HSS domain may gate the DNA at the entry site of the nucleosome only allowing DNA to enter after 7 bp have exited. In addition, the HSS domain may locally change the nucleosome conformation proximal to the entry site. It could for example locally detach DNA from the histone surface as seen in Chd1 (170, 224) or induce a conformational change in the histone octamer. In fact, the HSS domain binds close to the entry site of the nucleosome not far from the H3-H4 interface that was shown to deform during remodeling (223). Consistently, the HSS domain was shown to change its position on the nucleosome during the reaction cycle (204).

3.3 Regulation of ISWI

Nucleosome remodelers of the ISWI family have evolved intricate mechanisms to regulate their activity in order to avoid wasteful ATP hydrolysis and to prevent targeting of false substrates. Regulation is inferred by nucleosomal epitopes including the H4 N-terminal tail and extranucleosomal linker DNA. In addition, ISWI contains autoinhibitory motifs N-terminal to the ATPase domain, which are critically involved in substrate discrimination.

3.3.1 Regulation by the H4 N-terminal tail

The reliance of ISWI on the H4 tail was established qualitatively in a series of *in vitro* studies (see section 1.3.5). Nevertheless, the quantitative degree of ISWI's H4-tail dependency remained unexplored. Beyond that, the molecular mechanism of H4-tail recognition by ISWI is poorly understood. To measure the effect of H4-tail deletion on the catalytic activity of ISWI, we established a quantitative *in vitro* remodeling assay (see section 2.4). The assay allowed us to extract rate constants for remodeling, which are key indicators for enzyme kinetics. Remodeling has traditionally been probed using mononucleosomes as a substrate. *In vivo* however, nucleosomes occur as extended arrays, which further fold into distinct structures. To better mimic the physiological situation, we developed a remodeling assay involving regularly spaced nucleosomal arrays, which can be reconstituted *in vitro* from recombinantly purified components (see section 2.1 and section 2.4). Using this assay, we quantitatively scrutinized the effect of H4 tail deletion on ISWI remodeling. We found that $ISWI_{WT}$ remodeled arrays lacking the H4 tail about sixfold more slowly compared to wild-type arrays.

To further narrow down the H4 tail interacting region in ISWI, we repeated the measurements with $ISWI_{26–648}$, which lacks the HSS domain. Notably, $ISWI_{26–648}$ was sensitive towards deletion of the H4 tail as well (16-fold). Consistent with this observation, the ATPase activity of $ISWI_{26–648}$ was stimulated by an N-terminal peptide of H4 in complex with DNA. These results imply that the H4 tail-binding site within ISWI is located inside the ATPase domain. Given that the ISWI ATPase domain engages the nucleosome at SHL-2, the site where the H4 tail protrudes, it seems likely that the ATPase directly associates with the H4 tail.

Interestingly, a recent electron paramagnetic resonance spectroscopy (EPR) study showed that binding of the H4 tail to SNF2H induced a conformational change in the ATPase domain (190). Specifically, the H4 tail promoted a closed state of the ATPase lobes competent for ATP hydrolysis. Notably, we observed a conformational change of the ISWI ATPase domain upon DNA-binding (section 2.1, Figure 2). However, using EPR, no shift towards the closed state of the ATPase domain was observed upon addition of DNA (190). This may indicate that the H4 tail and nucleosomal linker DNA are important for different reaction steps. Linker DNA could for instance act prior to ATP hydrolysis, whereas the H4 tail would stabilize a conformation poised for ATP hydrolysis by directly contacting the ATPase domain. In fact, the H4 tail was proposed to activate ATP turnover by displacing the autoregulatory AutoN motif from the ATPase domain (147). Since AutoN and the H4 tail display sequence similarity they may compete for a binding site of the ATPase domain.

To gain further insight into the regulation of ISWI by the H4 tail, we mapped the H4 tail-binding site using crosslinking coupled to mass spectrometry. Strikingly, we found the H4 tail to crosslink to the conserved ATPase lobe 2 of ISWI (see section 2.3, Figure 5). *In silico* docking guided by the identified crosslinks delineated the binding interface of the H4 tail on ATPase lobe 2. Consistent

with a binding pocket for a basic epitope, several of the residues on lobe 2 that were most frequently contacted during modeling were acidic.

During the revision of the manuscript presented in section 2.3, the crystal structure of MtISWI in complex with an H4 peptide became available (154). Even though electron density was only detected for the basic patch of the H4 peptide, its location overlaps with our modeled H4 tail-binding interface on lobe 2. In the crystal structure, the H4 basic patch was embedded in a negatively charged pocket on lobe 2 formed by three conserved residues: E474, E523 and D524 (corresponding to E415, E464 and D465 in DmISWI). Specifically, H4 K16 contacted E523 and D524 whereas the side chain of H4 R17 was proximal to E474 and D524 (154) (see Figure 6A,D). Consistent with the crystal structure, DmISWI E415 and D465 were among the amino acids most frequently contacted by H4 K16 during modeling. Additionally, we identified the binding interfaces of H4 T1 and H4 L10, which were not resolved in the crystal structure (see Figure 6B,C).

Direct binding of the H4 tail to the conserved ATPase domain may explain why otherwise divergent remodelers like the Chd1 and Alc1 families are regulated by the H4 tail in a manner similar to ISWI (70, 163, 225). To check for the general conservation of the H4 tail-binding interface, we aligned the amino acid sequences of several representative enzymes from H4 tail-dependent and H4 tail-independent remodeler families (Figure 6A–C). In the simplest case, the H4 tail-binding amino acids would be conserved exclusively in remodelers, that are dependent on the H4 tail for full activity. Intriguingly however, many H4 tail-binding residues on lobe 2 are conserved in remodeler families, that are thought not rely on the H4 tail for full activation. Among those families are for instance the Snf2, Mi-2 (135) and Ino80 (226) families (Figure 6A–C). The recent cryo-EM structure of nucleosome-bound ScSnf2 indeed revealed an interaction between the H4 tail and ScSnf2 (Figure 6D). Furthermore, deletion of the H4 tail reduced the remodeling velocity of ScSnf2 by twofold (163). However, this effect is only marginal when compared to the sixfold reduction of remodeling activity in response to H4 tail-deletion we observed for ISWI. Notably, the H4 binding pocket in ScSnf2 corresponds to the acidic surface in MtISWI and DmISWI that is contacted by the H4 tail (Figure 6D). In conclusion, even though the H4 tail is not required as an allosteric activator of catalysis for many nucleosome remodeling enzymes, they may still harbor a binding site for H4. Binding of H4 tail to these remodelers may for example increase their affinity or specificity for the nucleosome.

As ISWI is usually found within larger remodeling factors *in vivo*, regulation is likely even more complex in the cellular context. Notably, the non-catalytic Acf1 subunit of the ACF complex was recently shown to engage the H4 tail at a defined stage during the sliding reaction (210). Specifically, it was proposed that Acf1 sequesters the H4 tail in case neighboring nucleosomes are in close proximity and thereby prevents the ATPase subunit to become active (210).

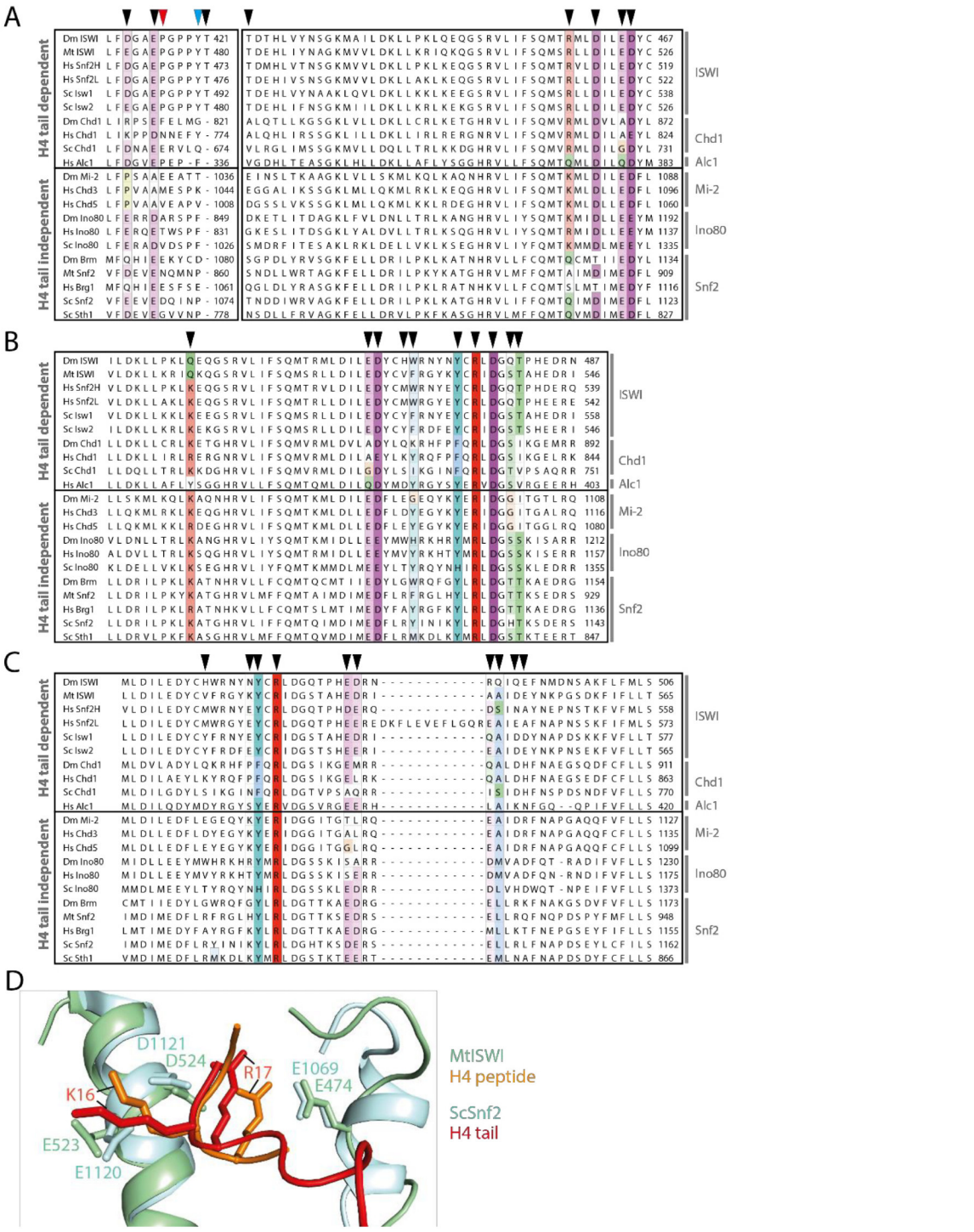

Figure 6: Conservation of the H4 tail-binding pocket across different nucleosome remodeler families. (A–C) Multiple sequence alignment of the H4 tail-binding pocket in several remodeler families. The binding pocket was identified by crosslink guided *in silico* docking of an H4 peptide (amino acids 1-20, see also section 2.3). The color intensity indicates the level of conservation. The arrowheads point to the ten amino acids, which were most frequently contacted during modeling. The alignment was calculated using the T-Coffee algorithm (http://tcoffee.crg.cat/apps/tcoffee/). **(A)** Binding pocket of H4 K16. Black arrowhead: The indicated amino acid is within 15 Å of H4 K16 (Cα-Cα distance) in the MtISWI (154) and in the ScSnf2 (163) structure. Approximately 15 Å can be spanned by a Bpa-mediated crosslink (156). Red arrowhead: The distance of the indicated amino acid from H4 K16 is larger than 15 Å in the MtISWI structure. Blue arrowhead: The distance of the indicated amino acid from H4 K16 is larger than 15 Å in the ScSnf2 structure. **(B)** Binding pocket of H4 L10. **(C)** Binding pocket of H4 T1. **(D)** Alignment of the MtISWI-H4 peptide crystal structure (PDB: 5JXR) and the ScSnf2-nucleosome structure (PDB: 5X0Y). Amino acids critical for the remodeler-H4 tail interaction are shown as sticks.

3.3.2 Regulation by N-terminal motifs

The NTR of ISWI contains several conserved motifs including ppHSA, AutoN and AcidicN (see section 2.3, Figure 1). Structures and functions of these motifs remain mostly unexplored to date. We found the ppHSA motif and the adjacent regions to crosslink to Lobe 2 of the ATPase domain in the absence of a nucleosome indicating spatial proximity. Based on this finding, we suggest the ppHSA motif to be important for docking the ISWI NTR against the ATPase domain. Consistent with a structural role of this motif, we found that N-terminal truncation mutants lacking ppHSA displayed no major catalytic defect, but were destabilized both *in vitro* and *in vivo* (see section 2.3, Figure 2 and Figure 3). Notably, ppHSA is conserved not only within the ISWI and Chd1 families, but also in unrelated families including Ino80, Lsh and Snf2. Like in ISWI, ppHSA may bind the ATPase domain of these remodeler families to confer structural stability. In fact, a helix containing ppHSA was found to bind ATPase lobe 1 of the *M. thermophila* Snf2 (152).

Our results fit well with the crystal structure of MtISWI (154), which was published during the revision of the manuscript presented in section 2.3. The sequence of MtISWI is about 46% identical to *Drosophila* ISWI and ppHSA, AutoN and AcidicN are conserved. The structure confirms the result from our crosslinking approach that the NTR folds back and contacts the ATPase domain. The photoreactive Bpa inserted at position 483, which is located within a loop region of lobe 2, crosslinked to several amino acids either inside or adjacent to the ppHSA motif (see section 2.3, Figure 4). Of these targeted amino acids, only two amino acids inside the ppHSA motif are conserved in MtISWI: H59 and F60 in DmISWI, which correspond to H108 and F109 in MtISWI. To investigate whether the crystal structure supports the identified crosslinks, we measured the Cα-Cα distances of the crosslinked residues in the MtISWI structure (Figure 7). We found the distances restraints obtained from crosslinking to be compatible with the crystal structure. Hence, we propose the docking site of the NTR to be conserved between DmISWI and MtISWI.

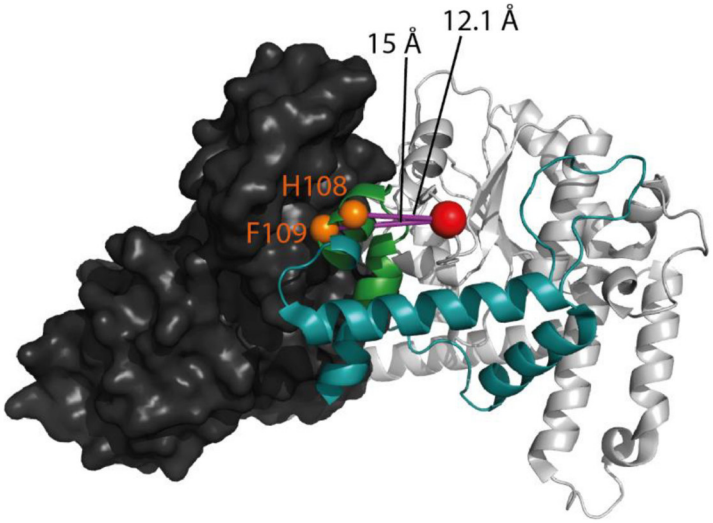

Figure 7: The ISWI NTR contacts lobe 2 of the ATPase domain. Illustrated are crosslinks (purple rods) connecting lobe 2 (light grey) and ppHSA (green) in the crystal structure of MtISWI (PDB 5JXR). The photocrosslinkable amino acid Bpa (red sphere) we inserted into DmISWI is shown at the corresponding position in MtISWI. Target amino acids within ppHSA are shown as orange spheres. Distances spanned by the crosslinks are indicated. The maximally allowed distance between crosslinked residues can be estimated from the maximal distance spanned by Bpa (9.6 Å) and the target amino acid (H: 4.7 Å; F: 5.1 Å). The crystal structure is thus largely consistent with the distance restraints provided by the crosslinks. Lobe 1 is shown in dark grey, the NTR in blue. NegC is omitted for clarity.

The conformation of the ISWI NTR is reminiscent of the architecture of the related Chd1 remodeler. In contrast to ISWI, the Chd1 NTR contains a double chromodomain, which binds within the central cleft of the ATPase domain in the absence of a nucleosomal substrate (153). The two chromodomains are connected by two helices. Interestingly, the C-terminal one of these helices is highly enriched in acidic amino acids and packs against a basic surface on the second ATPase lobe (Figure 8A). The acidic helix was suggested to occlude a DNA-binding surface on the ATPase domain to prevent activation of the enzyme in the absence of a substrate. Notably, we identified a novel motif in ISWI, which we named AcidicN, and which similarly contained a stretch of acidic amino acids. AcidicN is immediately adjacent to the previously identified AutoN motif implicated in negative regulation of the ISWI ATPase motor (147).

To functionally characterize AcidicN, we mutated conserved acidic residues to noncharged ones. Mutations in AcidicN resulted in abnormally high ATP hydrolysis activity of ISWI when bound to DNA. Strikingly, AcidicN mutants hydrolyzed ATP with comparable velocities when bound to nucleosomes (see section 2.3). The effects of AcidicN mutations were remarkably similar to AutoN mutations (147), indicating a collaborative regulatory role of both motifs.

Peptide docking algorithms predicted the docking site of the AutoN-AcidicN motif to localize to lobe 2 of the ISWI ATPase domain. To further corroborate this hypothesis, we inserted charge reversal mutations into the predicted binding interface of AutoN-AcidicN. Specifically, we replaced K403, R458 and R508 within the predicted interface on lobe 2 with acidic residues. As expected, these mutants phenocopied the AcidicN mutants. They hydrolyzed ATP with comparable velocities when bound to either naked DNA or nucleosomes while retaining their remodeling activity (see section 2.3, Figure 7).

Interestingly, Yan et al. introduced mutations into residues equivalent to K403 and R508 (K462 and R567) into MtISWI. Confirming our results, they found the mutants to have an increased DNA-stimulated ATPase activity. In contrast, the nucleosome sliding activity of the MtISWI mutants was severely diminished (154). However, whereas we probed remodeling of DmISWI mutants on nucleosomal arrays, sliding of MtISWI mutants was analyzed on mononucleosomes. The results may therefore not be directly comparable. There also remains the possibility that in MtISWI these residues are not only important for inhibition, but also crucial for the remodeling reaction.

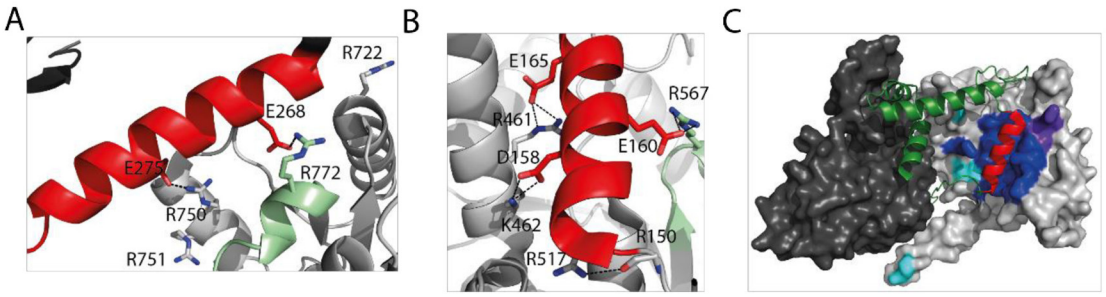

Figure 8: Comparison between the AcidicN binding pocket of DmISWI, MtISWI and Chd1. (A–B) Close-up view of the molecular contacts between the acidic helix (red) and lobe 2 (light grey) in Chd1 (PDB 3MWY) **(A)** and MtISWI (PDB 5JXR) **(B)**. Residues forming hydrogen bonds are shown in stick representation. The conserved motif V within lobe 2 is colored pale green. Hydrogen bonds are shown as dotted lines. **(C)** Comparison between the experimentally determined AcidicN-lobe 2 interface of the crystal structure of MtISWI and the predicted AcidicN interface in DmISWI. The AcidicN helix within the NTR (green) is indicated in red. Interface residues on lobe 2 detected in both approaches are shown in blue, residues uniquely detected in the MtISWI crystal structure are colored purple and residues unique to the prediction are cyan. Shown is the MtISWI structure (PDB 5JXR) (154). Lobe 1: dark grey, lobe 2: light grey.

Strikingly, our predicted AcidicN binding pocket on lobe 2 matched remarkably well with the crystal structure (Figure 8B,C) while AutoN crystallized closer to the H4 tail-binding site than suggested by modeling. The residues we analyzed by mutagenesis indeed lie in the AcidicN-lobe 2 interface giving a physical explanation for the deregulation of the respective mutants (Figure 8B). Furthermore, as predicted by us (see section 2.3, Figure 4—figure supplement 3), AcidicN forms an α-helix in the crystal structure.

AcidicN masks part of the helicase motif V, which is conserved among Snf2-family remodelers (95). Motif V was suggested to be required for coupling ATP hydrolysis to sliding activity in *S. cerevisiae* Swi2/Snf2 (227). It also participates in DNA-binding and may stabilize a catalytically active ATPase conformation (155, 163). Specifically, AcidicN binds to a highly conserved arginine residue within motif V (Figure 8B). Interestingly, in the Chd1 crystal structure the acidic helix also directly contacts the corresponding residue (Figure 8A). Notably, we did not observe a remodeling defect upon mutation of the arginine in the context of DmISWI while remodeling by MtISWI was severely diminished (see above) (154). In the context of Chd1, mutation of the conserved arginine decreased the ATPase activity about twofold whereas the effect on remodeling was not probed (153). Thus, it remains to be investigated how exactly motif V contributes to catalytic regulation of ISWI- and Chd1-type remodelers. Importantly, AcidicN appears to occlude a DNA-binding surface on lobe 2.

In summary, we propose that the overall structural architecture of the NTR-ATPase modules of Chd1 and ISWI is similar, even though their NTRs are not conserved at the sequence level. Both NTRs contact lobe 2 of the ATPase domain and the binding interface is required for substrate discrimination. Moreover, both NTRs confer sensitivity towards the H4 tail as discussed in the following section.

3.3.3 Interplay between the H4 tail and N-terminal motifs

Nucleosome remodeling enzymes of the ISWI- and Chd1-families have evolved complex regulatory mechanisms involving autoinhibitory motifs in their N-termini. A number of elegant studies have shown that autoinhibition is counteracted by binding of the H4 tail, but the molecular mechanism of activation remains elusive.

As AutoN is reminiscent of the H4 basic patch, it seems intuitive that AutoN acts as a pseudosubstrate that mimics the basic patch of the H4 tail. This model postulates a shared binding site of the H4 tail and AutoN on the ATPase domain. However, until recently no structural data supporting this hypothesis has been reported. In section 2.3, we demonstrated that AutoN does not function alone, but in concert with AcidicN to inhibit the ATPase motor. Contrary to expectations, we furthermore found the binding sites of the H4 tail and AutoN-AcidicN to be adjacent, but not overlapping. This is supported by the MtISWI crystal structure (154). It is thus conceivable that the ISWI ATPase motor is not regulated by direct competition between AutoN-AcidicN and the H4 tail. Instead, the negative charge of AcidicN may even promote binding of the positively charged basic patch of the H4 tail. Importantly, our data suggest that the NTR and the H4 tail can simultaneously bind to lobe 2. Whether simultaneous binding indeed occurs or whether it is a fleeting or stable intermediate remains to be investigated. A conformational change within the NTR is compatible with the model. Since AcidicN probably occludes a conserved DNA-binding site on lobe 2, a rearrangement during the remodeling cycle is likely. In fact, we observed a changed protease cleavage pattern in the NTR upon DNA binding to ISWI (see section 2.1, Figure 2).

Similarly, a conformational change of the NTR was postulated to be required for activation of Chd1 (153). Recently, site-specific protein-DNA crosslinking identified a loop inside the first chromodomain contacting nucleosomal DNA at SHL-1. The identified crosslinks suggested that the chromodomains remain close to the ATPase domain upon nucleosome binding. However, the distance restraints were consistent with a minor conformational change allowing the chromodomains to slightly shift away from the binding interface on ATPase lobe 2 (170). Interestingly, both deletion of the chromodomains and mutation of the acidic helix rendered remodeling by Chd1 independent of the H4 tail (153). Analogous to Chd1, AcidicN mutants of ISWI lost their reliance on the H4 tail during nucleosome remodeling (section 2.3 Figure 8). Binding of the H4 tail to lobe 2 may therefore trigger a minor rearrangement of AcidicN to facilitate DNA binding.

In the recent crystal structure of MtSnf2 (152), conserved DNA binding motifs including Motif V in the ATPase domain are solvent-accessible and not occluded by regulatory domains. Hence, Snf2 is maximally activated already in the presence of naked DNA and does not require additional epitopes to counteract autoinhibitory domains. This may also explain the fact that Snf2 is not strictly dependent on the H4 N-terminal tail (163).

Taken together, an intricate interplay between autoinhibitory motifs and the H4 tail determines the activity state of nucleosome remodeling enzymes belonging to the ISWI and Chd1 families. While our data provide unprecedented detail of the regulatory network, we are just beginning to understand the sophisticated mechanisms that regulate nucleosome remodeler ATPases.

3.3.4 Autoinhibition as a general mechanism for regulation of SF2 family members

Autoinhibitory motifs are found not only in ISWI and Chd1 family members, but also in distant remodeler families and DEAD-box helicases. In many cases, inhibitory domains contribute to regulation by either occluding a nucleic acid binding interface or by preventing the catalytic domain from adopting an active conformation, a concept described as modular allostery (228). In both cases, an intramolecular interaction must be broken to remove the gating element allowing the enzyme to become active. Consequently, false substrates are kept off and ATPase motors are prevented from wastefully hydrolyzing ATP. Regulatory motifs are frequently also supplied by auxiliary subunits and external effectors (210, 229-231).

Nucleosome remodelers belonging to subfamilies distinct from ISWI and Chd1 that carry autoinhibitory motifs include the SSO1653-like remodeler Cockayne syndrome group B protein (CSB) (232, 233) and Rad54 (234). CSB functions in transcription coupled nucleotide excision repair (235) and harbors an autoinhibitory region in the N-terminus (236). Deletion of the CSB N-terminus was shown to markedly increase DNA-stimulated ATPase activity. In the context of the *S. pombe* ortholog of CSB, Rhp26, the autoinhibitory region was narrowed down to the so-called leucine latch motif. Mutation of two conserved leucine residues within the leucine latch caused an increase of the ATPase activity accompanied by an increased remodeling activity. Reminiscent of ISWI and Chd1, the leucine latch motif was predicted to form a helix and crosslinked to lobe 2 of the Rhp26 ATPase domain. The exact binding site on lobe 2 however could not be identified from the data. The leucine latch was suggested to lock the ATPase domain in an inactive state (232). Rad54 is critically involved in homologous recombination. A systematic deletion analysis identified an autoinhibitory region in its N-terminus. Inhibition was shown to be counteracted by interaction of Rad54 with Rad51 and DNA (234).

The RecG-like helicase mutation frequency decline protein (Mfd) uses a similar strategy for regulation. Mfd contains the autoinhibitory UvrB homology module (BHM) in the N-terminus (237). The interaction of BHM with a C-terminal domain of Mfd in the apo state represses Mfd activity. Disruption of the binding interface was demonstrated to relieve autoinhibition and presumably stabilizes a conformation of Mfd competent for ATP hydrolysis and translocation (237-239).

Numerous examples for SF2 members that are inhibited in a comparable manner are found within the family of DEAD-box RNA helicases (section 1.2.4, Figure 2). Among them are the immune receptor retinoic acid inducible gene-I (RIG-I) (240, 241), DEAD-box protein 3 (DDX3) (242), the spliceosomal Prp5 (243) and DEAD-box protein 5 (Dbp5) (230, 244). RIG-I is an innate immune receptor responsible for detecting viral RNAs and triggering immune responses. In the autoinhibited state, two N-terminal caspase activation and recruitment domains (CARDs) interact with an insertion between the two ATPase lobes (240). This interaction was suggested to be critical for discrimination between viral and non-viral RNAs. Solely binding of the characteristic blunt-ended viral RNAs induces a conformational change of RIG-I, which releases the CARD domains. Consequently, the ATPase domain adopts an active conformation and the CARD domains become available for activation of a signaling cascade (241). Dbp5 plays a role in export of mRNA from the nucleus and is thought promote protein exchange from mRNA-containing complexes. Wild-type Dbp5 has a low ATPase activity in the absence of RNA. Interestingly, Dbp5 contains an α-helix in the N-terminus, which inserts between the two ATPase lobes and prevents them from adopting an active conformation (244). Gle1 in complex with the small molecule inositol hexakisphosphate (IP_6) robustly activates ATP hydrolysis of Dbp5 by displacing the α-helix. Deletion of the autoinhibitory helix resulted in Gle1-IP_6 and RNA independent ATP hydrolysis of Dbp5 (230, 244). Furthermore, Dbp5 can form a complex with the nuclear pore protein 159 (Nup159). Interaction with Nup159 was shown to occlude the RNA-binding surface of Dbp5 and prevented RNA-stimulated ATPase activity (230, 245, 246). Notably, the eukaryotic initiation factor 4A (eIF4A), which binds the 5'-untranslated region of mRNA and helps recruiting the small ribosomal subunit, is similarly regulated by occlusion of the RNA-binding region (231). The negative regulator programmed cell death protein 4 (PDCD4) was demonstrated to wedge itself into the cleft between the two ATPase lobes of eIF4A and sequestrates RNA-binding surfaces on both sides of the cleft (247, 248). In summary, inhibition of SF2 family ATPases by sterically blocking substrate binding sites or by locking the ATPase lobes in an inactive conformation emerges as a conserved mechanism.

3.4 Perspectives

Despite the tremendous progress in understanding mechanism and regulation of ISWI, many questions remain unanswered. While the work presented in this thesis provides answers to partial aspects of nucleosome sliding, it raises exciting new questions to be tackled by future research.

Exploring the mechanism and regulation of nucleosome remodeling enzymes has benefited from development of *in vitro* assays. The quantitative remodeling assay we developed (section 2.4) can easily be expanded to study the activity of remodelers distinct from ISWI. In the future, further development of this assay by addition of H1 or high salt concentrations to induce array compaction is desirable. This would provide an *in vitro* tool to quantitatively study remodeling of condensed chromatin and could potentially be used to study the relevance of H4 tail recognition by ISWI for formation of higher-order chromatin structures.

It will be important to investigate the contacts between ISWI domains and the nucleosome at different reaction steps during the remodeling cycle. Particularly revealing in this regard will be high-resolution structures of nucleosome-bound ISWI in different nucleotide states. While X-ray crystallography has long been considered the gold-standard for structural studies, emerging techniques like cryo-EM and NMR will provide powerful tools to study remodeler-nucleosome complexes. Additionally, crosslinking coupled to high resolution mass spectrometry may help to discover protein interactions and enable the construction of protein interaction networks. Ultimately, hybrid structural approaches may yield structural insights into complete ISWI factors bound to a nucleosome.

The ISWI ATPase domain as well as accessory domains most likely undergo complex conformational changes in response to substrate binding and during ATP hydrolysis. To understand the molecular mechanism of nucleosome sliding and the regulation of the catalytic domain, it will be pivotal to track these changes. Deciphering the movements of the HSS domain will be of special interest. FRET-based assays have revealed the HSS domain to change its position on the nucleosome during the catalytic cycle (204). However, the exact binding interfaces of these states and their functional significance are not yet clear. An important next step towards understanding the autoregulatory function of the N-terminal domains of ISWI will be to identify their structural rearrangements upon nucleosome binding. To address this issue, we have started to establish an approach that combines heavy isotope labeling (^{15}N) with crosslinking and quantitative mass spectrometry. Here, we use the identified crosslinks between the NTR and the ATPase domain (see section 2.3), which form in the absence of a substrate as a diagnostic tool. By comparing crosslinking efficiencies in ^{15}N-labeled ISWI bound to a nucleosome with substrate-free unlabeled ISWI we may be able to detect conformational changes of the NTR. Labeling with heavy isotopes allows us to simultaneously analyze both samples in the mass spectrometer and to extract quantitative data. To directly probe for a conformational change of the NTR induced by H4 tail binding, comparing crosslinking efficiencies of ISWI either bound to wild type H4-nucleosomes or to nucleosomes lacking the H4 tail will be critical. To obtain a more comprehensive picture of the movement of individual motifs in the NTR, a FRET approach in combination with quantitative crosslinking may prove useful.

Future work should not only focus on conformational changes of remodelers, but also on rearrangements within the nucleosome itself. A pioneering study by Sinha et al. has recently demonstrated that the histone octamer considerably deforms during remodeling by SNF2H (223). The protein core of the nucleosome is most likely not a static entity and may play a more active role than previously imagined. Investigating the structural plasticity of the nucleosome will importantly contribute to understand the basic remodeling reaction.

4. REFERENCES

1. A. L. Olins, D. E. Olins, Spheroid chromatin units (v bodies). *Science* **183**, 330-332 (1974).

2. C. L. Woodcock, J. P. Safer, J. E. Stanchfield, Structural repeating units in chromatin. I. Evidence for their general occurrence. *Exp Cell Res* **97**, 101-110 (1976).

3. K. Luger, A. W. Mader, R. K. Richmond, D. F. Sargent, T. J. Richmond, Crystal structure of the nucleosome core particle at 2.8 A resolution. *Nature* **389**, 251-260 (1997).

4. G. Arents, E. N. Moudrianakis, The histone fold: a ubiquitous architectural motif utilized in DNA compaction and protein dimerization. *Proceedings of the National Academy of Sciences of the United States of America* **92**, 11170-11174 (1995).

5. C. A. Davey, D. F. Sargent, K. Luger, A. W. Maeder, T. J. Richmond, Solvent mediated interactions in the structure of the nucleosome core particle at 1.9 a resolution. *Journal of molecular biology* **319**, 1097-1113 (2002).

6. M. A. Hall *et al.*, High-resolution dynamic mapping of histone-DNA interactions in a nucleosome. *Nature structural & molecular biology* **16**, 124-129 (2009).

7. E. Segal *et al.*, A genomic code for nucleosome positioning. *Nature* **442**, 772-778 (2006).

8. E. Segal, J. Widom, What controls nucleosome positions? *Trends Genet* **25**, 335-343 (2009).

9. A. Worcel, S. Han, M. L. Wong, Assembly of newly replicated chromatin. *Cell* **15**, 969-977 (1978).

10. S. Smith, B. Stillman, Stepwise assembly of chromatin during DNA replication in vitro. *The EMBO journal* **10**, 971-980 (1991).

11. Z. A. Gurard-Levin, J. P. Quivy, G. Almouzni, Histone chaperones: assisting histone traffic and nucleosome dynamics. *Annual review of biochemistry* **83**, 487-517 (2014).

12. T. Furuyama, C. A. Codomo, S. Henikoff, Reconstitution of hemisomes on budding yeast centromeric DNA. *Nucleic acids research* **41**, 5769-5783 (2013).

13. H. S. Rhee, A. R. Bataille, L. Zhang, B. F. Pugh, Subnucleosomal structures and nucleosome asymmetry across a genome. *Cell* **159**, 1377-1388 (2014).

14. H. Weintraub, A. Worcel, B. Alberts, A model for chromatin based upon two symmetrically paired half-nucleosomes. *Cell* **9**, 409-417 (1976).

15. M. Floer *et al.*, A RSC/nucleosome complex determines chromatin architecture and facilitates activator binding. *Cell* **141**, 407-418 (2010).

16. J. G. Henikoff, J. A. Belsky, K. Krassovsky, D. M. MacAlpine, S. Henikoff, Epigenome characterization at single base-pair resolution. *Proceedings of the National Academy of Sciences of the United States of America* **108**, 18318-18323 (2011).

17. S. Henikoff *et al.*, The budding yeast Centromere DNA Element II wraps a stable Cse4 hemisome in either orientation in vivo. *Elife* **3**, e01861 (2014).

18. C. L. Woodcock, A. I. Skoultchi, Y. Fan, Role of linker histone in chromatin structure and function: H1 stoichiometry and nucleosome repeat length. *Chromosome Res* **14**, 17-25 (2006).

19. R. T. Simpson, Structure of the chromatosome, a chromatin particle containing 160 base pairs of DNA and all the histones. *Biochemistry* **17**, 5524-5531 (1978).

20. J. Allan, T. Mitchell, N. Harborne, L. Bohm, C. Crane-Robinson, Roles of H1 domains in determining higher order chromatin structure and H1 location. *Journal of molecular biology* **187**, 591-601 (1986).

21. J. C. Hansen, Conformational dynamics of the chromatin fiber in solution: determinants, mechanisms, and functions. *Annu Rev Biophys Biomol Struct* **31**, 361-392 (2002).

22. G. Geeven *et al.*, Local compartment changes and regulatory landscape alterations in histone H1-depleted cells. *Genome Biol* **16**, 289 (2015).

23. J. T. Finch, A. Klug, Solenoidal model for superstructure in chromatin. *Proceedings of the National Academy of Sciences of the United States of America* **73**, 1897-1901 (1976).

24. M. Kruithof *et al.*, Single-molecule force spectroscopy reveals a highly compliant helical folding for the 30-nm chromatin fiber. *Nature structural & molecular biology* **16**, 534-540 (2009).

25. P. J. Robinson, L. Fairall, V. A. Huynh, D. Rhodes, EM measurements define the dimensions of the "30-nm" chromatin fiber: evidence for a compact, interdigitated structure. *Proceedings of the National Academy of Sciences of the United States of America* **103**, 6506-6511 (2006).

26. R. A. Horowitz, D. A. Agard, J. W. Sedat, C. L. Woodcock, The three-dimensional architecture of chromatin in situ: electron tomography reveals fibers composed of a continuously variable zig-zag nucleosomal ribbon. *The Journal of cell biology* **125**, 1-10 (1994).

27. C. L. Woodcock, L. L. Frado, J. B. Rattner, The higher-order structure of chromatin: evidence for a helical ribbon arrangement. *The Journal of cell biology* **99**, 42-52 (1984).

28. B. Dorigo *et al.*, Nucleosome arrays reveal the two-start organization of the chromatin fiber. *Science* **306**, 1571-1573 (2004).

29. T. Schalch, S. Duda, D. F. Sargent, T. J. Richmond, X-ray structure of a tetranucleosome and its implications for the chromatin fibre. *Nature* **436**, 138-141 (2005).

30. F. Song *et al.*, Cryo-EM study of the chromatin fiber reveals a double helix twisted by tetranucleosomal units. *Science* **344**, 376-380 (2014).

31. E. Fussner, R. W. Ching, D. P. Bazett-Jones, Living without 30nm chromatin fibers. *Trends Biochem Sci* **36**, 1-6 (2011).

32. K. Maeshima, R. Imai, S. Tamura, T. Nozaki, Chromatin as dynamic 10-nm fibers. *Chromosoma* **123**, 225-237 (2014).

33. Y. Joti *et al.*, Chromosomes without a 30-nm chromatin fiber. *Nucleus* **3**, 404-410 (2012).

34. K. Maeshima *et al.*, Nucleosomal arrays self-assemble into supramolecular globular structures lacking 30-nm fibers. *The EMBO journal* **35**, 1115-1132 (2016).

35. J. Dubochet, M. Adrian, P. Schultz, P. Oudet, Cryo-electron microscopy of vitrified SV40 minichromosomes: the liquid drop model. *The EMBO journal* **5**, 519-528 (1986).

36. Y. Nishino *et al.*, Human mitotic chromosomes consist predominantly of irregularly folded nucleosome fibres without a 30-nm chromatin structure. *The EMBO journal* **31**, 1644-1653 (2012).

37. E. Fussner *et al.*, Constitutive heterochromatin reorganization during somatic cell reprogramming. *The EMBO journal* **30**, 1778-1789 (2011).

38. E. Fussner *et al.*, Open and closed domains in the mouse genome are configured as 10-nm chromatin fibres. *EMBO reports* **13**, 992-996 (2012).

39. K. Ahmed *et al.*, Global chromatin architecture reflects pluripotency and lineage commitment in the early mouse embryo. *PloS one* **5**, e10531 (2010).

40. J. P. Langmore, C. Schutt, The higher order structure of chicken erythrocyte chromosomes in vivo. *Nature* **288**, 620-622 (1980).

41. M. P. Scheffer, M. Eltsov, A. S. Frangakis, Evidence for short-range helical order in the 30-nm chromatin fibers of erythrocyte nuclei. *Proceedings of the National Academy of Sciences of the United States of America* **108**, 16992-16997 (2011).

42. J. Dekker, Mapping in vivo chromatin interactions in yeast suggests an extended chromatin fiber with regional variation in compaction. *The Journal of biological chemistry* **283**, 34532-34540 (2008).

43. J. Dekker, M. A. Marti-Renom, L. A. Mirny, Exploring the three-dimensional organization of genomes: interpreting chromatin interaction data. *Nat Rev Genet* **14**, 390-403 (2013).

44. T. H. Hsieh *et al.*, Mapping Nucleosome Resolution Chromosome Folding in Yeast by Micro-C. *Cell* **162**, 108-119 (2015).

45. K. J. Polach, J. Widom, Mechanism of protein access to specific DNA sequences in chromatin: a dynamic equilibrium model for gene regulation. *Journal of molecular biology* **254**, 130-149 (1995).

46. G. Li, J. Widom, Nucleosomes facilitate their own invasion. *Nature structural & molecular biology* **11**, 763-769 (2004).

47. G. Li, M. Levitus, C. Bustamante, J. Widom, Rapid spontaneous accessibility of nucleosomal DNA. *Nature structural & molecular biology* **12**, 46-53 (2005).

48. W. J. Koopmans, A. Brehm, C. Logie, T. Schmidt, J. van Noort, Single-pair FRET microscopy reveals mononucleosome dynamics. *J Fluoresc* **17**, 785-795 (2007).

49. W. J. Koopmans, R. Buning, T. Schmidt, J. van Noort, spFRET using alternating excitation and FCS reveals progressive DNA unwrapping in nucleosomes. *Biophysical journal* **97**, 195-204 (2009).

50. J. D. Anderson, J. Widom, Sequence and position-dependence of the equilibrium accessibility of nucleosomal DNA target sites. *Journal of molecular biology* **296**, 979-987 (2000).

51. P. T. Lowary, J. Widom, New DNA sequence rules for high affinity binding to histone octamer and sequence-directed nucleosome positioning. *Journal of molecular biology* **276**, 19-42 (1998).

52. T. T. Ngo, Q. Zhang, R. Zhou, J. G. Yodh, T. Ha, Asymmetric unwrapping of nucleosomes under tension directed by DNA local flexibility. *Cell* **160**, 1135-1144 (2015).

53. V. Bohm *et al.*, Nucleosome accessibility governed by the dimer/tetramer interface. *Nucleic acids research* **39**, 3093-3102 (2011).

54. T. T. Ngo, T. Ha, Nucleosomes undergo slow spontaneous gaping. *Nucleic acids research* **43**, 3964-3971 (2015).

55. J. Mozziconacci, J. M. Victor, Nucleosome gaping supports a functional structure for the 30nm chromatin fiber. *Journal of structural biology* **143**, 72-76 (2003).

56. A. Lesne, J. M. Victor, Chromatin fiber functional organization: some plausible models. *Eur Phys J E Soft Matter* **19**, 279-290 (2006).

57. T. Suganuma, J. L. Workman, Signals and combinatorial functions of histone modifications. *Annual review of biochemistry* **80**, 473-499 (2011).

58. T. Jenuwein, C. D. Allis, Translating the histone code. *Science* **293**, 1074-1080 (2001).

59. P. Tessarz, T. Kouzarides, Histone core modifications regulating nucleosome structure and dynamics. *Nat Rev Mol Cell Biol* **15**, 703-708 (2014).

60. M. Lawrence, S. Daujat, R. Schneider, Lateral Thinking: How Histone Modifications Regulate Gene Expression. *Trends Genet* **32**, 42-56 (2016).

61. A. F. Kebede, R. Schneider, S. Daujat, Novel types and sites of histone modifications emerge as players in the transcriptional regulation contest. *The FEBS journal* **282**, 1658-1674 (2015).

62. M. Yun, J. Wu, J. L. Workman, B. Li, Readers of histone modifications. *Cell research* **21**, 564-578 (2011).

63. B. D. Strahl, C. D. Allis, The language of covalent histone modifications. *Nature* **403**, 41-45 (2000).

64. A. H. Hassan, K. E. Neely, J. L. Workman, Histone acetyltransferase complexes stabilize swi/snf binding to promoter nucleosomes. *Cell* **104**, 817-827 (2001).

65. A. H. Hassan *et al.*, Function and selectivity of bromodomains in anchoring chromatin-modifying complexes to promoter nucleosomes. *Cell* **111**, 369-379 (2002).

66. M. Kasten *et al.*, Tandem bromodomains in the chromatin remodeler RSC recognize acetylated histone H3 Lys14. *The EMBO journal* **23**, 1348-1359 (2004).

67. M. Shogren-Knaak *et al.*, Histone H4-K16 acetylation controls chromatin structure and protein interactions. *Science* **311**, 844-847 (2006).

68. C. R. Clapier, K. P. Nightingale, P. B. Becker, A critical epitope for substrate recognition by the nucleosome remodeling ATPase ISWI. *Nucleic acids research* **30**, 649-655 (2002).

69. D. F. Corona, C. R. Clapier, P. B. Becker, J. W. Tamkun, Modulation of ISWI function by site-specific histone acetylation. *EMBO reports* **3**, 242-247 (2002).

70. H. Ferreira, A. Flaus, T. Owen-Hughes, Histone modifications influence the action of Snf2 family remodelling enzymes by different mechanisms. *Journal of molecular biology* **374**, 563-579 (2007).

71. H. Klinker *et al.*, ISWI remodelling of physiological chromatin fibres acetylated at lysine 16 of histone H4. *PloS one* **9**, e88411 (2014).

72. H. Masumoto, D. Hawke, R. Kobayashi, A. Verreault, A role for cell-cycle-regulated histone H3 lysine 56 acetylation in the DNA damage response. *Nature* **436**, 294-298 (2005).

73. H. Neumann *et al.*, A method for genetically installing site-specific acetylation in recombinant histones defines the effects of H3 K56 acetylation. *Molecular cell* **36**, 153-163 (2009).

74. W. F. Marzluff, E. J. Wagner, R. J. Duronio, Metabolism and regulation of canonical histone mRNAs: life without a poly(A) tail. *Nat Rev Genet* **9**, 843-854 (2008).

75. K. Ahmad, S. Henikoff, The histone variant H3.3 marks active chromatin by replication-independent nucleosome assembly. *Molecular cell* **9**, 1191-1200 (2002).

76. R. D. Shelby, K. Monier, K. F. Sullivan, Chromatin assembly at kinetochores is uncoupled from DNA replication. *The Journal of cell biology* **151**, 1113-1118 (2000).

77. C. Bonisch, S. B. Hake, Histone H2A variants in nucleosomes and chromatin: more or less stable? *Nucleic acids research* **40**, 10719-10741 (2012).

78. L. M. Zink, S. B. Hake, Histone variants: nuclear function and disease. *Curr Opin Genet Dev* **37**, 82-89 (2016).

79. S. G. Franklin, A. Zweidler, Non-allelic variants of histones 2a, 2b and 3 in mammals. *Nature* **266**, 273-275 (1977).

80. J. R. Pehrson, V. A. Fried, MacroH2A, a core histone containing a large nonhistone region. *Science* **257**, 1398-1400 (1992).

81. S. Chakravarthy, A. Patel, G. D. Bowman, The basic linker of macroH2A stabilizes DNA at the entry/exit site of the nucleosome. *Nucleic acids research* **40**, 8285-8295 (2012).

82. C. Costanzi, J. R. Pehrson, Histone macroH2A1 is concentrated in the inactive X chromosome of female mammals. *Nature* **393**, 599-601 (1998).

83. Y. Bao *et al.*, Nucleosomes containing the histone variant H2A.Bbd organize only 118 base pairs of DNA. *The EMBO journal* **23**, 3314-3324 (2004).

84. T. Gautier *et al.*, Histone variant H2ABbd confers lower stability to the nucleosome. *EMBO reports* **5**, 715-720 (2004).

85. P. B. Talbert, S. Henikoff, Histone variants--ancient wrap artists of the epigenome. *Nat Rev Mol Cell Biol* **11**, 264-275 (2010).

86. P. B. Becker, J. L. Workman, Nucleosome remodeling and epigenetics. *Cold Spring Harb Perspect Biol* **5**, (2013).

87. C. R. Clapier, B. R. Cairns, in *Fundamentals of Chromatin,* J. L. Workman, S. M. Abmayr, Eds. (Springer, 2014).

88. S. Ghaemmaghami *et al.*, Global analysis of protein expression in yeast. *Nature* **425**, 737-741 (2003).

89. M. Weiss, S. Schrimpf, M. O. Hengartner, M. J. Lercher, C. von Mering, Shotgun proteomics data from multiple organisms reveals remarkable quantitative conservation of the eukaryotic core proteome. *Proteomics* **10**, 1297-1306 (2010).

90. B. Schwanhausser *et al.*, Global quantification of mammalian gene expression control. *Nature* **473**, 337-342 (2011).

91. R. Kumar, D. Q. Li, S. Muller, S. Knapp, Epigenomic regulation of oncogenesis by chromatin remodeling. *Oncogene*, (2016).

92. C. Kadoch, G. R. Crabtree, Mammalian SWI/SNF chromatin remodeling complexes and cancer: Mechanistic insights gained from human genomics. *Sci Adv* **1**, e1500447 (2015).

93. H. S. Subramanya, L. E. Bird, J. A. Brannigan, D. B. Wigley, Crystal structure of a DExx box DNA helicase. *Nature* **384**, 379-383 (1996).

94. M. R. Singleton, M. S. Dillingham, D. B. Wigley, Structure and mechanism of helicases and nucleic acid translocases. *Annual review of biochemistry* **76**, 23-50 (2007).

95. A. Flaus, D. M. Martin, G. J. Barton, T. Owen-Hughes, Identification of multiple distinct Snf2 subfamilies with conserved structural motifs. *Nucleic acids research* **34**, 2887-2905 (2006).

96. M. E. Fairman-Williams, U. P. Guenther, E. Jankowsky, SF1 and SF2 helicases: family matters. *Curr Opin Struct Biol* **20**, 313-324 (2010).

97. F. Mueller-Planitz, H. Klinker, P. B. Becker, Nucleosome sliding mechanisms: new twists in a looped history. *Nature structural & molecular biology* **20**, 1026-1032 (2013).

98. G. Mizuguchi *et al.*, ATP-driven exchange of histone H2AZ variant catalyzed by SWR1 chromatin remodeling complex. *Science* **303**, 343-348 (2004).

99. M. Papamichos-Chronakis, S. Watanabe, O. J. Rando, C. L. Peterson, Global regulation of H2A.Z localization by the INO80 chromatin-remodeling enzyme is essential for genome integrity. *Cell* **144**, 200-213 (2011).

100. I. Whitehouse *et al.*, Nucleosome mobilization catalysed by the yeast SWI/SNF complex. *Nature* **400**, 784-787 (1999).

101. Y. Lorch, M. Zhang, R. D. Kornberg, Histone octamer transfer by a chromatin-remodeling complex. *Cell* **96**, 389-392 (1999).

102. S. R. Kassabov, B. Zhang, J. Persinger, B. Bartholomew, SWI/SNF unwraps, slides, and rewraps the nucleosome. *Molecular cell* **11**, 391-403 (2003).

103. M. Bruno *et al.*, Histone H2A/H2B dimer exchange by ATP-dependent chromatin remodeling activities. *Molecular cell* **12**, 1599-1606 (2003).

104. M. L. Dechassa *et al.*, SWI/SNF has intrinsic nucleosome disassembly activity that is dependent on adjacent nucleosomes. *Molecular cell* **38**, 590-602 (2010).

105. A. Lusser, D. L. Urwin, J. T. Kadonaga, Distinct activities of CHD1 and ACF in ATP-dependent chromatin assembly. *Nature structural & molecular biology* **12**, 160-166 (2005).

106. C. Stockdale, A. Flaus, H. Ferreira, T. Owen-Hughes, Analysis of nucleosome repositioning by yeast ISWI and Chd1 chromatin remodeling complexes. *The Journal of biological chemistry* **281**, 16279-16288 (2006).

107. L. R. Racki *et al.*, The chromatin remodeller ACF acts as a dimeric motor to space nucleosomes. *Nature* **462**, 1016-1021 (2009).

108. J. Pointner *et al.*, CHD1 remodelers regulate nucleosome spacing in vitro and align nucleosomal arrays over gene coding regions in S. pombe. *The EMBO journal* **31**, 4388-4403 (2012).

109. L. K. Elfring, R. Deuring, C. M. McCallum, C. L. Peterson, J. W. Tamkun, Identification and characterization of Drosophila relatives of the yeast transcriptional activator SNF2/SWI2. *Molecular and cellular biology* **14**, 2225-2234 (1994).

110. T. Tsukiyama, C. Daniel, J. Tamkun, C. Wu, ISWI, a member of the SWI2/SNF2 ATPase family, encodes the 140 kDa subunit of the nucleosome remodeling factor. *Cell* **83**, 1021-1026 (1995).

111. T. Tsukiyama, C. Wu, Purification and properties of an ATP-dependent nucleosome remodeling factor. *Cell* **83**, 1011-1020 (1995).

112. T. Ito, M. Bulger, M. J. Pazin, R. Kobayashi, J. T. Kadonaga, ACF, an ISWI-containing and ATP-utilizing chromatin assembly and remodeling factor. *Cell* **90**, 145-155 (1997).

113. P. D. Varga-Weisz *et al.*, Chromatin-remodelling factor CHRAC contains the ATPases ISWI and topoisomerase II. *Nature* **388**, 598-602 (1997).

114. L. Vanolst, C. Fromental-Ramain, P. Ramain, Toutatis, a TIP5-related protein, positively regulates Pannier function during Drosophila neural development. *Development* **132**, 4327-4338 (2005).

115. A. V. Emelyanov *et al.*, Identification and characterization of ToRC, a novel ISWI-containing ATP-dependent chromatin assembly complex. *Genes & development* **26**, 603-614 (2012).

116. G. LeRoy, G. Orphanides, W. S. Lane, D. Reinberg, Requirement of RSF and FACT for transcription of chromatin templates in vitro. *Science* **282**, 1900-1904 (1998).

117. O. Barak *et al.*, Isolation of human NURF: a regulator of Engrailed gene expression. *The EMBO journal* **22**, 6089-6100 (2003).

118. G. S. Banting *et al.*, CECR2, a protein involved in neurulation, forms a novel chromatin remodeling complex with SNF2L. *Human molecular genetics* **14**, 513-524 (2005).

119. M. Chioda, S. Vengadasalam, E. Kremmer, A. Eberharter, P. B. Becker, Developmental role for ACF1-containing nucleosome remodellers in chromatin organisation. *Development* **137**, 3513-3522 (2010).

120. K. Borner *et al.*, A role for tuned levels of nucleosome remodeler subunit ACF1 during Drosophila oogenesis. *Developmental biology* **411**, 217-230 (2016).

121. O. Barak, M. A. Lazzaro, N. S. Cooch, D. J. Picketts, R. Shiekhattar, A tissue-specific, naturally occurring human SNF2L variant inactivates chromatin remodeling. *The Journal of biological chemistry* **279**, 45130-45138 (2004).

122. M. A. Lazzaro *et al.*, Characterization of novel isoforms and evaluation of SNF2L/SMARCA1 as a candidate gene for X-linked mental retardation in 12 families linked to Xq25-26. *BMC Med Genet* **9**, 11 (2008).

123. M. Eckey *et al.*, Nucleosome remodeler SNF2L suppresses cell proliferation and migration and attenuates Wnt signaling. *Molecular and cellular biology* **32**, 2359-2371 (2012).

124. F. Erdel, K. Rippe, Chromatin remodelling in mammalian cells by ISWI-type complexes--where, when and why? *The FEBS journal* **278**, 3608-3618 (2011).

125. T. Stopka, A. I. Skoultchi, The ISWI ATPase Snf2h is required for early mouse development. *Proceedings of the National Academy of Sciences of the United States of America* **100**, 14097-14102 (2003).

126. R. Deuring *et al.*, The ISWI chromatin-remodeling protein is required for gene expression and the maintenance of higher order chromatin structure in vivo. *Molecular cell* **5**, 355-365 (2000).

127. D. F. Corona *et al.*, ISWI regulates higher-order chromatin structure and histone H1 assembly in vivo. *PLoS biology* **5**, e232 (2007).

128. G. Mizuguchi, T. Tsukiyama, J. Wisniewski, C. Wu, Role of nucleosome remodeling factor NURF in transcriptional activation of chromatin. *Molecular cell* **1**, 141-150 (1997).

129. P. Badenhorst, M. Voas, I. Rebay, C. Wu, Biological functions of the ISWI chromatin remodeling complex NURF. *Genes & development* **16**, 3186-3198 (2002).

130. H. Song, C. Spichiger-Haeusermann, K. Basler, The ISWI-containing NURF complex regulates the output of the canonical Wingless pathway. *EMBO reports* **10**, 1140-1146 (2009).

131. N. Collins *et al.*, An ACF1-ISWI chromatin-remodeling complex is required for DNA replication through heterochromatin. *Nature genetics* **32**, 627-632 (2002).

132. J. A. Vincent, T. J. Kwong, T. Tsukiyama, ATP-dependent chromatin remodeling shapes the DNA replication landscape. *Nature structural & molecular biology* **15**, 477-484 (2008).

133. L. Lan *et al.*, The ACF1 complex is required for DNA double-strand break repair in human cells. *Molecular cell* **40**, 976-987 (2010).

134. S. Sanchez-Molina *et al.*, Role for hACF1 in the G2/M damage checkpoint. *Nucleic acids research* **39**, 8445-8456 (2011).

135. A. Brehm *et al.*, dMi-2 and ISWI chromatin remodelling factors have distinct nucleosome binding and mobilization properties. *The EMBO journal* **19**, 4332-4341 (2000).

136. A. Hamiche, R. Sandaltzopoulos, D. A. Gdula, C. Wu, ATP-dependent histone octamer sliding mediated by the chromatin remodeling complex NURF. *Cell* **97**, 833-842 (1999).

137. A. Eberharter *et al.*, Acf1, the largest subunit of CHRAC, regulates ISWI-induced nucleosome remodelling. *The EMBO journal* **20**, 3781-3788 (2001).

138. D. F. Corona *et al.*, ISWI is an ATP-dependent nucleosome remodeling factor. *Molecular cell* **3**, 239-245 (1999).

139. A. Eberharter, I. Vetter, R. Ferreira, P. B. Becker, ACF1 improves the effectiveness of nucleosome mobilization by ISWI through PHD-histone contacts. *The EMBO journal* **23**, 4029-4039 (2004).

140. J. G. Yang, T. S. Madrid, E. Sevastopoulos, G. J. Narlikar, The chromatin-remodeling enzyme ACF is an ATP-dependent DNA length sensor that regulates nucleosome spacing. *Nature structural & molecular biology* **13**, 1078-1083 (2006).

141. C. Lieleg *et al.*, Nucleosome spacing generated by ISWI and CHD1 remodelers is constant regardless of nucleosome density. *Molecular and cellular biology* **35**, 1588-1605 (2015).

142. N. Krietenstein *et al.*, Genomic Nucleosome Organization Reconstituted with Pure Proteins. *Cell* **167**, 709-721 e712 (2016).

143. T. Ito *et al.*, ACF consists of two subunits, Acf1 and ISWI, that function cooperatively in the ATP-dependent catalysis of chromatin assembly. *Genes & development* **13**, 1529-1539 (1999).

144. A. Loyola *et al.*, Functional analysis of the subunits of the chromatin assembly factor RSF. *Molecular and cellular biology* **23**, 6759-6768 (2003).

145. A. Loyola, G. LeRoy, Y. H. Wang, D. Reinberg, Reconstitution of recombinant chromatin establishes a requirement for histone-tail modifications during chromatin assembly and transcription. *Genes & development* **15**, 2837-2851 (2001).

146. S. E. Torigoe, A. Patel, M. T. Khuong, G. D. Bowman, J. T. Kadonaga, ATP-dependent chromatin assembly is functionally distinct from chromatin remodeling. *Elife* **2**, e00863 (2013).

147. C. R. Clapier, B. R. Cairns, Regulation of ISWI involves inhibitory modules antagonized by nucleosomal epitopes. *Nature* **492**, 280-284 (2012).

148. L. Aravind, D. Landsman, AT-hook motifs identified in a wide variety of DNA-binding proteins. *Nucleic acids research* **26**, 4413-4421 (1998).

149. N. H. Thoma *et al.*, Structure of the SWI2/SNF2 chromatin-remodeling domain of eukaryotic Rad54. *Nature structural & molecular biology* **12**, 350-356 (2005).

150. H. Durr, C. Korner, M. Muller, V. Hickmann, K. P. Hopfner, X-ray structures of the Sulfolobus solfataricus SWI2/SNF2 ATPase core and its complex with DNA. *Cell* **121**, 363-373 (2005).

151. G. Shaw *et al.*, Structure of RapA, a Swi2/Snf2 protein that recycles RNA polymerase during transcription. *Structure (London, England : 1993)* **16**, 1417-1427 (2008).

152. X. Xia, X. Liu, T. Li, X. Fang, Z. Chen, Structure of chromatin remodeler Swi2/Snf2 in the resting state. *Nature structural & molecular biology* **23**, 722-729 (2016).

153. G. Hauk, J. N. McKnight, I. M. Nodelman, G. D. Bowman, The chromodomains of the Chd1 chromatin remodeler regulate DNA access to the ATPase motor. *Molecular cell* **39**, 711-723 (2010).

154. L. Yan, L. Wang, Y. Tian, X. Xia, Z. Chen, Structure and regulation of the chromatin remodeller ISWI. *Nature* **540**, 466-469 (2016).

155. T. Sengoku, O. Nureki, A. Nakamura, S. Kobayashi, S. Yokoyama, Structural basis for RNA unwinding by the DEAD-box protein Drosophila Vasa. *Cell* **125**, 287-300 (2006).

156. I. Forné, J. Ludwigsen, A. Imhof, P. B. Becker, F. Mueller-Planitz, Probing the conformation of the ISWI ATPase domain with genetically encoded photoreactive crosslinkers and mass spectrometry. *Molecular & cellular proteomics : MCP* **11**, M111 012088 (2012).

157. T. Grune *et al.*, Crystal structure and functional analysis of a nucleosome recognition module of the remodeling factor ISWI. *Molecular cell* **12**, 449-460 (2003).

158. D. P. Ryan, R. Sundaramoorthy, D. Martin, V. Singh, T. Owen-Hughes, The DNA-binding domain of the Chd1 chromatin-remodelling enzyme contains SANT and SLIDE domains. *The EMBO journal* **30**, 2596-2609 (2011).

159. K. Ogata *et al.*, Solution structure of a specific DNA complex of the Myb DNA-binding domain with cooperative recognition helices. *Cell* **79**, 639-648 (1994).

160. T. H. Tahirov *et al.*, Mechanism of c-Myb-C/EBP beta cooperation from separated sites on a promoter. *Cell* **108**, 57-70 (2002).

161. A. Sharma, K. R. Jenkins, A. Heroux, G. D. Bowman, Crystal structure of the chromodomain helicase DNA-binding protein 1 (Chd1) DNA-binding domain in complex with DNA. *The Journal of biological chemistry* **286**, 42099-42104 (2011).

162. K. Yamada *et al.*, Structure and mechanism of the chromatin remodelling factor ISW1a. *Nature* **472**, 448-453 (2011).

163. X. Liu, M. Li, X. Xia, X. Li, Z. Chen, Mechanism of chromatin remodelling revealed by the Snf2-nucleosome structure. *Nature*, (2017).

164. M. N. Kagalwala, B. J. Glaus, W. Dang, M. Zofall, B. Bartholomew, Topography of the ISW2-nucleosome complex: insights into nucleosome spacing and chromatin remodeling. *The EMBO journal* **23**, 2092-2104 (2004).

165. W. Dang, B. Bartholomew, Domain architecture of the catalytic subunit in the ISW2-nucleosome complex. *Molecular and cellular biology* **27**, 8306-8317 (2007).

166. R. Schwanbeck, H. Xiao, C. Wu, Spatial contacts and nucleosome step movements induced by the NURF chromatin remodeling complex. *The Journal of biological chemistry* **279**, 39933-39941 (2004).

167. M. Zofall, J. Persinger, S. R. Kassabov, B. Bartholomew, Chromatin remodeling by ISW2 and SWI/SNF requires DNA translocation inside the nucleosome. *Nature structural & molecular biology* **13**, 339-346 (2006).

168. A. Saha, J. Wittmeyer, B. R. Cairns, Chromatin remodeling through directional DNA translocation from an internal nucleosomal site. *Nature structural & molecular biology* **12**, 747-755 (2005).

169. M. L. Dechassa *et al.*, Architecture of the SWI/SNF-nucleosome complex. *Molecular and cellular biology* **28**, 6010-6021 (2008).

170. I. M. Nodelman *et al.*, Interdomain Communication of the Chd1 Chromatin Remodeler across the DNA Gyres of the Nucleosome. *Molecular cell*, (2017).

171. S. Tan, C. A. Davey, Nucleosome structural studies. *Curr Opin Struct Biol* **21**, 128-136 (2011).

172. Y. Zhang *et al.*, DNA translocation and loop formation mechanism of chromatin remodeling by SWI/SNF and RSC. *Molecular cell* **24**, 559-568 (2006).

173. Y. Lorch, B. Davis, R. D. Kornberg, Chromatin remodeling by DNA bending, not twisting. *Proceedings of the National Academy of Sciences of the United States of America* **102**, 1329-1332 (2005).

174. R. Strohner *et al.*, A 'loop recapture' mechanism for ACF-dependent nucleosome remodeling. *Nature structural & molecular biology* **12**, 683-690 (2005).

175. G. Langst, P. B. Becker, ISWI induces nucleosome sliding on nicked DNA. *Molecular cell* **8**, 1085-1092 (2001).

176. J. N. McKnight, K. R. Jenkins, I. M. Nodelman, T. Escobar, G. D. Bowman, Extranucleosomal DNA binding directs nucleosome sliding by Chd1. *Molecular and cellular biology* **31**, 4746-4759 (2011).

177. H. Schiessel, The nucleosome: a transparent, slippery, sticky and yet stable DNA-protein complex. *Eur Phys J E Soft Matter* **19**, 251-262 (2006).

178. S. Deindl *et al.*, ISWI remodelers slide nucleosomes with coordinated multi-base-pair entry steps and single-base-pair exit steps. *Cell* **152**, 442-452 (2013).

179. A. Flaus, T. Owen-Hughes, Mechanisms for nucleosome mobilization. *Biopolymers* **68**, 563-578 (2003).

180. I. M. Kulic, H. Schiessel, Chromatin dynamics: nucleosomes go mobile through twist defects. *Physical review letters* **91**, 148103 (2003).

181. K. van Holde, T. Yager, Models for chromatin remodeling: a critical comparison. *Biochemistry and cell biology = Biochimie et biologie cellulaire* **81**, 169-172 (2003).

182. T. J. Richmond, C. A. Davey, The structure of DNA in the nucleosome core. *Nature* **423**, 145-150 (2003).

183. R. D. Makde, J. R. England, H. P. Yennawar, S. Tan, Structure of RCC1 chromatin factor bound to the nucleosome core particle. *Nature* **467**, 562-566 (2010).

184. S. Aoyagi, J. J. Hayes, hSWI/SNF-catalyzed nucleosome sliding does not occur solely via a twist-diffusion mechanism. *Molecular and cellular biology* **22**, 7484-7490 (2002).

185. X. He, H. Y. Fan, G. J. Narlikar, R. E. Kingston, Human ACF1 alters the remodeling strategy of SNF2h. *The Journal of biological chemistry* **281**, 28636-28647 (2006).

186. A. Sala *et al.*, The nucleosome-remodeling ATPase ISWI is regulated by poly-ADP-ribosylation. *PLoS biology* **6**, e252 (2008).

187. R. Ferreira *et al.*, Site-specific acetylation of ISWI by GCN5. *BMC molecular biology* **8**, 73 (2007).

188. C. R. Clapier, G. Langst, D. F. Corona, P. B. Becker, K. P. Nightingale, Critical role for the histone H4 N terminus in nucleosome remodeling by ISWI. *Molecular and cellular biology* **21**, 875-883 (2001).

189. A. Hamiche, J. G. Kang, C. Dennis, H. Xiao, C. Wu, Histone tails modulate nucleosome mobility and regulate ATP-dependent nucleosome sliding by NURF. *Proceedings of the National Academy of Sciences of the United States of America* **98**, 14316-14321 (2001).

190. L. R. Racki *et al.*, The histone H4 tail regulates the conformation of the ATP-binding pocket in the SNF2h chromatin remodeling enzyme. *Journal of molecular biology* **426**, 2034-2044 (2014).

191. L. A. Boyer, R. R. Latek, C. L. Peterson, The SANT domain: a unique histone-tail-binding module? *Nat Rev Mol Cell Biol* **5**, 158-163 (2004).

192. T. G. Fazzio, M. E. Gelbart, T. Tsukiyama, Two distinct mechanisms of chromatin interaction by the Isw2 chromatin remodeling complex in vivo. *Molecular and cellular biology* **25**, 9165-9174 (2005).

193. B. Dorigo, T. Schalch, K. Bystricky, T. J. Richmond, Chromatin fiber folding: requirement for the histone H4 N-terminal tail. *Journal of molecular biology* **327**, 85-96 (2003).

194. J. Zhou, J. Y. Fan, D. Rangasamy, D. J. Tremethick, The nucleosome surface regulates chromatin compaction and couples it with transcriptional repression. *Nature structural & molecular biology* **14**, 1070-1076 (2007).

195. P. J. Robinson *et al.*, 30 nm chromatin fibre decompaction requires both H4-K16 acetylation and linker histone eviction. *Journal of molecular biology* **381**, 816-825 (2008).

196. A. Allahverdi *et al.*, The effects of histone H4 tail acetylations on cation-induced chromatin folding and self-association. *Nucleic acids research* **39**, 1680-1691 (2011).

197. W. J. Shia, S. G. Pattenden, J. L. Workman, Histone H4 lysine 16 acetylation breaks the genome's silence. *Genome Biol* **7**, 217 (2006).

198. O. Bell *et al.*, Accessibility of the Drosophila genome discriminates PcG repression, H4K16 acetylation and replication timing. *Nature structural & molecular biology* **17**, 894-900 (2010).

199. K. P. Nightingale *et al.*, Acetylation increases access of remodelling complexes to their nucleosome targets to enhance initiation of V(D)J recombination. *Nucleic acids research* **35**, 6311-6321 (2007).

200. D. Angelov *et al.*, SWI/SNF remodeling and p300-dependent transcription of histone variant H2ABbd nucleosomal arrays. *The EMBO journal* **23**, 3815-3824 (2004).

201. J. A. Goldman, J. D. Garlick, R. E. Kingston, Chromatin remodeling by imitation switch (ISWI) class ATP-dependent remodelers is stimulated by histone variant H2A.Z. *The Journal of biological chemistry* **285**, 4645-4651 (2010).

202. V. K. Gangaraju, B. Bartholomew, Dependency of ISW1a chromatin remodeling on extranucleosomal DNA. *Molecular and cellular biology* **27**, 3217-3225 (2007).

203. M. Zofall, J. Persinger, B. Bartholomew, Functional role of extranucleosomal DNA and the entry site of the nucleosome in chromatin remodeling by ISW2. *Molecular and cellular biology* **24**, 10047-10057 (2004).

204. J. D. Leonard, G. J. Narlikar, A nucleotide-driven switch regulates flanking DNA length sensing by a dimeric chromatin remodeler. *Molecular cell* **57**, 850-859 (2015).

205. I. M. Nodelman *et al.*, The Chd1 chromatin remodeler can sense both entry and exit sides of the nucleosome. *Nucleic acids research*, (2016).

206. S. K. Hota *et al.*, Nucleosome mobilization by ISW2 requires the concerted action of the ATPase and SLIDE domains. *Nature structural & molecular biology* **20**, 222-229 (2013).

207. J. C. Liu, C. G. Ferreira, T. Yusufzai, Human CHD2 is a chromatin assembly ATPase regulated by its chromo- and DNA-binding domains. *The Journal of biological chemistry* **290**, 25-34 (2015).

208. A. Patel *et al.*, Decoupling nucleosome recognition from DNA binding dramatically alters the properties of the Chd1 chromatin remodeler. *Nucleic acids research* **41**, 1637-1648 (2013).

209. J. N. McKnight, T. Tsukiyama, G. D. Bowman, Sequence-targeted nucleosome sliding in vivo by a hybrid Chd1 chromatin remodeler. *Genome Res* **26**, 693-704 (2016).

210. W. L. Hwang, S. Deindl, B. T. Harada, X. Zhuang, Histone H4 tail mediates allosteric regulation of nucleosome remodelling by linker DNA. *Nature* **512**, 213-217 (2014).

211. M. Pinskaya, A. Nair, D. Clynes, A. Morillon, J. Mellor, Nucleosome remodeling and transcriptional repression are distinct functions of Isw1 in Saccharomyces cerevisiae. *Molecular and cellular biology* **29**, 2419-2430 (2009).

212. A. Yildiz, M. Tomishige, A. Gennerich, R. D. Vale, Intramolecular strain coordinates kinesin stepping behavior along microtubules. *Cell* **134**, 1030-1041 (2008).

213. D. D. Hackney, M. F. Stock, J. Moore, R. A. Patterson, Modulation of kinesin half-site ADP release and kinetic processivity by a spacer between the head groups. *Biochemistry* **42**, 12011-12018 (2003).

214. T. H. Evers, E. M. van Dongen, A. C. Faesen, E. W. Meijer, M. Merkx, Quantitative understanding of the energy transfer between fluorescent proteins connected via flexible peptide linkers. *Biochemistry* **45**, 13183-13192 (2006).

215. I. M. Nodelman, G. D. Bowman, Nucleosome sliding by Chd1 does not require rigid coupling between DNA-binding and ATPase domains. *EMBO reports* **14**, 1098-1103 (2013).

216. M. S. Dillingham, D. B. Wigley, M. R. Webb, Demonstration of unidirectional single-stranded DNA translocation by PcrA helicase: measurement of step size and translocation speed. *Biochemistry* **39**, 205-212 (2000).

217. E. J. Tomko, C. J. Fischer, A. Niedziela-Majka, T. M. Lohman, A nonuniform stepping mechanism for E. coli UvrD monomer translocation along single-stranded DNA. *Molecular cell* **26**, 335-347 (2007).

218. M. Gyimesi, K. Sarlos, M. Kovacs, Processive translocation mechanism of the human Bloom's syndrome helicase along single-stranded DNA. *Nucleic acids research* **38**, 4404-4414 (2010).

219. W. Cheng, S. G. Arunajadai, J. R. Moffitt, I. Tinoco, Jr., C. Bustamante, Single-base pair unwinding and asynchronous RNA release by the hepatitis C virus NS3 helicase. *Science* **333**, 1746-1749 (2011).

220. B. T. Harada *et al.*, Stepwise nucleosome translocation by RSC remodeling complexes. *Elife* **5**, (2016).

221. H. Y. Fan, X. He, R. E. Kingston, G. J. Narlikar, Distinct strategies to make nucleosomal DNA accessible. *Molecular cell* **11**, 1311-1322 (2003).

222. M. L. Dechassa *et al.*, Disparity in the DNA translocase domains of SWI/SNF and ISW2. *Nucleic acids research* **40**, 4412-4421 (2012).

223. K. K. Sinha, J. D. Gross, G. J. Narlikar, Distortion of histone octamer core promotes nucleosome mobilization by a chromatin remodeler. *Science* **355**, (2017).

224. R. Sundaramoorthy *et al.*, Structural reorganization of the chromatin remodeling enzyme Chd1 upon engagement with nucleosomes. *Elife* **6**, (2017).

225. D. Ahel *et al.*, Poly(ADP-ribose)-dependent regulation of DNA repair by the chromatin remodeling enzyme ALC1. *Science* **325**, 1240-1243 (2009).

226. M. Udugama, A. Sabri, B. Bartholomew, The INO80 ATP-dependent chromatin remodeling complex is a nucleosome spacing factor. *Molecular and cellular biology* **31**, 662-673 (2011).

227. C. L. Smith, C. L. Peterson, A conserved Swi2/Snf2 ATPase motif couples ATP hydrolysis to chromatin remodeling. *Molecular and cellular biology* **25**, 5880-5892 (2005).

228. J. E. Dueber, B. J. Yeh, R. P. Bhattacharyya, W. A. Lim, Rewiring cell signaling: the logic and plasticity of eukaryotic protein circuitry. *Curr Opin Struct Biol* **14**, 690-699 (2004).

229. K. Zhao *et al.*, Rapid and phosphoinositol-dependent binding of the SWI/SNF-like BAF complex to chromatin after T lymphocyte receptor signaling. *Cell* **95**, 625-636 (1998).

230. B. Montpetit *et al.*, A conserved mechanism of DEAD-box ATPase activation by nucleoporins and InsP6 in mRNA export. *Nature* **472**, 238-242 (2011).

231. A. Marintchev, Roles of helicases in translation initiation: a mechanistic view. *Biochimica et biophysica acta* **1829**, 799-809 (2013).

232. L. Wang *et al.*, Regulation of the Rhp26ERCC6/CSB chromatin remodeler by a novel conserved leucine latch motif. *Proceedings of the National Academy of Sciences of the United States of America* **111**, 18566-18571 (2014).

233. R. J. Lake, A. Geyko, G. Hemashettar, Y. Zhao, H. Y. Fan, UV-induced association of the CSB remodeling protein with chromatin requires ATP-dependent relief of N-terminal autorepression. *Molecular cell* **37**, 235-246 (2010).

234. V. Alexiadis, A. Lusser, J. T. Kadonaga, A conserved N-terminal motif in Rad54 is important for chromatin remodeling and homologous strand pairing. *The Journal of biological chemistry* **279**, 27824-27829 (2004).

235. E. Citterio *et al.*, ATP-dependent chromatin remodeling by the Cockayne syndrome B DNA repair-transcription-coupling factor. *Molecular and cellular biology* **20**, 7643-7653 (2000).

236. D. A. Hill, A. N. Imbalzano, Human SWI/SNF nucleosome remodeling activity is partially inhibited by linker histone H1. *Biochemistry* **39**, 11649-11656 (2000).

237. A. M. Deaconescu *et al.*, Structural basis for bacterial transcription-coupled DNA repair. *Cell* **124**, 507-520 (2006).

238. M. N. Murphy *et al.*, An N-terminal clamp restrains the motor domains of the bacterial transcription-repair coupling factor Mfd. *Nucleic acids research* **37**, 6042-6053 (2009).

239. L. Manelyte, Y. I. Kim, A. J. Smith, R. M. Smith, N. J. Savery, Regulation and rate enhancement during transcription-coupled DNA repair. *Molecular cell* **40**, 714-724 (2010).

240. E. Kowalinski *et al.*, Structural basis for the activation of innate immune pattern-recognition receptor RIG-I by viral RNA. *Cell* **147**, 423-435 (2011).

241. A. Ramanathan *et al.*, The autoinhibitory CARD2-Hel2i Interface of RIG-I governs RNA selection. *Nucleic acids research* **44**, 896-909 (2016).

242. S. N. Floor, K. J. Condon, D. Sharma, E. Jankowsky, J. A. Doudna, Autoinhibitory Interdomain Interactions and Subfamily-specific Extensions Redefine the Catalytic Core of the Human DEAD-box Protein DDX3. *The Journal of biological chemistry* **291**, 2412-2421 (2016).

243. Z. M. Zhang *et al.*, Crystal structure of Prp5p reveals interdomain interactions that impact spliceosome assembly. *Cell Rep* **5**, 1269-1278 (2013).

244. R. Collins *et al.*, The DEXD/H-box RNA helicase DDX19 is regulated by an {alpha}-helical switch. *The Journal of biological chemistry* **284**, 10296-10300 (2009).

245. H. von Moeller, C. Basquin, E. Conti, The mRNA export protein DBP5 binds RNA and the cytoplasmic nucleoporin NUP214 in a mutually exclusive manner. *Nature structural & molecular biology* **16**, 247-254 (2009).

246. J. Napetschnig *et al.*, Structural and functional analysis of the interaction between the nucleoporin Nup214 and the DEAD-box helicase Ddx19. *Proceedings of the National Academy of Sciences of the United States of America* **106**, 3089-3094 (2009).

247. J. H. Chang *et al.*, Crystal structure of the eIF4A-PDCD4 complex. *Proceedings of the National Academy of Sciences of the United States of America* **106**, 3148-3153 (2009).

248. P. G. Loh *et al.*, Structural basis for translational inhibition by the tumour suppressor Pdcd4. *The EMBO journal* **28**, 274-285 (2009).